A METHOD FOR COMPUTING THE CORE FLOW IN THREE-DIMENSIONAL LEADING-EDGE VORTICIES

By

James Michael Luckring

A Dissertation

Submitted to the Graduate Faculty of

North Carolina State University at Raleigh

in Partial Fulfillment of the Requirements

for the Degree of Doctor of Philosophy

in the department of Mechanical and Aerospace Engineering

Raleigh, North Carolina

May 1985

A METHOD FOR COMPUTING THE CORE FLOW IN THREE-DIMENSIONAL LEADING-EDGE VORTICES

BY

James Michael Luckring

A Dissertation submitted to the Graduate Faculty of
North Carolina State University at Raleigh
in partial fulfillment of the requirements
for the Degree of Doctor of Philosphy

DEPARTMENT OF MECHANICAL AND AEROSPACE ENGINEERING
RALEIGH, NORTH CAROLINA

1985

Approved by:

Fred R. DeJarnette
Professor of Mechanical and
Aerospace Engineering
(Chairman of Advisory Committee)

H. D. Hagerson
Professor of Mechanical and
Aerospace Engineering
(Member of Advisory Committee)

Frederick O. Smetana
Professor of Mechanical and
Aerospace Engineering
(Member of Advisory Committee)

R. E. Chandler
Professor of Mathematics
(Member of Advisory Committee)

ABSTRACT

Luckring, James Michael. A Method for Computing the Core Flow in Three-Dimensional Leading-Edge Vortices (under the direction of Dr. Fred R. DeJarnette.)

A theory is presented for calculating the flow in the core of a separation-induced leading-edge vortex. The method is based on matching inner and outer representations of the vortex. The inner model of the vortex is based on the quasicylindrical Navier-Stokes equations; the flow is assumed to be steady, axially symmetric, and incompressible and, in addition, gradients in the radial direction are assumed to be much larger than gradients in the axial direction. The outer model is based on the three-dimensional free-vortex-sheet theory, a higher-order panel method which solves the Prandtl-Glauert equation including nonlinear boundary conditions pertinent to the concentrated vorticity representation of the leading edge vortex. The initial conditions for the inner representation draw upon conical flow notions and include an asymptotic viscous subcore. All matching is based on identifying overlapping zones among the various theories which are either derived analytically from asymptotic concepts or demonstrated numerically. The resultant flow is evaluated a posteriori for evidence of incipient vortex breakdown and the critical helix angle concept, in conjunction with an adverse longitudinal pressure gradient, is found to correlate well with the occurrence of vortex breakdown at the trailing edge of delta, arrow, and diamond wings.

BIOGRAPHY

James M. Luckring was born [redacted] in [redacted] He received his elementary and secondary education in Glen Ellyn, Illinois, graduating from Glenbard West High School in 1969.

He received a Bachelor of Science degree in aeronautical and astronautical engineering in 1973 from Purdue University. This was followed by a Master of Science degree in aeronautics and astronautics in 1974, also from Purdue University.

From 1974 to the present, he has been employed by NASA at the Langley Research Center, Hampton, Virginia. Under the auspices of NASA's graduate training program, he attended North Carolina State University in the fall of 1979 and the spring of 1980 to complete academic requirements pertinent to the subject degree.

ACKNOWLEDGEMEMTS

The advice provided by Dr. Fred R. DeJarnette during the course of this study is greatfully acknowledged. Sincere appreciation is also extended to Dr. Richard W. Barnwell and Mr. Edward C. Polhamus for their technical assistance and intuitive guidance.

The financial and professional support of the NASA-Langley Research Center through its graduate training program is particularly appreciated. Without such support this endeavor could not have been undertaken.

A special note of thanks is expressed to Mrs. Sue Seward of the Technical Library Staff at NASA Langley. Her persistence and success in obtaining many technical documents played a vital role in the completion of this research. I am also grateful to Mrs. Bernice Barrack and Miss Karen Cole for the careful preparation of this text.

Finally, sincere appreciation is expressed to my wife, Karen, whose personal sacrifice made this research possible, and to my parents who continue to be a source of inspiration.

TABLE OF CONTENTS

LIST OF FIGURES

NOMENCLATURE

All nonreference quantities are nondimensional, unless otherwise indicated. Lengths are referenced to wing root chord, velocities to the free-stream reference velocity, and pressures to twice the free-stream dynamic pressure. Nondimensionalization is explicitly shown for deviations from this convention or for purposes of clarity.

A	inner radial flow expansion, eq. (3.18a)
AR	aspect ratio
a	Burgers' vortex coefficient, eq. (4.16)
B	inner swirl flow expansion, eq. (3.18b)
C	inner axial flow expansion, eq. (3.18c)
$C_{B,D}$	dynamic wing root bending moment coefficient, $\tilde{M}_D/\tilde{q}_\infty \tilde{S}_{ref} \bar{c}$
C_D	drag coefficient, drag/$\tilde{q}_\infty \tilde{S}_{ref}$
C_L	lift coefficient, lift/$\tilde{q}_\infty \tilde{S}_{ref}$
C_m	pitching moment coefficient, pitching moment/$\tilde{q}_\infty \tilde{S}_{ref} \bar{c}$
$C_{m,o}$	zero lift pitching moment coefficient
C_p	static pressure coefficient, $(\tilde{p} - \tilde{p}_\infty)/\tilde{q}_\infty$
$C_{p,t}$	total pressure coefficient, $(\tilde{p}_t - \tilde{p}_\infty)/\tilde{q}_\infty$
c	constant
$\bar{c}$	reference chord
cs_i	quasicylindrical numerical coefficients, $i = 1,2,3$, eq. (D.9)
D	inner pressure expansion, eq. (3.18d)

$\hat{e}$	unit edge vector
$\vec{F}$	force vector
f	radial scale factor, eq. (4.1)
H	radial flow parameter, eq. (4.4b)
h	enthalpy
h_o	stagnation enthalpy, h + 1/2 Q^2
K	circulation parameter, eq. (4.4.c)
l	length
M	Mach number
$\tilde{M}_D$	time averaged rms value of dynamic wing root bending moment
m	chordwise index
N	radial index at edge of core
$\hat{n}$	unit normal vector
p	static pressure, $\tilde{p}_t/2\tilde{q}_\infty$
p_t	total pressure, $\tilde{p}_t/2\tilde{q}_\infty$
Q	velocity
q	dynamic pressure, 1/2 ρU^2
R	scaled radial coordinate, eq. (4.1a)
Rn	Reynolds number, $\tilde{U}_\infty \tilde{l}/\tilde{\nu}_\infty$
(r,θ,z)	core axis radial, angular, and axial coordinate system
S	entrophy
S_{ref}	reference area
s	conical coordinate, $(r^2+z^2)^{1/2}$; also local semispan
T	temperature

t	conical coordinate, r/z
(U,V,W)	body axis cartesian velocites
(u,v,w)	core axis radial, angular, and axial velocities
v_r^*	$(r/v)\ v_{,r}$
w_r^*	$(r/v)\ w_{,r}$
ws_i	quasicylindrical numerical coefficients, i = 1,2,3,4,5, eq. D13
(X,Y,Z)	body axis cartesian coordinate system
(x,y,z)	core axis orthogonal coordinates
α	angle of attack, degrees; also swirl function, eq. (3.6b)
α_a	angle of attack for vortex assymmetry onset
α_b	angle of attack for vortex breakdown at trailing edge
β	swirl function, eq. (A.8); also Prandtl-Glauert factor, $(1-M_\infty^2)^{1/2}$
γ	ratio of specific heats
Δ	difference operator
δ	slenderness function, eq. (A.5)
ε	small constant
ζ	vorticity
η	transverse inner variable, eq. (3.14b)
Λ	leading edge sweep angle, degrees
λ	radial parameter, eq. (4.4d)
μ	viscosity, also doublet strength
ν	kinematic viscosity, $\nu=\mu/\rho$

ξ	transverse inner variable, eq. (4.4a)
ρ	density
τ	function of t, eq. (A.6); also radial stretching factor, eq. (4.7)
Φ	velocity potential
ϕ	helix angle parameter, v/w, eq. (3.6a); also pertubation velocity potential
χ	core-wise inner variable, eq. (3.14a)
ϕ	spherical coordinate
ω	frequency, radians/sec.
$\cdot$	vector dot product
$\times$	vector cross product
∇	vector gradient operator

Subscripts

a	axis of vortex core
av	average
c	core; also critical
e	edge of vortex core
i	inner variable
le	leading edge
max	maximum
o	outer variable
te	trailing edge
1	first order

2	second order
∞	freestream reference conditions
,j	partial differentiation, eg, $\frac{\partial}{\partial j}$

Superscripts

T	transpose
~	dimensional quantity
$\rightarrow$	vector quantity
$(\bar{})$	lagged quantity

1.0 INTRODUCTION

Interest in vortical flows embraces a rather broad spectrum of aerodynamics and, for that matter, fluid mechanics. Aerodynamically, vortices are a natural consequence of lifting flow and are manifested at scales ranging from a boundary layer thickness to characteristic wing dimensions. They can persist for miles downstream from a typical transport aircraft or, on the other hand, undergo an abrupt disruption commonly referred to as bursting or vortex breakdown. In addition, vorticies are a usual consequence of flow instability, play a role in the large scale structure of turbulence, and are a dominant feature of separated flows. They are prevalent in flows such as a draining basin and can be manifested on geophysical scales in the form of tornadoes and hurricanes. The fluid mechanics of vortical flows has been addressed by several authors, among them Küchemann (1966) and, in a broader sense, Lugt (1983).

The research of one class of vortical flow, the separation induced leading edge vortex phenomena, is largely motivated by the advent of high speed aircraft with supersonic capability. The design of these aircraft for efficient supersonic cruise often requires consideration of slender wing concepts which include comparatively high leading-edge sweep angles, thin wing sections, and in some cases, relatively sharp leading edges. At the higher angles of attack encountered for take-off and landing as well as for subsonic-transonic maneuver, the subject vortex flow naturally occurs on these wings and

can be exploited for a variety of beneficial effects. The application of slender wing benefits to military aircraft has recently been reviewed by Polhamus (1983).

The computation of these vortex flow effects which are dominant for aerodynamic applications has proven to be a challenging task. Even for simple three-dimensional geometries with sharp edges at subsonic speeds, it has only been during the last ten years or so that methods have been developed to provide reasonable estimates of inviscid force-moment properties and, subsequently, pressure distributions. Most of these methods are based upon explicit representations of the vortex by various approximate means, as opposed to solving a globally applicable formulation such as the Reynolds averaged Navier Stokes equations or, possibly, the Euler equations. Apart from the usual drawback of turbulence closure for the Navier-Stokes equations, problems affiliated with large memory requirements along with the large execution times for these equations are particularly exacerbated for the subject flow. As opposed to attached flows where large gradients occur in narrow regions near the wing surface, the zone of high gradients for the vortex flow case can easily extend for distances on the order of the local wing semispan or more, thus requiring a comparatively large zone over which a fine grid would have to be employed. This situation is particularly acute when viewed in the context of current limitations to algorithms for solving three-dimensional, nonlinear flows as discussed by South (1985). While progress in this area will no doubt be realized, the presently

available methods with explicit vortex modeling will continue to be useful for some time. This will particularly be true if they are extended by embedding representations of additional flow effects (such as those due to viscosity), much as has been done for attached flows.

The purpose of the present research is to formulate a composite representation of a fully three-dimensional, separation-induced, leading-edge vortex with emphasis on the flow in the vortex core. The primary objectives of the research are, first, to calculate the general properties of the vortex core flow for the fully three-dimensional outer flow of simple wing shapes, and, second, to examine the resultant flow a posteriori for evidence of incipient vortex breakdown. The approach taken is to embed an inner representation of the core flow in an outer representation of the overall wing/vortex flow field. With this approach, considerable advantage can be taken of the extensive modeling studies that have been performed for isolated vortex cores as well as for three-dimensional leading-edge vortices, so long as appropriate matching conditions can be established between the two models.

The present investigation draws heavily on the isolated vortex core solutions of Stewartson and Hall (1963) and Hall (1967) as well as the vortex sheet solution of Johnson, et al. (1980). These theories were found to be appropriate for the present study and offered adequate growth potential for future investigations. The composite representation of the vortex is formulated by matching an

inner representation of the vortex core which accounts for viscosity and continuously distributed vorticity to an outer representation of the vortex which is inviscid and has concentrated sheets of spiral vorticity. A sketch illustrating the theoretical model of the present investigation is presented in figure 1.1.

Select background and review material is presented in section 2. Included are a discussion of prominent leading-edge vortex flow features as well as a focused review of vortex core theory, leading-edge vortex theory, and vortex breakdown theory. Some additional review material addressing these disciplines in a broader sense is also cited. The particular theoretical methods, as implemented in the present formulation, are then developed in detail. In section 3, the initial plane solution for the inner representation of the vortex core is presented. The solution is conical and includes a viscous sub core which is asymptotic to an analytical solution of the incompressible and conical Euler equations. This solution is advanced in space with the nonconical quasicylindrical Navier-Stokes equations, section 4. The three-dimensional boundary conditions for the inner vortex core representation are provided by the free-vortex-sheet theory (section 5) and the matching of these solutions is described in section 6. Results and discussion of the coupled formulation are presented in section 7. Future considerations based upon these results are contained in section 8, and some general conclusions are presented in section 9. Some frequently used parameters are shown in figure 1.2.

2.0 BACKGROUND AND REVIEW

2.1 Leading-Edge Vortex Flow Features

The basic flow structure of the separation-induced leading-edge vortex is shown in figure 2.1. For slender wings with relatively sharp leading edges, the flow is dominated at moderate to high angles of attack by spiral shear layers of concentrated vorticity emanating from the leading edges. These shear layers roll up in the presence of the wing under their own influence into what is commonly referred to as the vortex core; collectively, this flow structure constitutes the primary vortex. The primary vortex induces a transverse boundary-layer flow on the wing upper surface which can separate and cause a smaller secondary vortex. The chief attribute of the overall flow is the development of large vortex lift increments which are nonlinear and stable at moderate to high angles of attack. The stable vortices persist well downstream of the generating wing and eventually diffuse.

As angle of attack is increased further, the stable vortex flow pattern drastically changes as the vortices exhibit an abrupt breakdown (or burst) downstream of the generating surface. With additional angle-of-attack increases, the burst point propagates rapidly upstream, and over the lifting surface. A water-tunnel photograph from Erickson (1981) illustrates strake vortices bursting in the vicinity of the wing trailing edge and empennage for a YF-17 model (figure 2.2). Although the present effort is directed primarily at delta wings, this photograph emphasizes the complexity of the

vortex breakdown flow field for practical geometries. The occurrence of breakdown in the vicinity of the lifting surface has many adverse effects; these include lift loss, pitchup, buffet onset, control decrements, nonlinearities, and configurational sensitivities. As a consequence, the "usable lift" range for configurations employing the vortex lift concept is often limited to angles of attack sufficiently below the critical angle of attack (α_b) at which bursting has reached the near field of lifting or control surfaces. The near-field breakdown stability boundary, α_b, is presented in figure 2.3, along with the near-field vortex asymmetry boundary, α_a, for sharp edged delta wings at incompressible conditions. This figure (after Polhamus (1971)) is a summary of experimental data; there are presently no theoretical methods available for predicting these boundaries or aerodynamic properties under conditions when the angle of attack exceeds the appropriate critical value.

Some examples of the adverse effects affiliated with near-field vortex breakdown are presented in figures 2.4 and 2.5 for a 65° delta wing. In figure 2.4 the water-tunnel photograph of Lambourne and Bryer (1962) illustrates clearly the flow of a core streamline near the axis of a vortex undergoing breakdown; both axisymmetric and spiral type core flows are demonstrated directly down stream of the burst point. Also shown, the lift losses due to breakdown are substantial. The theoretical lift from which experimental losses are judged was determined with the free-vortex-sheet theory of Johnson, et al. (1980). For this case, the losses occur gradually and precede

α_b. At lower angles of attack, some of the differences between the theory and experiment are also due to the relative accuracies of both.

The effects of breakdown on longitudinal stability and buffet properties are equally pronounced as shown in figure 2.5. The experimental pitching moment data of Wentz and Kohlman (1968) demonstrate a marked pitchup somewhat prior to the onset of breakdown. The correlation between theory and experiment at low to moderate values of lift coefficient is less accurate than usually achieved with the FVS theory, primarily because of experimental effects such as free-stream curvature and support-strut interference. (This aspect of the pitching moment data has been confirmed in a private communication with Dr. Wentz.) The dynamic data of Boyden and Johnson (1982) exhibit buffet onset in the vicinity of α_b as indicated by the dynamic root bending moment coefficient. In this experiment, the buffet intensity for $\alpha > \alpha_b$ was chiefly a function of reduced frequency, although buffet onset itself was insensitive to this parameter as well as to Reynolds number, dynamic pressure, and subsonic Mach number.

Other aerodynamic consequences of near-field breakdown can be equally pronounced, particularly with regard to lateral-directional effects as discussed by J. L. Johnson, et al (1980). Collectively, these adverse effects emphasize the need to be able to predict this phenomena.

2.2 Vortex Core Theory

Representations of the flow in the core of a vortex generally include the effects of distributed vorticity and viscosity. Virtually all of the theories are axisymmetric, and most model the vortex in isolation from natural surroundings for simplified boundary conditions, e.g., the models are usually appropriate for a vortex in a tube, or at best, conical edge flow. Newman (1959) modeled the flow in a laminar viscous trailing vortex for moderate to large Reynolds numbers by assuming the axial flow deficit and (unnecessarily) the swirl velocity to be small when compared to freestream reference conditions. As a consequence of the high Reynolds number and small axial perturbation assumptions the governing equations decouple, and the analytic solution is the familiar exponential vortex which, by virtue of the impulsive flow analogy, is identical to Lamb's (1932) for the time development of a viscous vortex. A different class of core flow was derived by Hall (1960) as well as Ludwieg (1962) for the conical incompressible Euler equations. The chief feature of these analytic solutions are radial logarithmic singularities as contrasted to the potential (1/r) form. This inviscid solution was extended by Stewartson and Hall (1963) to formally account for viscous effects by asymptotic means and the resultant solutions exhibit an asymptotic viscous subcore.

Brown (1965) extended Hall's Euler vortex solution to compressible conditions. Brown showed that the adiabatic conical

governing equations imply the flow to be isentropic and that momentum and continuity equations contain the energy integral

$$\frac{1}{2} Q^2 + \frac{\gamma}{\gamma-1} \frac{p}{\rho} = \text{const.} \tag{2.1}$$

which, for isentropic flow, will yield the compressible Bernoulli equation. The governing equations indicate that the velocity and vorticity are locally aligned which is consistant with Crocco's vortex theorem for steady inviscid flow:

$$\nabla h_0 - T\nabla S = \vec{Q} \times \vec{\zeta} \tag{2.2}$$

The chief feature of Brown's solution is that compressibility removes the radial singularities at the vortex axis but does so by achieving vacuum conditions there.

Nonaxisymmetric effects for conical flows were studied by Mangler and Weber (1966) by modeling a spiral sheet of vorticity in an otherwise potential flow. An asymptotic solution was derived, valid for a slender core, with the noteworthy result that the lead terms of the solution were axisymmetric and identical to Hall's (1960) solution. This solution was later extended by Brown and Mangler (1967) to account for compressibility yielding a similar result, when compared to the axisymmetric solution of Brown (1965). A more general treatment of the asymptotic structure of spiral vortex sheets including nonconical effects has been given by Guiraud and Zeytounian (1977).

A method valid for both nonconical and conical external flows was developed by Hall (1967). The flow is assumed to be steady, axisymmetric, and imcompressible. With the additional assumption of high Reynolds number a boundary layer-like approximation valid for a slender core is made and the resultant equations, referred to as quasicylindrical Navier-Stokes equations, are parabolic in the axial direction, i.e., down the core. The equations are solved numerically by a finite difference technique and the resultant solutions are shown to exhibit many of the general features of vortex core flow for both generic wake and leading edge vortex flows. These equations were also solved by Bossel (1972) by a method of weighted residuals for wake-like initial conditions in a study directed at vortex breakdown phenomena. The slenderness assumption was removed by Grabowski and Berger (1976) who solved the resultant elliptic system of equations with downstream Neumann boundary conditions by an ADI technique for initial and edge boundary conditions indicative of wake-like vorticies. Their solutions exhibit some features of the vortex breakdown flow field which are at least qualitatively similar to experiment.

2.3 Leading Edge Vortex Theory

In contrast to vortex core formulations, leading edge vortex formulations, which are generally directed at wing applications, tend to emphasize global flow effects while incorporating very approximate representations of the vortex core region. Early work in this area

was mostly for conical flows and focused on developing appropriate models for the leading edge vortex sheet and vortex core. Contributors to this research include Legender (1953), Brown and Michael (1955), Mangler and Smith (1959), and Smith (1966). Smith's resultant model incorporated a segmented free vortex sheet (alligned with the local flow and locally force free) terminated with a "cut" or fed sheet to a line vortex representation of the vortex core. By imposing that the combination of the fed sheet and vortex core be force free in conjunction with no flow boundary conditions for the wing and a leading-edge Kutta condition, the problem is solved numerically in an iterative fashion. The solutions achieved are qualitatively correct but suffer quantitatively due to the assumption of conical flow.

Several models have been developed for computing the subject flow in three dimensions. One approach is to represent the leading edge vortex by a system of discrete vortex filaments whose strength and location is determined iteratively so that they are force free. Contributors to this formulation include Rebach (1973), Mook and Maddox (1974), and Kandil, et al. (1974). This formulation has generally been coupled with a vortex lattice representation of the wing or, in the case of Mehrotra and Lan (1978), a quasi vortex lattice. The filament approach generally yields good estimates of force-moment properties but published correlations for wing pressure distributions are sparce and can be less than satisfactory. An alternate approach is to represent the leading edge vortex (as well as the wing and near wakes) by higher order panel techniques. The vortex

sheets satisfy the usual boundary conditions and the resultant formulation takes advantage of the higher order panel methodology to provide reasonable estimates of wing pressures as well as resultant force/moment properties. This formulation has primarily been developed by Brune, et al. (1975) as well as Johnson, et al. (1980) and has been applied to a fairly broad class of simple wing shapes.

The most recent approach to computing leading-edge vortex flows is based on solving the three-dimensional Euler equations. The calculations are usually founded on a finite volume formulation coupled with a fourth-order Runge-Kutta time-stepping scheme as put forth by Jameson, et al. (1981). Rotational effects are inherently represented in the governing equations, thereby offering the distinct advantage of implicitly capturing regions of vortical flow as contrasted to the previously discussed methods which (a priori) explicitly model these regions. Calculations by Hitzel and Schmidt (1983), as well as by Raj (1984), have shown encouraging correlations with experiment; in addition, Hoeijmakers and Rizzi (1984) have recently demonstrated an encouraging correlation between Euler and "vortex-fitted potential" solutions for a 70-degree delta wing at 20 degrees angle of attack. However, some controversy regarding the application of these Euler methods to the calculation of leading-edge vortex flows has arisen. For wings with blunt leading edges, Newsome (1985) recently demonstrated for supersonic flow that the Euler solutions are extremely grid dependent due to the nature of the artificial damping required for numerical stability; this result will hold true for

subsonic and transonic applications as well. Of possibly greater significance are the occurrence of extensive loses in total conditions (entropy production) in regions coincident with the vortical flow, as shown by Krause, et al. (1983b) for the sharp leading-edge case. For these shockless flows, there is no physically realistic mechanism for the entropy production; its source is numerical error. Further research into the nature and consequences of these effects will be required for a better understanding of leading-edge vortex solutions by Euler formulations.

Additional discussion of computational vortex flow methods may be found in the recent and comprehensive review of Hoeijmakers (1983).

2.4 Vortex Breakdown Theory

Vortex breakdown analysis can be accomplished either in the context of a stability theory or in terms of flow field analysis. Even for the simplified case of an isolated vortex in a tube, vortex breakdown (or bursting) has proven to be a very elusive phenomena to predict. Although some breakdown theories have enjoyed wider acceptance than others, a fully satisfactory and generally applicable explanation of this phenomena has yet to be developed. A review of many theories directed at this phenomena has recently been performed by Leibovich (1983); additional contributions to the problem of vortex breakdown can also be found in AGARD CP-342 (1983). Accurate computation of the vortex breakdown flow field has also been hindered, chiefly by the turbulent, unsteady nature of this flow as well as by

its inherent three dimensionality. Even so, computations based on various subclasses of the full governing equations have shown some success in capturing various features of this flow field for an isolated vortex.

Ludwieg (1962) derived a stability criterion, often referred to as hydrodynamic, by analyzing annular flow with a small disturbance theory for spiral perturbations. The stability criterion

$$(1 - v_r^*)\,(1 - v_r^{*2}) - (5/3 - v_r^*)\, w_r^{*2} > 0. \qquad (2.3)$$

emphasizes the strongly destabilizing effect of radial gradients in the axial flow, figure 2.6. Application of this criteria to the inviscid, analytic and conical solution of Hall (1960) predicted instability when the helix angle tangent, ϕ, exceeded 1.16. This critical value occurred at the edge of the vortex and was roughly confirmed experimentally by Hummel (1965). Ludwieg's criterion predicts that the flow will always become unstable to nonaxisymmetric modes prior to axisymmetric modes so long as $w_r^* \neq 0$.

The concept of a critical helix angle, ϕ_c, has been addressed by several authors. Bossel (1968) demonstrated, for a simplified vortex model with rigid rotation, that small edge disturbances would amplify in the core for $\phi_c \geq \sqrt{2}$. For a more elaborate model, Bossel (1969) found $\phi_c \geq 1.92$ corresponded to the occurrence of a breakdown bubble on the axis of the vortex core. Under rather general conditions, Hall (1966) showed, for the inviscid quasicylindrical equations, that

gradients in the edge axial flow can be amplified at the vortex core axis for a retarding flow. This relationship can be be expressed as

$$\frac{dw_a^2}{dz} = \frac{dw_e^2}{dz} - 4 \int_0^{r_e} \phi \frac{u}{r^2} k_{,r} \, dr \, . \tag{2.4}$$

For the retarded flow, the integrand is positive. Critical values of ϕ, therefore, not only promote instability of the edge flow, but also greatly promote deceleration of the inner core flow, primarily at the axis. A more general treatment of this feature has recently been given by Krause (1983) including viscous effects; the amplifying feature is retained although modulated by viscosity.

An alternate interpretation of vortex breakdown has been put forth by Benjamin (1962) by drawing an analogy to the hydraulic jump from a supercritical state of the flow to a subcritical state. Drawing upon variational methods, Benjamin shows that a finite transition between the conjugate flows is possible for inviscid parallel flow in a cylinder. The supercritical flow corresponds to the concentrated vortex and cannot support standing waves whereas the opposite is true for the subcritical case. By this theory, vortex breakdown corresponds to a transition from the supercritical to the subcritical flows.

Finally, the quasicylindrical Navier-Stokes formulation of Hall (1967) can provide an indication of vortex breakdown in a manner analogous to the boundary layer equations. As breakdown is approached, the flow undergoes rapid axial deceleration and some of

the assumptions of the theory are no longer valid. Hall (1967b) draws an analogy between this case and the calculation of boundary layer flows for conditions resulting in separation. Vortex breakdown, therefore, is related to a failure of the quasicylindrical approximation and comparisons by Hall (1967b) to the experimental results of Kirkpatrick (1965) for a tube vortex show reasonable correlation. The predicted breakdown location was several core diameters downstream from the measured location consistent with the parabolic nature of the theory. Continuation of the calculation beyond the breakdown point is impossible by Hall's method. This would require either an inverse boundary layer approach or some treatment of elliptic effects such as in Grabowski and Berger (1976), or Bossel (1969).

Additional review material regarding vortex breakdown has been given by Hall (1972) and Liebovich (1978).

3.0 INITIAL PLANE (CONICAL) CORE FORMULATION

For the initial plane of the inner vortex core model the outer flow is assumed to be representable in some fashion by conical flow notions. Matching of this conical solution to the nonconical outer flow will be addressed in section 6.

3.1 Intermediate Inviscid Solution

When the flow is considered to be steady, incompressible, inviscid, and axisymmetric the nondimensional governing equations are, without approximation

$$\frac{1}{r}(ru)_{,r} + w_{,z} = 0 \tag{3.1a}$$

$$uu_{,r} + wu_{,z} - \frac{v^2}{r} = -p_{,r} \tag{3.1b}$$

$$u(rv)_{,r} + w(rv)_{,z} = 0 \tag{3.1c}$$

$$uw_{,r} + ww_{,z} = -p_{,z} \tag{3.1d}$$

Transforming the independent variables from the cylindrical (r, z) system to the spherical-like (t, s) system yields

$$-t\left(w - \frac{u}{t}\right)_{,t} + 2\frac{u}{t} = \frac{-s}{1 + t^2}(w + tu)_{,s} \tag{3.2a}$$

$$-t\left(w - \frac{u}{t}\right)u_{,t} - \frac{v^2}{t} + p_{,t}$$

$$= \frac{-s}{1 + t^2}\left[(w + tu)\, u_{,s} + tp_{,s}\right] \tag{3.2b}$$

$$-t\left(w - \frac{u}{t}\right)v_{,t} + \frac{uv}{t} = \frac{-s}{1 + t^2}\left[(w + tu)\, v_{,s}\right] \tag{3.2c}$$

$$-t\left(w - \frac{u}{t}\right)w_{,t} - tp_{,t} = \frac{-s}{1 + t^2}\left[(w + tu)\, w_{,s} + p_{,s}\right] \tag{3.2d}$$

By further assuming conical flow all s-derivatives are zero and the t-derivatives become total derivatives:

$$-t\,\frac{d}{dt}\left(w - \frac{u}{t}\right) + \frac{2u}{t} = 0 \tag{3.3a}$$

$$-t\,\left(w - \frac{u}{t}\right)\frac{du}{dt} - \frac{v^2}{t} = \frac{-dp}{dt} \tag{3.3b}$$

$$-t\,\left(w - \frac{u}{t}\right)\frac{dv}{dt} + \frac{(uv)}{t} = 0 \tag{3.3c}$$

$$-\left(w - \frac{u}{t}\right)\frac{dw}{dt} = \frac{dp}{dt} \tag{3.3d}$$

Hall (1961) showed that the resultant system of equations may be integrated in closed form. The boundary conditions appropriate to the inviscid vortex core flow are

$$\{u = 0;\quad t = 0\} \tag{3.4a}$$

$$\{v = v_e,\ w = w_e,\ p = p_e;\ t = t_e\} \tag{3.4b}$$

and Hall's solution, neglecting effects of $O(t^2)$ is

$$\frac{u}{w_e} = \frac{-\alpha_e}{2} t \tag{3.5a}$$

$$\frac{v}{w_e} = \left[\phi_e^2 - \alpha_e^2 \ln \left(\frac{t}{t_e}\right)\right]^{1/2} \tag{3.5b}$$

$$\frac{w}{w_e} = 1 - \alpha_e \ln \left(\frac{t}{t_e}\right) \tag{3.5c}$$

$$\frac{p - p_e}{w_e^2} = \phi_e^2 \ln \left(\frac{t}{t_e}\right) - \frac{1}{2} \alpha_e^2 \ln^2 \left(\frac{t}{t_e}\right) \tag{3.5d}$$

where

$$\phi_e = \frac{v_e}{w_e} \tag{3.6a}$$

$$\alpha_e = (1 + 2\phi_e^2)^{1/2} - 1 \tag{3.6b}$$

or, equivalently,

$$\phi_e^2 = \alpha_e \left(1 + \frac{\alpha_e}{2}\right) \tag{3.6c}$$

The same solution was derived independently by Ludwieg (1962). Hall indicates that equations (3.3) can be solved exactly, without the slender core ($t^2 << 1$) assumption, but that the exact solution is

algebraically complicated and does not alter the character of the approximate solution. The exact solution is presented in Appendix 10.A and compared to the slender core solution in figure 3.1. The consequences of the slenderness assumption are, in general, small; near the axis, the nonslender terms are negligible ($t/t_e << 1$) while, near the edge, both the slender and nonslender solutions approach the same boundary condition values except for the radial flow which has no edge boundary condition, but which is small as compared to the other velocities. For practical applications, $t_e \leq 0.1$ and the slender core assumption constitutes a very good approximation.

Several aspects of this solution are noteworthy. Perhaps its most prominent feature is the logarithmic singularity in the swirl and axial velocities as well as in the pressure. For this distributed vorticity solution the singularity is much weaker than for the potential vortex. Moreover, the solution never approaches a potential form.

Further insights are gained by examining the vorticity of this solution. From Appendix 10.B, the solution is seen to be highly rotational; the axial component of the vorticity is dominant. As indicated in section 1.0, the vorticity and velocity vectors for this incompressible Euler vortex are locally aligned so that

$$\vec{Q} \times \vec{\zeta} = 0 \tag{3.7}$$

A simple calculation, though algebraically cumbersome, can confirm this result; vorticity contours are also streamlines. As a consequence, the

pressure field of this highly rotational flow is governed by the Bernoulli equation and total pressure losses are identically zero. These aspects are important to the matching of this flow to the outer formulation.

3.2 Inner Viscous Subcore

The governing equations for a steady, incompressible, and axisymmetric flow including the effects of viscosity for laminar flow are

$$\frac{1}{r}(ru)_{,r} + w_{,z} = 0 \tag{3.8a}$$

$$uu_{,r} + wu_{,z} - \frac{v^2}{r} + p_{,r}$$

$$= \frac{1}{Rn}\left(u_{,rr} + \frac{1}{r}u_{,r} + u_{,zz} - \frac{u}{r^2}\right) \tag{3.8b}$$

$$u(rv)_{,r} + w(rv)_{,z}$$

$$= \frac{1}{Rn}\left[(rv)_{,rr} - \frac{1}{r}(rv)_{,r} + (rv)_{,zz}\right] \tag{3.8c}$$

$$uw_{,r} + ww_{,z} + p_{,z}$$

$$= \frac{1}{Rn}\left(w_{,rr} + \frac{1}{r}w_{,r} + w_{,zz}\right) \tag{3.8d}$$

Evaluating these equations for the slender core conical solution

(equations (3.5)) yields

$$\frac{w_e^2\,\alpha_e t}{2z}\left(\frac{w}{w_e} + \frac{\alpha_e}{2}\right) = \frac{-1}{Rn}\left(\frac{w_e \alpha_e t}{z^2}\right) \tag{3.9a}$$

$$\frac{w_e^2 \alpha_e^2}{2z}\{0\} = \frac{-w_e \alpha_e}{2Rn\ r^2}\left[\frac{\alpha_e^2}{2}\left(\frac{w}{w_e} + \frac{\alpha_e}{2}\right)^{-1}(1 + t^2)\right.$$

$$\left. + \alpha_e\, t^2 + 2\left(\frac{w}{w_e} + \frac{\alpha_e}{2}\right)\right] \tag{3.9b}$$

$$\frac{w_e^2 \alpha_e}{z}\{0\} = \frac{-1}{Rn}\left(\frac{w_e \alpha_e}{z^2}\right) \tag{3.9c}$$

and continuity is identically satisfied. The nonzero left-hand side of equation (3.9a) arises due to the slender core approximation; the solution of Appendix A integrates these terms identically. The viscous terms for the radial and axial momentum equations arise solely from corewise diffusion and will be small for $z >> Rn^{-1/2}$. The swirl momentum equation alone imparts a scale for the viscous subcore which, following Stewartson and Hall (1963), is given by

$$r = 0\left[z(w_e \alpha z Rn)^{-1/2}\right] \tag{3.10}$$

Stewartson and Hall (1963) proceed to construct an inner solution for the viscous vortex which will be asymptotic to the outer inviscid

solution, equations (3.5). They follow a standard approach from singular perturbation theory, the basic steps of which are outlined below. By comparing the size of the viscous and inviscid terms, a boundary-layer like approximation to equations (3.8) is made by taking the limit

$$[w_e \alpha_e zRn \to \infty \; ; \; (\tfrac{r}{z})(w_e \alpha_e zRn)^{1/2} \text{ fixed}] \tag{3.11}$$

to yield

$$\frac{1}{r}(ru_i)_{,r} + w_{i,z} = 0 \tag{3.12a}$$

$$\frac{v_i^2}{r} = p_{i,r} \tag{3.12b}$$

$$u_i(rv_i)_{,r} + w_i(rv_i)_{,z} = \frac{1}{Rn}[(rv_i)_{,rr} - \frac{1}{r}(rv_i)_{,r}] \tag{3.12c}$$

$$u_i w_{i,r} + w_i w_{i,z} = -p_{i,z} + \frac{1}{Rn}(w_{i,rr} + \frac{1}{r} w_{i,r}) \tag{3.12d}$$

where the subscript i denotes an inner solution. The boundary conditions appropriate to the inner flow are

$$\{u_i = v_i = w_{i,r} = 0; \quad r = 0\} \tag{3.13a}$$

$$\{(v_i, w_i, p_i)^T \to (v, w, p)^T; \quad (\tfrac{r}{z})\,(w_e \alpha_e zRn)^{1/2} \to \infty\} \tag{3.13b}$$

Equations (3.12) govern the inner viscous flow. In the limit $Rn \to \infty$

equations (3.12) revert to the outer equations (3.1) but with the slender core approximation, $t^2 << 1$; the boundary layer like approximation (3.11) is equivalent to the slender core approximation in this limit.

Next a new set of independent variables appropriate to the inner flow are set down:

$$\chi = \ln \left[\frac{r_e}{z}(w_e \alpha_e z Rn)^{1/2}\right] \tag{3.14a}$$

$$\eta = \frac{r}{z}(w_e \alpha_e \chi z Rn)^{1/2} \tag{3.14b}$$

$$= \frac{r}{r_e}\, \chi^{1/2} e^{\chi} \tag{3.14c}$$

The outer flow expressed in these inner variables is

$$\frac{u}{w_e} = \frac{-\alpha_e}{2}(w_e \alpha_e \chi z Rn)^{-1/2} \eta \tag{3.15a}$$

$$\frac{v}{w_e} = \alpha_e \chi^{1/2} \left[1 + \frac{1}{2}\frac{\ln \chi}{\chi} + \frac{1}{\chi}\left(-\ln \eta + \frac{1}{2} + \frac{1}{\alpha_e}\right)\right]^{1/2} \tag{3.15b}$$

$$= \alpha_e \chi^{1/2} \left[1 + \frac{\ln \chi}{4\chi} + \frac{1}{2\chi}\left(-\ln \eta + \frac{1}{2} + \frac{1}{\alpha_e}\right) + \ldots\right] \tag{3.15c}$$

$$\frac{w}{w_e} = \alpha_e \chi \left[1 + \frac{\ln \chi}{2\chi} + \left(\frac{1}{\chi} - \ln \eta + \frac{1}{\alpha_e}\right)\right] \tag{3.15d}$$

$$\frac{p - p_e}{w_e^2} = \frac{-\alpha_e^2 \chi^2}{2} \left\{1 + \frac{\ln \chi}{\chi} + \frac{1}{\chi}\left(-2 \ln \eta + 1 + \frac{2}{\alpha_e}\right)\right.$$

$$+ \frac{\ln^2 \chi}{4\chi^2} + \frac{\ln \chi}{\chi^2}\left(-\ln \eta + \frac{1}{2} + \frac{1}{\alpha_e}\right)$$

$$\left. + \frac{1}{\chi^2}\left[\ln^2 \eta - \left(1 + \frac{2}{\alpha_e}\right) \ln \eta\right]\right\} \qquad (3.15e)$$

The expansion for the swirl velocity is valid for

$$\left| \frac{1}{2} \frac{\ln \chi}{\chi} + \frac{1}{\chi}\left(-\ln \eta + \frac{1}{2} + \frac{1}{\alpha_e}\right) \right| < 1 \qquad (3.16a)$$

or

$$e^{(1/2+1/\alpha_e)} \chi^{1/2} e^{-\chi} < \eta < e^{(1/2+1/\alpha_e)} \chi^{1/2} e^{\chi} \qquad (3.16b)$$

Equations (3.15) are exact. They represent the outer limit of the inner flow and suggest the following series expansion for the inner flow:

$$\frac{u_i}{w_e} = \frac{-1}{2} \alpha_e (w_e \alpha_e \chi z Rn)^{-1/2} \eta A(\chi, \eta) \qquad (3.17a)$$

$$\frac{v_i}{w_e} = \alpha_e \chi^{1/2} B(\chi, \eta) \qquad (3.17b)$$

$$\frac{w_i}{w_e} = \alpha_e \chi C(\chi,\eta) \tag{3.17c}$$

$$\frac{p_i - p_e}{w_e^2} = \frac{-1}{2} \alpha_e^2 \chi^2 D(\chi,\eta) \tag{3.17d}$$

with

$$A(\chi,\eta) = \frac{1}{2} + A_0(\eta) + \frac{\ln \chi}{\chi} A_1(\eta) + \frac{1}{4\chi} + \frac{1}{\chi} A_2(\eta) + \ldots \tag{3.18a}$$

$$B(\chi,\eta) = B_0(\eta) + \frac{\ln \chi}{\chi} B_1(\eta) + \frac{1}{\chi} B_2(\eta) + \ldots \tag{3.18b}$$

$$C(\chi,\eta) = 1 + \frac{\ln \chi}{2\chi} + \frac{1}{\chi} C_1(\eta) + \frac{\ln \chi}{\chi^2} C_2(\eta) + \frac{1}{\chi^2} C_3(\eta) + \ldots \tag{3.18c}$$

$$D(\chi,\eta) = 1 + \frac{\ln \chi}{\chi} + \frac{1}{\chi} D_1(\eta) + \frac{\ln^2 \chi}{4\chi^2} + \frac{\ln \chi}{\chi^2} D_2(\eta) + \frac{1}{\chi^2} D_3(\eta) + \ldots \tag{3.18d}$$

At this point the character of the inner solution and its relationship to the outer solution are clear. Stewartson and Hall (1963) proceed to cast the boundary conditions (3.13) in terms of the series representation (3.18) and to express the governing equations (3.12) for the inner flow in terms of the inner variables. The resultant system of equations is algebraically complex, but upon equating terms of like order of

magnitude, coupled systems of ordinary differential equations may be set down and solved in descending order. Initiation of computation is expedited by the governing equation for B_0. The solution for B_0 satifying all boundary conditions can be expressed analytically in terms of a confluent hypergeometric function. In addition, Stewartson and Hall (1963) cleverly disect the functions of equations (3.18) into subsidiary functions which are either universal functions of η or functions of the edge boundary condition term α_e. Evaluation of the outer limit for the universal η functions is performed numerically and the (universal) α_e functions are then established once and for all. In practice, this allows the inner equations to be uniformly integrated in the proper order from the centerline to the edge without iteration. Additional details may be found in Appendix C.

For the present application these equations are integrated with a fourth order Runge-Kutta scheme; some typical results are presented in figure 3.2. Here the asymptotic nature of the solution is evident as well as the consequences of the outer expansion of the swirl velocity, equation (3.15c). Unfortunately this approximation renders the convergence of the entire formulation to be algebraic as opposed to asymptotic, and additional terms in the outer expansion as well as their counterparts for the inner expansion would have to be included for increased accuracy.

Because the inner solution is asymptotic the choice of the "edge" has no appreciable effect on the resultant solutions so long as condition (3.16) is met and the outer and inner solutions agree at the

"edge." A comparison of solutions demonstrating the effects of the edge location is presented in figure 3.3. For this comparison, the values of the $t_e = 0.10$ solution at $t/t_e = 0.05$ are imposed as boundary conditions for the $t_e = 0.05$ solution and the results are presented as normalized by the edge quantities of the $t_e = 0.10$ solution. Small differences arise chiefly due to the outer swirl expansion and the definition of χ. Matching is part of the solution.

The edge helix angle and the Reynolds number have strong effects on the vortex core solution properties. As shown in figure 3.4, an increase in edge helix angle, ϕ_e, greatly increased the magnitudes of the velocity components as well as the magnitude of the static pressure. An increase in Reynolds number decreases the extent of the viscous subcore, much as would be expected (figure 3.5). Reynolds number has little effect on the radial flow. However, increases in Reynolds number results in increases in the magnitudes of the other velocity components as well as the magnitude of the static pressure near the axis. Because the radial extent of the inner vortex representation (not the viscous subcore) is given by the outer vortex representation (section 6), a minimum Reynolds number for which the theory is applicable may be derived. This limitation is consistent with the assumptions of the outer vortex formulation, namely that the flow is inviscid and that free vorticity can be represented by infinitely thin free vortex sheets.

4.0 NONCONICAL INNER FORMULATION

4.1 Governing Equations

As in the case of the viscous subcore, the flow is considered to be steady, incompressible, axisymmetric, viscous, and laminar, equations (3.8). A boundary-layer like stretching is introduced such that

$$R = \frac{Rn^{1/2}}{f} r \tag{4.1a}$$

$$U = \frac{Rn^{1/2}}{f} u \tag{4.1b}$$

$$1 \leq f << Rn^{1/2} \tag{4.1c}$$

and R and U are presumed to be of unit order of magnitude. The governing equations (3.8) then become

$$\frac{1}{R}(RU)_{,R} + w_{,z} = 0 \tag{4.2a}$$

$$\frac{f^2}{Rn}(UU_{,R} + wU_{,z}) - \frac{v^2}{R} = -p_{,R}$$

$$+ \frac{1}{Rn}\left(U_{,RR} + \frac{1}{R}U_{,R} - \frac{U}{R^2} + \frac{f^2}{Rn}U_{,zz}\right) \tag{4.2b}$$

$$U(Rv)_{,R} + w(Rv)_{,z} = \frac{1}{f^2}\left[(Rv)_{,RR} - \frac{1}{R}(Rv)_{,R} + \frac{f^2}{Rn}(Rv)_{,zz}\right] \tag{4.2c}$$

$$Uw_{,R} + ww_{,z} = -p_{,z} + \frac{1}{f^2}\left(w_{,RR} + \frac{1}{R} w_{,R} + \frac{f^2}{Rn} w_{,zz}\right) \qquad (4.2d)$$

In the high Reynolds number limit with the constraint of equation (4.1c) these equations collapse to the quasicylindrical formulation of Hall (1967):

$$\frac{1}{R}(RU)_{,R} + w_{,z} = 0 \qquad (4.3a)$$

$$\frac{v^2}{R} = p_{,R} \qquad (4.3b)$$

$$U(Rv)_{,R} + w(Rv)_{,z} = (Rv)_{,RR} - \frac{1}{R}(Rv)_{,R} \qquad (4.3c)$$

$$Uw_{,R} + ww_{,z} = -p_{,z} + w_{,RR} + \frac{1}{R} w_{,R} \qquad (4.3d)$$

In practice the quasicylindrical scaling ($f = 1$) can result in values of R and U greater than unit order of magnitude, and the scale factor f is useful in analyzing the consequences of these effects with equations (4.2). As long as scaling is appropriate (equation (4.1c)), it is observed that corewise diffusion effects are uniformly negligible among the viscous terms. The remaining viscous terms in the swirl and axial momentum equations become less significant for $f > 1$ (much as would be expected); this effect is included in equations (4.3c) and (4.3d). The radial momentum equation viscous effects are wholly negligible, while the bracketed inertia terms are negligible in terms of equations (4.1c). However, these are the

"largest" terms of those excluded in the quasicylindrical approximation, and their chief effect is to lessen the magnitude of the radial pressure gradient. Nonetheless, the quasicylindrical equations (4.3) are reasonable for high Reynolds number flows and are used for this study. It should be noted that the quasicylindrical equations which were derived with a simple boundary layer stretching notion are identical to the initial plane inner equations (3.12) which were derived more formally from a boundary layer limit viewpoint. Consequently, the equations used to advance the solution in space are consistent with the equations used to generate the initial plane solution.

Following Hall (1967) the equations (4.3) are cast in terms of more convenient variables

$$\xi = \frac{R}{\lambda} \tag{4.4a}$$

$$H = \frac{U}{\lambda} \tag{4.4b}$$

$$K = \lambda \xi v \tag{4.4c}$$

$$\lambda = \frac{R_e(z_m)}{R_e(z_1)} \tag{4.4d}$$

to yield

$$(\xi H)_{,\xi} = -\xi w_{,z} + \xi^2 \frac{\lambda'}{\lambda} w_{,\xi} \tag{4.5a}$$

$$p_{,\xi} = \frac{K^2}{\lambda^2 \xi^3} \tag{4.5b}$$

$$wK_{,z} - \frac{1}{\lambda^2} K_{,\xi\xi} + \left(H - \frac{\lambda'}{\lambda} \xi w + \frac{1}{\lambda^2 \xi}\right) K_{,\xi} = 0 \qquad (4.5c)$$

$$ww_{,z} - \frac{1}{\lambda^2} w_{,\xi\xi} + \left(H - \frac{\lambda'}{\lambda} \xi w - \frac{1}{\lambda^2 \xi}\right) w_{,\xi} = \frac{\lambda'}{\lambda^3} \frac{K^2}{\xi^2} - p_{,z} \qquad (4.5d)$$

with

$$\lambda' = \frac{d\lambda}{dz} \qquad (4.5e)$$

In equation (4.4d) lambda is defined as the ratio of the edge radius at any longitudinal station, z_m, to the edge radius at the initial plane, z_1.

The equations (4.3) or equivalently (4.5) are parabolic in the axial direction and therefore can be marched downstream so long as appropriate initial and boundary conditions are provided. Although the complete flow field in the initial plane is available (section 3) for the wing case, only the bounding radius as well as the radial distributions of the circulation parameter, K, and the axial flow, w, are required to initiate the marching procedure. The boundary conditions for the present problem are

$$\{u = k = w_{,\xi} = 0; \quad \xi = 0, \; z > z_1\} \qquad (4.6a)$$

$$\{k = k_e, \quad w = w_e, \quad p = p_e; \quad \xi = \xi_e, \; z > z_1\} \qquad (4.6b)$$

$$\lambda(z) \text{ given.} \qquad (4.6c)$$

Other edge boundary conditions may be constructed for stream surfaces, solid surfaces, or alternate choices of known and unknown edge parameters as discussed by Hall (1967). These alternate conditions will only be addressed for appropriate validation cases presented later in this section.

4.2 Numerical Solution Technique

The solution is advanced in space by replacing the differential equations (4.5) with an implicit set of difference equations for each computational sub-domain

$$\{(\xi,z)\,|\,0 \leq \xi \leq \xi_e,\ z_m \leq z \leq z_{m+1}\}$$

Second order accurate central differences are used for a grid with variable Δz_m and a simple stretched radial spacing

$$\tau = \frac{\Delta\xi_n}{\Delta\xi_{n-1}} \tag{4.7}$$

where τ is a constant greater than or equal to 1. This permits improved radial resolution near the core centerline. Nonlinearities are treated with full Newton linearization. The continuity, radial, angular, and axial momentum equations are written about points (m + 1/2, n - 1/2), (m + 1, n + 1/2), (m + 1/2, n), and (m + 1/2, n), respectively. Two solution techniques were investigated, the iterative decoupled formulation of Hall (1967) and an iterative coupled formulation based on the Davis modified tridiagonal algorithm as reported by Blottner (1979). For the coupled formulation, iteration was required

because of the boundary conditions for the continuity and radial momentum equations; the continuity, angular momentum, and axial momentum equations were coupled while the radial momentum equation was lagged. The decoupled formulation was found to converge rather quickly (seven iterations, on average) and as such the usual advantages of a coupled formulation were offset by the increased level of work per iteration. In addition, the run time for a typical core computation is small (≈ 3 seconds on CY175) particularly with regard to the outer flow calculation. Therefore, the decoupled formulation was used to advance the solution.

Convergence was judged by computing normalized L_2 residuals across the entire core for the four computational plane dependent variables, H, p, K, and w. The solution at each corewise station m was considered converged when all four residuals were of order of magnitude 10^{-4} or less. Additional details may be found in Appendix D.

4.3 Isolated Core Computations

Computations were performed for several isolated core cases. The purpose of the computations is to validate the present formulation with comparisons to published numerical results and exact solutions as well as to highlight general features of the computed flow.

The first case considered was published by Hall (1967) and is appropriate to a trailing vortex. The initial conditions at $z_1 = 0.25$ are

$$K = \frac{1}{2}\left(1 - e^{-\xi^2}\right) \tag{4.8a}$$

$$w = 1 - \frac{1}{4} e^{-\xi^2} \tag{4.8b}$$

The boundary conditions at $\xi_e = 6$ are

$$K = \frac{1}{2} \tag{4.9a}$$

$$w = 1 \tag{4.9b}$$

$$p = \text{const} \tag{4.9c}$$

$$\lambda = 1 \tag{4.9d}$$

The results (figure 4.1) are identical to Hall's (1967) and illustrate a diffusion dominated vortex flow with an axial velocity deficit. A similar result is shown in figure 4.2 for the same initial and boundary conditions but with an initial axial flow excess at $z = 0.25$:

$$w = 1 + \frac{1}{4} e^{-\xi^2} \tag{4.10}$$

For these solutions, the longitudinal decrease in the axial velocity excess (figure 4.2b) exceeded in magnitude the longitudinal increase in the axial velocity deficit (figure 4.1b).

The second case considered, also published by Hall (1967) is appropriate to a generic leading edge vortex. Initial conditions are derived from the tabulated solutions of Stewartson and Hall (1963) which

neglect some of the higher order terms. The edge conditions for $z_1 = 50$ are:

$$v_e = 210 \tag{4.11a}$$

$$w_e = 392 \tag{4.11b}$$

$$\xi_e = 9.6295 \tag{4.11c}$$

The boundary conditions are of two types. The first portion models a conical "edge" with constant velocity and pressure and, hence, increasing circulation:

$50 \leq z \leq 100$

$$v_e = 210 \tag{4.12a}$$

$$w_e = 392 \tag{4.12b}$$

$$p_e = \text{const} \tag{4.12c}$$

$$\lambda(z) = \frac{z}{50} \tag{4.12d}$$

The second portion models a stream surface of unspecified shape but with a specified pressure distribution, taken in this case to illustrate the effects of an adverse pressure gradient. The stream surface will have fixed circulation and negligible diffusion across it. These conditions necessitate a different treatment at the edge of the core:

$100 < z < 140$

$$K_e(z) = K_e(100) \tag{4.13a}$$

$$p_e(z) = \text{prescribed} \tag{4.13b}$$

$$\frac{H_e}{w_e} = \xi_e \frac{\lambda'}{\lambda} \tag{4.13c}$$

$$w_e \frac{dw_e}{dz} = \frac{\lambda'}{\lambda^3} \frac{K_e^2}{\xi_e^2} - \frac{dp_e}{dz} \tag{4.13d}$$

The edge parameters w_e, H_e, and λ are unknown, and the solution process must therefore be extended to the edge itself. This is accomplished with an additional outer iteration procedure where the shape parameter λ is relaxed and the edge conditions of equations (4.13) are satisfied.

The results (figure 4.3) agree well with those obtained by Hall. For the conical zone the solution shows axial acceleration even though the edge velocities and pressure are held constant and the core is expanding. This can be attributed to the longitudually increasing edge circulation boundary condition. The radial extent of the viscous subcore does not increase appreciably for this case. For the stream tube zone the effects of the adverse pressure gradient are to decelerate the flow and expand the stream tube, much as would be expected.

The final validation case is for a vortex in a tube with breakdown. This problem was studied theoretically by Hall (1967b) for the experimental results of Kirkpatrick (1964). The test was conducted in air with a reference Mach number of approximately 0.08 corresponding to a unit Reynolds number of approximately 0.5 million per foot. The initial swirl was imparted to the flow by guide vanes and the experimental profiles of initial swirl and axial flow can be approximated by

$$v = \frac{.315}{(r/r_e)} \left[1 - e^{-24.8(r/r_e)^2}\right] \tag{4.14a}$$

$$w = .961 + .394\, e^{-69.3(r/r_e)^2} \tag{4.14b}$$

The test section of the tube included a small contraction to fix the location of breakdown, figure 4.4.

Stream tube boundary conditions are once again applied for the edge, taken as the tube radius. This time, however, the geometry of the tube is fixed and the edge quantities H_e, w_e, p_e must be solved for to satisfy conditions (4.13c) and (4.13d). Following Hall (1967) these edge boundary conditions are incorporated directly into the solution process without requiring any additional outer iteration schemes.

As in the previous cases, the results agree well with those published by Hall (1967b), figure 4.5. They demonstrate the type of breakdown predicted by the quasicylindrical formulation, a rapid deceleration of the axial flow in the vicinity of the vortex axis. As the value of the nondimensional axial velocity drops below unity, the quasicylindrical assumptions become invalid and the computation will

eventually fail. Because the equations are parabolic, the failure tends to occur downstream of the experimental location.

A final correlation is presented for the Burgers vortex, an exact solution for the axisymmetric incompressible equations for the following assumed form:

$$u = u(r) \tag{4.15a}$$

$$v = v(r) \tag{4.15b}$$

$$w = zw(r) = 2az \tag{4.15c}$$

The solution is

$$u = -ar \tag{4.16a}$$

$$v = \frac{K}{r}\left(1 - e^{-Rna/2\ r^2}\right) \tag{4.16b}$$

$$w = 2az \tag{4.16c}$$

Comparisons between the exact and numerical solutions (figure 4.6) show good correlation. This comparison stresses one of the neglected terms in the radial momentum equation, $uu_{,r}$, as well as numerical errors.

5.0 OUTER FORMULATION - FREE VORTEX SHEET

5.1 Governing Equations and Boundary Conditions

The free-vortex-sheet (FVS) theory of Johnson et al. (1980) is a fully three-dimensional, inviscid, potential flow formulation which models steady subsonic flow about wing or wing-body configurations with separation-induced leading- and/or side-edge vortex flow. It is assumed that the separation line, a viscous flow phenomenon, is known and that boundary layer effects are negligible. Adopting a potential flow approach, particularly with regard to the free vortex sheets, is a common practice which is supported by experimental studies such as Maskell (1964) or Peckham (1961) where the basic shape and strength of these vortices were demonstrated to be only weakly dependent on Reynolds number (i.e., viscous effects) for slender, sharp-edged wings. The flow is governed by the Prandtl Glauert equation

$$\beta^2 \phi_{,x_o x_o} + \phi_{,y_o y_o} + \phi_{,z_o z_o} = 0; \quad \beta^2 = 1 - M_\infty^2 \tag{5.1}$$

accounting for linear compressibility effects. Here ϕ is the perturbation velocity potential.

A higher order panel method approach is adopted to solve the problem (figure 5.1). The panels incorporate either quadratic doublet or linear source distributions. Doublet panels are used to model thin wings, wakes, and vortex networks while source panels are used to model thickness effects. Thick wings may be modeled with surface source

networks and internal mean plane doublet networks. However, most wings of interest are sufficiently thin to render the thin wing assumption a good approximation which reduces computational expenses.

The method differs from conventional higher order panel methods by virtue of the boundary conditions which must be satisfied to model the vortex flow case. The wing must satisfy the usual zero mass flux boundary condition locally ("no flow"), but with the Kutta condition imposed along network edges with either vortex separation or wake flow. The Kutta condition is implemented by matching not only doublet strength, but also the component of the vorticity along the appropriate edges. This approach, as originally proposed by Rubbert of Boeing, in conjunction with the vortex sheet updating procedure, results in all the usual flow phenomena at the wing edges associated with the Kutta condition, i.e., zero pressure jump, finite flow, smooth off-flow, etc.

Wakes must satisfy the usual zero pressure jump boundary condition locally ("no load"), but with the near wake doing so to second order accuracy in perturbation velocity quantities. (The trailing wake is formulated in the usual sense and persists far downstream.) This higher order formulation is necessary due to the large spanwise velocities induced on the wake by the primary vortices, thus rendering the linearized ΔC_p approximation invalid. A consequence of this higher order formulation is that the wake vorticity will skew laterally in the process of satisfying the no-load boundary condition and thereby influence the Kutta condition at the wing trailing edge. The near wake accounts for the effect which was approximated by the simple transverse wake of

Johnson et al. (1976). Inclusion of the near wake has been shown by Johnson et al. (1980) to significantly improve correlations between theoretical and experimental lift coefficients over a range of delta wing aspect ratios.

The free vortex sheet must have no local flow through it and simultaneously support no local pressure jump across it. This duality in boundary conditions is balanced by the fact that both the geometry of the free sheet as well as its singularity strength are unknown. However, by virtue of these boundary conditions the resultant integral solution equation is nonlinear. Solution of the subject vortex flow via the present approach results, therefore, in a boundary value problem for which both the location and strength of a portion of the boundary, the vortex sheets, is part of the solution.

As in conical flow (Smith, 1966), the fed vortex sheet represents an approximation to the inner wrappings of the free vortex sheet and serves the purpose of terminating free sheet rollup as well as condensing free sheet vorticity into the vortex core. The fed sheet's strength is dictated by the free sheet, while its size and position are determined by imposing a boundary condition "consistent with those that would be applicable to an infinitely rolled-up vortex sheet as well, namely, that the total force normal to the core be zero" (Johnson, 1980) at each chord station. Such an approach is analogous to the conical flow formulation. In practice, free sheet rollup is terminated at approximately one half of a revolution, near the crest of the vortex. Sensitivity studies for both conical flow and the FVS theory have demonstrated the

wing pressures to be reasonably converged at this value of free sheet rollup; additional quantities of free sheet rollup do not change the solution appreciably.

Because of the nonlinearity associated with the vortex sheets, an iterative solution procedure must be employed. The basic approach is to initiate singularity values for a fixed, initial geometry by satisfying some but not all of the boundary conditions. The full problem is then usually solved by a quasi-Newton scheme with controlled step size. Results are considered to be converged when the sum of the squares of the residuals is less than 10^{-6}.

5.2 Inviscid Computations

A correlation with the experimental pressure distributions from Luckring, et al. (1982) is reproduced in figure 5.2. Also shown are conical vortex flow as well as attached flow estimates. Differences between the thoeretical and experimental primary vortex suction peak are primarily due to secondary separation effects in the experiment. Although the data are for turbulent secondary separation, the secondary vortex effects are not small as is evident in the experimental results for the outer 20 to 25 percent of the local semispan. Diminishing this effect experimentally or adding a representation of the secondary separation to the theory would improve the correlation. Even without this effect, the correlation is reasonable and substantially better than that given by conical vortex flow or attached flow theories. In addition, correlation between theoretical and experimental vortex

trajectories is quite good, as shown in figure 5.3, also from Luckring, et al. (1982).

A correlation with the experimental force/moment properties of Hummel, et al. (1972) is presented in figure 5.4 for an aspect ratio one delta wing. This sharp-edged wing was beveled asymmetrically with the upper surface being flat. The mean plane camber surface effectively has a trailing edge flap deflected upward six degrees and the correlation between theory and experiment, including this effect, is quite good.

The free-vortex-sheet theory generally gives good estimates of inviscid surface pressure distributions as well as integral properties. The formulation has been validated for a fairly broad class of generic configurations; these include the geometric effects of leading- and trailing-edge sweep, leading- and trailing-edge camber, and edge cropping, as well as the flow effects of angle of attack, angle of sideslip, and freestream Mach number (linear compressibility). Applications of this theory have been addressed by Luckring, et al. (1982) as well as by Lamar and Campbell (1983), Lamar and Luckring (1979), and, most recently, Polhamus (1983). The theory was selected to model the outer flow because of the range of documented applications for which reasonable pressure estimates have been achieved prior to vortex breakdown.

6.0 MATCHING - INNER TO OUTER SOLUTION

The inner flow representation of the vortex core requires "edge" values of axial flow, circulation, and pressure as well as the region of the edge itself. In the overlap region to be sought between the inner and outer theories, both represent inviscid vortices, the former modeling axisymmetric, continuously distributed vorticity and the latter modeling nonaxisymmetric, concentrated vorticity. Matching requires that the two formulations accurately model the flow through this overlap zone to a consistent order. For conventional boundary layer flows (two-dimensional, axisymmetric) the matching process along with the requisite viscous-inviscid interaction has been developed to a fairly mature science. However, application of these concepts to the current problem is not straightforward; matching must be accomplished in space, away from any wing surfaces and the differences between the inner and outer formulations must be reconciled.

6.1 Nonaxisymmetric Effects

Mangler and Weber (1966) studied the steady incompressible flow near the center of a rolled up vortex sheet. They considered a conical flow with sheets of concentrated vorticity embedded in an otherwise potential flow, which is incompressible. The usual boundary conditions are to be satisfied; the sheet must be a stream surface and sustain no pressure jump across it. These require the flow to be locally aligned with the sheet and, with the additional constraint of constant total pressure, that the magnitude of the velocity vector be the same across

the sheet. The direction of the velocity vectors across the sheet will differ.

The problem is cast in spherical coordinates by first defining a dual stream function to integrate the continuity equation and satisfy implicitly the stream surface boundary condition. Next a conical potential function is defined and by equating potential and stream function representations of the velocity components three coupled first order partial differential equations are derived. After transforming coordinates and introducing new independent variables an alternate system of equations is derived which readily allows the pressure jump boundary condition to be implemented exactly; there is no small perturbation assumption. The resultant system of equations is solved in an asymptotic sense, valid for a slender core.

The resultant velocity field expressed in cylindrical coordinates is

$$\frac{u}{w_e} = \frac{-\alpha_e}{2} t - \frac{t^2}{\alpha_e}\left[\alpha_e + 1 - \alpha_e \ln\left(\frac{t}{t_e}\right)\right]\left[\phi_e^2 - \alpha_e^2 \ln\left(\frac{t}{t_e}\right)\right]^{1/2}\left[\theta_s(t) - \theta - \pi\right] + \ldots \tag{6.1a}$$

$$\frac{v}{w_e} = \left[\phi_e^2 - \alpha_e^2 \ln\left(\frac{t}{t_e}\right)\right]^{1/2} + t\left[1 - \alpha_e \ln\left(\frac{t}{t_e}\right)\right]\left[\theta_s(t) - \theta - \pi\right] + \ldots \tag{6.1b}$$

$$\frac{w}{w_e} = 1 - \alpha_e \ln\left(\frac{t}{t_e}\right)$$

$$- t\left[\phi_e^2 - \alpha_e^2 \ln\left(\frac{t}{t_e}\right)\right][\theta_s(t) - \theta - \pi] + \ldots \qquad (6.1c)$$

where θ_s is the sheet geometry given by

$$\frac{d\theta_s(t)}{dt} = \frac{-\alpha_e}{t^2\left[\phi_e^2 - \alpha_e^2 \ln\left(\frac{t}{t_e}\right)\right]^{1/2}} + O[\ln(t)] \qquad (6.1d)$$

and

$$\theta_s(t) - 2\pi \leq \theta \leq \theta_s(t) \qquad (6.1e)$$

The most noteworthy result of the Mangler and Weber solution is that "the leading terms of the velocity components for a potential flow with the vorticity concentrated along a vortex sheet are the same as for an axisymmetric flow with distributed vorticity" as given by Hall (1961) and used herein. In addition, these lead terms of the asymptotic expansion are continuous across the vortex sheet, and the pressure is determined from the Bernoulli equation. To be consistent with the axisymmetric vortex core formulation these (higher order) nonaxisymmetric effects are neglected in the present formulation and an appropriate set of axisymmetric conditions are determined from the outer free vortex sheet formulation. The Mangler and Weber solution serves in the capacity of an intermediate theory to the matching process of the inner and outer formulations.

6.2 Matching Criteria

For conventional free vortex sheet computations the vortex sheet is explicitly modeled through approximately $\pi/2$ radians of rollup from the horizontal, roughly to the crest of the vortex, and terminated with a construction commonly referred to as the fed vortex sheet. The fed sheet approximates the far field effects of the inner wrappings of the free sheet and the amount of rollup explicitly modeled has been shown by Johnson et al. (1980) to be sufficient for converging solution properties such as wing pressures and vortex geometry much as was the case for conical flows (Smith, 1966). A typical result taken from Johnson et al. (1980) is reproduced as figure 6.1. It must be recognized that the flow properties due to the fed sheet are valid only in its far field; flow details in the immediate vicinity of the fed sheet may be physically fictitious though mathematically correct.

The matching between the outer free vortex sheet formulation and the intermediate vortex core formulation of Hall is determined numerically in an asymptotic spirit; the outer limit of the inner flow and the inner limit of the outer flow are studied with the intent of determining an overlap zone for which both models describe the flow accurately and to a consistent order. Results are presented for the conical initial plane formulation at a longitudinal station slightly aft of the apex. The conditions chosen for this study are a 70° delta wing at 20° angle of attack and a freestream Mach number of zero.

The inner vortex properties of the outer free vortex sheet formulation are determined by systematically increasing the amount of sheet

rollup modeled beyond the conventional amount. Solutions were obtained in increments of additional rollup of $\pi/2$ radians up to a total rollup of 3π radians beyond the datum amount. Typical vortex geometries are shown in figure 6.2 for several rollup values. The vortex sheet is oblate and its geometry was relatively independent of the amount of rollup modeled. The oblateness of the vortex is one manifestation of nonaxisymmetric effects. With increased rollup, the radial distance from the vortex core to the free sheet decreases and, thus, the solutions modeling various extents of modeled free-sheet rollup can be used to probe the inner properties of the inviscid vortex at discrete intervals. The vortex core properties are determined in a coordinate system which locally follows the converged vortex core trajectory as given by the free vortex sheet. (See figure 1.1.) The radial extent of the vortex is taken as the distance perpendicular to the core trajectory from the core to the free sheet terminus; it is measured in the fed sheet plane.

Flow field studies were conducted for the various rollup solutions between the free sheet and the core. It was found that, away from the immediate vicinity of the free vortex sheet, the circulation was constant both in the radial and angular direction and that, as would be expected,

$$k = \frac{\mu_c}{2\pi} \tag{6.2}$$

where μ_c is the doublet strength of the vortex core. The axial flow

was found to be constant radially and to vary linearly in the angular direction, consistent to the feeding nature of the fed sheet.

The nonaxisymmetric effects are eliminated from the free vortex sheet solutions by taking an angular average at a fixed radial extent within the free sheet; e.g.,

$$w_{av} = \frac{1}{2\pi} \int_{\theta_s - 2\pi}^{\theta_s} w d\theta \tag{6.3}$$

as suggested by the form of the nonaxisymmetric terms in the Mangler and Weber solution. These properties reflect an inner limit of the outer formulation for a given angular extent, and equations (6.2) and (6.3) are therefore appropriate for providing boundary condition quantities for the vortex core model. These boundary conditions may be interpreted as maintaining the same axial mass flow and circulation (as well as circulation gradient) for the axisymmetric and nonaxisymmetric flows.

A comparison of vortex trajectories for the free-vortex-sheet solutions with two rollup values and the Mangler and Weber solution based on boundary condition quantities extracted from the base line free-vortex-sheet calculation ($\Delta\theta=0$) is also shown in figure 6.2. The correlation is reasonable except for the portion of the sheet given by $\pi<\Delta\theta<2\pi$. Radial correlations between the free vortex sheet and Hall inviscid solutions are presented in figure 6.3 for the axial and swirl velocities as well as the longitudinal circulation gradient. The base or "edge" solution is taken as the free vortex sheet solution with

either the standard amount of rollup (solid line) or an additional amount of rollup of $\pi/2$ (dashed line). The correlation is quite good among the points in the fed sheet plane, but not as good among the points $\pi/2$ out of phase. The difference between these two sets of results is viewed in part as a remaining nonaxisymmetric effect most probably due to the oblate nature of the free vortex sheet. Additional studies using the solutions with π and $3\pi/2$ of additional rollup as the "edge" showed the correlation in the base fed sheet plane to be equally good while the correlation in the plane π out of phase was still not as good. The character of these solutions together with the results of Mangler and Weber suggest that an asymptotic approach could account for these nonaxisymmetric effects. Because the calculations in the plane of the fed sheet with no additional rollup correlated best with the inner formulation, they were chosen to provide the appropriate boundary conditions. It is to be emphasized that within this plane the overlap is independent of the amount of rollup modeled.

Consistent to the theoretical studies of Hall and Mangler and Weber, the free vortex sheet boundary conditions result in a pressure field which is continuous across the vortex sheet and given by the Bernoulli equation; there are no total losses. Specification of the velocity field therefore implies the pressure field and the requisite boundary conditions for the vortex core from the free vortex sheet are complete.

It must be emphasized that the particular boundary conditions chosen for this initial formulation are not the only ones available.

Additional studies should yeild improved correlations as implied by the excellent correlation achieved by Küchemann and Weber (1965) by fitting the Mangler and Weber solution to an experimentally determined trajectory. The correlation was not limited to the inner wrappings but extended well into the outer portion of the vortex. A more rigorous treatment of the subject boundary conditions could also entail quantification of nonaxisymmetric effects, a candidate topic for future studies.

With the exception of radial flow, the solutions are fully matched. As in boundary layer analysis, the edge value of radial flow may not be specified but must be accommodated through an appropriate viscous/inviscid interaction scheme. Various schemes have been studied to adjust the overall flow in such a fashion as to fully match the inner and outer representations. Lighthill (1958) studied several approaches to account for the viscous zone effects on the outer flow and a fairly recent review of viscous-inviscid interaction may be found in AGARD CP-291 (1981), in particular, in the papers by Melnik (1981) and Lock (1981). For the present formulation these effects are not addressed. Consistent to the assumed vortex core model, the radial flow is small and, for most cases, will have a correspondingly small effect on the overall solution. Calculations by Hoeijmakers et al. (1979) showed that the additional entrainment increments as modeled by free line source/sinks along the vortex core have a small effect on the free vortex sheet geometry while affecting the vortex strength to a larger extent. Radial flow effects will become increasingly important as the axial flow gradients become large, such as in the vicinity of a burst as

modeled by the Hall theory. Here the radial flow effects, properly accounted for, would cause the vortex to flair and the longitudinal pressure gradients to increase as suggested by Bossel (1968) thus promoting the upstream propagation of the burst point. Inclusion of radial flow matching by an appropriate viscous-inviscid interaction scheme is left as a candidate topic for future studies.

6.3 Nonconical Effects

Matching the initial-plane formulation to the inner solution requires detailed consideration of the nonconical aspects of three-dimensional subsonic flows near the apex of a slender wing. Conical flow theories such as those due to Jones (1946) for attached flow or Smith (1966) for leading-edge vortex flow are often used subsonically as a qualitative datum to judge three-dimensional effects, most commonly the trailing-edge flow effects affiliated with the Kutta condition. However, the subsonic flow near the apex of a delta wing is also fundamentally nonconical. Sketches highlighting this nonconical nature of the flow are presented in figure 6.4 for attached flow on a delta wing. The sketches illustrate trends in pressure coefficinet and are indicative of other flow properties as well. From symmetry considerations the isobars down the wing center line are normal to it and, as indicated by Thwaites (1960) among others, this condition results in large isobar curvature near the apex region. As a consequence, wing properties take on a singular form along a ray in this region.

The nature of this singularity has been studied for the semi-infinite delta wing by Germain (1955) who showed that the linearized apex flow is dominated by eigensolutions of the form

$$\Phi = s^{1+\varepsilon}\, \phi(\psi,\theta) \;;\; -1<\varepsilon<0 \tag{6.4}$$

where ϕ is a perturbation velocity potential, s is the distance from the apex, and ε is a measure of the singularity strength. Values of ε have been determined numerically by Rossiter (1970) who also reports several series expansion solutions valid for leading-edge sweep angles near zero or 90 degrees; ε is generally small for conventional delta wing sweep values. The apex singularity is weak and similar in form to two-dimensional wedge flow (see Van Dyke (1964)).

The nonconical nature of this solution is manifested as a uniformly scaled flow. For example in spherical coordinates the velocity components

$$v_s = \Phi_{,s} \tag{6.5a}$$

$$v_\psi = \frac{1}{s}\Phi_{,\psi} \tag{6.5b}$$

$$v_\theta = \frac{1}{s \sin\psi}\Phi_{,\theta} \tag{6.5c}$$

take on the form

$$v_s = (1 + \varepsilon)\, s^{\varepsilon}\phi(\psi,\theta) \tag{6.6a}$$

$$v_\psi = s^\varepsilon \phi_{,\psi} \tag{6.6b}$$

$$v_\theta = \frac{1}{\sin \psi} s^\varepsilon \phi_{,\theta} \tag{6.6c}$$

For $\varepsilon = 0$ the conical form is recovered. However, even for $\varepsilon \neq 0$ ratios of velocities have no s dependence.

Flows in the general class of equation (6.4) are weakly singular along a ray and take on the form

$$s^\varepsilon = 1 + \varepsilon \ln s + \frac{\varepsilon^2}{2} \ln^2 s + \ldots \tag{6.7}$$

This term contributes the major nonconical effect. Consider, for example the flow with continuously distributed vorticity governed by equations (3.2). If the velocities take on the form

$$\vec{Q}(s,t) = s^\varepsilon \vec{Q}(t) \tag{6.8}$$

the subject governing equations (3.2) take on the form

$$-t \frac{d}{dt}\left(w - \frac{u}{t}\right) + \frac{2u}{t} = \frac{-\varepsilon}{1 + t^2}(w + tu) \tag{6.9a}$$

$$-t \left(w - \frac{u}{t}\right) \frac{du}{dt} - \frac{v^2}{t} + \frac{dp}{dt} = \frac{-\varepsilon}{1 + t^2}[(w + tu)\, u + 2tp] \tag{6.9b}$$

$$-t \left(w - \frac{u}{t}\right) \frac{dv}{dt} + \frac{uv}{t} = \frac{-\varepsilon}{1 + t^2}[(w + tu)\, v] \tag{6.9c}$$

$$-t \left(w - \frac{u}{t}\right) \frac{dw}{dt} - t \frac{dp}{dt} = \frac{-\varepsilon}{1 + t^2}[(w + tu)\, w + 2p] \tag{6.9d}$$

These equations exhibit no s dependence but differ from the conical equations (3.3) by virtue of the right-hand side being of $O(\varepsilon)$ as opposed to being equal to zero. Equation (6.9) along with equation (6.7) suggest an asymptotic solution with the lead solution given by Hall, equations (3.5). A similar result can be demonstrated for the conical solution of Mangler and Weber. Closed form solutions to this class of flow and not pursued in this report.

For the present problem, the free-vortex-sheet theory removes the strong leading-edge singularity with the leading-edge Kutta condition. However, the weak apex singularity remains and its form, as determined from numerical experimentation, is similar to the attached flow case. Representative velocity boundary condition values are presented in figure 6.5. Because of the particular form of the apex singularity, matching the three-dimensional outer flow to the conical flow initial plane solution can be accomplished in terms of locally scaled variables. An example is presented in figure 6.6. Shown on the left portion of this figure are radial distributions of inviscid axial flow in the vortex core at three-chordwise stations near the apex of a 70° delta wing at 20 degrees angle of attack. These were obtained by matching the intermediate solution to the free vortex sheet boundary conditions as previously described. Shown on the right portion of the figure are the same results, each scaled by the value of the edge axial flow for the three longitudinal stations. In this locally scaled plane there is virtually no dependence on longitudinal position and the conical initial plane solution can be implemented without constraint.

Numerical studies have verified the solutions to be virtually independent of the initial plane location.

6.4 Downstream Continuation of Boundary Conditions

As described in section 5, the near wake is modeled 2 1/2 to 3 vortex diameters at the trailing edge downstream. By this point the vortex is essentially fully fed and the corewise gradients of circulation and axial flow boundary conditions are nearly zero:

$$K_{e,s} \approx w_{e,s} \approx 0 \tag{6.10}$$

Continuation of the free vortex sheet modeling much beyond this distance can result in convergence difficulties because the strength of the sheet is becoming very small and (unmodeled) trailing edge wake rollup effects are becoming more significant. However, as described by Hall (1967b) the bursting phenomena represented by this vortex core model can occur several vortex diameters downstream of the experimental location due to the parabolic nature of the governing equations; in an analogous fashion simple boundary layer methods can separate several boundary layer thicknesses downstream of the correct location. Consequently, it is desirable to continue the vortex core calculation downstream of the modeled near wake extent. Free vortex sheet quantities in this zone are inadequate for these purposes because the modeling is that of potential flow trailing wakes and valid only in a far field sense.

Boundary condition quantities for this zone were obtained from the free vortex sheet by means of analytic continuation. By virtue of the

diminished free sheet strength in the aft portion of the near wake, the radial gradients of the circulation and axial flow near the edge of the vortex core are also virtually zero. In this portion of the vortex core the flow has become that of a potential vortex, and the radial extent or "edge" of the core no longer affects the calculation. The boundary condition quantities K_e, w_e, and R_e are extended downstream by first establishing their values and nominal corewise gradients several stations upstream from the trailing wake to minimize any near field errors affiliated with the trailing wake itself. Using the vortex core diameter at this location, the quantities are then extended several diameters downstream by maintaining continuity of corewise derivatives and stipulating that these derivatives go to zero. From this location the calculation are continued downstream by maintaining the zero gradient condition. The edge pressure always follows from the Bernoulli equation. Numerical studies demonstrated that the extent over which the analytic continuation was employed had no appreciable effect on the computed core properties.

7.0 RESULTS AND DISCUSSION

Calculations for the composite formulation have been performed for delta wings ranging in leading-edge sweep angle from 55 degrees to 85 degrees over an angle-of-attack range from 5 degrees to 50 degrees. Select arrow and diamond wings have also been analyzed. All composite calculations have been performed for incompressible conditions at Reynolds numbers on the order of one million based on the wing root chord. Some results highlighting the character of the composite solutions are presented below.

7.1 General Flow Features

The core flow properties of a 75-degree delta wing at 15 degrees angle of attack are presented in figure 7.1 as a function of radial distance from the core axis normalized by the local edge radius for various longitudinal stations. The radial velocity (figure 7.1a) distributions remain essentially linear and decrease in magnitude down the core. In figure 7.1b, the circulation parameter radially increases at all stations throughout the core. Near the axis, the quadratic region, indicative of solid-body rotation, is very small. At the edge, the inner solution matches to the outer solution without necessarily achieving zero slope radially; a potential-like vortex flow begins to be evidenced towards the edge of the most downstream station shown. As part of the solution, this inviscid flow transitions from the highly rotational leading-edge vortex structure to the irrotational wake-like

vortex structure; this transition comes about as the feeding of the vortex core from the free vortex sheet goes to zero.

These effects are also manifested in the angular velocity (figure 7.1c) as well as the axial velocity (figure 7.1d). Near the edge of the most downstream station shown, the angular velocity begins to evidence a potential (1/r) form while the axial flow is becoming constant. Although the edge flow is decelerating, the angular and axial velocity components near the axis show a longitudinal acceleration over the forward portion of the wing followed by a deceleration over the aft section of the wing as well as the wake. In addition, the normalized radial extent of the viscous subcore decreases downstream (Fig. 7.1c).

Consistent with the velocity profiles, the static pressure coefficient (figure 7.1e) shows an adverse longitudinal pressure gradient at a fixed fraction of core radius away from the axis. Both proverse and adverse longitudinal pressure gradients are evidenced in the vicinity of the axis. The total pressure coefficient distributions (figure 7.1f) emphasize the confinement of total losses to the viscous subcore by this theoretical method. It should be noted, though, that the magnitude of the total losses for this flow are less than the total losses associated with simple boundary-layer flow because of the flow acceleration which occurs in the viscous region of the vortex core. The erroneous overshoot in the initial plane of the total pressure coefficient is seen to quickly damp out.

These same results are presented in figure 7.2 for an unscaled abscissa. The positive radial flow, figure 7.1a, occurs at the

trailing-edge station as a consequence of comparatively large longitudinal retardation of the axial flow in this region. For this flow, the stream tubes will exhibit a bulge in the vicinity of the trailing edge. In figure 7.2b the circulation distributions are seen to roughly overlay one another; the circulation for an inner portion of the core is chiefly established by conditions upstream in these solutions. Related to this effect, the radial extent of the viscous subcore (figure 7.2c), though increasing, changes very little for the range of computations shown. At the downstream stations, the angular and axial velocity components, as well as static and total pressure coefficients, show little dependence on axial distance for the outer portion of the core. However, the entire core flow over the forward three-quarters of the wing is highly three dimensional as is the inner portion of the core flow over the entire computed range.

Longitudinal variations for select flow parameters are presented in figure 7.3. The nonconical and, in general, three-dimensional nature of the solution is evident. Even though the edge boundary condition for the axial flow is continually decelerating (figure 7.3b), the centerline value accelerates over the forward portion of the wing. This is due to the vigorous increases in circulation which the vortex experiences longitudinally in this region; the circulation and axial flow are closely coupled by the governing equations, chiefly through the pressure. Accordingly, the static pressure coefficient exhibits a proverse pressure gradient over the forward portion of the wing even though the edge condition is uniformly adverse (figure 7.3c). Losses in

total pressure accummulate down the length of the wing along the centerline and appear to be approaching an asymptote by the last station shown (figure 7.3d).

The effects of angle of attack and leading edge sweep angle are summarized in figure 7.4 and 7.5, respectively, at a longitudinal distance down the core of one half root chord, $z = 0.5$. With increasing angle of attack the vortex is strengthened and, correspondingly, velocities increase through the core while pressures become more negative. Angle of attack has a strong effect on the magnitude of the velocities, particularly near the vortex core axis. For the largest angle of attack shown, this flow is already approaching a condition where compressibility effects are no longer negligible and for angles of attack approaching those conducive to near field vortex breakdown, compressibility effects will become increasingly significant. An increase in angle of attack is also seen to increase the radial extent of the viscous subcore over which total pressure losses are manifested, (figure 7.4d).

An increase in leading edge sweep angle has the opposite effect of an increase in angle of attack; the vortex is weakened and, correspondingly, velocities decrease through the core while pressures become more positive due to this effect. The solutions of figure 7.5 show essentially the opposite trends of the solutions of figure 7.4.

7.2 Experimental Correlation

Calculations for the 75° delta wing at 15° incidence are compared to the experimental results of Earnshaw (1962) in figure 7.6. The test was conducted with an aspect-ratio-one delta wing (76° leading-edge sweep) at 14.9 degrees incidence with a freestream reference Mach number of approximately 0.09 and a Reynolds number of approximately 3 million. The measured velocity and pressure profiles through the vortex core were obtained with a five tube Conrad probe aligned to the local flow and were taken along mutually perpendicular traverses in the wind axes at 70-percent root chord. These data were also used by Hall (1960) to correlate an earlier vortex core theory. This predecessor theory was conical, and the intermediate formulation was empirically fit to the experimental results for the boundary conditions at the edge of the vortex. In addition, the viscous subcore was treated in a simpler fashion than the Stewartson and Hall theory.

Comparisons between the theoretical and experimental velocity profiles show reasonable correlations for the outer region of the vortex core and for the radial extent of the viscous subcore. The major discrepancy of this correlation is the centerline axial flow, and both theory and experiment are probable contributors to this case. Although the probe was very small compared to the local wing semispan, its diameter was still appreciable compared to the scale of the viscous subcore. Apart from perturbing the flow itself, gradients across the probe head will also affect the measurements. In addition, the relatively small probe size was achieved in part by use of a rather

large model set at high incidence relative to the test section, thereby creating possibly large wall interference effects. Theoretically, the major factors affecting the subcore flow are probably the incompressible and laminar flow assumptions. Because these flows have a local maximum in velocity at or near the vortex axis, they can be locally compressible at incompressible reference conditions. The current solution is approaching this condition, and further angle-of-attack increases will aggravate the incompressible assumption. The compressible flow would undergo less acceleration than the incompressible counterpart, an effect which has been studied by Brown (1965) for inviscid conical flows. With regard to the laminar flow assumption, the implementation of a simple eddy viscosity model or, for that matter, performing the computation at a lower Reynolds number, will result in reduced centerline axial flow due to the correspondingly increased radial diffusion effects. Hall (1960) put forth this argument as the chief reason for the similar lack of correlation between his conical theory and this data set.

The correlation between theoretical and experimental pressure coefficients (figure 7.6b) is consistent with the velocity correlations. The centerline static pressure coefficient is more negative than the experimental value chiefly because of the increased axial flow. However, static pressures of this magnitude at the core axis are not unusual for vortex core flow. At a higher angle of attack Earnshaw (1962) recorded C_p values of approximately -24; for a 65° swept wing at 15° incidence Lambourne and Bryer (1960) recorded C_p values in the vicinity of -13. The theoretical total pressure losses are confined to

the viscous subcore, whereas, experimentally, they are spread over the majority of the region shown. Further understanding of the differences between theoretical and experimental results will require correlation studies for additional configurations and flow conditions.

7.3 Vortex Breakdown Analysis

As stated in the background and review section, the variety of theories directed at vortex stability and, in particular, vortex breakdown, have yet to yield satisfactory correlations with experiment, even for the isolated vortex case. For the present analysis, two criteria of differing types are selected to evaluate the subject flow, the bounday layer analogy of Hall (1967b) and the stability theory of Ludwieg (1962). In addition, an empirical analysis of the solutions is performed in terms of the maximal helix angle tangent, ϕ_{max}, a parameter to which breakdown has been shown theoretically to be sensitive.

A common attribute of vortex breakdown is the rapid axial deceleration of the core centerline flow, which can lead to an axial stagnation point. Under these conditions, some of the assumptions leading to the quasicylindrical equations are no longer valid. As pointed out by Hall (1967b), this is in close analogy to the calculation of boundary-layer flows for conditions resulting in separation and, therefore, vortex breakdown could be related to a failure of the quasi-cylindrical approximation. Hall proceeded to quantify this observation and included a correlation to the experimental results of Kirkpatrick

(1965). The calculations were performed at 1/50th the experimental Reynolds number as a means to simulate the turbulent experiment in the laminar theory by an eddy viscosity concept. Breakdown was predicted several core diameters downstream of the experimental location consistent with the parabolic nature of the formulation. This particular criterion emphasizes flow properties in the viscous subcore of the vortex.

For the present delta wing applications, no breakdown of this type was observed. Although the axial core flow is decelerating, its magnitude at breakdown conditions, as determined by Wentz and Kohlman (1968), is still sufficient to prevent the quasicylindrical equations from failing. The computations were performed without Hall's eddy viscosity scaling because the status of the core flow (laminar or turbulent) is uncertain and because compressibility will also affect this flow by reducing the axial magnitudes.

In contrast to the boundary-layer analogy of Hall (1967b), Ludwieg's hydrodynamic stability criterion is derived from flow stability considerations, is inviscid, and tends to be manifested near the edge of vortices. An application of this criterion is shown in figure 7.7 for a 70° delta wing at 30° angle of attack. Experimentally, Wentz and Kohlman (1968) determined $\alpha_b \approx 29°$ for this wing. In this figure, contours of the stability relationship in the vortex core are presented; the roughly diagonal edge where the contours terminate corresponds to the edge of the inner computational space as given by the free-vortex-sheet theory. In the shaded region, the flow is unstable by

Ludwieg's criterion. The zone differs in character from the conical case in that it does not correspond to maximum values of helix angle. It was found for other wings and other angles of attack, but, in general, it did not move so far upstream as the trailing edge. Two aspects of the present formulation which would inhibit the forward propagation of the unstable zone are the parabolic assumption and the lack of viscous-inviscid interaction effects.

The final criterion chosen for analysis of vortex breakdown was the occurrence of a critical helix angle in conjunction with a longitudinally retarding flow, or equivalently, a longitudinal adverse pressure gradient. As put forth by Hall (1972), these two effects, along with a divergence of stream tubes in the vortex core, commonly occur in conjunction with vortex breakdown. The critical helix angle is also a consequence of simplified stability analyses, such as those due to Ludwieg (1962) or Bossel (1968), as well as more advanced flow field analyses given by Bossel (1969, 1972).

Contours of ϕ in the vortex core are presented in figure 7.8 for a 70° delta wing at an angle of attack below, essentially at, and above α_b, respectively, as determined experimentally by Wentz and Kohlman (1968). Several aspects of these solutions are noteworthy. For a given angle of attack, there are two regions of maximum ϕ. Both are at the edge of the vortex, one near the apex and the other in the vicinity of the trailing edge. The structure of the vortex in terms of this parameter changes from the wing to the wake; over the wing, the maximum ϕ occurs at the vortex edge, whereas, in the wake, this maximum occurs

well within the vortex. Finally, the maximum ϕ is seen to exceed unity as α_b is surpassed, figure 7.8b.

In terms of quantifying the condition of incipient vortex breakdown at the wing trailing edge, the longitudinal regions of maximum ϕ are considered. Longitudinal pressure gradients for this wing are qualitatively similar to those shown for the 75° delta wing (figure 7.3). Near the apex, the flow may achieve critical ϕ, but the core axis is in a favorable pressure gradient. Near the trailing edge, however, the local maxima of ϕ occur in conjunction with an adverse pressure gradient down the core axis. The combination of these effects along with the low total energy of the core down the centerline could be conducive to vortex breakdown.

The various solutions were analyzed for these conditions at the trailing edge. The flows were in general decelerating (adverse pressure gradient) and exhibited maximum ϕ at the edge of the vortex; these values are presented in figure 7.9 for several of the delta wings analyzed. For these wings, the experimentally determined value of α_b from Wentz and Kohlman (1968) is also indicated. The experimental condition of vortex breakdown at the trailing edge of the delta wings roughly correlates with a constant theoretical value of $\phi_{te,max}$. With the present formulation, this value is slightly greater than one; for reference purposes, the conical value of 1.16 is also shown in figure 7.9.

This correlation is shown in figure 7.10 for a more familiar parameter space; the theoretical results of this figure are based on

$\phi_c = 1$. In addition to the reasonable correlation with delta wing leading-edge sweep effects (which are generally strong), the correlation with trailing-edge sweep effects (which are generally weak) is also shown to be reasonable for 70° arrow and diamond wings. The significant aspect of this correlation is that the single concept of a critical helix angle in conjunction with the adverse pressure gradient provides reasonable estimates of both the strong leading edge and the weak trailing-edge effects and does so with one value of ϕ_c. The particular value of ϕ_c is less significant. It should also be noted that ϕ_c occurs in a region of the vortex core model where three-dimensional effects are strong and, in addition, where the chief theoretical concern is the matching of inner and outer representations.

In light of these results, the lack of a physically realistic burst in the computation can be attributed to neglected effects, many of which affect the subcore flow to a much greater extent than they do the rest of the core flow. Virtually all of these, when considered individually, are conducive to the occurrence of a physically realistic burst.

8.0 RECOMMENDATIONS FOR FUTURE STUDIES

Several effects currently not included in the leading-edge vortex-core formulatiom could readily be implemented. The method could be extended to account for compressibility in a straightforward fashion. This would account for the local effects near the vortex axis, reducing the magnitude of the velocities there. Implementing a simple eddy-viscosity model to approximate turbulence effects would also result in decreased velocity magnitudes in this region. Of more importance, though, would be the implementation of a viscous/inviscid interaction scheme to fully match the inner and outer flow models. This will be most important under conditions conducive to vortex breakdown where deceleration of the axial flow in the core must be accompanied by a radial expansion of the vortex. This expansion would tend to promote the upstream propagation of a burst.

Additional matching studies should yield improved correlations of the vortex sheet trajectories between the inner and outer representations of the vortex. In addition, nonaxisymmetric effects may be addressable for the parabolic formulation.

Application of the present approach to computing vortex flows is not strictly limited to the methods currently in use. For example, elliptic effects could be addressed by embedding a form of the Grabowski and Berger (1976) model of the vortex core into the free vortex sheet. In addition, other vortex flow problems such as forebody vortex effects of importance to missile aerodynamics could be addressed in a similar fashion with models appropriate to that flow.

9.0 CONCLUSIONS

The flow in the core of a three-dimensional separation-induced, leading-edge vortex can be calculated by appropriately matching inner and outer representations of the vortex. This procedure is not strictly limited to the theories implemented in the present formulation; it is applicable for other representations of the inner and outer flows as well.

The calculated results of the present formulation exhibit many of the general features of the subject flow. Some prominent aspects of these solutions can be summarized as follows:

1. At practical Reynolds numbers, the majority of the core flow is inviscid, rotational, and weakly singular in the radial direction.

2. Near the vortex axis, the flow exhibits velocity magnitudes several times the freestream reference value along with total pressure losses; these losses arise because of modeled viscous effects.

3. The solutions are highly three-dimensional and begin to evidence a transition in the near wake from the leading-edge class of vortex flow to a more wake-like vortex flow structure.

Although the experimental comparison was limited in scope, the correlation with measured vortex core properties is encouraging. However, extensions to the model may be required for more accurate estimates of the viscous subcore flow, particularly under conditions conducive to vortex breakdown.

The experimental condition of vortex breakdown at the trailing edge of delta, arrow, and diamond wings was found to correlate closely with

the theoretical criterion of a critical helix angle in conjunction with an adverse pressure gradient. The calculations also exhibited a zone of unstable flow by Ludwieg's criterion, but did not exhibit failure of the quasicylindrical approximations. The lack of an axial stagnation point or other realistic aspects of the vortex breakdown flow field is related to approximations chiefly affecting the viscous subcore. Systematic extension of the present formulation should provide additional insights to the vortex breakdown phenomena for three-dimensional flows.

10.0 APPENDICES

10.A Exact Solution for Hall's Vortex

The governing equations (3.3) are appropriate for steady, inviscid, incompressible, and conical flow. The solution procedure of Hall (1961) may be used with more complicated integrals to yield the following exact solution subject to boundary conditions (3.4):

$$\frac{u}{w_e} = \frac{-\beta_e}{2}\,\tau \tag{A.1}$$

$$\frac{v}{w_e} = \left[\phi_e^2\left(\frac{2+\delta\beta_e}{2+\delta_e\beta_e}\right) - \beta_e^2 \ln\left(\frac{\tau}{\tau_e}\right)\right]^{1/2} \tag{A.2}$$

$$\frac{w}{w_e} = 1 - \beta_e \ln\left(\frac{\tau}{\tau_e}\right) \tag{A.3}$$

$$\frac{p - p_e}{w_e^2} = \frac{\phi_e^2\beta_e}{2}\left(\frac{\delta_e - \delta}{2+\delta_e\beta_e}\right) + \frac{1}{2}\left(\frac{\tau_e\beta_e}{2}\right)^2\left[1 - \left(\frac{\tau}{\tau_e}\right)^2\right]$$

$$+ \beta_e\left(1 + \frac{1}{2}\beta_e\right)\ln\left(\frac{\tau}{\tau_e}\right) - \frac{\beta_e^2}{2}\ln^2\left(\frac{\tau}{\tau_e}\right) \tag{A.4}$$

where

$$\delta = \frac{2}{t^2}\left[(1+t^2)^{1/2} - 1\right] \tag{A.5}$$

$$\tau = \frac{2t}{1 + (1+t^2)^{1/2}} \tag{A.6}$$

$$\phi = \frac{v}{w} \tag{A.7}$$

$$\beta_e = \frac{(1 + 2\delta_e \phi_e^2)^{1/2} - 1}{\delta_e} \tag{A.8}$$

and, equivalently,

$$\tau = t\delta \tag{A.9}$$

$$\phi_e^2 = \beta_e(1 + \frac{1}{2}\,\delta_e\beta_e) \tag{A.10}$$

The relationship of this exact solution to Hall's slender core solution ($t^2 << 1$) is apparent with the following expansions:

$$\delta = \frac{2}{t^2}\,(1 + \frac{1}{2}\,t^2 - \frac{1}{8}\,t^4 + \ldots - 1) \tag{A.11}$$

$$= 1 - \frac{1}{4}\,t^2 + \ldots \tag{A.12}$$

$$\tau = t - \frac{1}{4}\,t^3 + \ldots \tag{A.13}$$

Neglecting $O(t^2)$

$$\delta \approx 1 \tag{A.14}$$

$$\tau \approx t \tag{A.15}$$

$$\beta_e \approx \alpha_e \tag{A.16}$$

and the slender core solution is recovered.

10.B Vortical Aspects of Hall's Vortex

For axisymmetric flows

$$\vec{\zeta} = \vec{\nabla} \times \vec{Q} \tag{B.1}$$

$$= (\zeta_r, \zeta_\theta, \zeta_z) \tag{B.2}$$

$$= \{[-v_{,z}], [u_{,z} - w_{,r}], [\tfrac{1}{r}(rv)_{,r}]\} \tag{B.3}$$

For the conical flow at hand the components of vorticity for the slender core solution are

$$\zeta_r = \frac{w_e \alpha_e}{r} \frac{u}{v} \tag{B.4}$$

$$= \frac{-w_e^2 \alpha_e^2}{2v} \frac{\sqrt{1 + t^2}}{s} \tag{B.5}$$

$$\zeta_\theta = \frac{-u}{r} \left(\frac{2}{t} + t\right) \tag{B.6}$$

$$= \frac{w_e \alpha_e \sqrt{1 + t^2}}{s} \left(\frac{t}{2} + \frac{1}{t}\right) \tag{B.7}$$

$$\zeta_z = \frac{1}{rv}\left(v^2 - \frac{w_e^2\alpha_e^2}{2}\right) \tag{B.8}$$

$$= \frac{\sqrt{1 + t^2}}{stv}\left(v^2 - \frac{w_e^2\alpha_e^2}{2}\right) \tag{B.9}$$

Near the axis ($t << 1$) the vorticity has the form

$$\vec{\zeta} \approx \frac{1}{s}\left[\left(\frac{-w_e^2\alpha_e^2}{2v}\right), \left(\frac{w_e\alpha_e}{t}\right), \left(\frac{v}{t}\right)\right] \tag{B.10}$$

10.C Stewartson and Hall Inner Solution

Transforming equations (3.12) to the inner dependent and independent variables results in the following coupled system of ordinary differential equations written in descending order:

O(1)

$$\eta A_0' + 2A_0 = -\eta C_1' \tag{C.1a}$$

$$D_1' = \frac{-2}{\eta} B_0^2 \tag{C.1b}$$

$$B_0'' + (\frac{1}{2}\eta + \frac{1}{\eta}) B_0' - \frac{1}{\eta^2} B_0 = 0 \tag{C.1c}$$

$$C_1'' + (\frac{1}{2}\eta + \frac{1}{\eta}) C_1' = \frac{-1}{4} \eta D_1' \tag{C.1d}$$

O $(\frac{\ln \chi}{\chi})$

$$\eta A_1' + 2A_1 = -\eta C_2' \tag{C.2a}$$

$$D_2' = \frac{-4}{\eta} B_0 B_1 \tag{C.2b}$$

$$B_1'' + (\frac{1}{2}\eta + \frac{1}{\eta}) B_1' - \frac{1}{\eta^2} B_1 = \frac{-1}{4} \eta B_0' \tag{C.2c}$$

$$C_2'' + (\frac{1}{2}\eta + \frac{1}{\eta}) C_2' = \frac{1}{4} \eta D_2' - \frac{1}{4} \eta C_1' \tag{C.2d}$$

$0\ (\frac{1}{\chi})$

$$\eta A_2' + 2A_2 = \frac{1}{2}\,\eta C_1' - \eta C_3' \tag{C.3a}$$

$$D_3' = \frac{-4}{\eta}\,B_0 B_2 \tag{C.3b}$$

$$B_2'' + (\frac{1}{2}\,\eta + \frac{1}{\eta})\,B_2' - \frac{1}{\eta^2}\,B_2 = \frac{-1}{2}\,\eta C_1 B_0'$$

$$- \frac{1}{2}\,A_0 B_0 - \frac{1}{2}\,\eta A_0 B_0' \tag{C.3c}$$

$$C_3'' + (\frac{1}{2}\,\eta + \frac{1}{\eta})\,C_3' = \frac{1}{4}\,\eta D_3' - \frac{1}{4}\,D_1 - \frac{1}{8}\,\eta D_1'$$

$$+ \frac{1}{2}\,C_1 - \frac{1}{2}\,\eta C_1'(C_1 + A_0) \tag{C.3d}$$

Here the prime denotes a total derivative with repect to η. The boundary conditions are

$\eta = 0$

$$\{\eta A_i = B_i = C_i' = 0;\quad i = 1, 2, \ldots\} \tag{C.4}$$

$\eta\chi^{-1/2} \to \infty$

$$B_0 \to 1 \tag{C.5a}$$

$$C_1 \to -\ln \eta + \frac{1}{\alpha_e} \tag{C.5b}$$

$$D_1 \to -2 \ln \eta + 1 + \frac{2}{\alpha_e} \tag{C.5c}$$

$$B_1 \to \frac{1}{4} \tag{C.6a}$$

$$C_2 \to 0 \tag{C.6b}$$

$$D_2 \to - \ln \eta + \frac{1}{2} + \frac{1}{\alpha_e} \tag{C.6c}$$

$$B_2 \to - \frac{1}{2} \ln \eta + \frac{1}{4} + \frac{1}{2\alpha_e} \tag{C.7a}$$

$$C_3 \to 0 \tag{C.7b}$$

$$D_3 \to \ln^2 \eta - (1 + \frac{2}{\alpha_e}) \ln \eta \tag{C.7c}$$

The treatment of edge boundary conditions is further simplified by introducing subsidiary functions:

O(1)

$$\eta A_0' + 2A_0 = \eta C_{11}' \tag{C.8a}$$

$$D_{11}' = \frac{2}{\eta} B_0^2 \tag{C.8b}$$

$$B_0'' + (\frac{1}{2} \eta + \frac{1}{\eta}) B_0' - \frac{1}{\eta^2} B_0 = 0 \tag{C.8c}$$

$$C_{11}'' + \left(\frac{1}{2}\eta + \frac{1}{\eta}\right) C_{11}' = \frac{1}{2} B_0^2 \tag{C.8d}$$

with

$$A_0 = A_0(\eta) \tag{C.9a}$$

$$B_0 = B_0(\eta) \tag{C.9b}$$

$$C_1 = C_{10}(\alpha) - C_{11}(\eta) \tag{C.9c}$$

$$D_1 = D_{10}(\alpha) - D_{11}(\eta) \tag{C.9d}$$

$O\left(\frac{\ln \chi}{\chi}\right)$

$$\eta A_{11}' + 2A_{11} = \eta C_{21}' \tag{C.10a}$$

$$D_{21}' = \frac{4}{\eta} B_0 B_{11} \tag{C.10b}$$

$$B_{11}'' + \left(\frac{1}{2}\eta + \frac{1}{\eta}\right) B_{11}' - \frac{1}{\eta^2} B_{11} = \frac{1}{4}\eta B_0' \tag{C.10c}$$

$$C_{21}'' + \left(\frac{1}{2}\eta + \frac{1}{\eta}\right) C_{21}' = B_0 B_{11} + \frac{\eta}{4} C_{11}' \tag{C.10d}$$

with

$$A_1 = 2B_{10}(\alpha)\, A_0(\eta) - A_{11}(\eta) \tag{C.11a}$$

$$B_1 = B_{10}(\alpha)\, B_0(\eta) - B_{11}(\eta) \tag{C.11b}$$

$$C_2 = C_{20}(\alpha) - 2B_{10}(\alpha)\, C_{11}(\eta) + C_{21}(\eta) \tag{C.11c}$$

$$D_2 = D_{20}(\alpha) - 2B_{10}(\alpha)\, D_{11}(\eta) + D_{21}(\eta) \tag{C.11d}$$

$O\left(\frac{1}{\chi}\right)$

$$\eta A'_{21} + 2A_{21} = \eta C'_{31} \tag{C.12a}$$

$$\eta A'_{22} + 2A_{22} = \eta C'_{32} \tag{C.12b}$$

$$D'_{31} = \frac{4}{\eta} B_0 B_{21} \tag{C.12c}$$

$$B''_{21} + \left(\frac{1}{2}\eta + \frac{1}{\eta}\right) B'_{21} - \frac{1}{\eta^2} B_{21}$$

$$= \frac{\eta}{2} B'_0 \left(A_0 + \frac{1}{2} - C_{11}\right) + \frac{1}{2} A_0 B_0 \tag{C.12d}$$

$$C''_{31} + \left(\frac{1}{2}\eta + \frac{1}{\eta}\right) C'_{31} = \frac{1}{2} \tag{C.12e}$$

$$C''_{32} + \left(\frac{1}{2}\eta + \frac{1}{\eta}\right) C'_{32} = B_0 B_{21} + \frac{1}{4} D_{11} - \frac{1}{2} C_{11}$$

$$+ \frac{1}{2}\eta C'_{11}\left(A_0 + \frac{1}{2} - C_{11}\right) \tag{C.12f}$$

with

$$A_2 = [2B_{20}(\alpha) - 1]\, A_0(\eta) - [2C_{10}(\alpha) - 1]\, A_{11}(\eta)$$

$$+ \left[\tfrac{1}{2} D_{10}(\alpha) - C_{10}(\alpha)\right] A_{21}(\eta) - A_{22}(\eta) \qquad \text{(C.13a)}$$

$$B_2 = B_{20}(\alpha)\, B_0(\eta) - [2C_{10}(\alpha) - 1]\, B_{11}(\eta) - B_{21}(\eta) \qquad \text{(C.13b)}$$

$$C_3 = C_{30}(\alpha) - \left[2B_{20}(\alpha) - \tfrac{1}{2}\right] C_{11}(\eta) + [2C_{10}(\alpha) - 1]\, C_{21}(\eta)$$

$$- \left[\tfrac{1}{2} D_{10}(\alpha) - C_{10}(\alpha)\right] C_{31}(\eta) + C_{32}(\eta) \qquad \text{(C.13c)}$$

$$D_3 = D_{30}(\alpha) - 2B_{20}(\alpha)\, D_{11}(\eta)$$

$$+ [2C_{10}(\alpha) - 1]\, D_{21}(\eta) + D_{31}(\eta) \qquad \text{(C.13d)}$$

10.D Numerical Aspects of Inner Core Solution

Equations (4.5) are evaluated in difference form about points $(m + 1/2, n - 1/2)$, $(m + 1, n + 1/2)$, $(m + 1/2, n)$, and $(m + 1/2, n)$ respectively. The difference approximations are formally second order accurate:

$$K_{m+1/2,n} = \frac{K_{m+1,n} + K_{m,n}}{2} \tag{D.1}$$

$$K_{,z\ m+1/2,n} = \frac{K_{m+1,n} - K_{m,n}}{\Delta z_m} \tag{D.2}$$

$$K_{,\xi\ m+1/2,n} = \frac{(\frac{1}{\tau + 1})\ (K_{m+1,n+1} + K_{m,n+1}) + (\tau - 1)(K_{m+1,n} + K_{m,n})}{2\Delta\xi_n}$$

$$+ \frac{-\ (\frac{\tau^2}{\tau + 1})(K_{m+1,n-1} + K_{m,n-1})}{2\Delta\xi_n} \tag{D.3}$$

$$K_{,\xi\xi\ m+1/2,n} = \frac{(\frac{\tau}{\tau + 1})(K_{m+1,n+1} + K_{m,n+1}) - \tau(K_{m+1,n} + K_{m,n})}{\Delta\xi_n^2}$$

$$+ \frac{(\frac{\tau^2}{\tau + 1})\ (K_{m+1,n-1} + K_{m,n-1})}{\Delta\xi_n^2} \tag{D.4}$$

where

$$\tau = \frac{\Delta\xi_n}{\Delta\xi_{n-1}} \tag{D.5}$$

$$\Delta\xi_1 = \xi_N \frac{(\tau - 1)}{(\tau^{N-1} - 1)} \tag{D.6}$$

The resultant difference equations are

$$H_{m+1/2,n} = \frac{\xi_{n-1}}{\xi_n} H_{m+1/2,n-1}$$

$$- \frac{1 + \frac{\xi_{n-1}}{\xi_n}}{4\Delta z_m} \left[\Delta\xi_{n-1}\left(w_{m+1,n} - w_{m,n} + w_{m+1,n-1} - w_{m,n-1}\right)\right.$$

$$- \xi_n\left(1 + \frac{\xi_{n-1}}{\xi_n}\right)\left(\frac{\lambda_{m+1} - \lambda_m}{\lambda_{m+1} + \lambda_m}\right)$$

$$\left.\times \left(w_{m+1,n} - w_{m+1,n-1} + w_{m,n} - w_{m,n-1}\right)\right] \tag{D.7}$$

$$p_{m+1,n} = p_{m+1,n+1} - \frac{2\Delta\xi_n\left(K_{m+1,n+1} + K_{m+1,n}\right)^2}{\lambda_{m+1}^2\left(\xi_{n+1} + \xi_n\right)^3} \tag{D.8}$$

$$\left[\frac{1}{(\tau+1)}\,cs_3 - \frac{\tau}{(\tau+1)}\,cs_2\right] K_{m+1,n+1}$$

$$+ \left[cs_1 + \tau cs_2 + (\tau - 1)\,cs_3\right] K_{m+1,n}$$

$$+ \left[\frac{-\tau^2}{(\tau+1)}\,cs_3 - \frac{\tau^2}{(\tau+1)}\,cs_2\right] K_{m+1,n-1}$$

$$= \left[\frac{-1}{(\tau+1)}\,cs_3 + \frac{\tau}{(\tau+1)}\,cs_2\right] K_{m,n+1}$$

$$+ \left[cs_1 - \tau cs_2 - (\tau - 1)\,cs_3\right] K_{m,n}$$

$$+ \left[\frac{\tau^2}{(\tau+1)}\,cs_3 + \frac{\tau^2}{(\tau+1)}\,cs_2\right] K_{m,n-1} \qquad (D.9)$$

where

$$cs_1 = \frac{\bar{w}_{m+1,n} + w_{m,n}}{2\Delta z_m} \qquad (D.10)$$

$$cs_2 = \frac{4}{(\lambda_{m+1} + \lambda_m)^2 \Delta\xi_n^2} \qquad (D.11)$$

$$cs_3 = \frac{1}{\Delta\xi_n}\left[\frac{H_{m+1/2,n}}{2} - \xi_n \frac{\lambda_{m+1} - \lambda_m}{\lambda_{m+1} + \lambda_m}\,cs_1 + \frac{2}{\xi_n(\lambda_{m+1} + \lambda_m)^2}\right] \qquad (D.12)$$

$$[AU]\, w_{m+1,n+1} + [AD]\, w_{m+1,n} + [AL]\, w_{m+1,n-1} = [AR] \qquad (D.13)$$

where

$$AU = \frac{1}{(\tau + 1)\Delta\xi_n}\left[\frac{H_{m+1/2,n}}{2} - \frac{\xi_n(\lambda_{m+1} - \lambda_m)}{2\Delta z_m(\lambda_{m+1} + \lambda_m)}\, ws_1 - \frac{2\Delta\xi_n + 4\tau\xi_n}{\xi_n\Delta\xi_n(\lambda_{m+1} + \lambda_m)^2}\right] \tag{D.14}$$

$$AD = \frac{\bar{w}_{m+1,n}}{\Delta z_m} + \frac{1}{\Delta\xi_n}\left\{\frac{(\tau - 1)\, H_{m+1/2,n}}{2} - \frac{\xi_n(\lambda_{m+1} - \lambda_m)}{2\Delta z_m(\lambda_{m+1} + \lambda_m)} \times [ws_2 + (\tau - 1)\, ws_1] - \frac{2\Delta\xi_n(\tau - 1) + 4\tau\xi_n}{\xi_n\Delta\xi_n(\lambda_{m+1} + \lambda_m)^2}\right\} \tag{D.15}$$

$$AL = -\tau^2\left[AU + \frac{4}{\Delta\xi_n^2(\lambda_{m+1} + \lambda_m)^2}\right] \tag{D.16}$$

$$AR = \frac{ws_3}{2\Delta z_m} - \frac{4\tau^2}{\Delta\xi_n^2(\lambda_{m+1} + \lambda_m)}\, ws_4 - AU\, ws_5 - \frac{\xi_n(\lambda_{m+1} - \lambda_m)}{2\Delta\xi_n\Delta z_m(\lambda_{m+1} + \lambda_m)} \times ws_2\, \bar{w}_{m+1,n} + \frac{2(\lambda_{m+1} - \lambda_m)}{\Delta z_m\xi_n^2(\lambda_{m+1} + \lambda_m)^3}(K_{m+1,n} + K_{m,n})^2 - \frac{p_{m+1,n} - p_{m,n}}{\Delta z_m} \tag{D.17}$$

and

$$ws_1 = \bar{w}_{m+1,n} + w_{m,n} \tag{D.18}$$

$$ws_2 = \frac{1}{\tau + 1}(\bar{w}_{m+1,n+1} + w_{m,n+1}) + (\tau - 1)(\bar{w}_{m+1,n} + w_{m,n})$$

$$- \frac{\tau^2}{\tau + 1}(\bar{w}_{m+1,n-1} + w_{m,n-1}) \tag{D.19}$$

$$ws_3 = \bar{w}^2_{m+1,n} + w^2_{m,n} \tag{D.20}$$

$$ws_4 = w_{m,n} - w_{m,n-1} \tag{D.21}$$

$$ws_5 = w_{m,n+1} + (\tau + 1)(\tau - 1)\, w_{m,n} - \tau^2 w_{m,n-1} \tag{D.22}$$

The superscript ($\bar{}$) denotes a value from the previous iterate. For the centerline the coefficients of equations (D.13) take the form

$$AU = \frac{-8}{\Delta\xi_n^2(\lambda_{m+1} + \lambda_m)^2} \tag{D.23}$$

$$AD = \frac{\bar{w}_{m+1,n}}{\Delta z_m} - AU \tag{D.24}$$

$$AL = 0 \tag{D.25}$$

$$AR = \frac{ws_3}{2\Delta z_m} - AU(w_{m,n+1} - w_{m,n}) - \frac{p_{m+1,n} - p_{m,n}}{\Delta z} \tag{D.26}$$

The difference equations are valid for the decoupled iterative solution procedure of Hall (1967). With an estimate of the axial flow at station (m + 1), the continuity equation is integrated for the radial flow parameter H. Next the swirl momentum equations are solved simultaneously for the circluation parameter K with the Thomas algorithm. With this result the radial momentum equation is integrated for the pressure. Finally the axial momentum equations are solved simultaneously for a new estimate of the axial flow. Convergence is judged as described in the text.

11.0 BIBLIOGRAPHY

AGARD CP-291 (1981), Computation of Viscious-Inviscid Interactions. February.

AGARD CP-342 (1983), Aerodynamics of Vortical Type Flows in Three Dimensions. July.

Benjamin, T. B. (1962), Theory of the Vortex Breakdown Phenomena. Journal of Fluid Mechanics, Vol. 14, Part 4, pp. 593-629, December.

Blottner, F. G. (1979), Introduction to Computational Techniques for Boundary Layers. SAND 79-0893, September.

Bossel, H. H. (1968), Stagnation Criterion for Vortex Flows. AIAA Journal, Vol. 6, No. 6, pp. 1192-1193, June.

Bossel, H. H. (1969), Vortex Breakdown Flowfield. Physics of Fluids, Vol. 12, No. 3, pp. 498-508, March.

Bossel, H. H. (1972), Vortex Equations: Singularities, Numerical Solution, and Axisymmetric Vortex Breakdown. NASA CR 2090, July.

Boyden, R. P.; and Johnson, W. G., Jr. (1982), Results of Buffet Tests in a Cryogenic Wind Tunnel. NASA TM-84520.

Brown, C. E.; and Michael, W. H. (1955), On Slender Delta Wings with Leading-Edge Separation. NACA TN 3430.

Brown, S. N. (1965), The Compressible Inviscid Leading-Edge Vortex. Journal of Fluid Mechanics, Vol. 22, pp. 17-32.

Brown, S. N.; and Mangler, K. W. (1967), An Asymptotic Solution for the Centre of a Rolled-Up Conical Vortex Sheet in Compressible Flow. Aeronautical Quarterly, Vol. 18, pp. 354-366, November.

Brune, G. W.; Weber, J. A.; Johnson, F. T.; Lu, P.; and Rubbert, P. E. (1975), A Three Dimensional Solution of Flow over Wings with Leading-Edge Separation, Part I - Engineering Document. NASA CR-132709.

Earnshaw, P. B. (1962), An Experimental Investigation of the Structure of a Leading-Edge Vortex. ARC R&M No. 3281.

Erickson, G. E. (1981), Vortex Flow Correlation. AFWAL-TR-80-3143, January.

Germain, P. (1955), Sur L'Écoulement Subsonique au Voisinage de la Pointe Avant d'une Aille Delta. La Recherche Aéronautique, No. 44, pp. 3-8, March.

Grabowski, W. J.; and Berger, S. A. (1976), Solutions of the Navier-Stokes Equations for Vortex Breakdown. Journal of Fluid Mechanics, Vol. 75, pp. 525-544.

Guiraud, J. P.; and Zeytounian, R. Kh. (1977), A Double-Scale Investigation of the Asymptotic Structure of Rolled-Up Vortex Sheets. Journal of Fluid Mechanics. Vol. 79, Part 1, pp. 93-112.

Hall, M. G. (1960), A Theory for the Core of a Leading Edge Vortex. RAE Report No. Aero. 2644, December.

Hall, M. G. (1961), A Theory for the Core of a Leading-Edge Vortex. Journal Fluid Mechanics, Vol. 11, p. 209.

Hall, M. G. (1966), The Structure of Concentrated Vortex Cores. Progress in Aeronautical Sciences, Vol. 7, pp. 53-110.

Hall, M. G. (1967), A Numerical Method for Solving the Equations of a Vortex Core. ARC R&M 3467.

Hall, M. G. (1967b), A New Approach to Vortex Breakdown. Proceedings of the 1967 Heat Transfer and Fluid Mechanics Institute, Stanford University Press, pp. 319-340.

Hall, M. G. (1972), Vortex Breakdown. Annual Review of Fluid Mechanics, Vol. 4, pp. 195-218.

Hitzel, S. M.; and Schmidt, W. (1983), Slender Wings with Leading-Edge Vortex Separation--A Challenge for Panel-Methods and Euler Codes. AIAA Paper No. 83-0562, January.

Hoeijmakers, H. W. M.; and Bennekers, B. (1979), A Computational Model for the Calculation of the Flow About Wings with Leading-Edge Vortices. AGARD CP-247, Paper No. 25, January.

Hoeijmakers, H. W. M. (1983), Computational Vortex Flow Aerodynamics. AGARD CP-342, Paper No. 18, July.

Hoeijmakers, H. W. M.; and Rizzi, A. (1984), Vortex-Fitted Potential Solution Compared with Vortex-Captured Euler Solution for Delta Wing with Leading-Edge Vortex-Separation. AIAA Paper No. 84-2144, August.

Hummel, D. (1965), Untersuchungen über das Aufplatzen der Wirbel an Schlanken Deltaflügeln. ZFW, Vol. 13, No. 5, pp. 158-168.

Hummel, D.; and Redeker, G. (1973), Experimental Determination of Bound Vortex Lines and Flow in the Vicinity of the Trailing Edge of a Slender Wing. NASA TTF-15,012. Translation of "Experimentelle

Bestimmung der Gebundenen Wirbellinien Sowie des Strömungsverlaußs in der Umgebung der Hinterkante eines Schlanken Deltaflügels", Braunschweigische Wissenschaftliche Gesellschaft, Abhandlungen pp. 273-290, 1972.

Jameson, A.; Schmidt, W.; and Turkel, E. (1981), Numerical Solutions of the Euler Equations by Finite Volume Methods Using Runge-Kutta Time-Stepping Schemes. AIAA Paper No. 81-1259, June.

Johnson, F. T.; Lu, P.; Brune, G. W.; Weber, J. A.; and Rubbert, P. E. (1976), An Improved Method for the Prediction of Completely Three-Dimensional Aerodynamic Load Distributions of Configurations with Leading Edge Vortex Separation. AIAA Paper No. 76-417, July.

Johnson, F. T.; Lu, P.; Tinoco, E. N.; and Epton, M. A. (1980), An Improved Panel Method for the Solution of Three-Dimensional Leading-Edge Vortex Flows. Volume 1--Theory Document. NASA CR-3278, July.

Johnson, J. L., Jr.; Grafton, S. B.; and Yip, L. P. (1980), Exploratory Investigation of Vortex Bursting on the High-Angle-of-Attack Lateral-Directional Stability Characteristics of Highly-Swept Wings. AIAA Paper No. 80-0463, March.

Jones, R. T. (1946), Properties of Low-Aspect-Ratio Pointed Wings at Speeds Below and Above the Speed of Sound. NACA Report No. 835.

Kandil, O. A.; Mook, D. T.; and Nayfeh, A. H. (1974), Nonlinear Prediction of the Aerodynamic Loads of Lifting Surfaces. AIAA Paper No. 74-503.

Kirkpatrick, D. L. I. (1965), Experimental Investigation of the Breakdown of a Vortex in a Tube. ARC CP No. 821.

Krause, E. (1983), A Contribution to the Problem of Vortex Breakdown. AGARD CP-342, Paper No. 26, July.

Krause, E.; Shi, X. G.; and Hartwich, P. M. (1983b), Computation of Leading Edge Vortices. AIAA Paper No. 83-1907, July.

Küchemann, D. (Editor) (1966), Progress in Aeronautical Sciences. Vol. 7. Pergamon Press Ltd.

Küchemann, D.; and Weber, J. (1965), Vortex Motions. ZAMM, Vol. 45, pp. 457-474, December.

Lamar, J. E.; and Luckring, J. M. (1979), Recent Theoretical Developments and Experimental Studies Pertinent to Vortex Flow Aerodynamics-With a View Towards Design. High Angle of Attack Aerodynamics, AGARD CP-247, Paper No. 24, January.

Lamar, J. E.; and Campbell, J. F. (1983), Recent Studies at NASA Langley of Vortical Flows Interacting with Neighboring Surfaces. Aeodynamics of Vortical Type Flows in Three Dimensions, AGARD CP-342, Paper No. 10, July.

Lamb, H. (1932), Hydrodynamics. Cambridge University Press, 6th Edition.

Lambourne, N. C.; and Bryer, D. W. (1960), Some Measurements of the Vortex Flow Generated by a Sharp Leading Edge Having 65 Degrees Sweep. ARC CP No. 477.

Lambourne, N. C.; and Bryer, D. W. (1962), The Bursting of Leading Edge Vortices--Some Observations and Discussion of the Phenomena. ARC R&M No. 3282.

Legendre, R. (1953), E'coulement an voisinage de la pointe avant d'une aile à forte fleche aux incidences moyennes. Rechere Aeronautique (ONERA), No. 35, pp. 7-8.

Leibovich, S. (1978), The Structure of Vortex Breakdown. Annual Review of Fluid Mechanics, Vol. 10, pp. 221-246.

Leibovich, S. (1983), Vortex Stability and Breakdown. AGARD CP-342, Paper 23, July.

Lighthill, M. J. (1958), On Displacement Thickness. Journal Fluid Mechanics, Vol. 4, Part 4, pp. 383-392, August.

Lock, R. C. (1981), A Review of Methods for Predicting Viscous Effects on Aerofoils and Wings at Transonic Speeds. Computation of Viscous-Inviscid Interactions, AGARD CP-291, Paper No. 2, February.

Luckring, J. M.; Schoonover, W. E., Jr.; and Frink, N. T. (1982), Recent Advances in Applying Free Vortex Sheet Theory for the Estimation of Vortex Flow Aerodynamics. AIAA Paper No. 82-0095.

Ludwieg, H. (1962), Zur Erklärung der Instabilität der über angestellten Deltaflügeln auftretenden freien Wirkbelkerne. ZFW, Vol. 10, No. 6, pp. 242-248, June. See also, An Explanation of the Instability of the Free Vortex Cores Occurring Over Delta Wings with Raised Edges. NASA TM-75861, September 1980. (Technical translation.)

Lugt, H. J. (1983), Vortex Flow in Nature and Technology. John Wiley & Sons, Inc.

Maskell, E. C. (1962), Some Recent Developments in the Study of Edge Vortices. Proceedings of the 3rd Congress of ICAS, Spartan Books, Inc., Washington, pp. 737-749, 1964.

Mangler, K. W.; and Smith, J. H. B. (1959), A Theory of the Flow Past a Slender Delta Wing with Leading-Edge Separation. Proceedings of the Royal Society, Series A, Vol. 251, No. 1265, pp. 200-217, May.

Mangler, K. W.; and Weber, J. (1966), The Flow Field Near the Center of a Rolled-Up Vortex Sheet. RAE TR No. 66324.

Mehrotra, S. C.; and Lan, C. E. (1978), A Theoretical Investigation of the Aerodynamics of Low Aspect-Ratio Wings with Partial Leading-Edge Separation. NASA CR-145304, January.

Melnik, R. E. (1981), Turbulent Interactions on Airfoils at Transonic Speeds--Recent Developments. Computation of Viscous-Inviscid Interactions, AGARD CP-291, Paper No. 10, February.

Mook, D. T.; and Maddox, S. A. (1974), Extension of a Vortex-Lattice Method to Include the Effects of Leading-Edge Separation. Journal of Aircraft, Vol. 11, pp. 127-128, February.

Newman, B. G. (1959), Flow in a Viscous Trailing Vortex. Aeronautical Quarterly, Vol. 10, Part 2, pp. 149-162, May.

Newsome, R. W. (1985), A Comparison of Euler and Navier-Stokes Solutions for Supersonic Flow Over a Conical Delta Wing. AIAA Paper No. 85-0111, January.

Peckham, D. H. (1961), Low-Speed Wind-Tunnel Tests on a Series of Uncambered Slender Pointed Wings with Sharp Edges. ARC RM No. 3186.

Polhamus, E. C. (1971), Predictions of Vortex-Lift Characteristics by a Leading-Edge Suction Analogy. Journal of Aircraft, Vol. 8, No. 4, pp. 193-199, April.

Polhamus, E. C. (1983), Application of Slender Wing Benefits to Military Aircraft. AIAA Paper No. 83-2566. See also AIAA Journal of Aircraft, Vol. 21, No. 8, pp. 545-558, August 1984.

Raj, P. (1984), Computational Simulation of Free Vortex Flows Using an Euler Code. Proceedings of the 14th Congress of ICAS, Paper No. ICAS-84-1.3.1, September.

Rehbach, C. (1973), Étude Numérique de Nappes Tourbillonnaires Issues D'une Ligne de Décollement Prés du Bord D'attaque. La Recherche Aérospatiale, No. 6, pp 325-330. See also, Numerical Investigation of Vortex Sheets Issuing from a Separation Line Near the Leading-Edge, NASA TTF-15530, 1974. (Technical translation.)

Rossiter, P. J. (1970), The Linearised Subsonic Flow Over the Centre-Section of a Lifting Swept Wing. ARC R&M No. 3630.

Stewartson, K.; and Hall, M. G. (1963), The Inner Viscous Solution for the Core of a Leading-Edge Vortex. Journal of Fluid Mechanics, Vol. 15, pp. 306-318.

Smith, J. H. B. (1966), Improved Calculations of Leading-Edge Separation from Slender Delta Wings. RAE TR No. 66070, March.

South, J. C., Jr. (1985), Recent Advances in Computational Transonic Aerodynamics. AIAA Paper No. 85-0366, January.

Thwaites, B. (Editor), (1960), Incompressible Aerodynamics. Oxford University Press.

Van Dyke, M. (1964), Perturbation Methods in Fluid Mechanics. Academic Press.

Wentz, W. H., Jr.; and Kohlman, D. L. (1968), Wind-Tunnel Investigation of Vortex Breakdown on Slender Sharp-Edged Wings. NASA CR-98737, November.

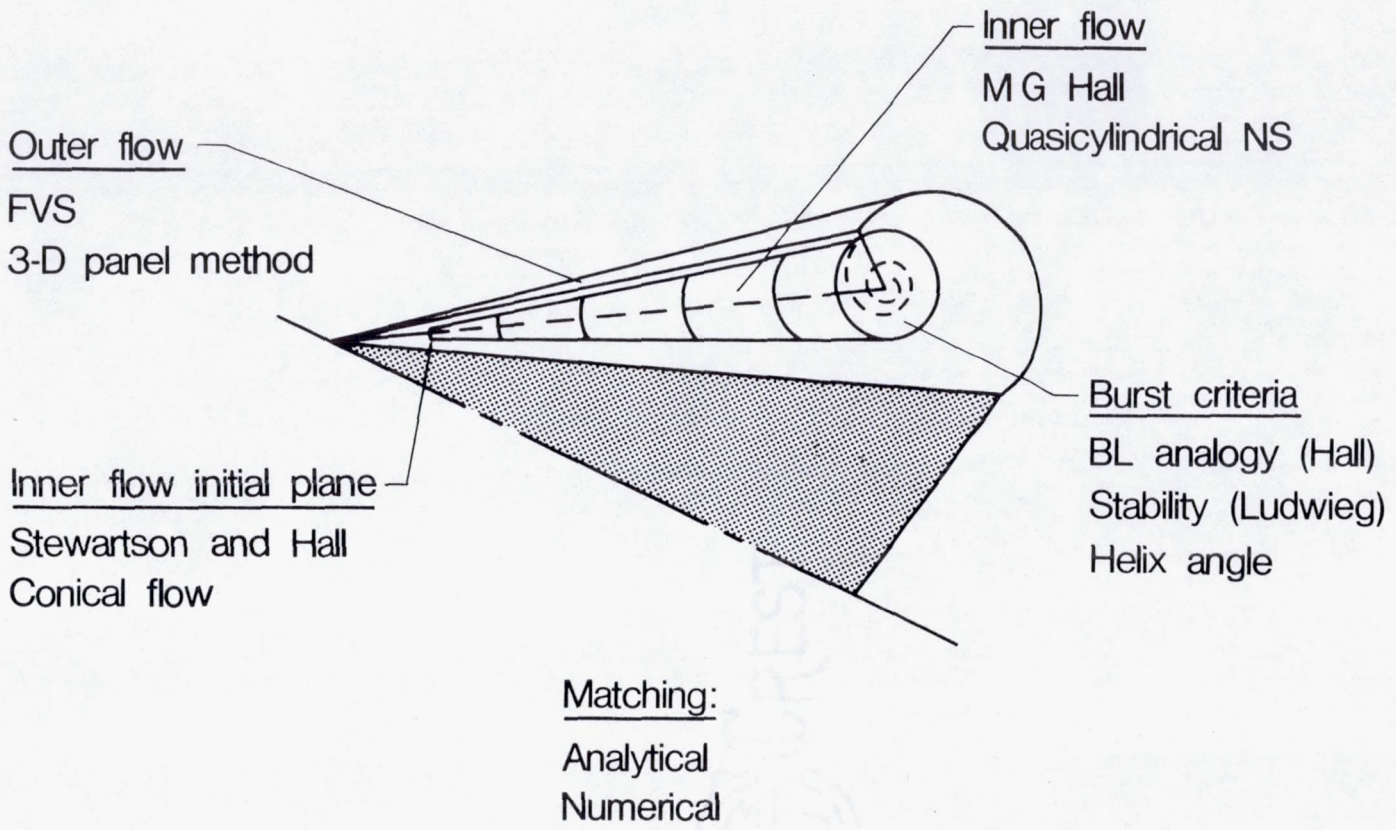

Figure 1.1- Theoretical flow model. Rn >> 1.

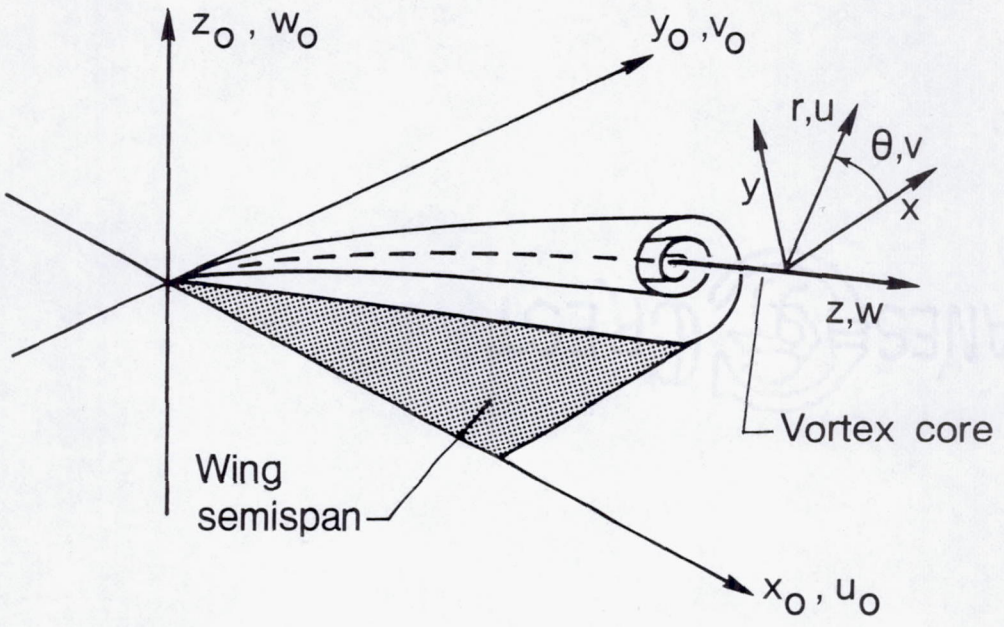

a) Global definitions

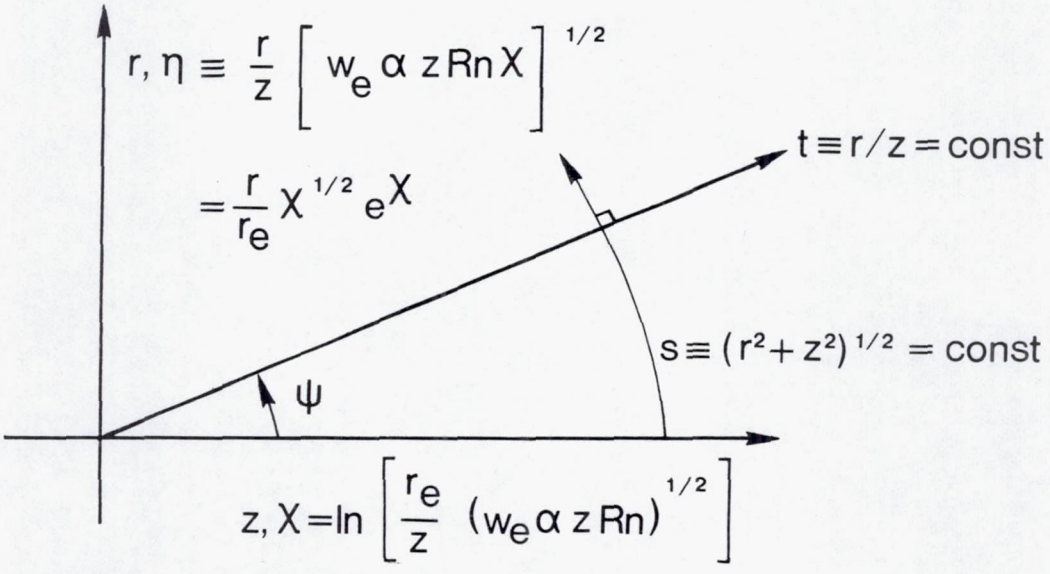

b) Near vortex core

Figure 1.2- Frequently used parameters.

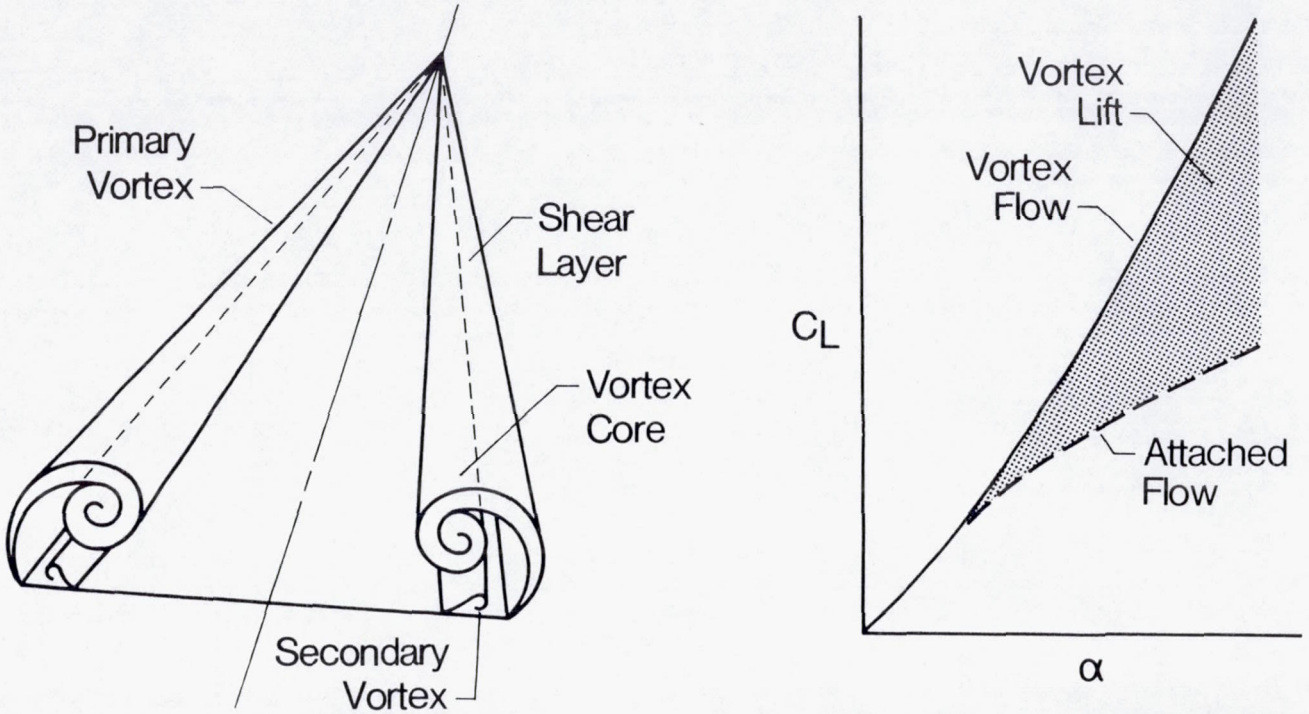

Figure 2.1- Vortex flow structure and lift effect - slender wings.

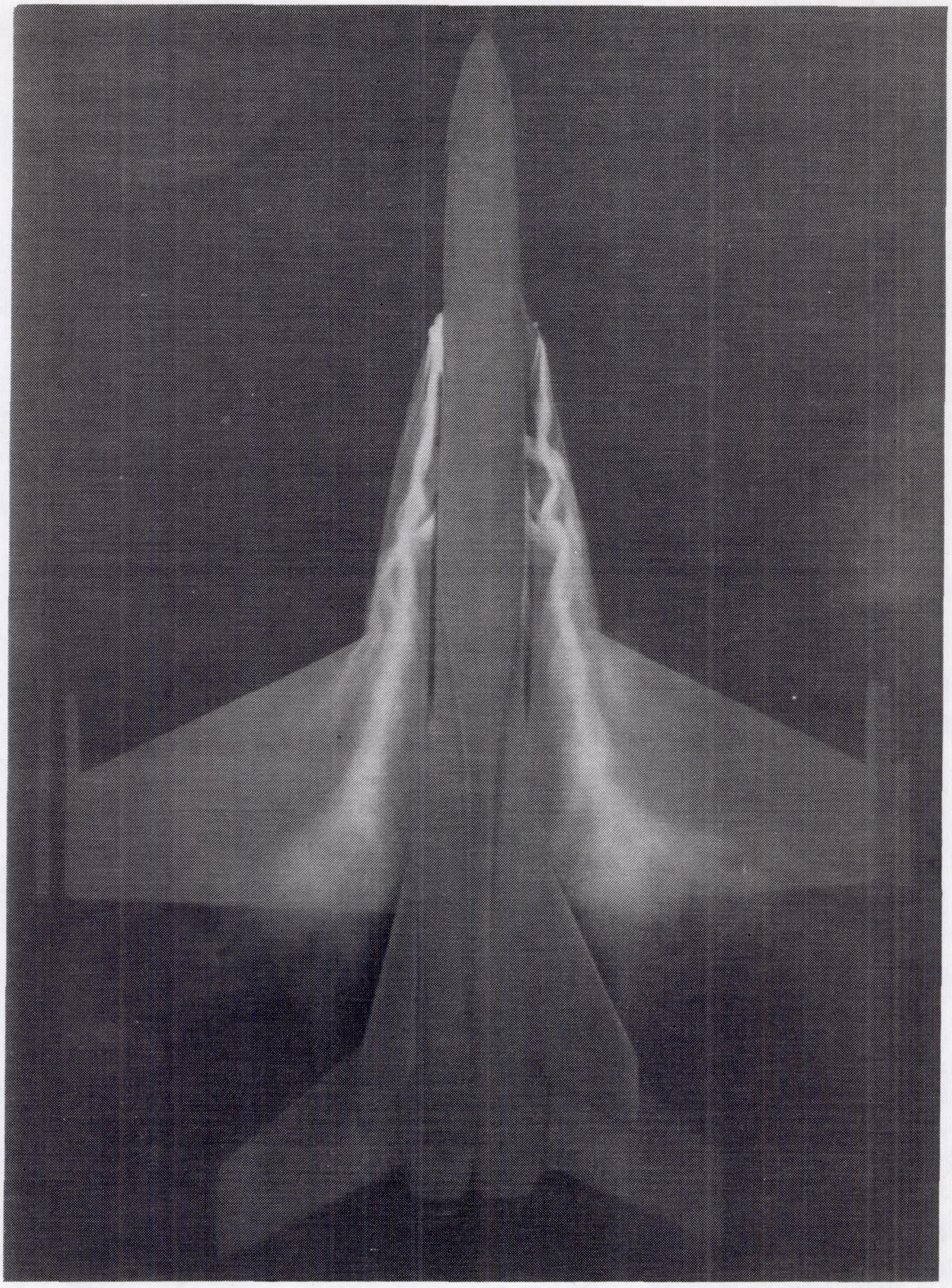

Figure 2.2- Near field vortex breakdown.

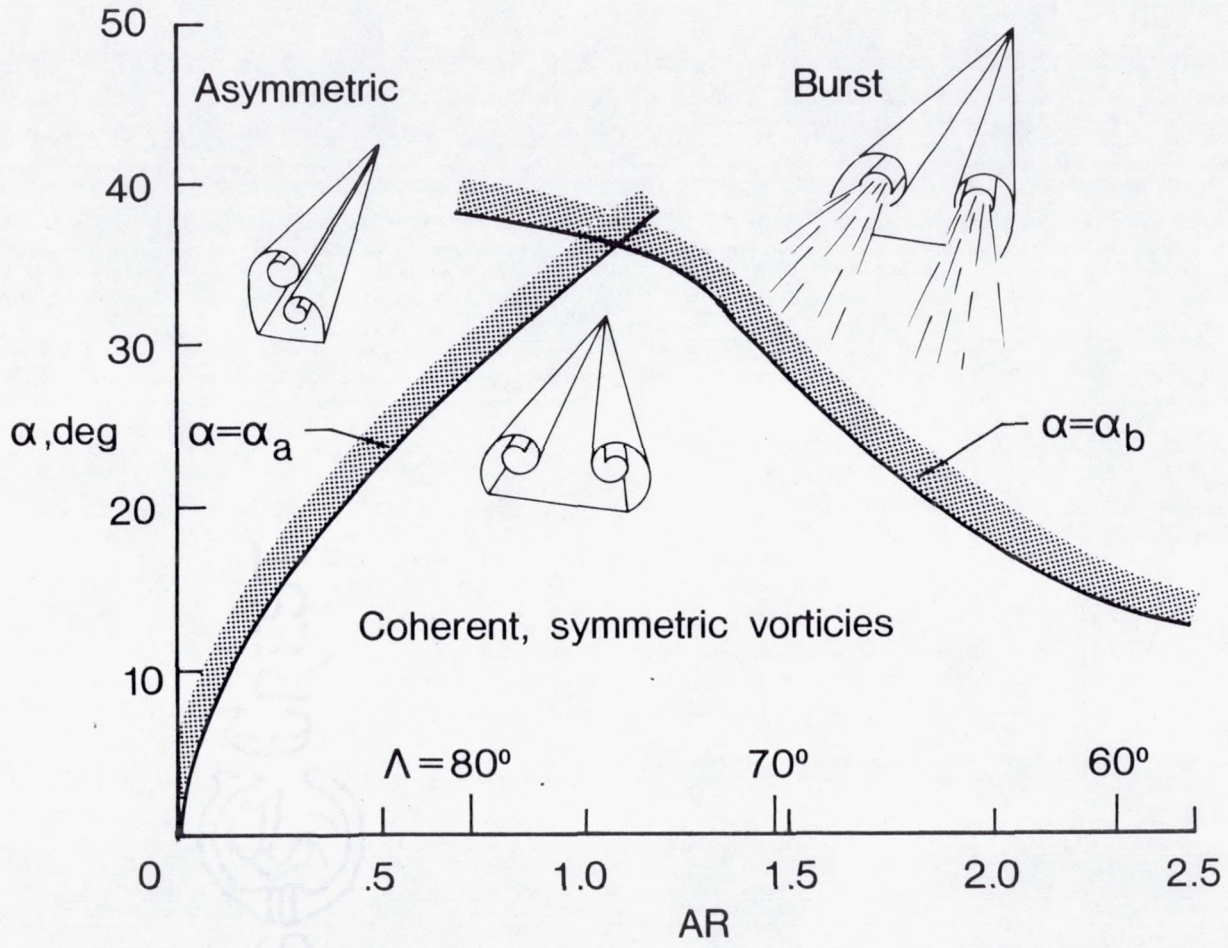

Figure 2.3- Incompressible vortex flow regimes for sharp-edged delta wings.

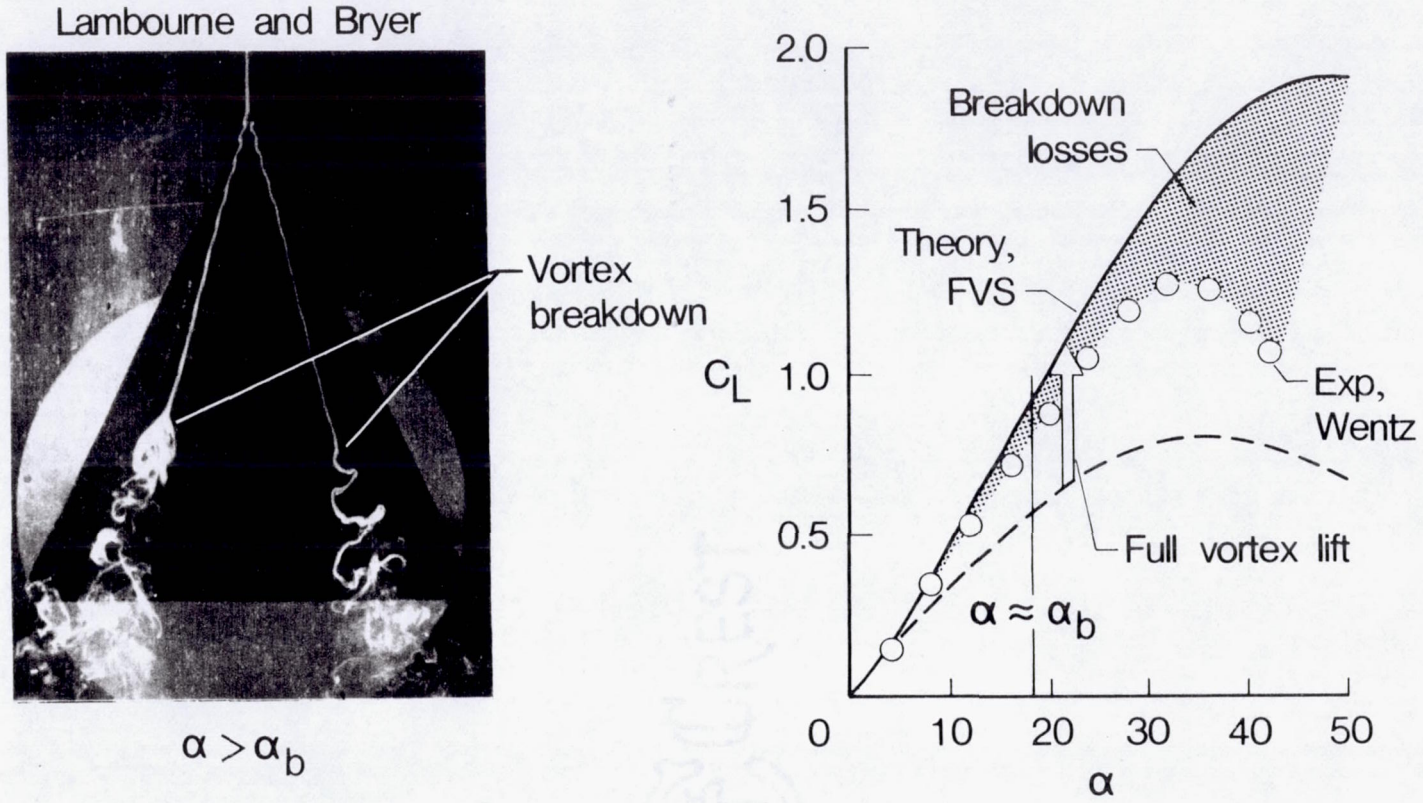

Figure 2.4- Vortex breakdown and lift effects. $\Lambda = 65°$

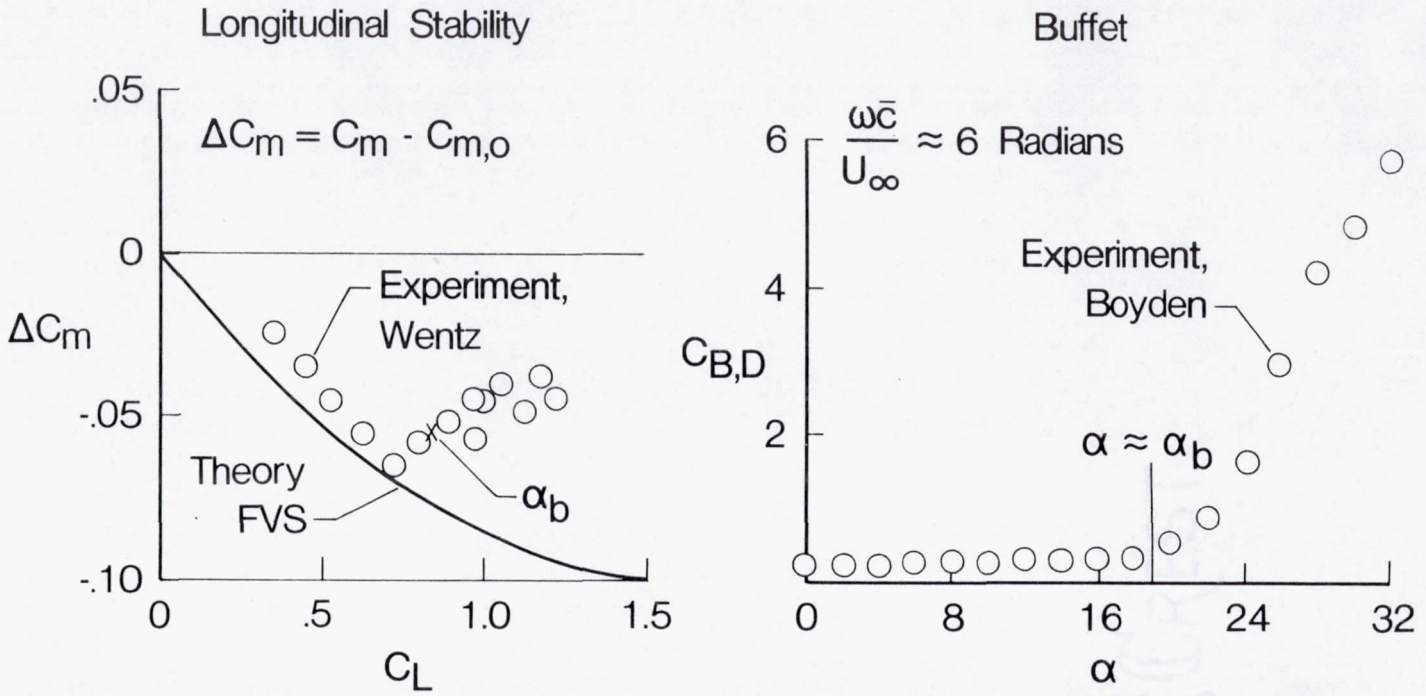

Figure 2.5- Vortex breakdown moment effects. $\Lambda = 65°$

$$(1-v_r^*)(1-v_r^{*2}) - (5/3-v_r^*)\ w_r^{*2} > 0$$

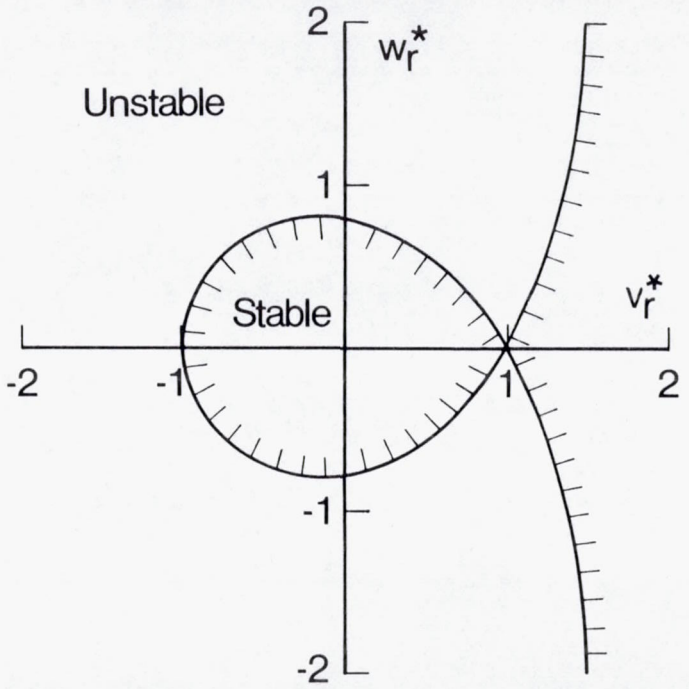

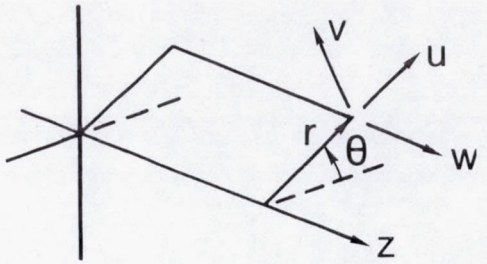

$$v_r^* \equiv \frac{r}{v}\, v_{,r}$$

$$w_r^* \equiv \frac{r}{v}\, w_{,r}$$

Figure 2.6- Hydrodynamic stability criterion - Ludwieg.

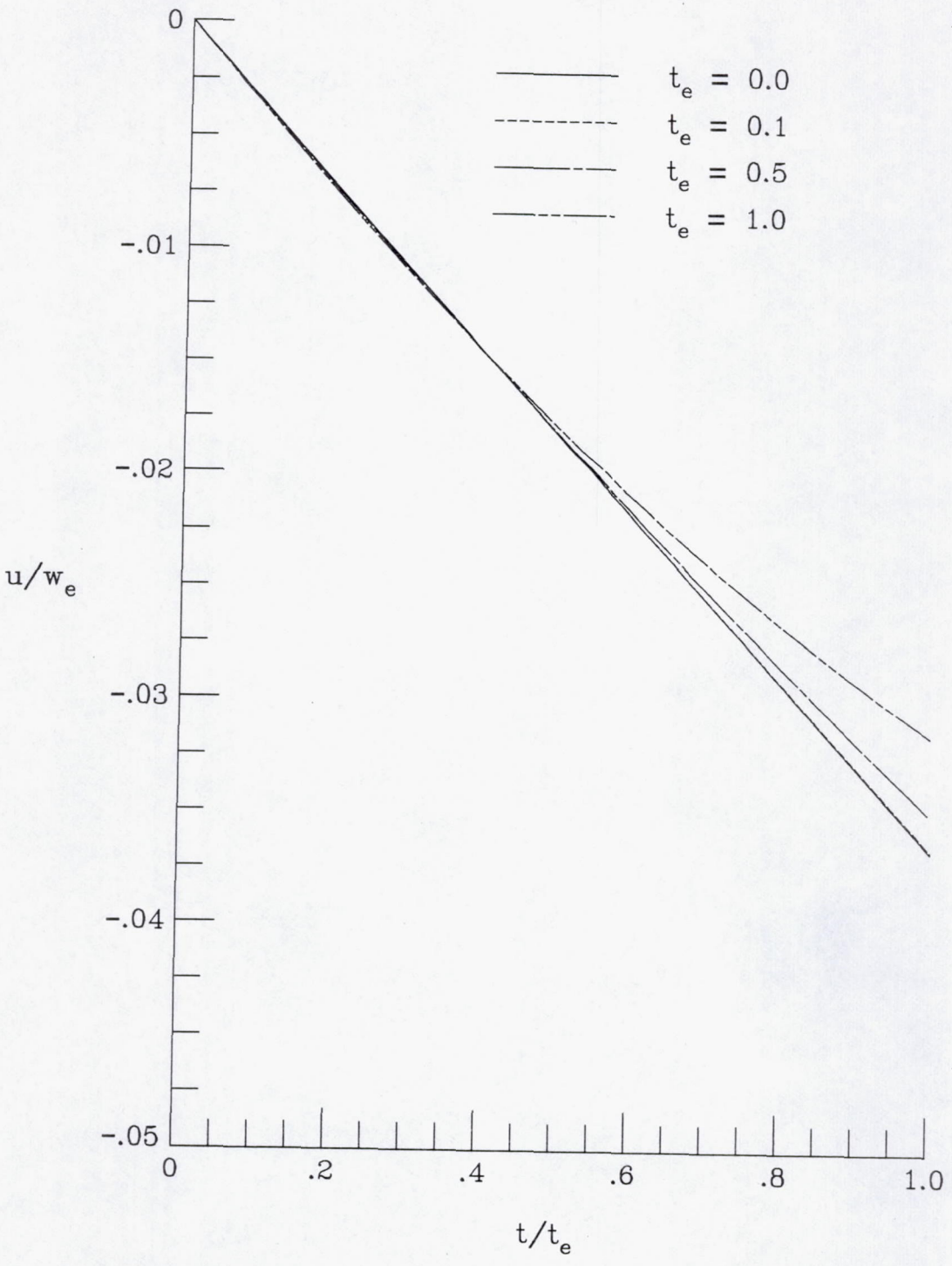

a) radial velocity

Figure 3.1- Comparison of slender and exact inviscid solutions.
$Rn = 10^6$, $\phi_e = 1.$

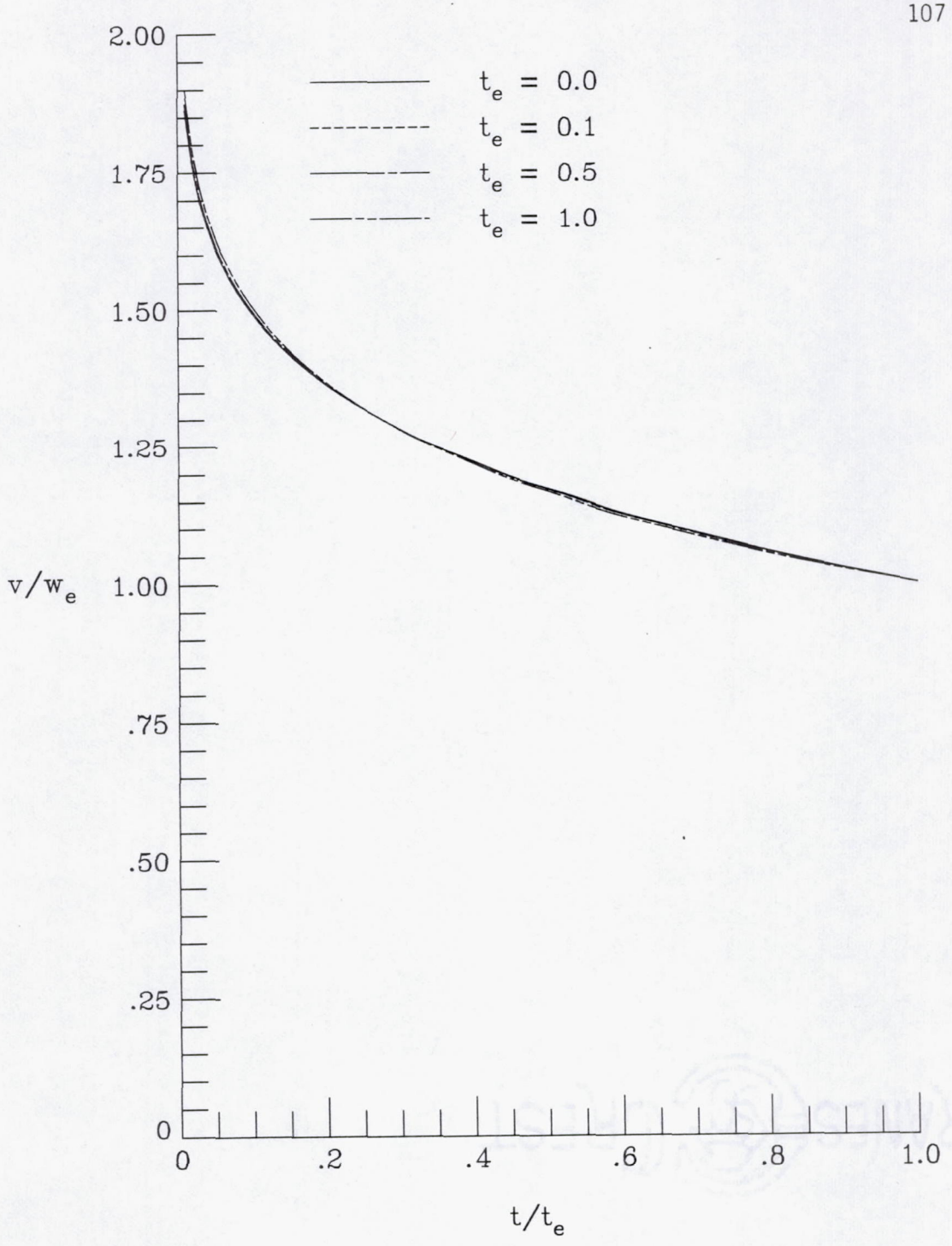

b) angular velocity

Figure 3.1- Continued

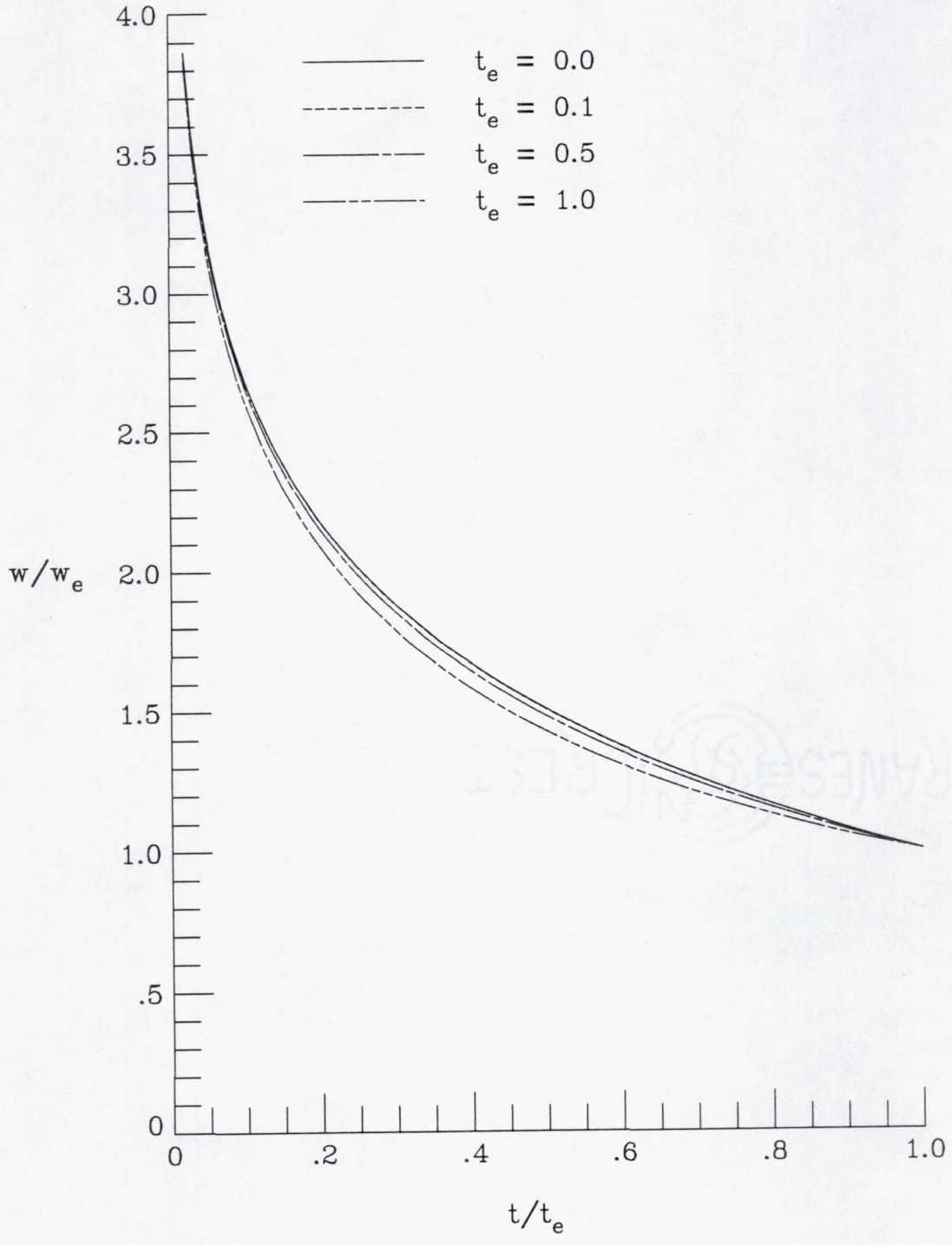

c) axial velocity

Figure 3.1- Continued

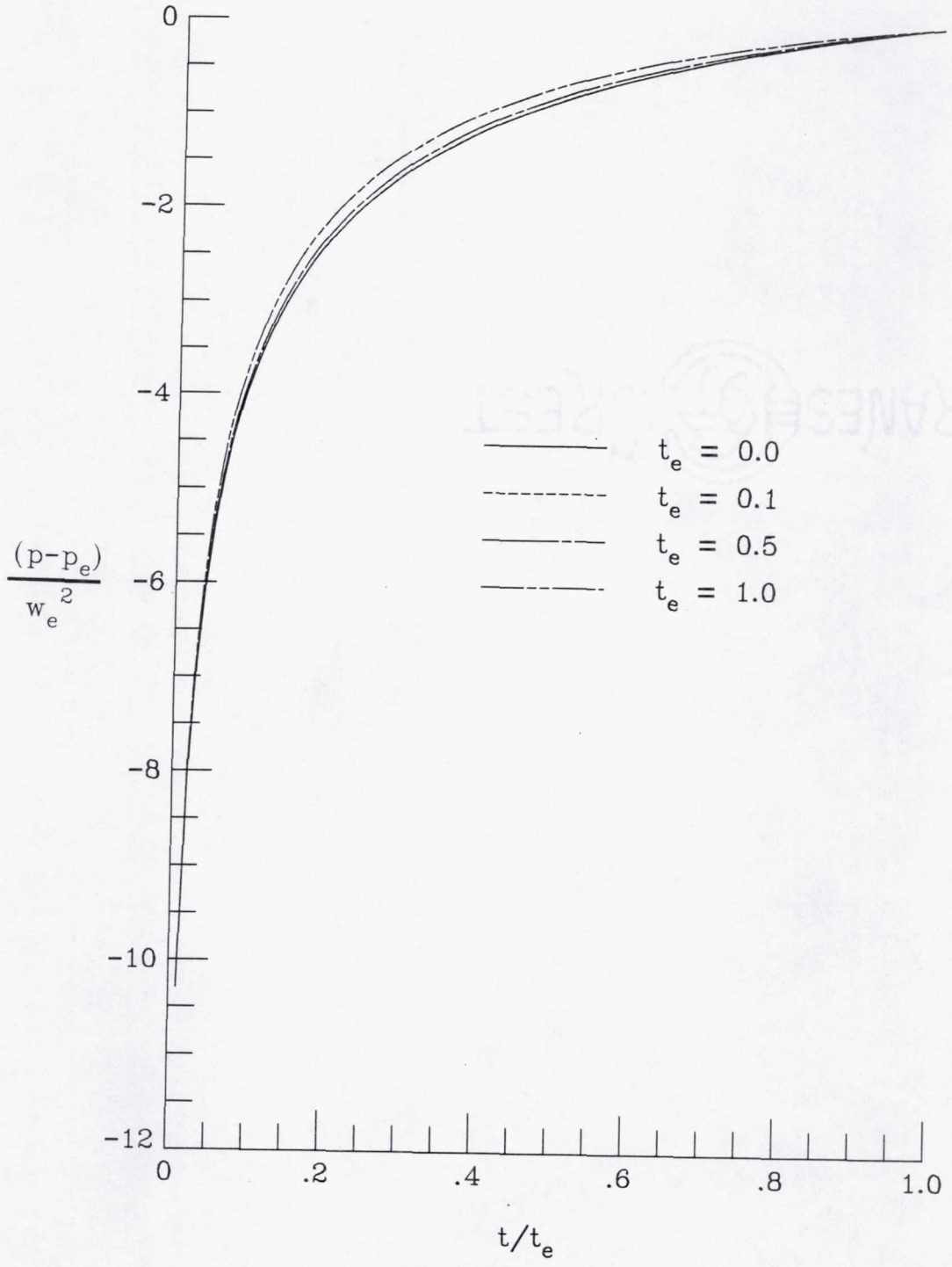

d) static pressure

Figure 3.1- Concluded.

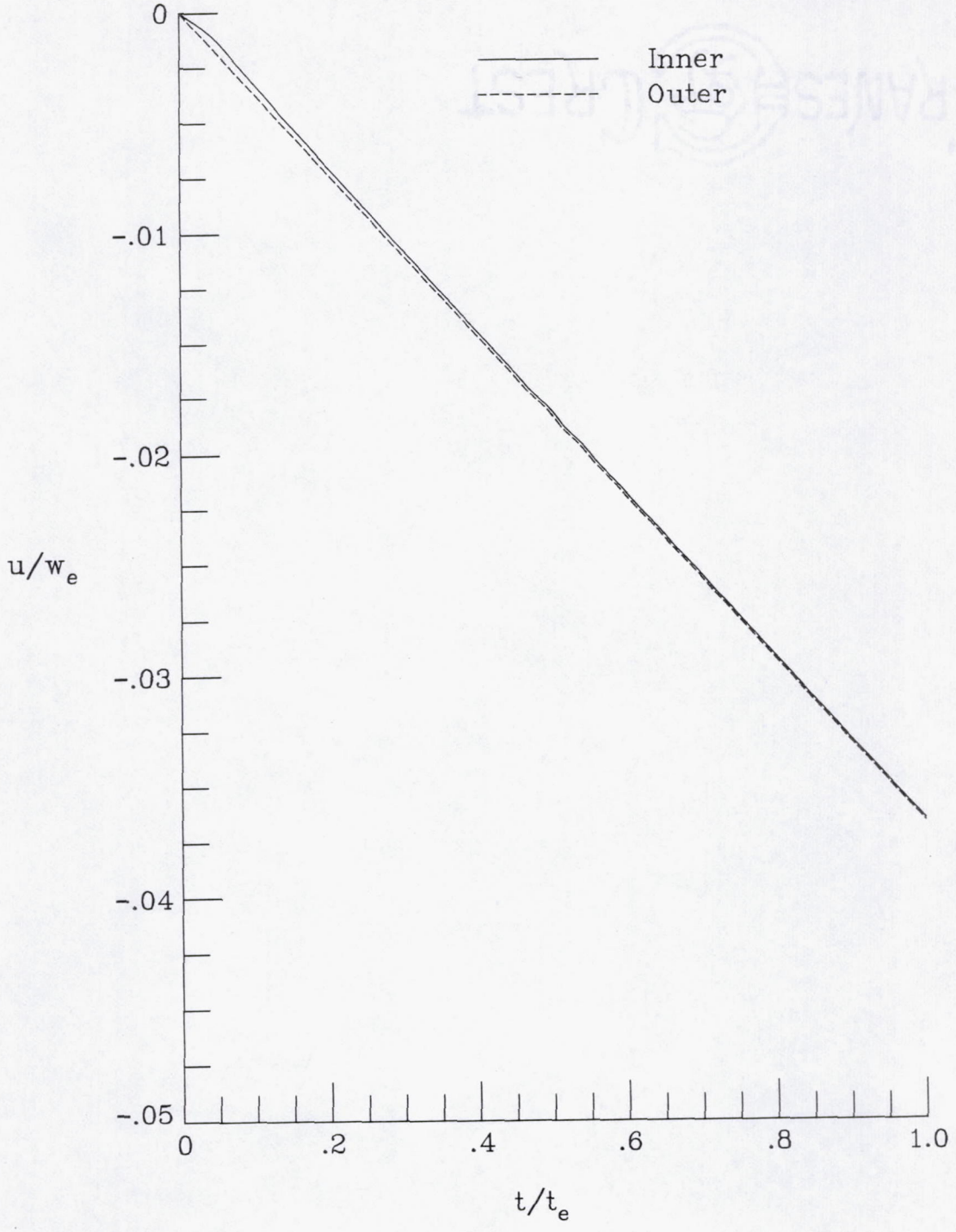

a) radial velocity

Figure 3.2- Inner and outer initial plane solutions.

$Rn = 10^6$, $\phi_e = 1.$

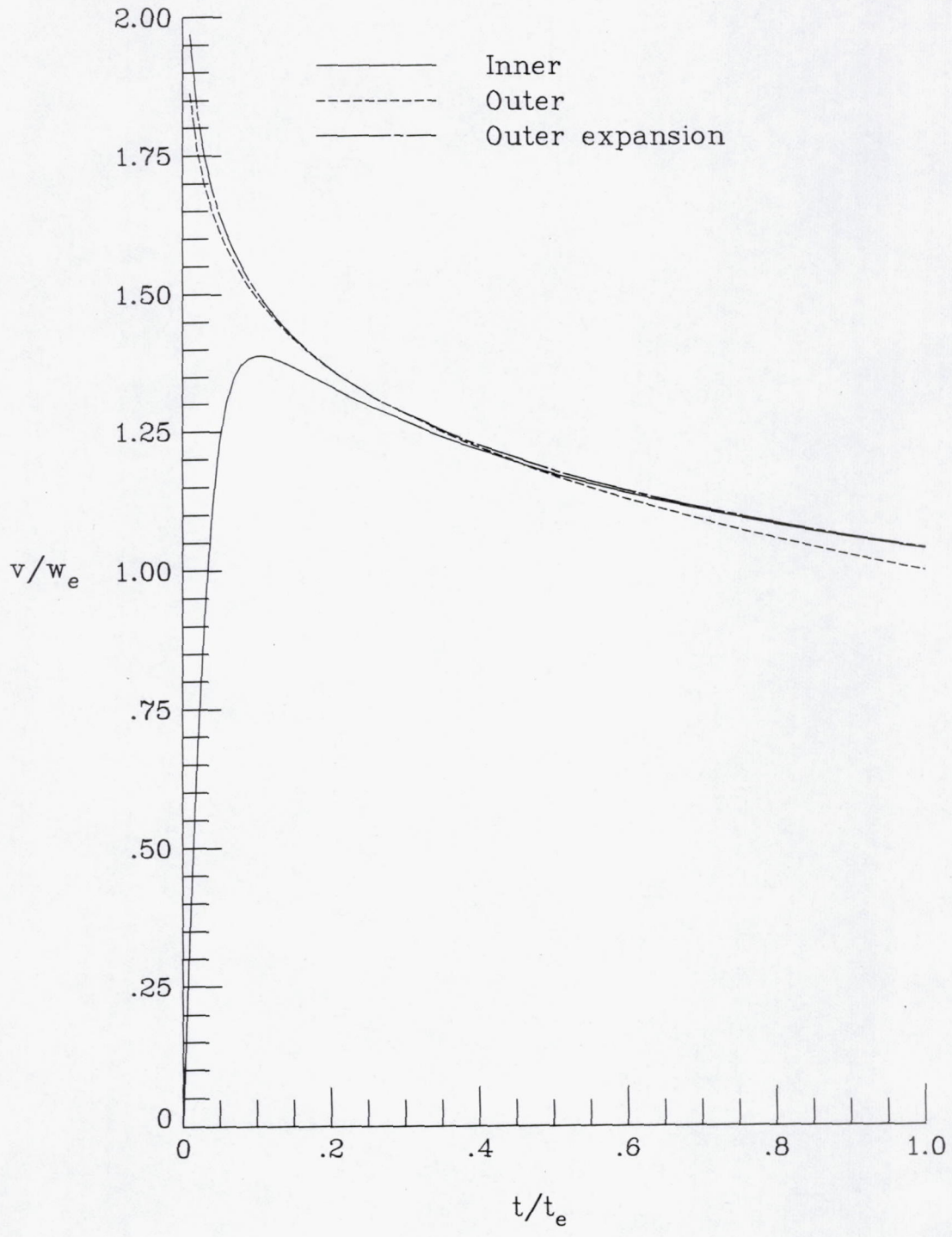

b) angular velocity

Figure 3.2- Continued

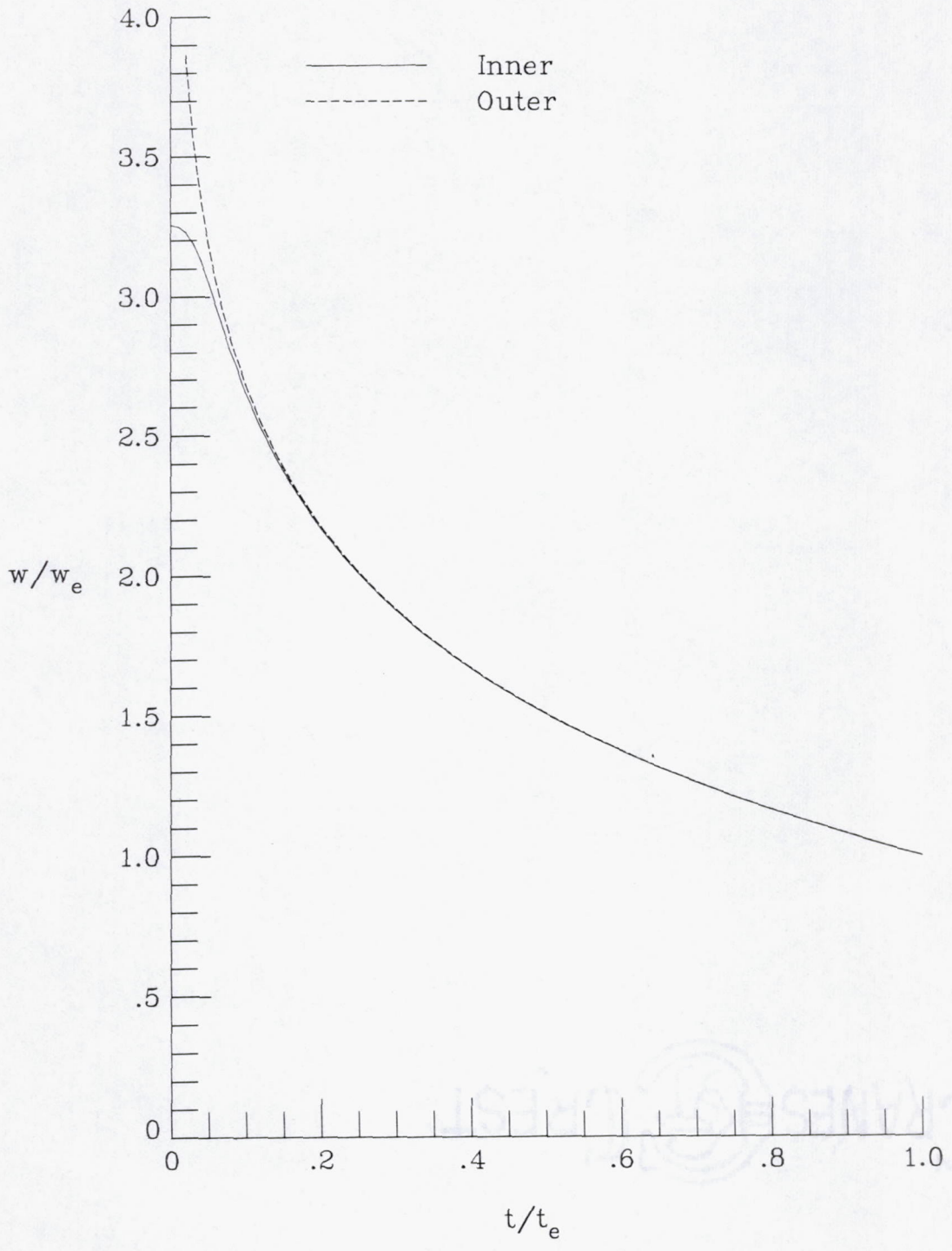

c) axial velocity

Figure 3.2- Continued

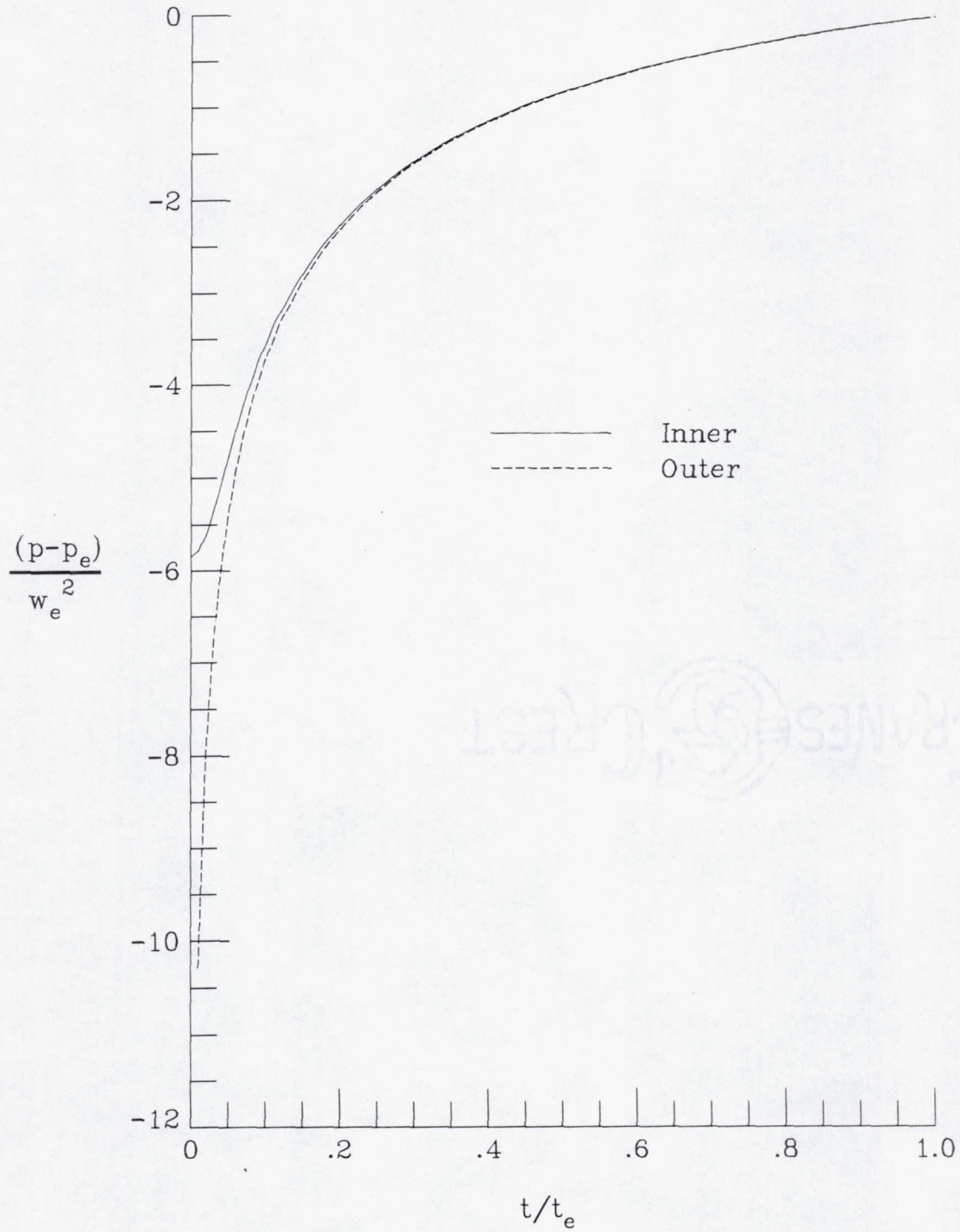

d) static pressure

Figure 3.2- Concluded.

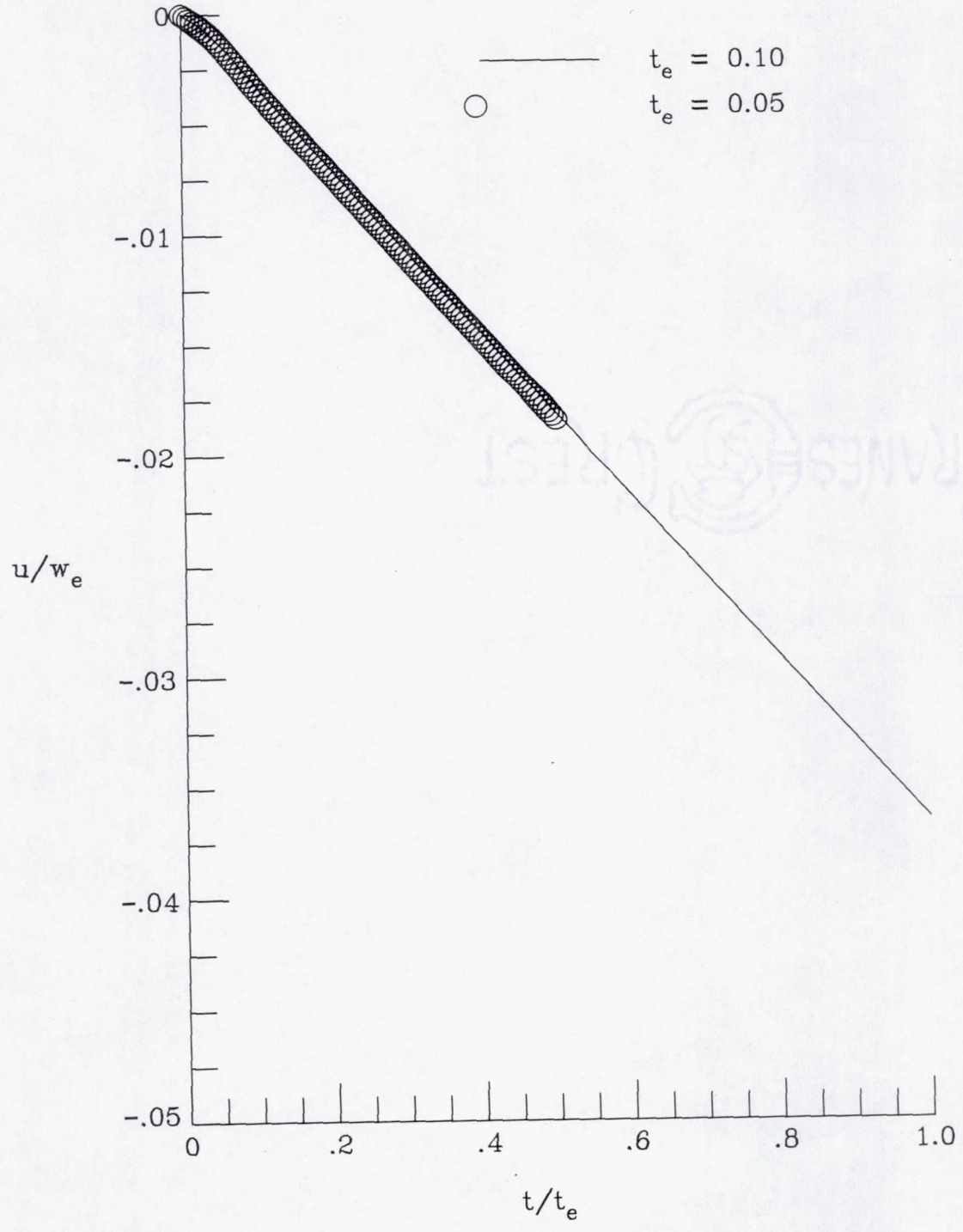

a) radial velocity

Figure 3.3- Edge location effect. Rn = 10^6, ϕ_e = 1.

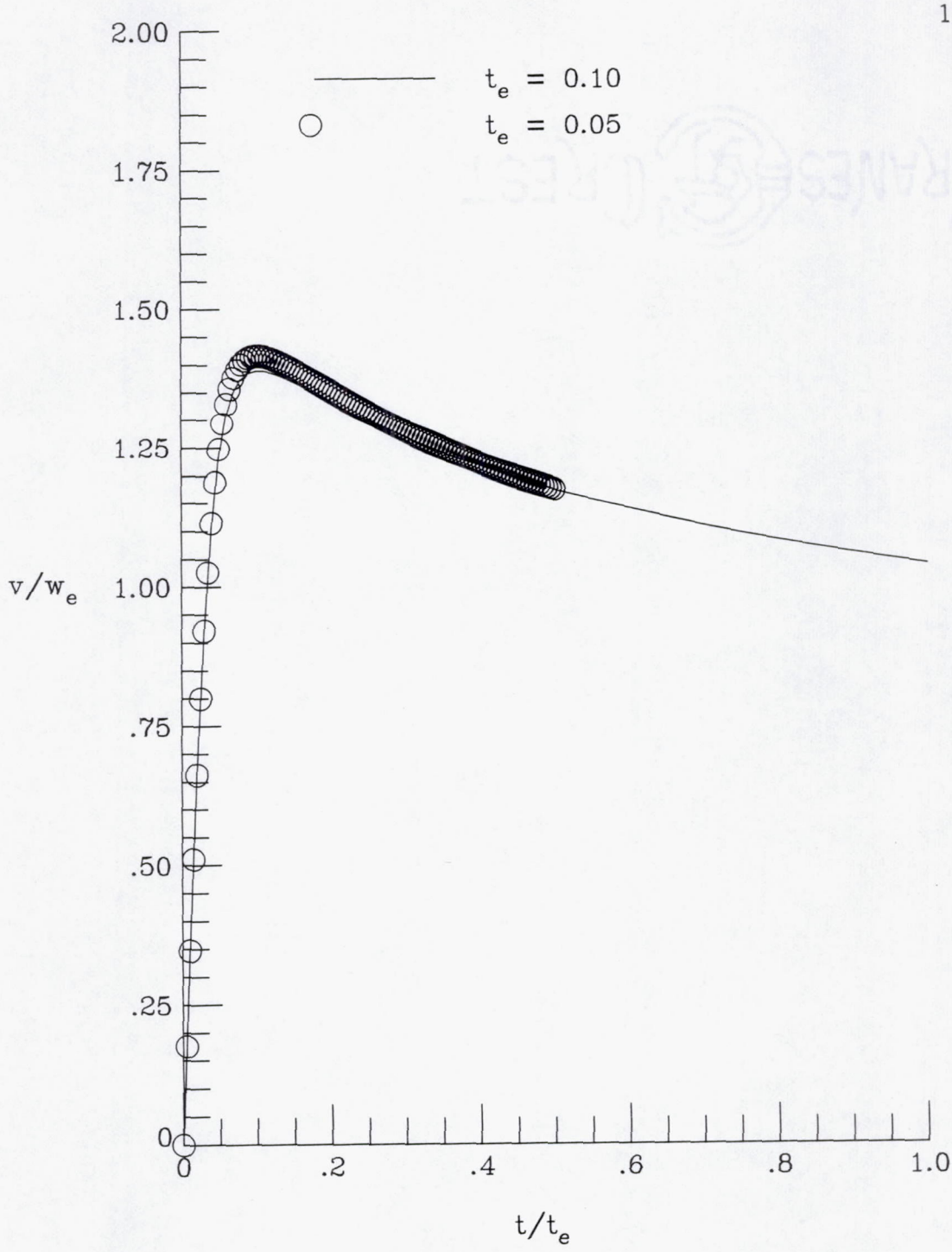

b) angular velocity

Figure 3.3- Continued

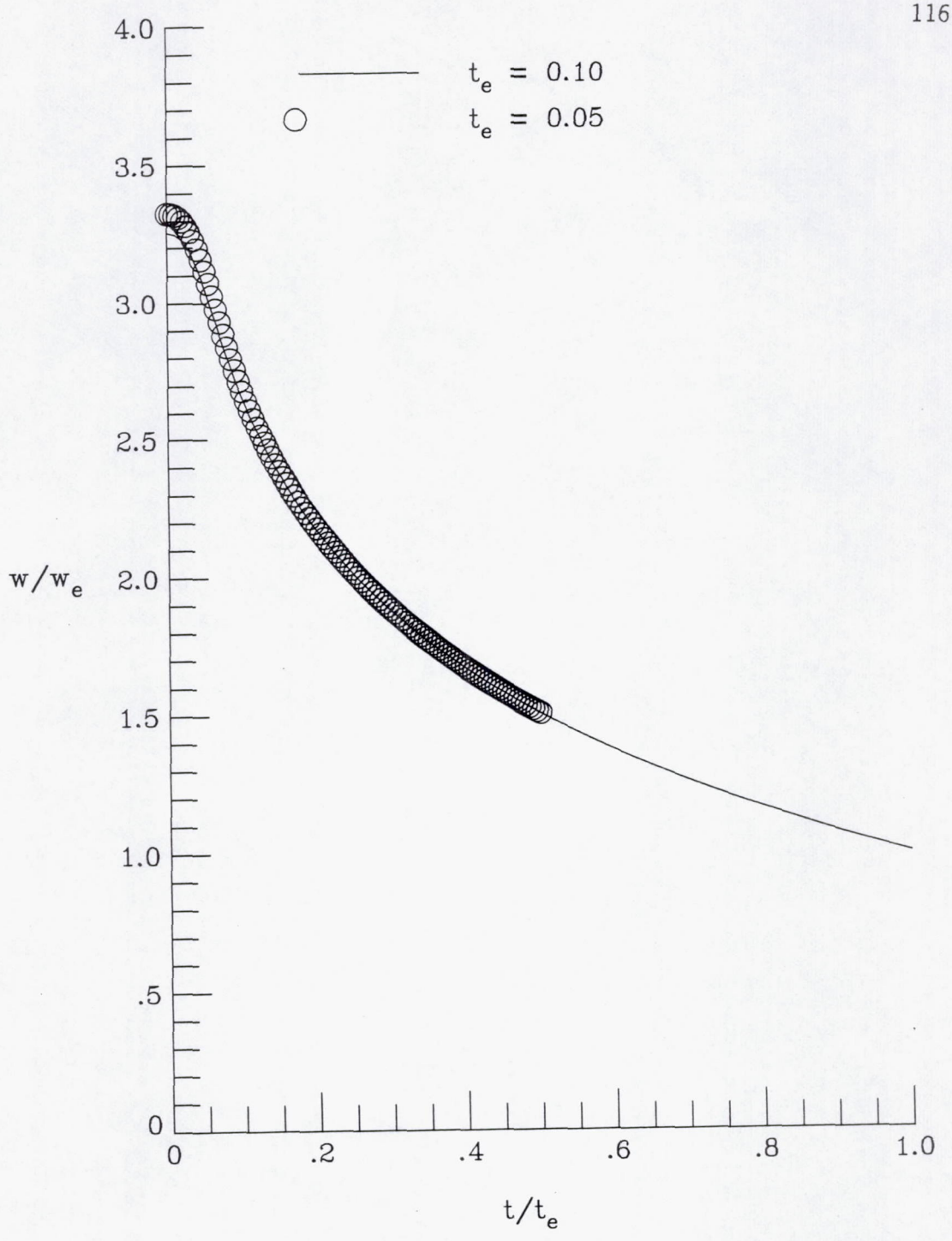

c) axial velocity

Figure 3.3- Continued

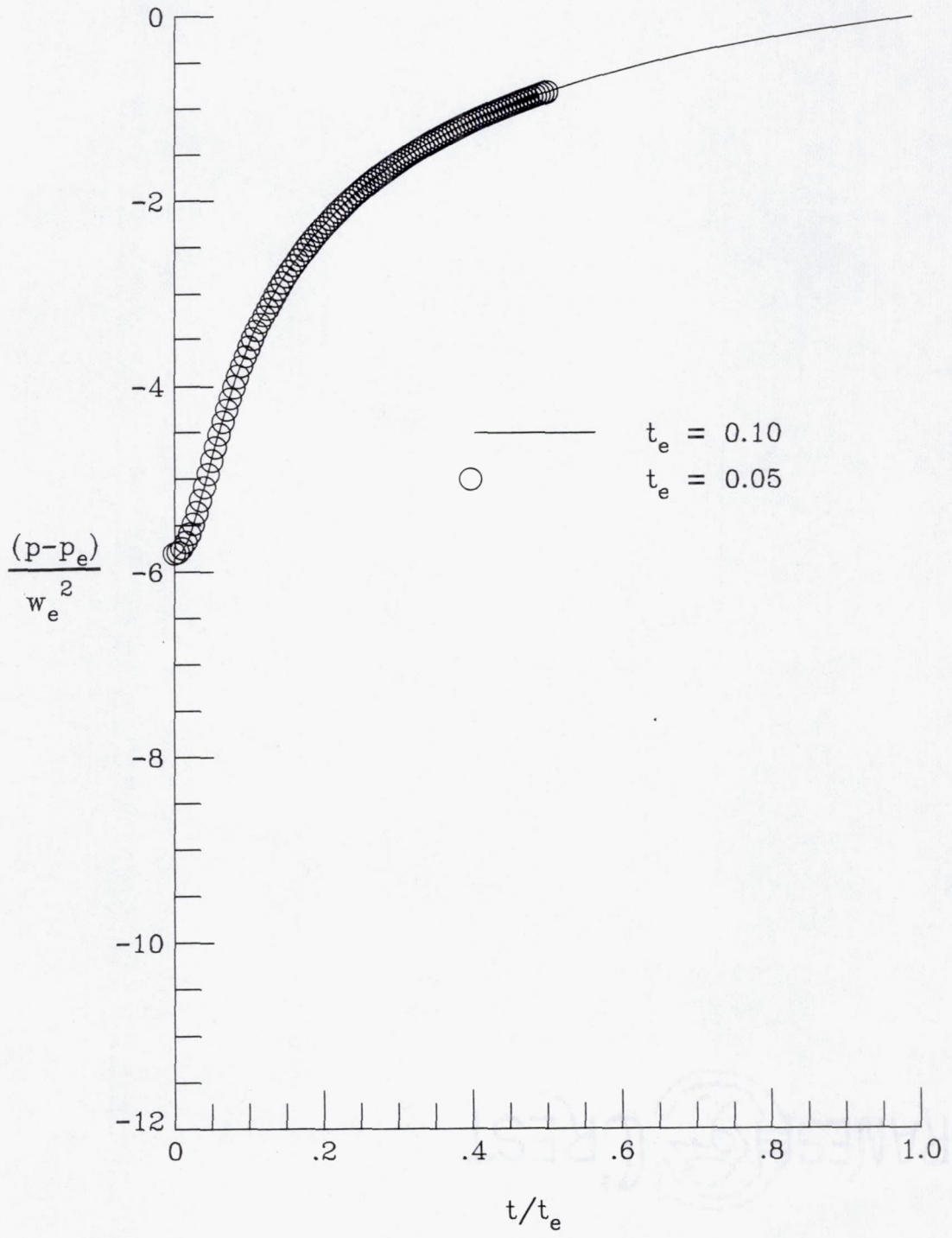

d) static pressure

Figure 3.3- Concluded.

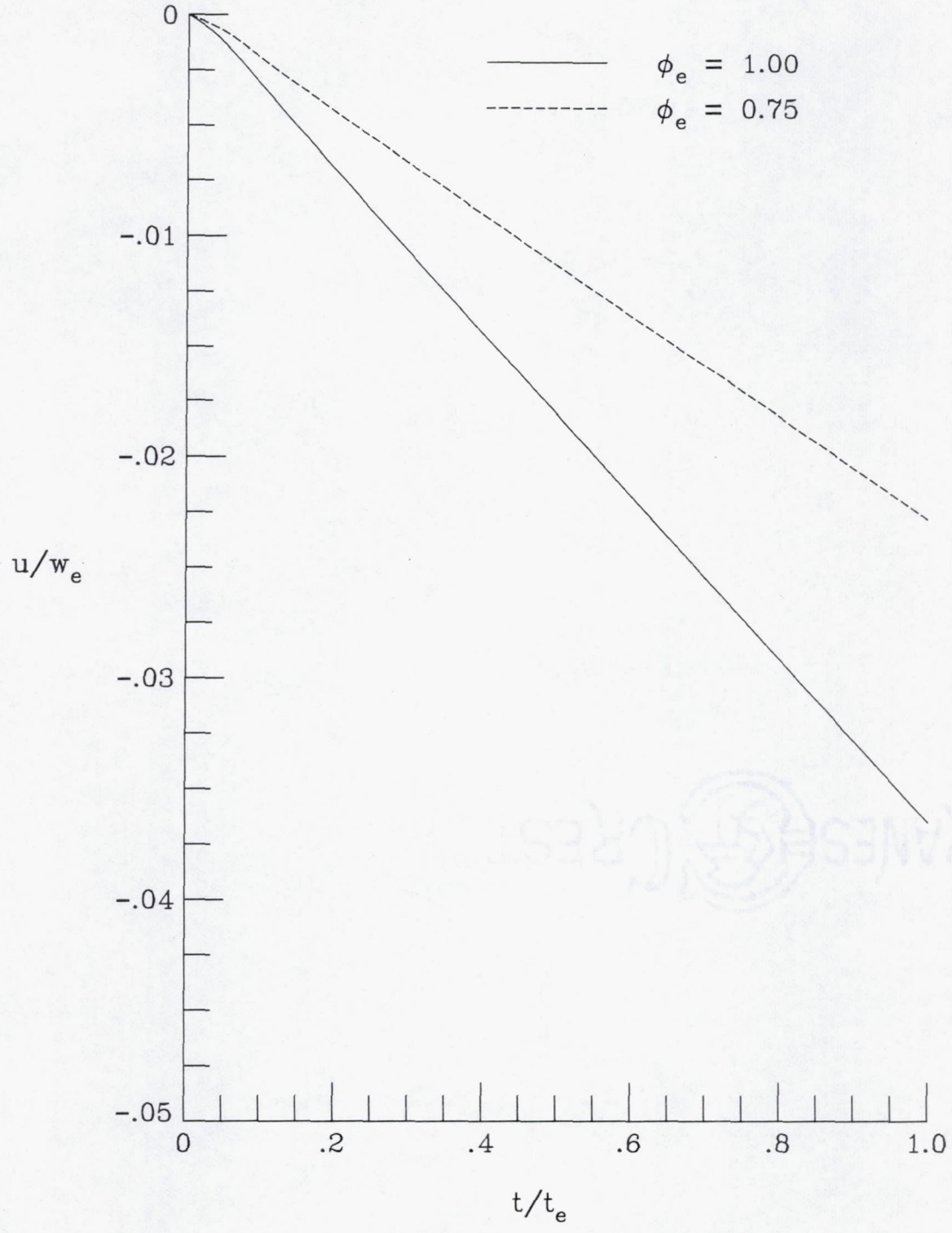

a) radial velocity

Figure 3.4- Edge helix angle effect. Rn = 10^6

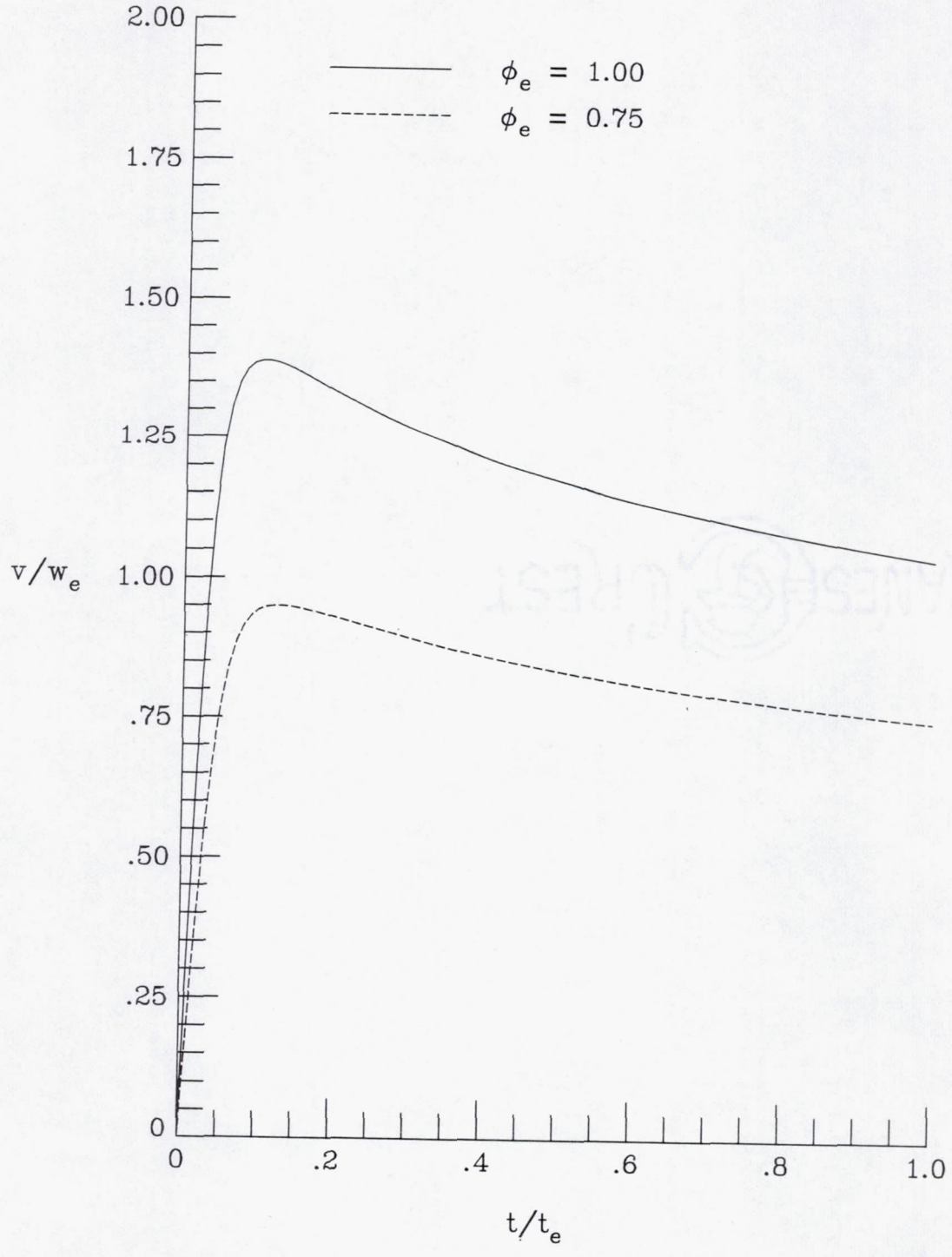

b) angular velocity

Figure 3.4- Continued

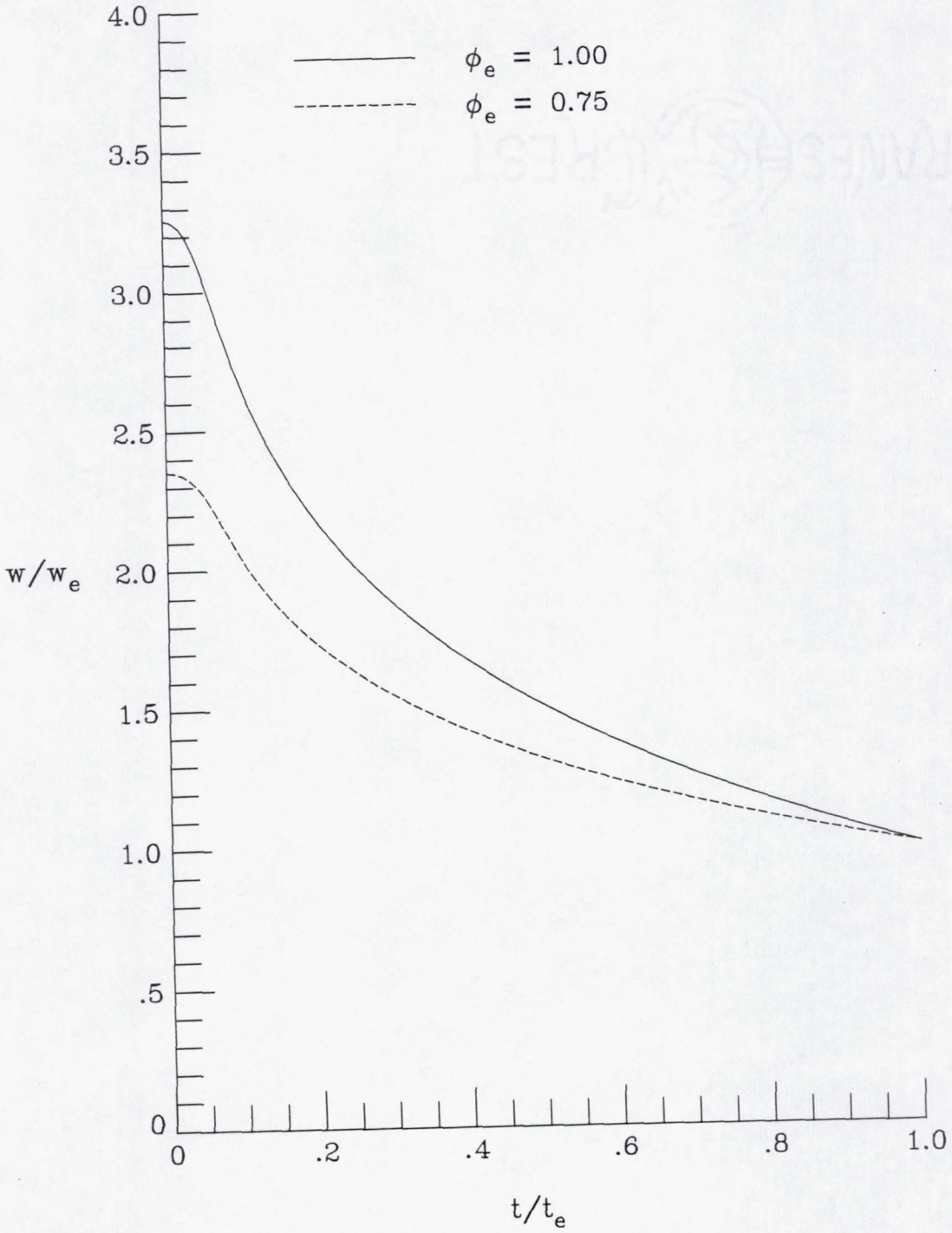

c) axial velocity

Figure 3.4- Continued

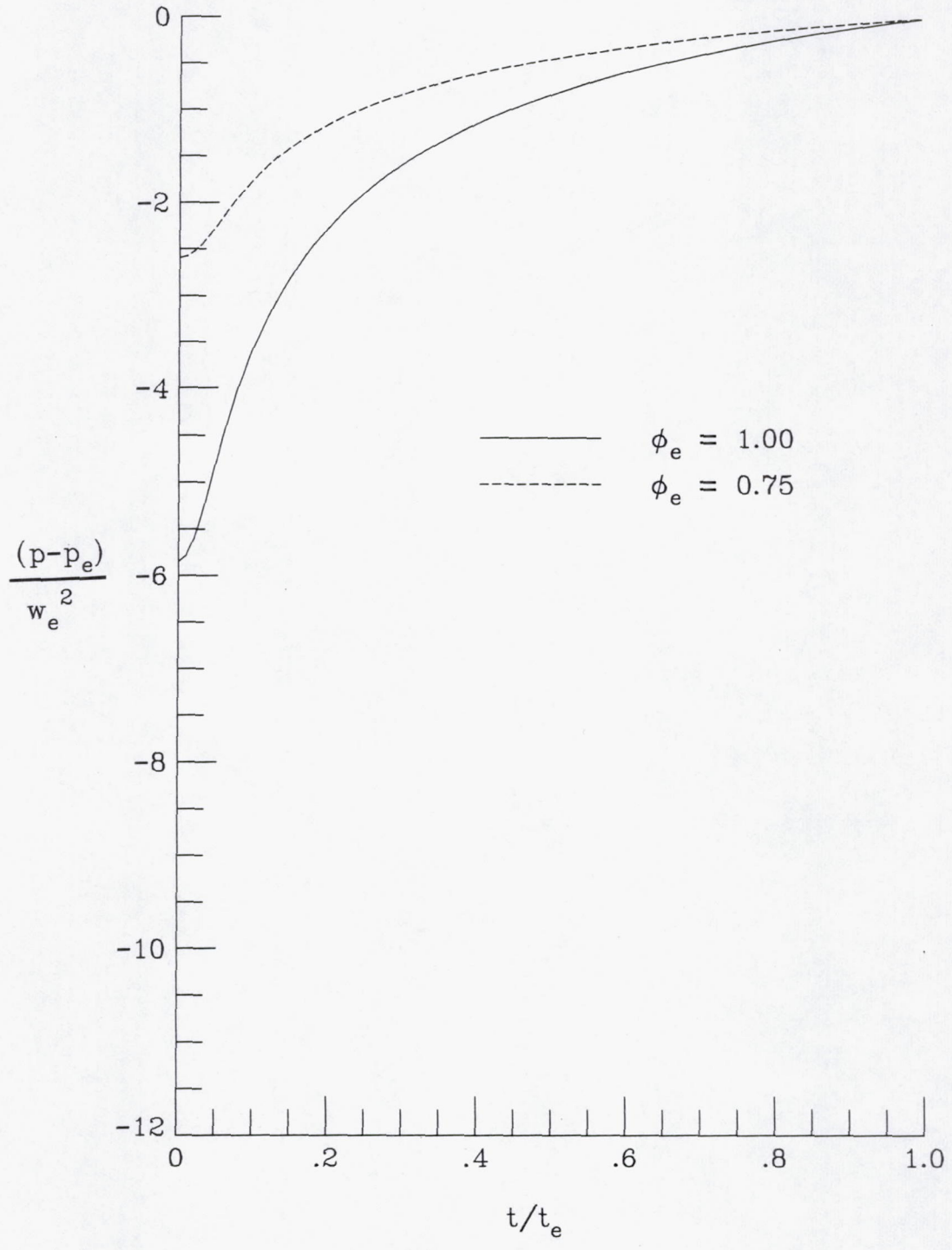

d) static pressure

Figure 3.4- Concluded.

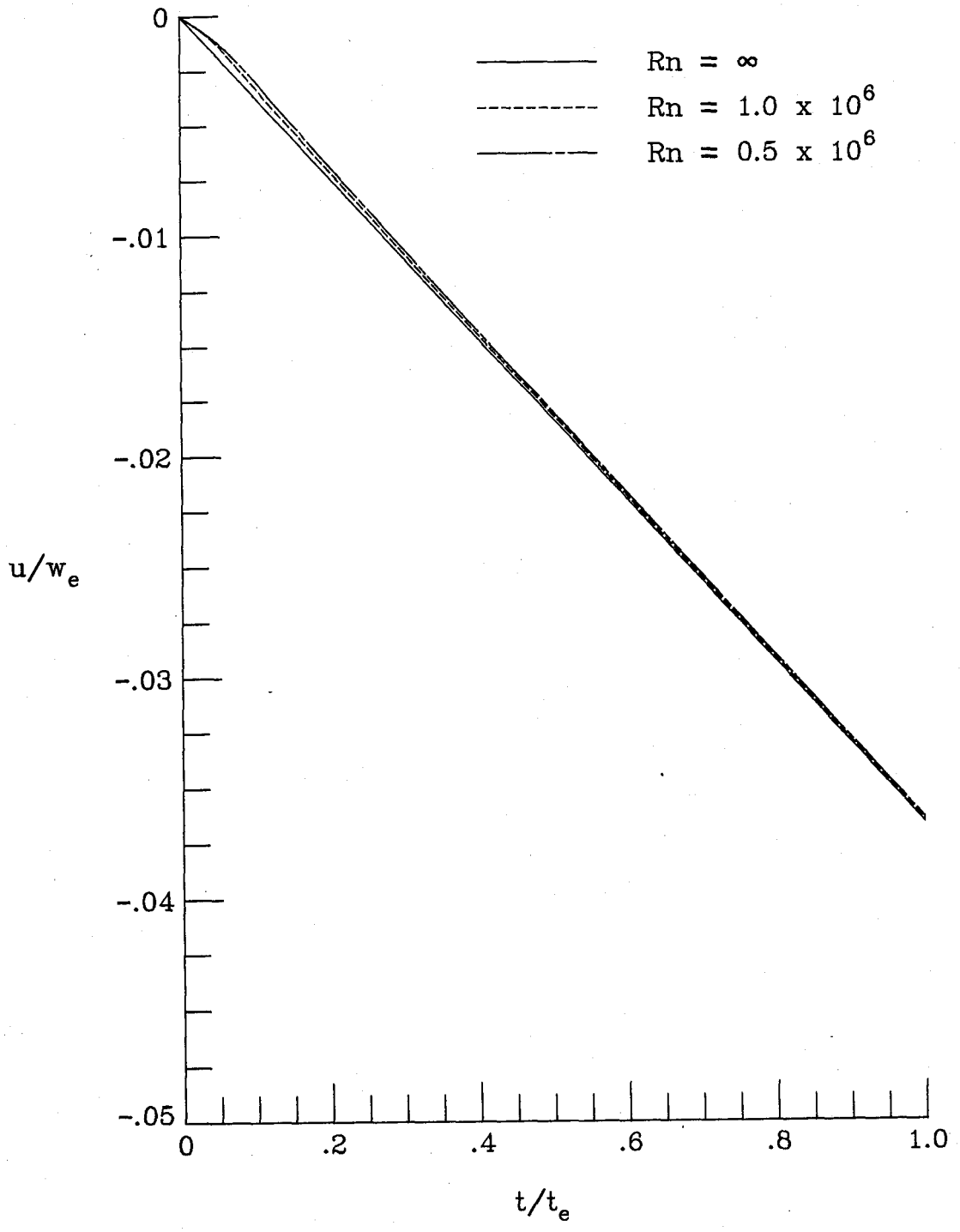

a) radial velocity

Figure 3.5- Reynolds number effect. $\phi_e = 1.$

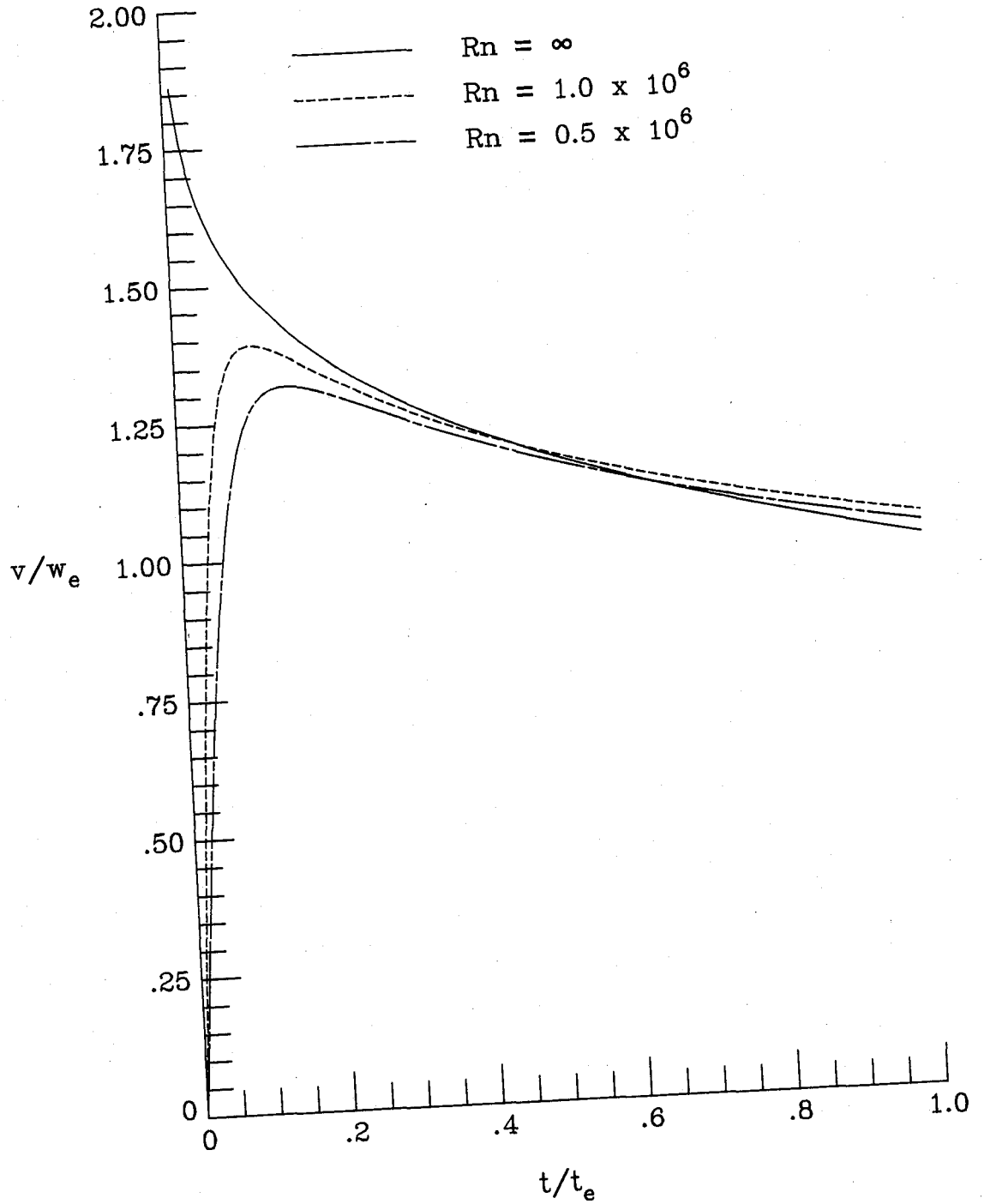

b) angular velocity

Figure 3.5- Continued

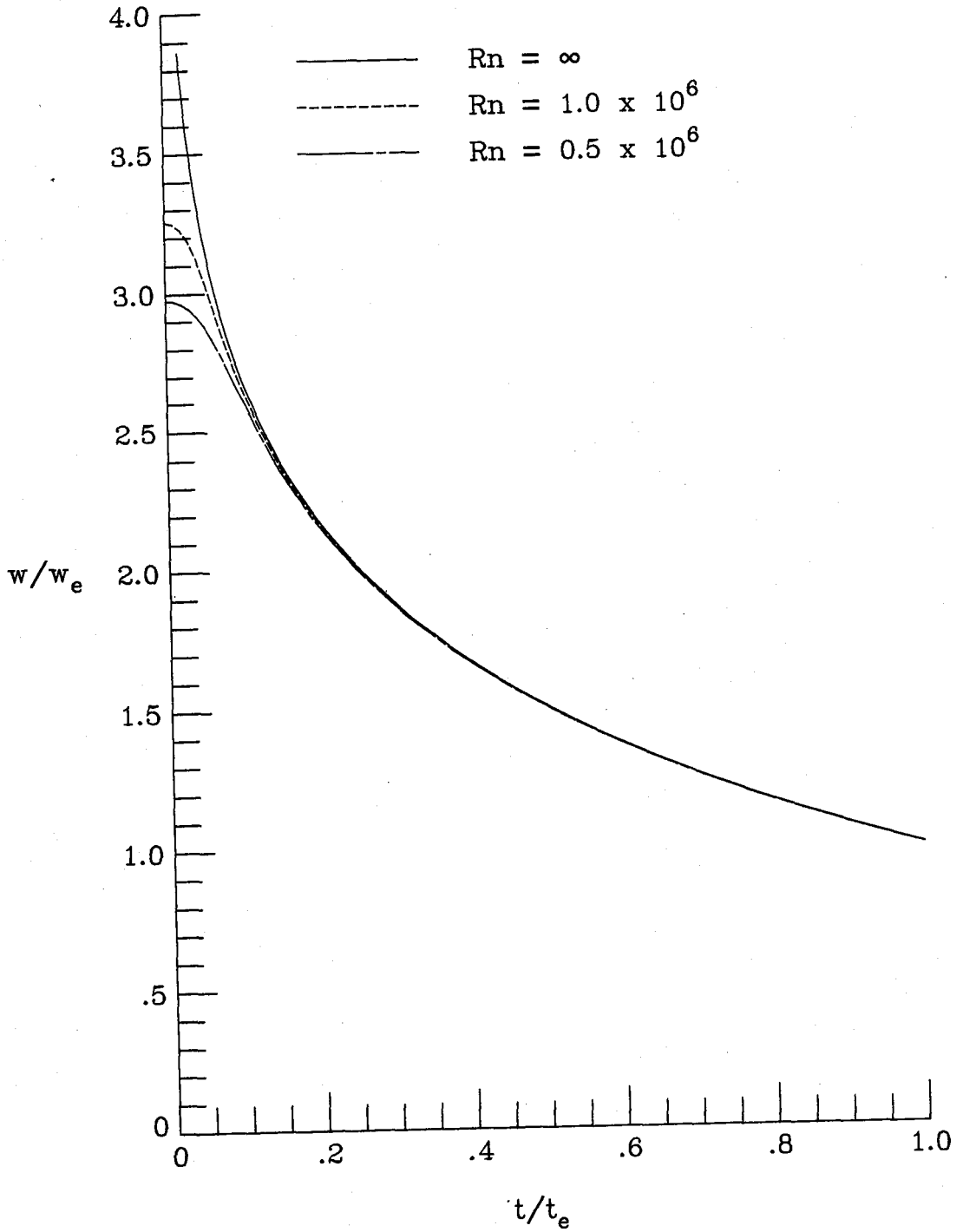

c) axial velocity

Figure 3.5- Continued

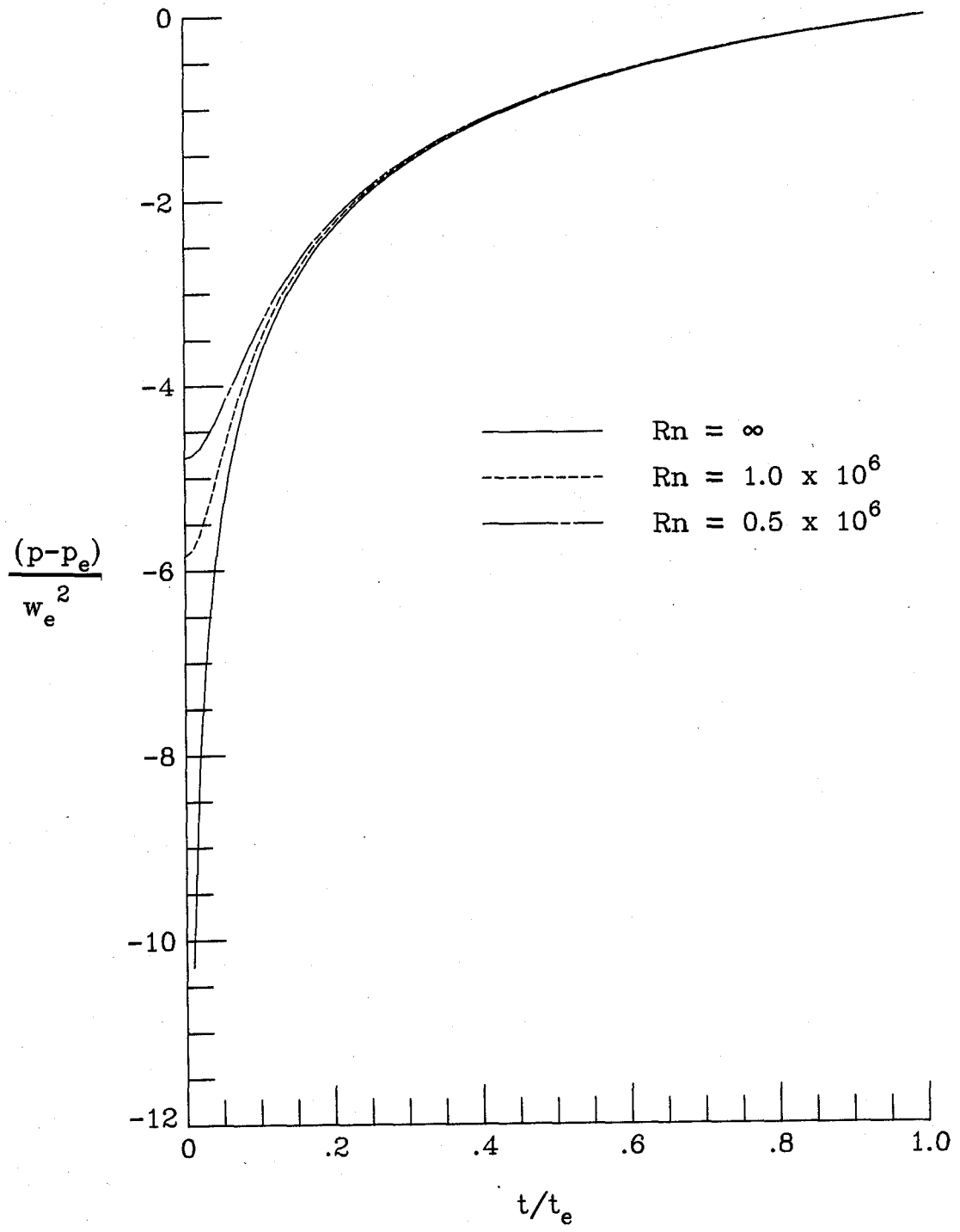

d) static pressure

Figure 3.5- Concluded.

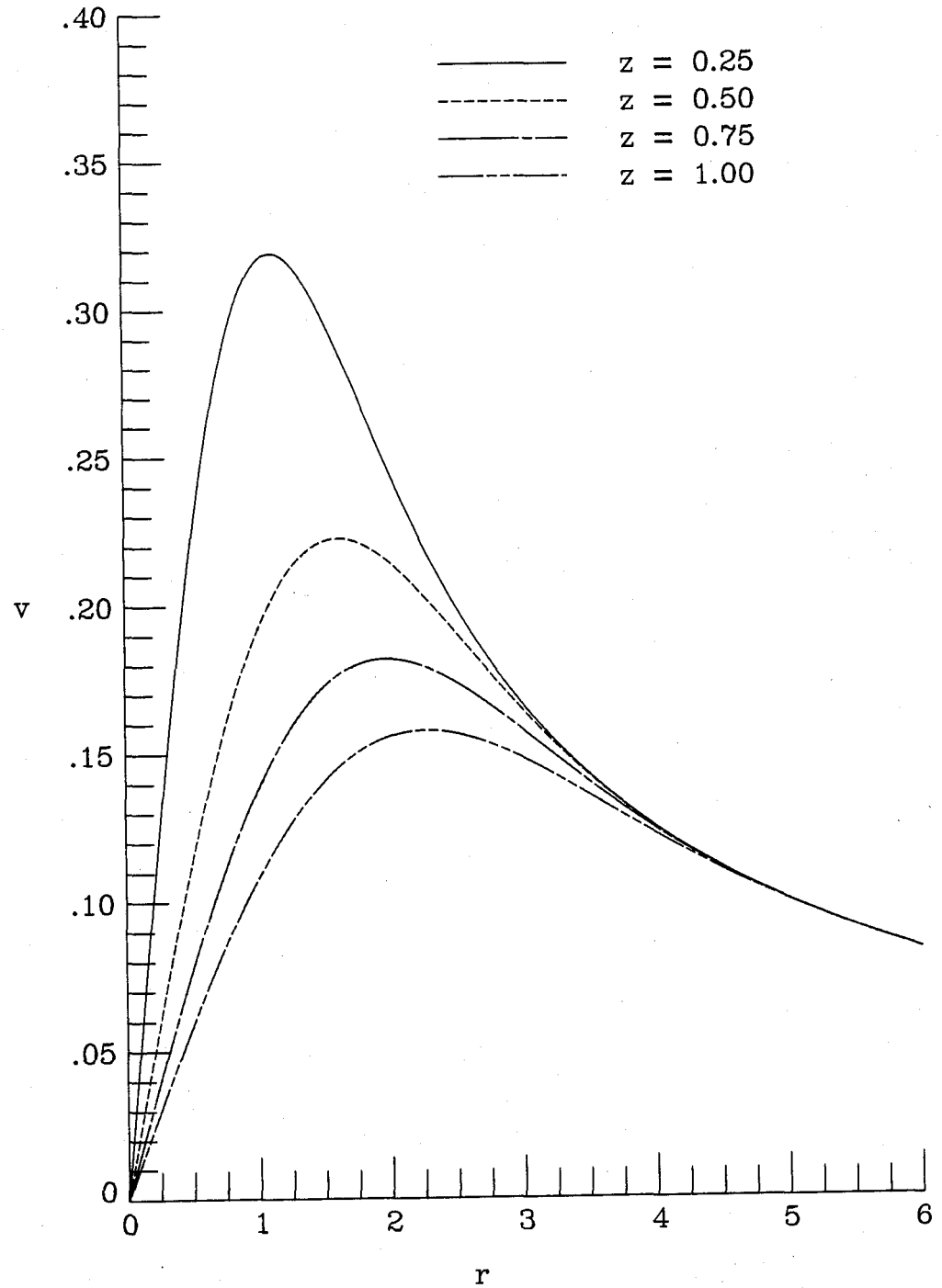

a) angular velocity

Figure 4.1- Generic trailing vortex solution - axial velocity deficit.

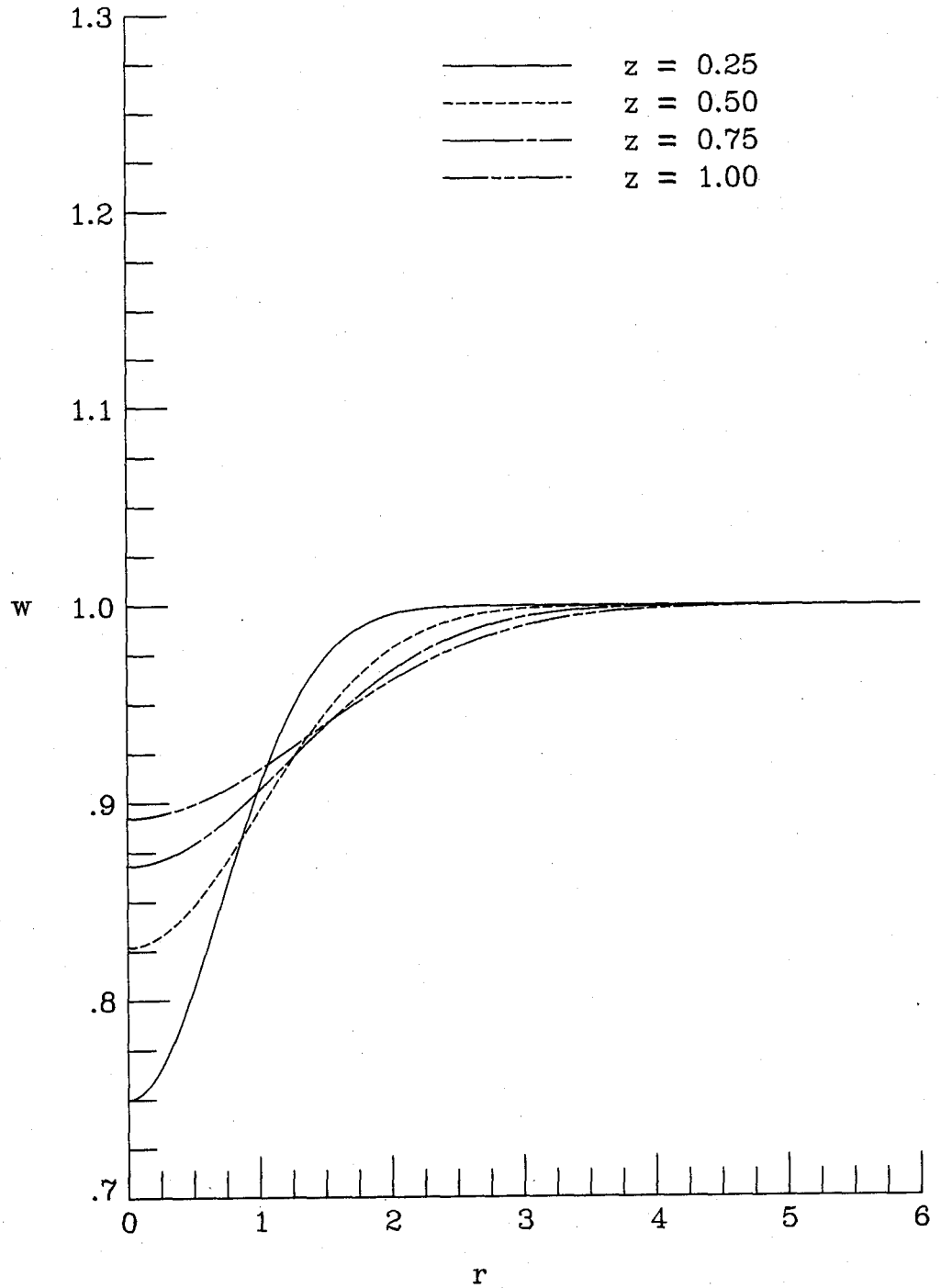

b) axial velocity

Figure 4.1- Concluded.

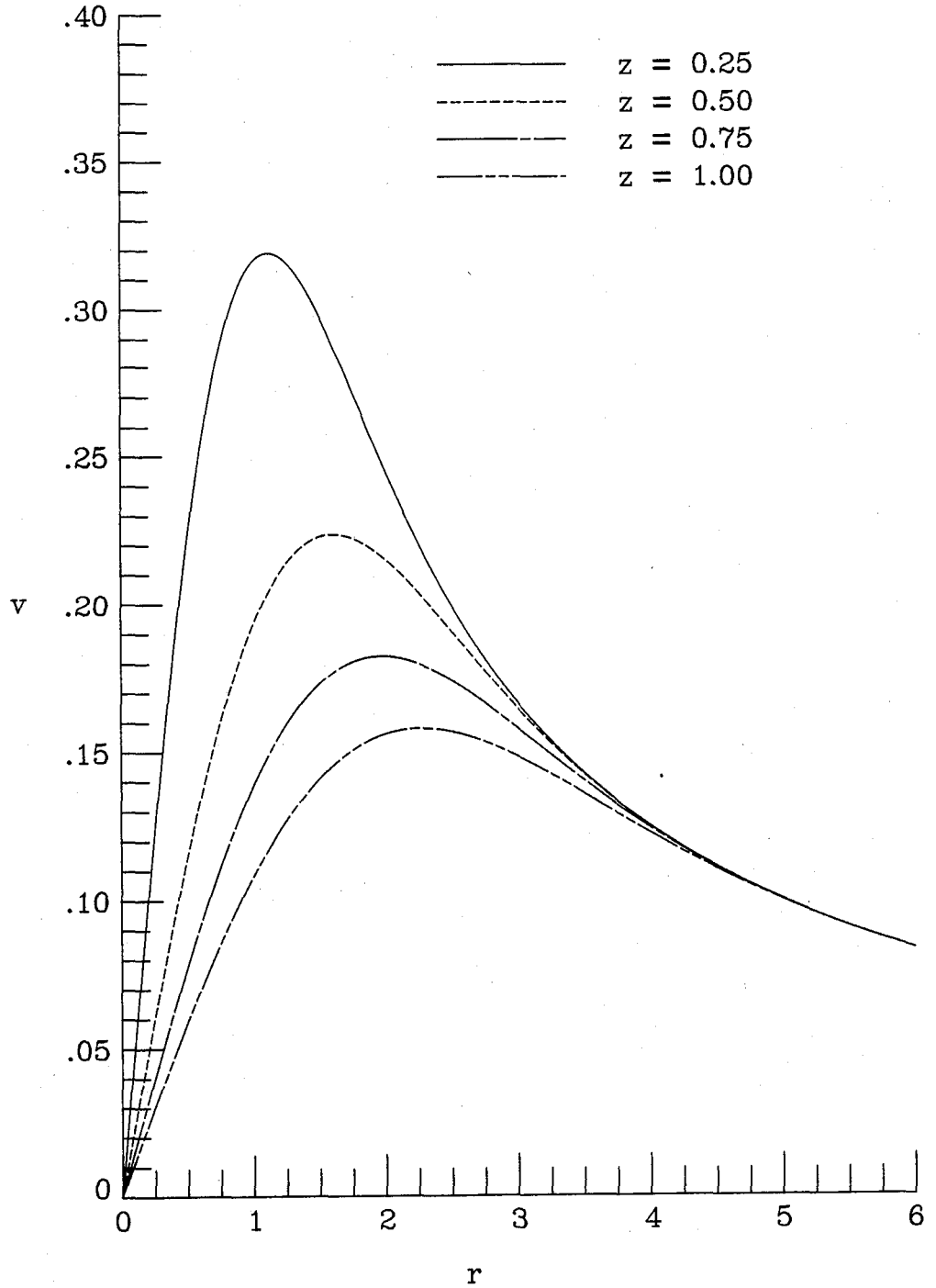

a) angular velocity

Figure 4.2- Generic trailing-vortex solution - axial velocity excess.

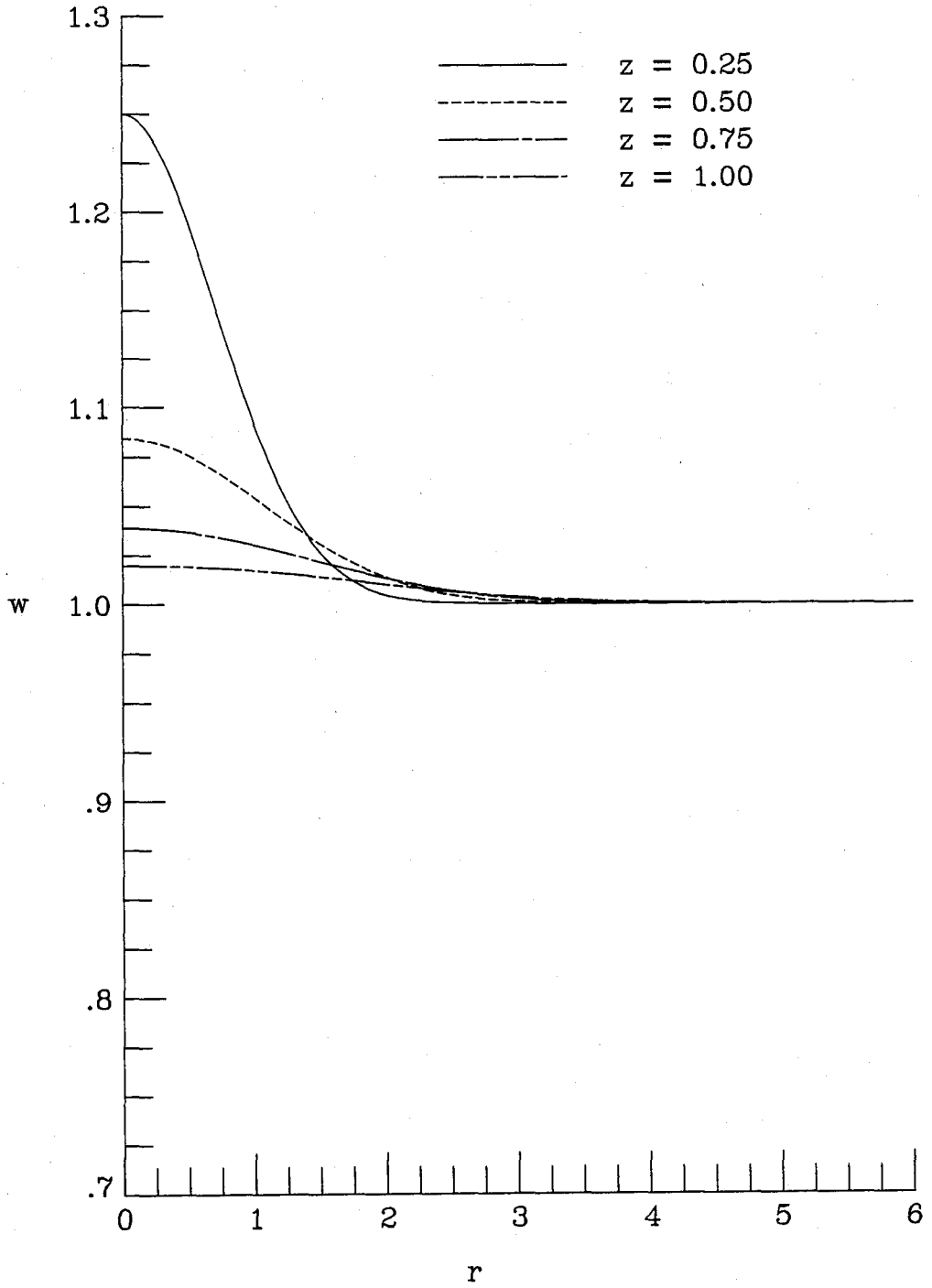

b) axial velocity

Figure 4.2- Concluded.

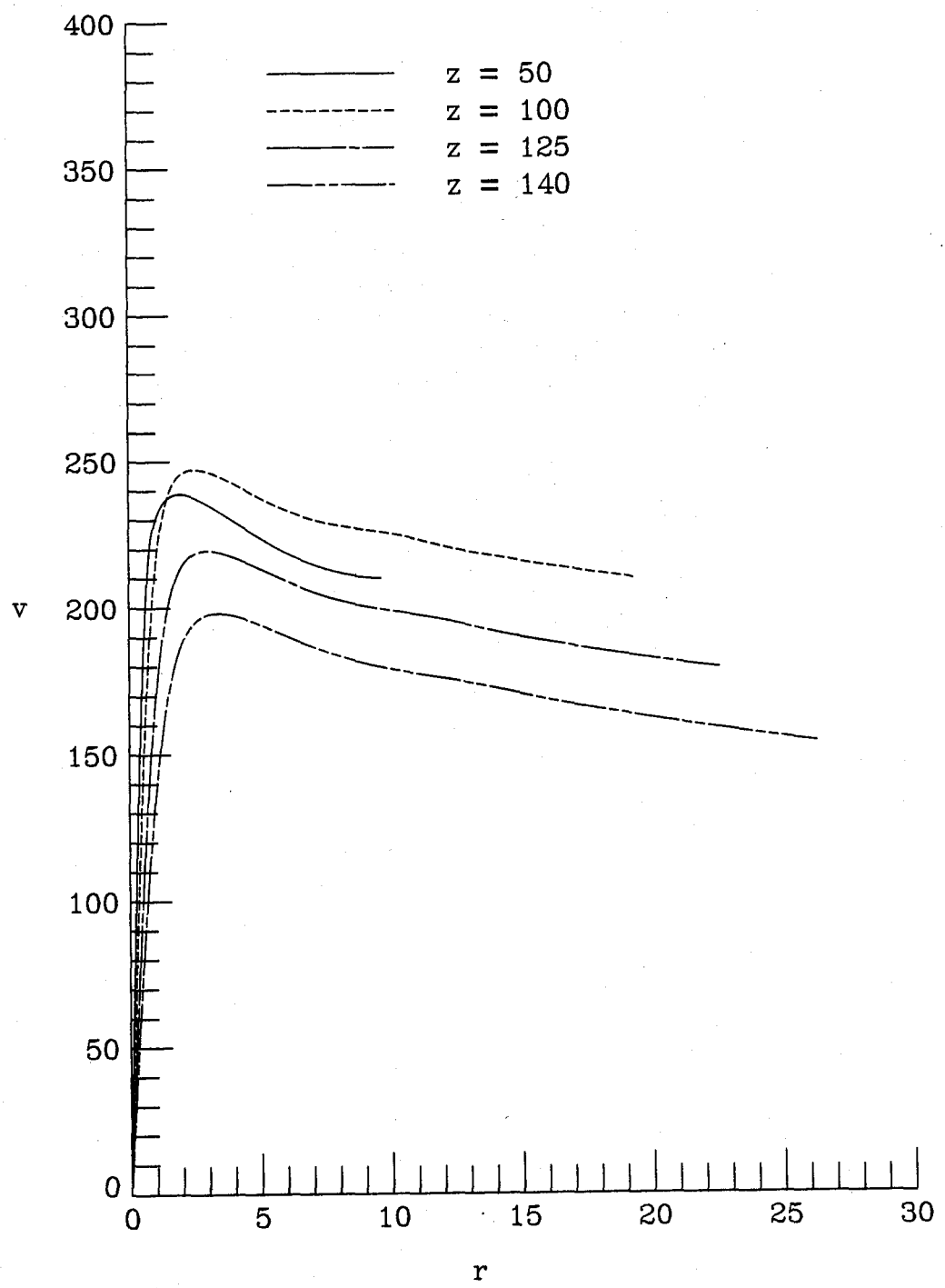

a) angular velocity

Figure 4.3- Generic leading-edge vortex solution.

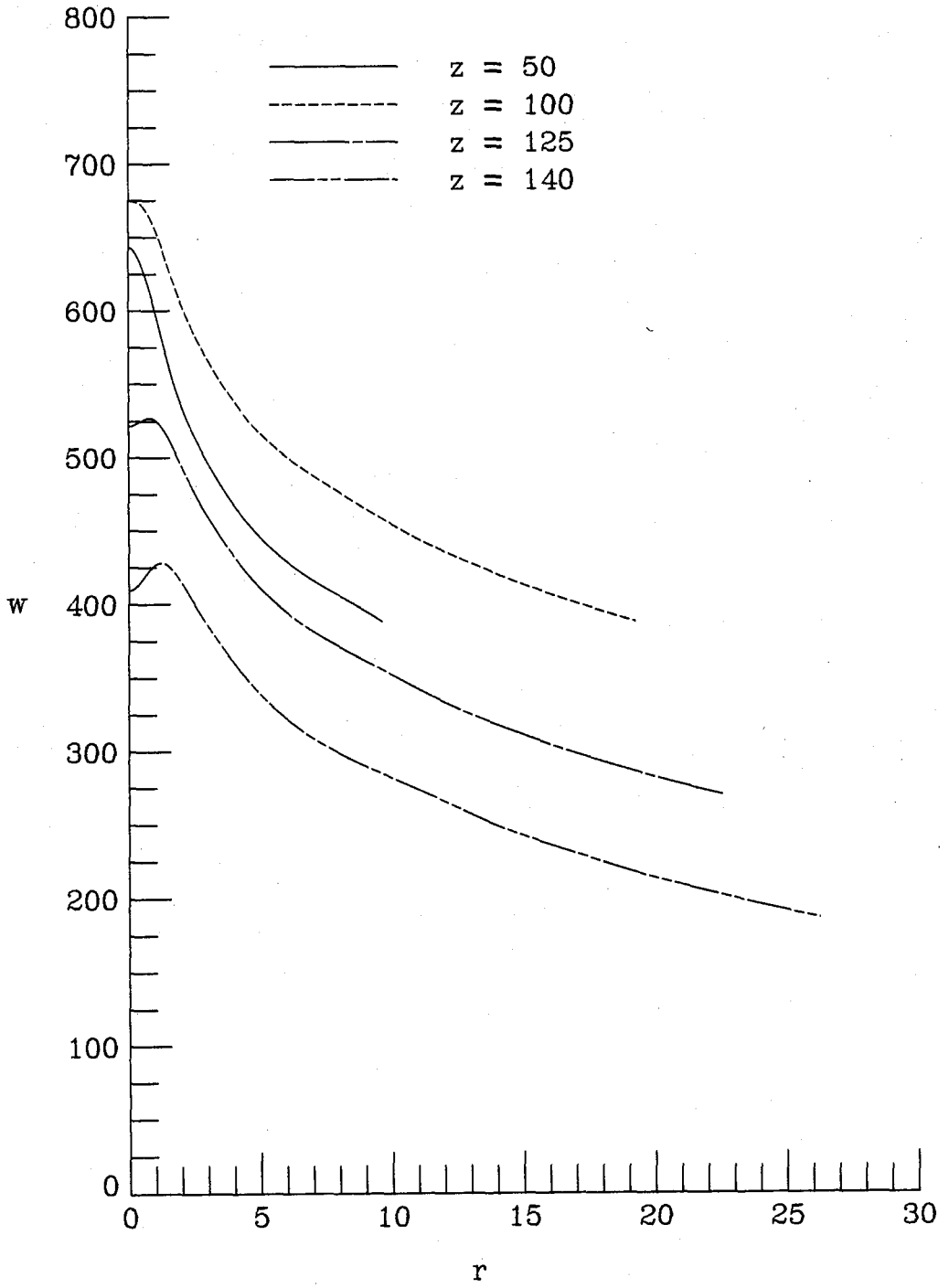

b) axial velocity

Figure 4.3- Continued

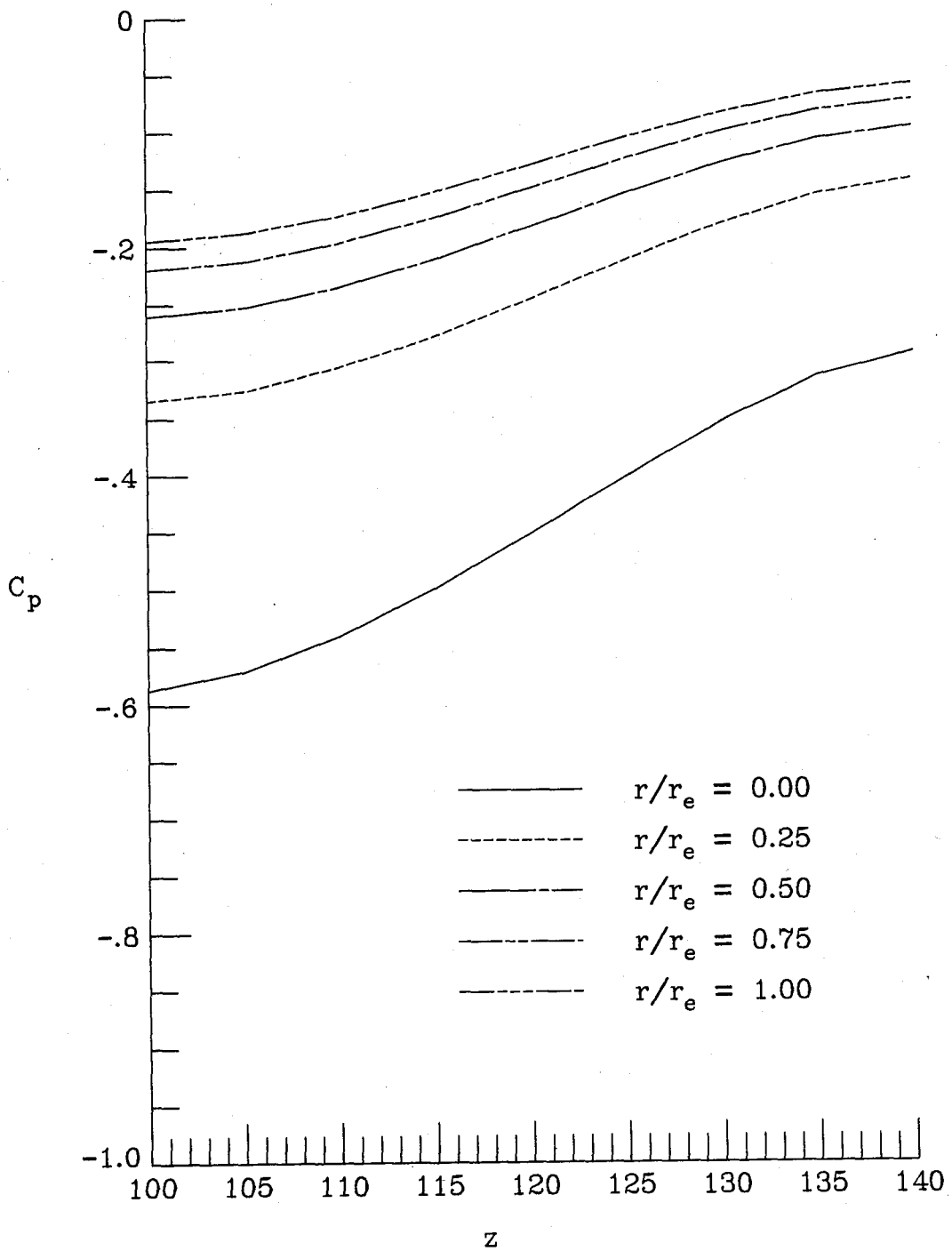

c) static pressure

Figure 4.3- Continued

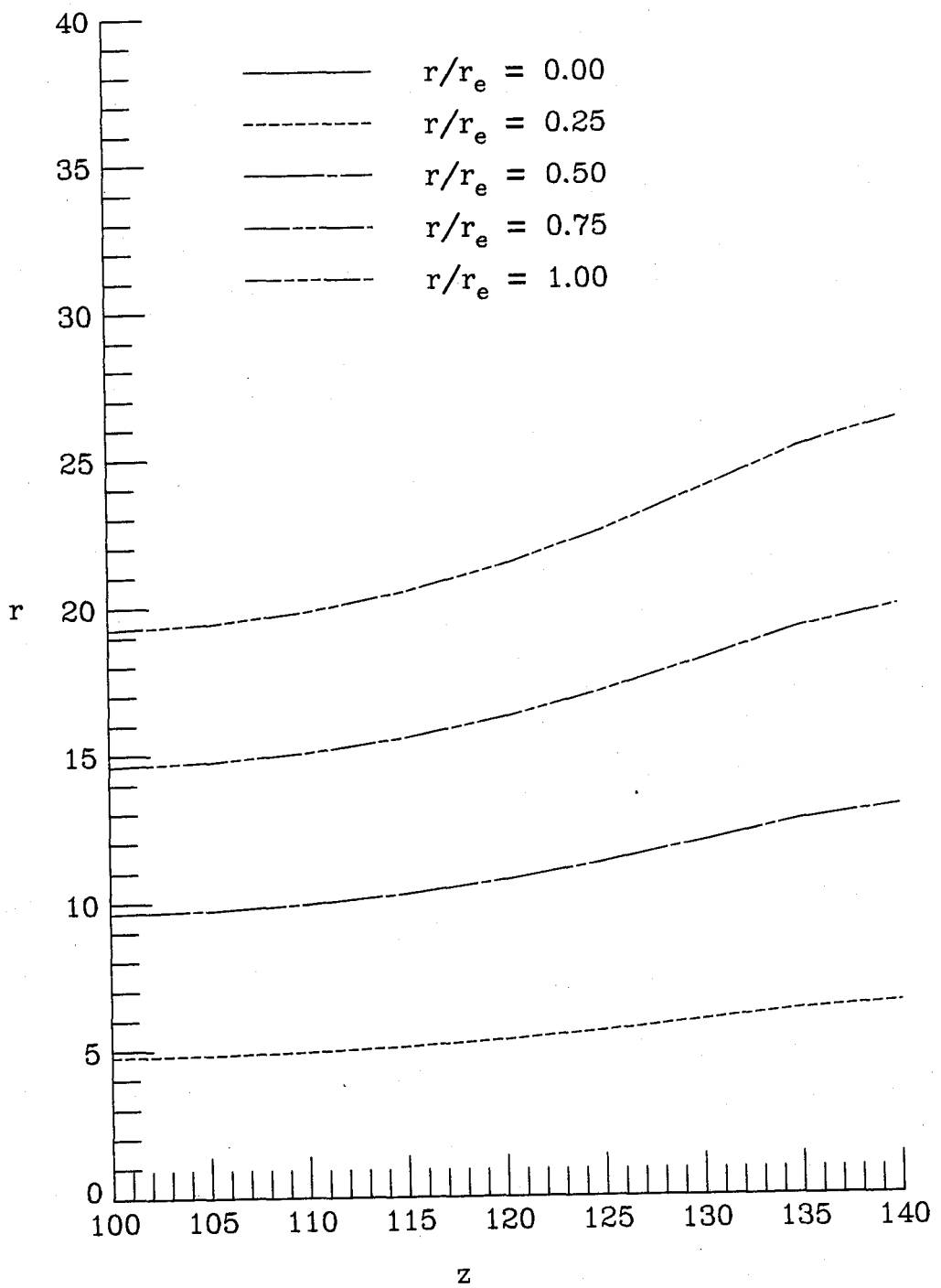

d) stream tube geometry

Figure 4.3- Concluded.

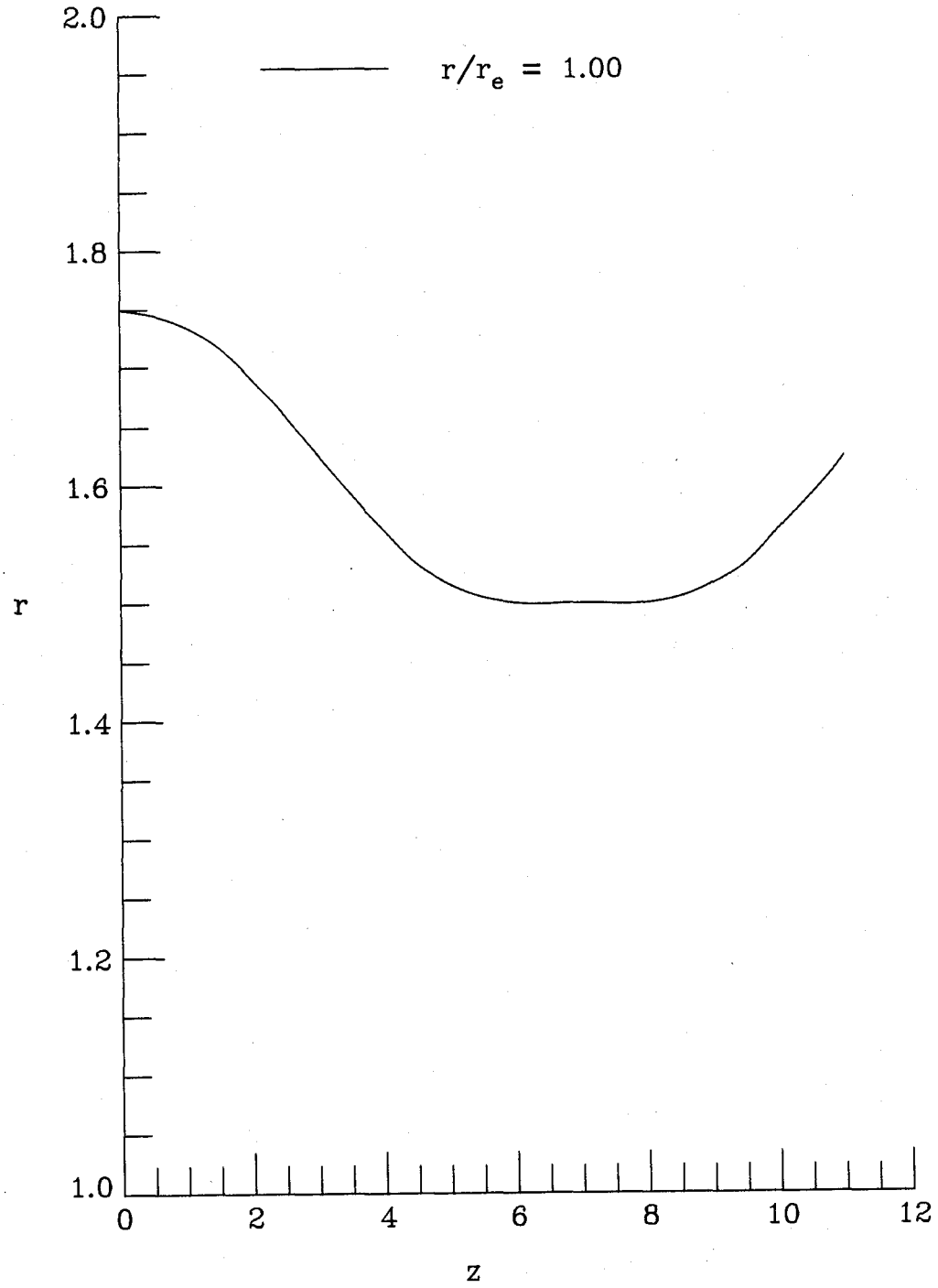

Figure 4.4- Test section contraction of Kirkpatrick (1964).

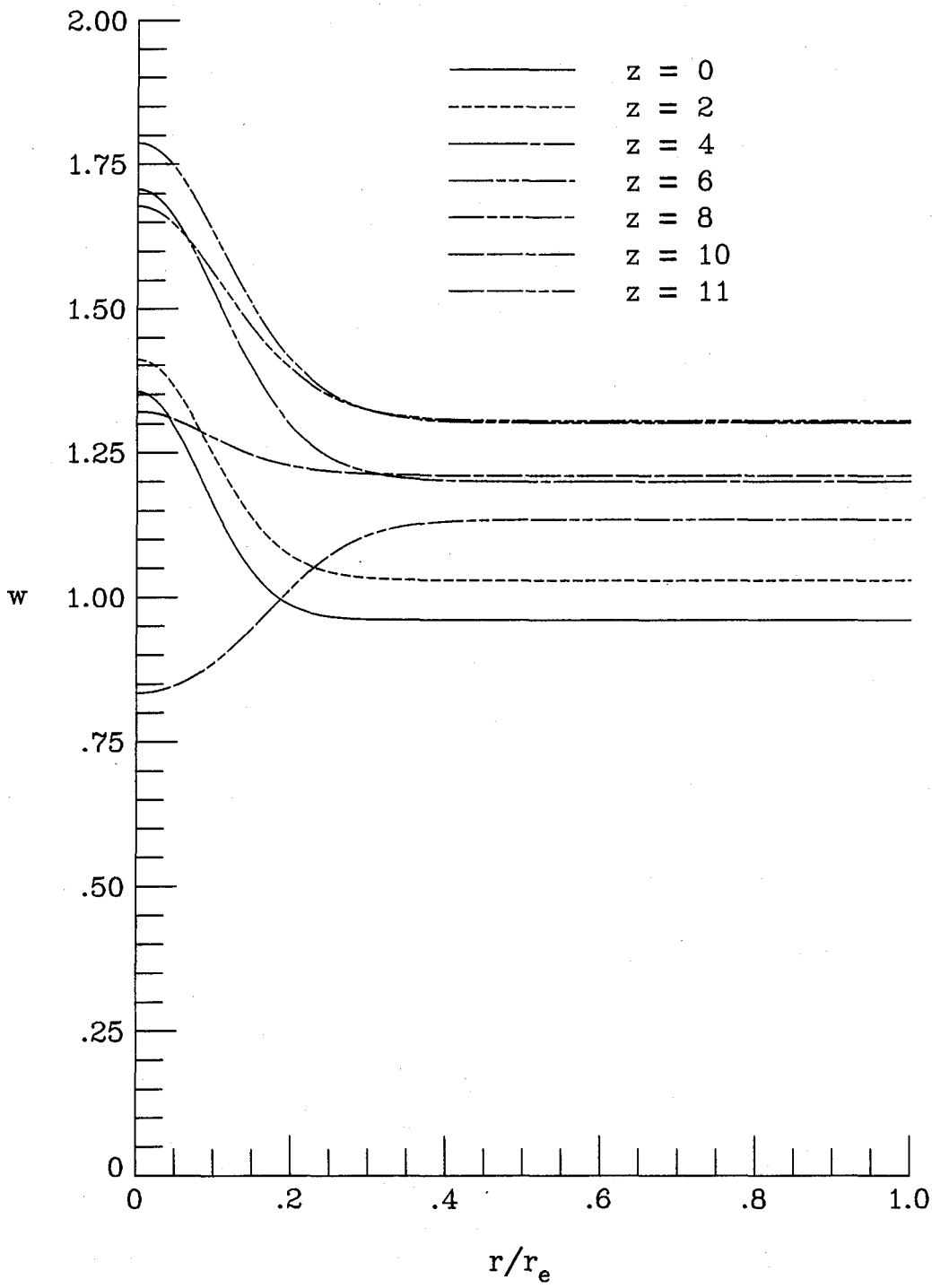

a) axial velocity

Figure 4.5- Tube vortex solution with breakdown.

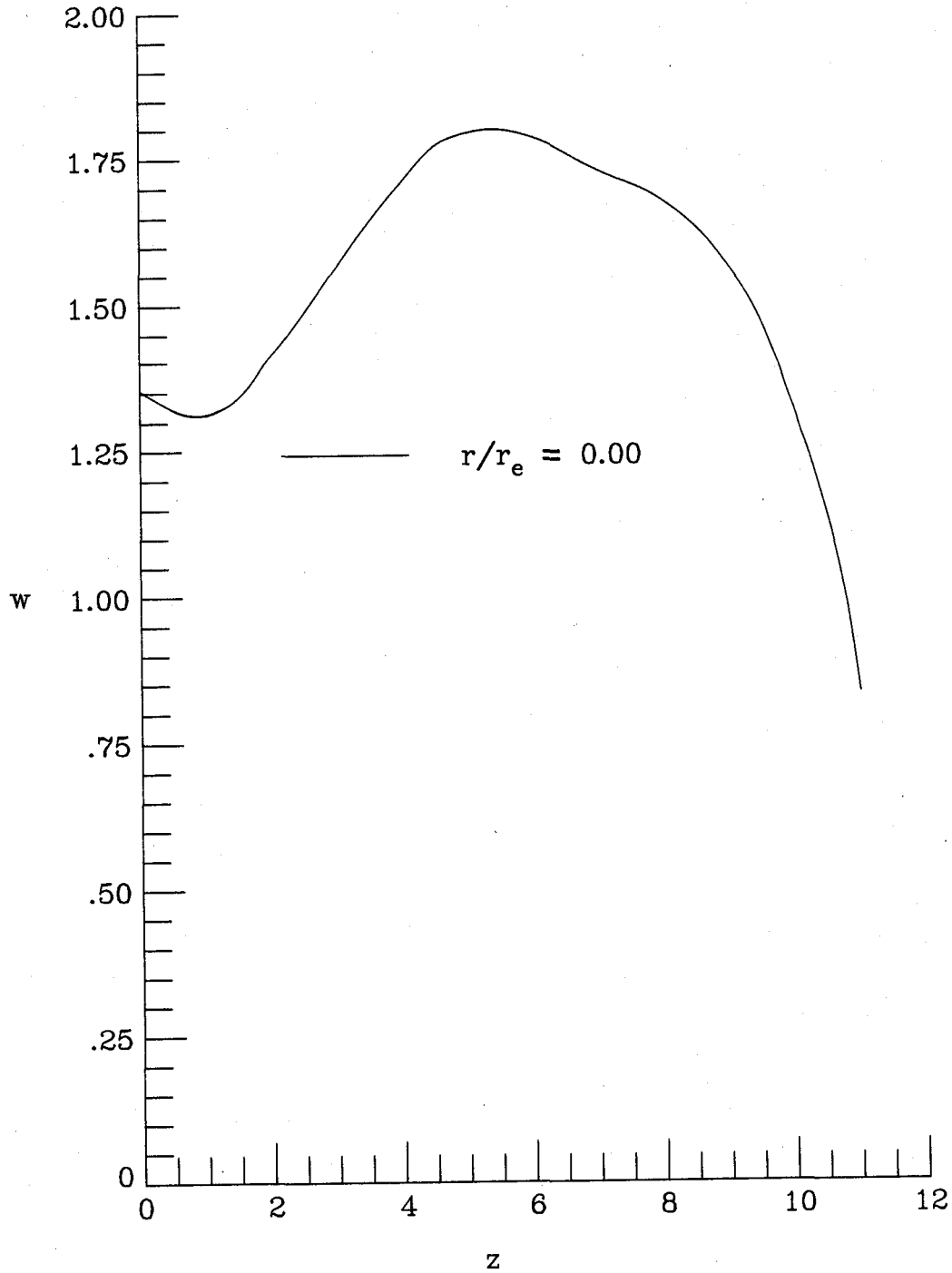

b) axial velocity at axis

Figure 4.5- Concluded.

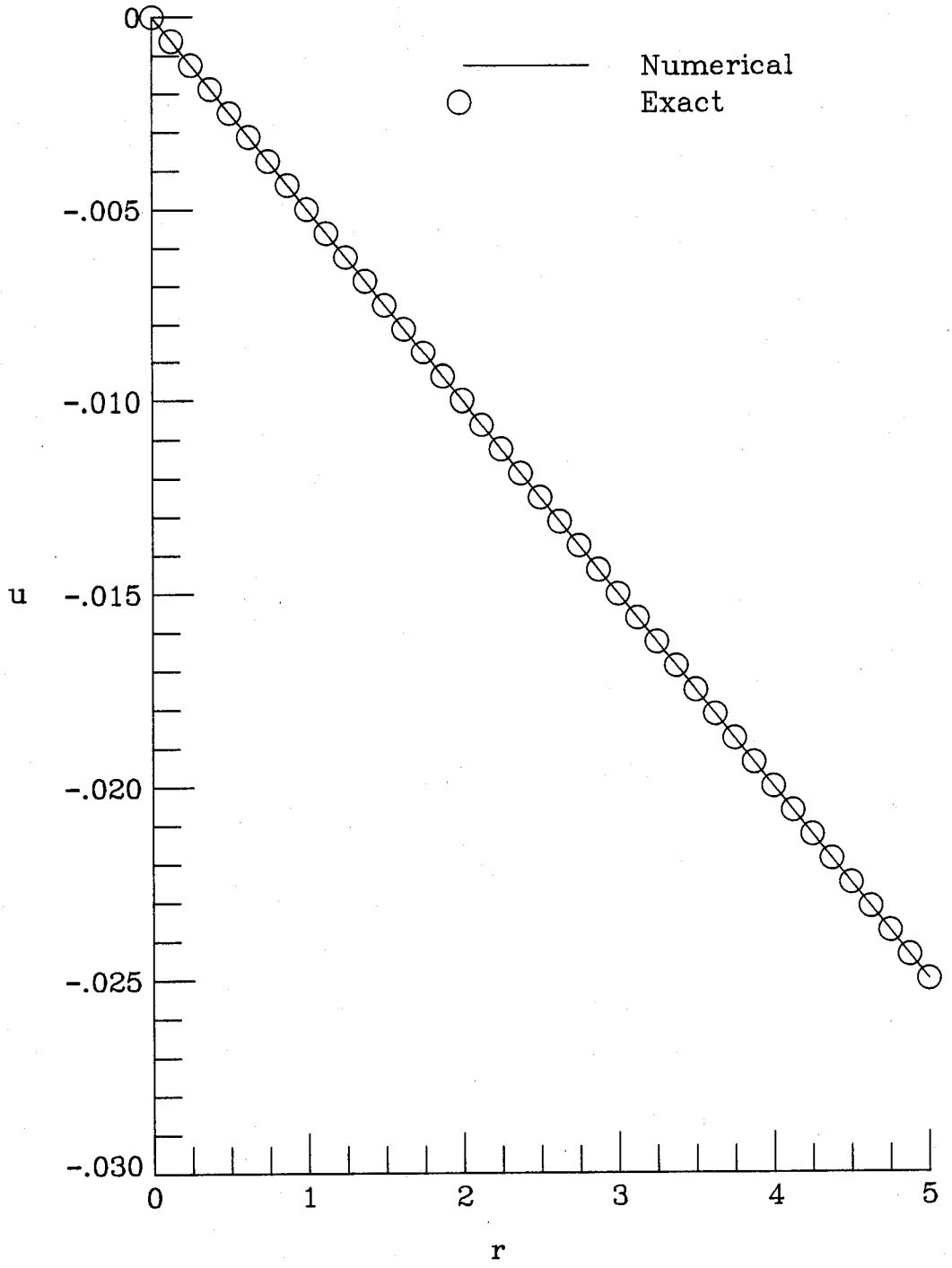

a) radial velocity

Figure 4.6- Calculation of Burgers' vortex.

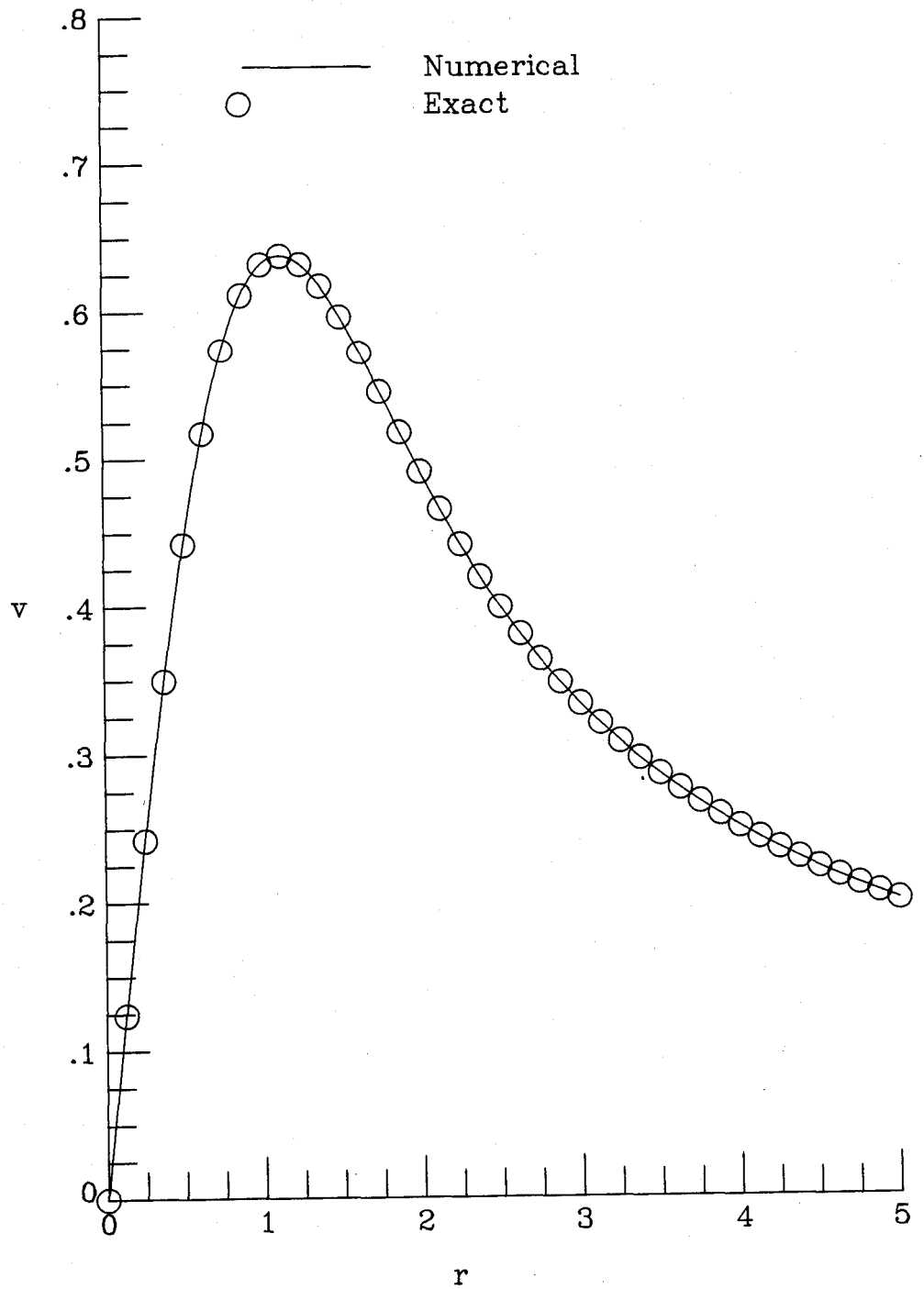

b) angular velocity

Figure 4.6- Continued

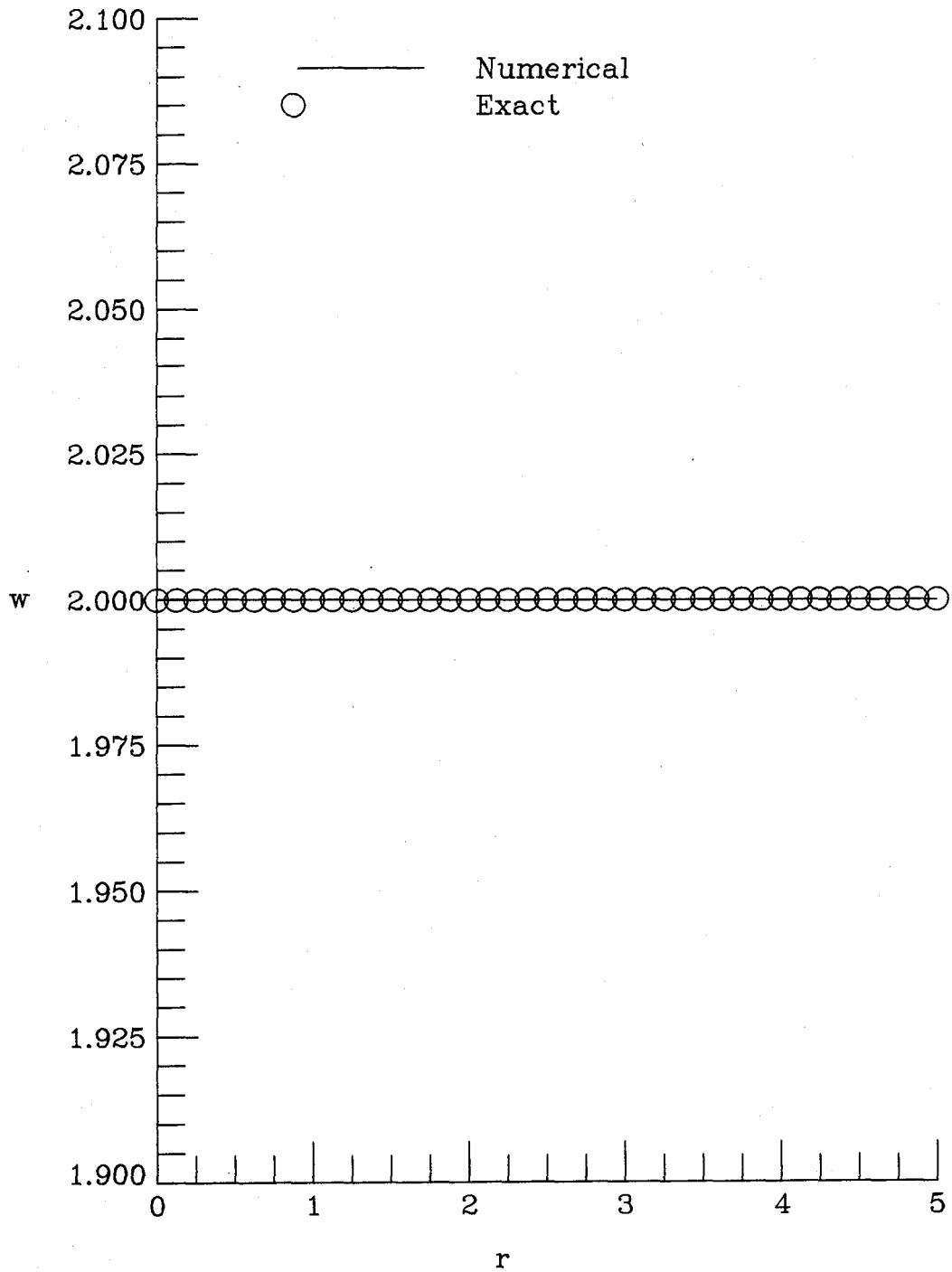

c) axial velocity

Figure 4.6- Continued

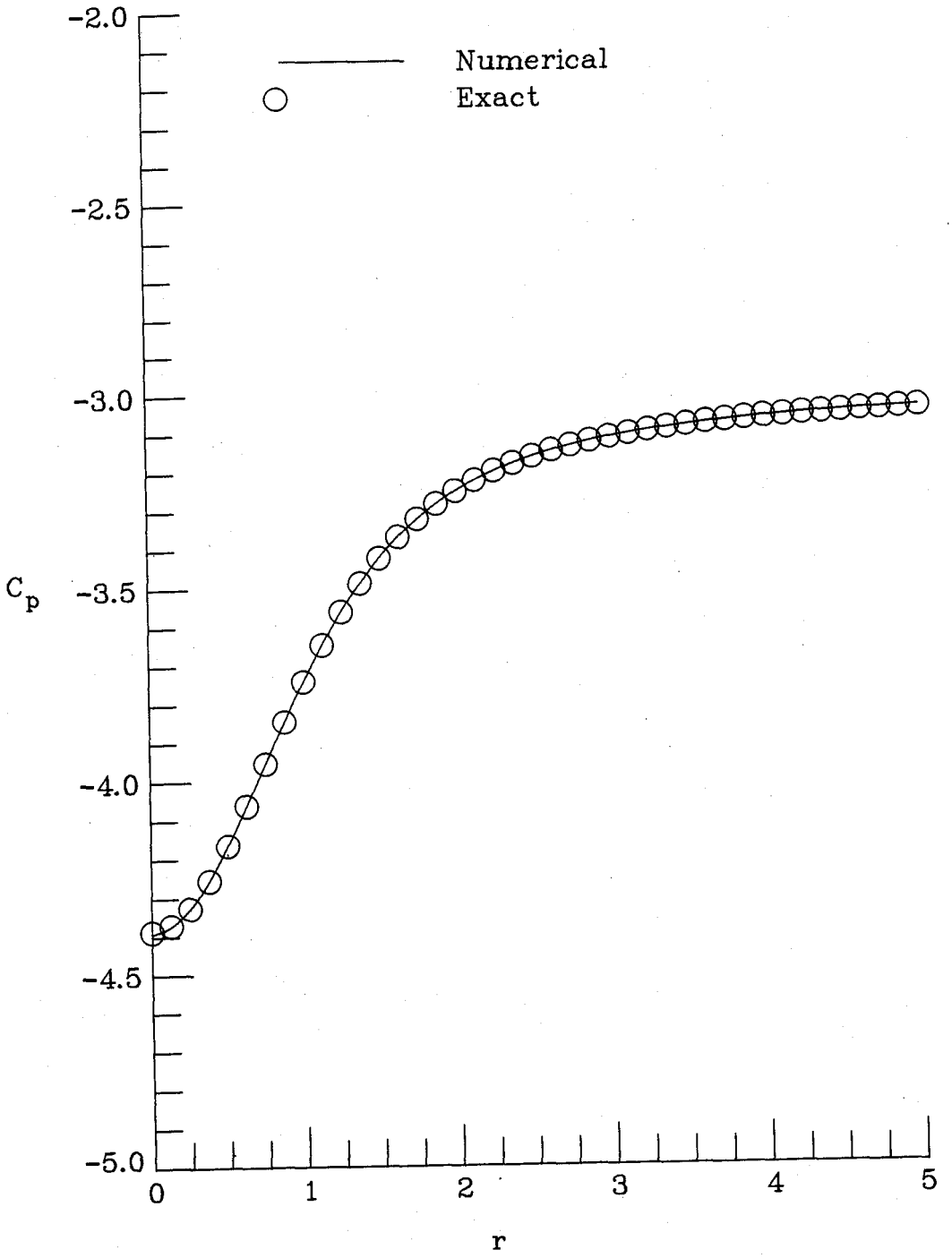

d) static pressure

Figure 4.6- Continued

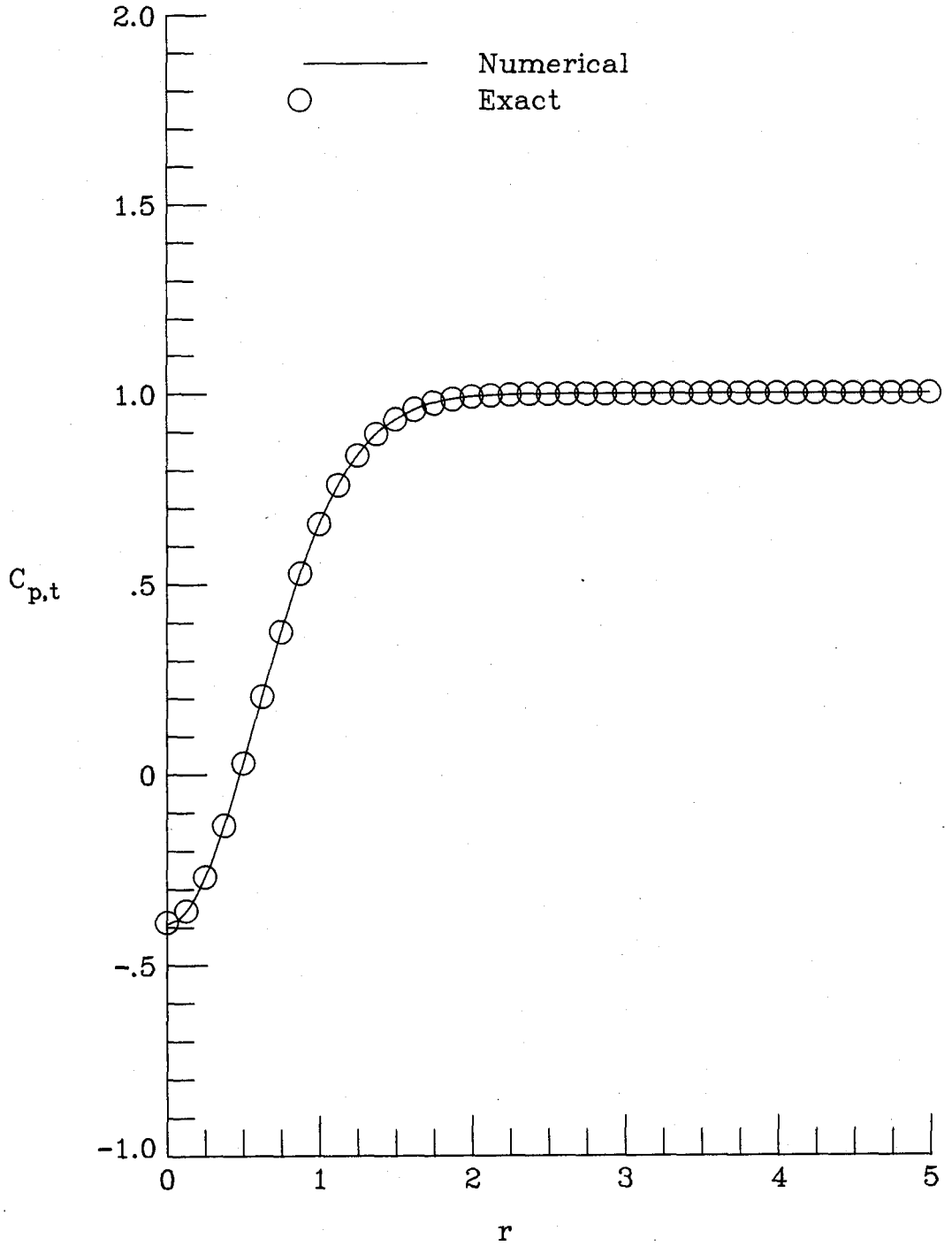

e) Total pressure

Figure 4.6- Concluded.

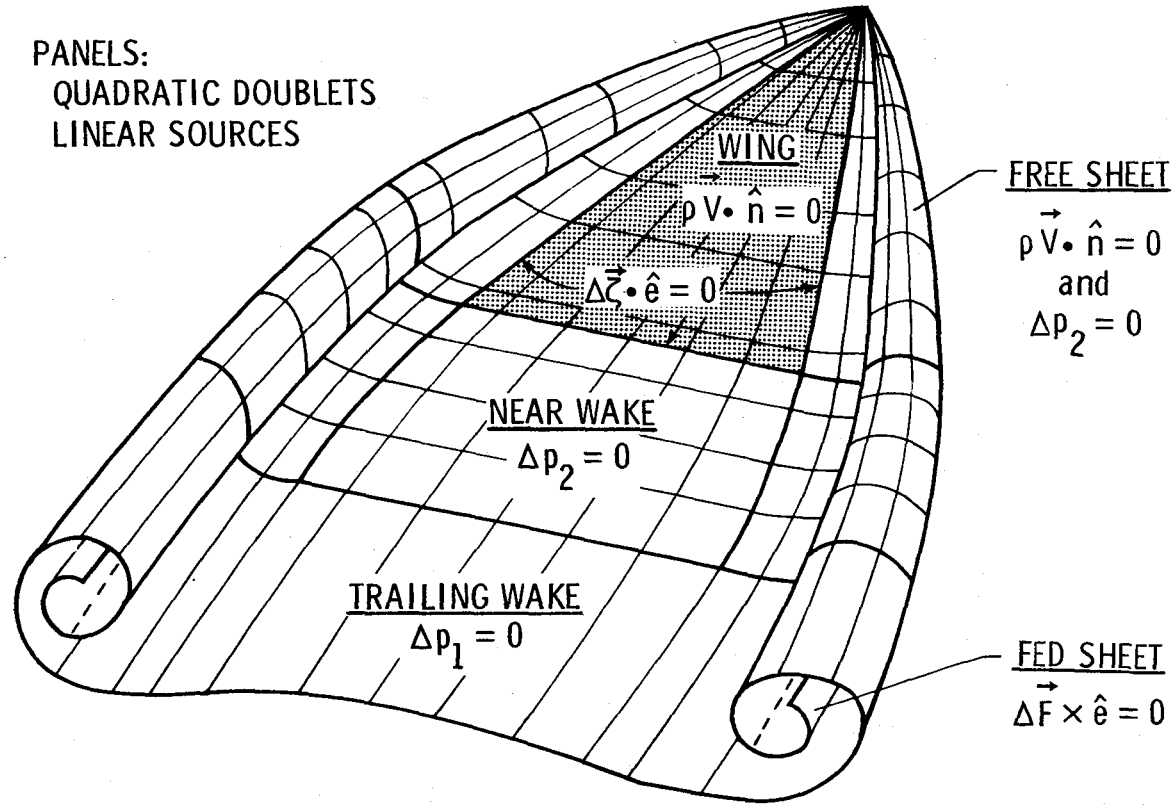

Figure 5.1- Free vortex sheet formulation.

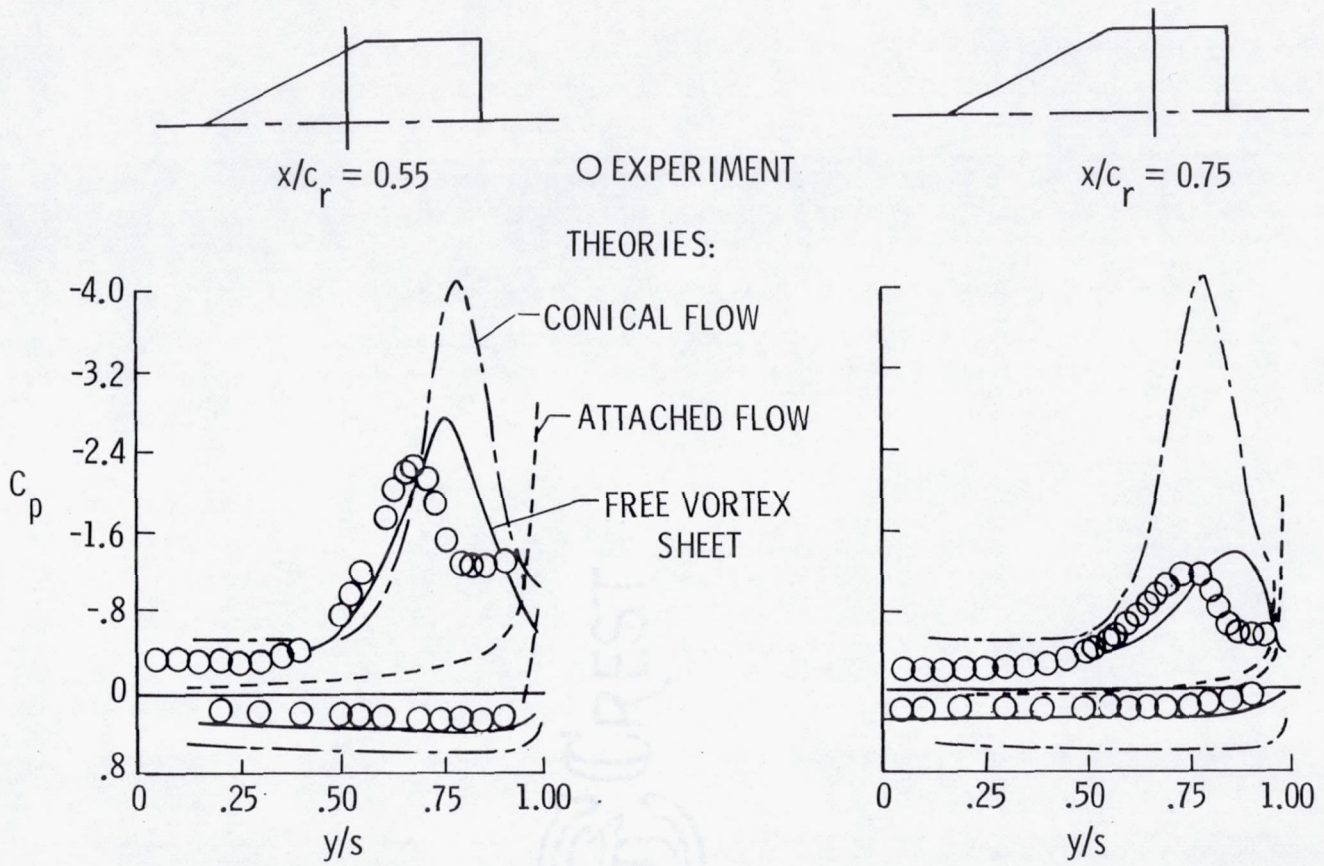

Figure 5.2- Spanwise pressure distributions. $\Lambda = 63^0$, $c_t/c_r = 0.4$, $\alpha = 20°$, $M_\infty = 0.3$. From Luckring, et al. (1982).

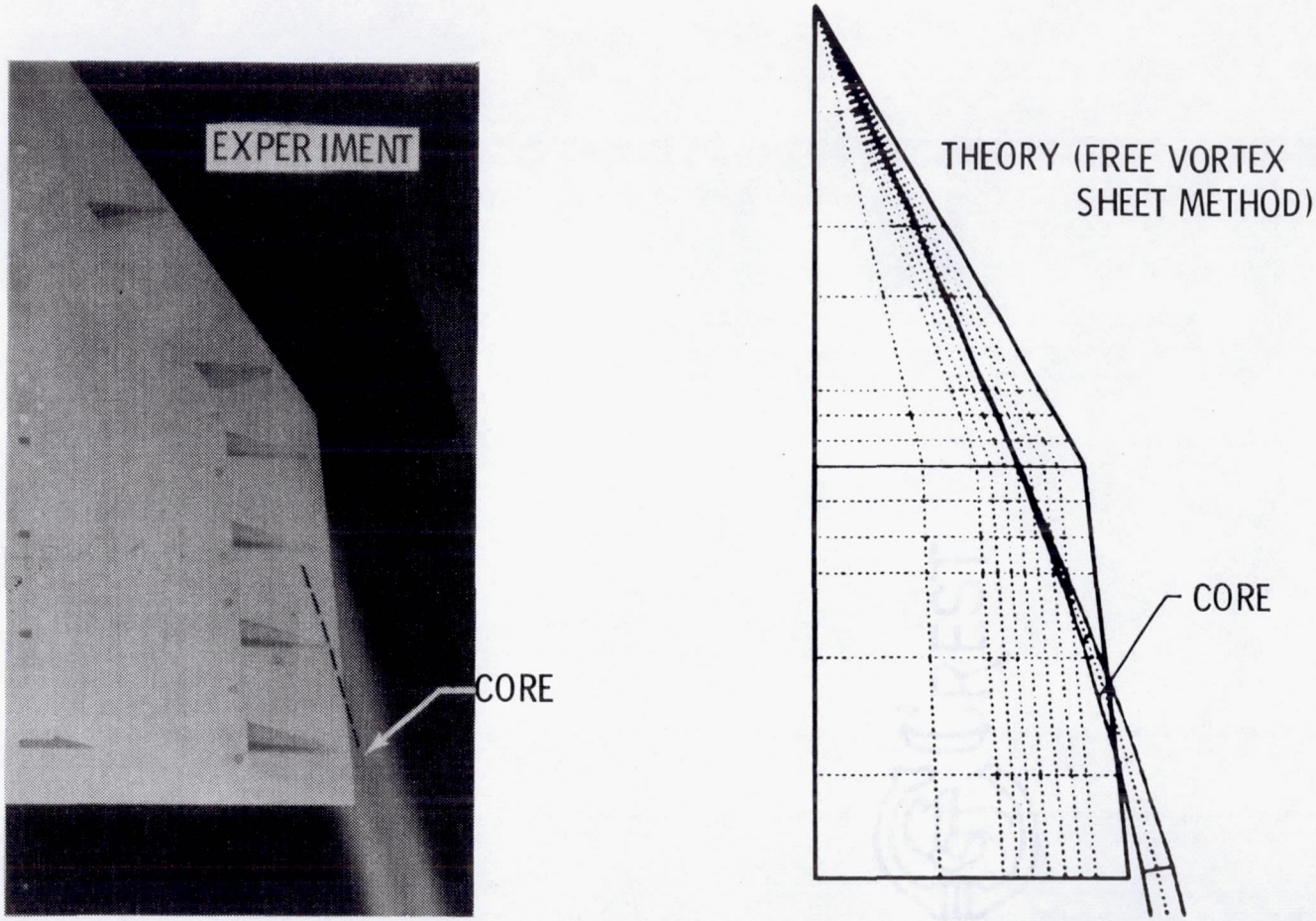

Figure 5.3- Calculation of vortex core trajectory. From Luckring, et al. (1982).

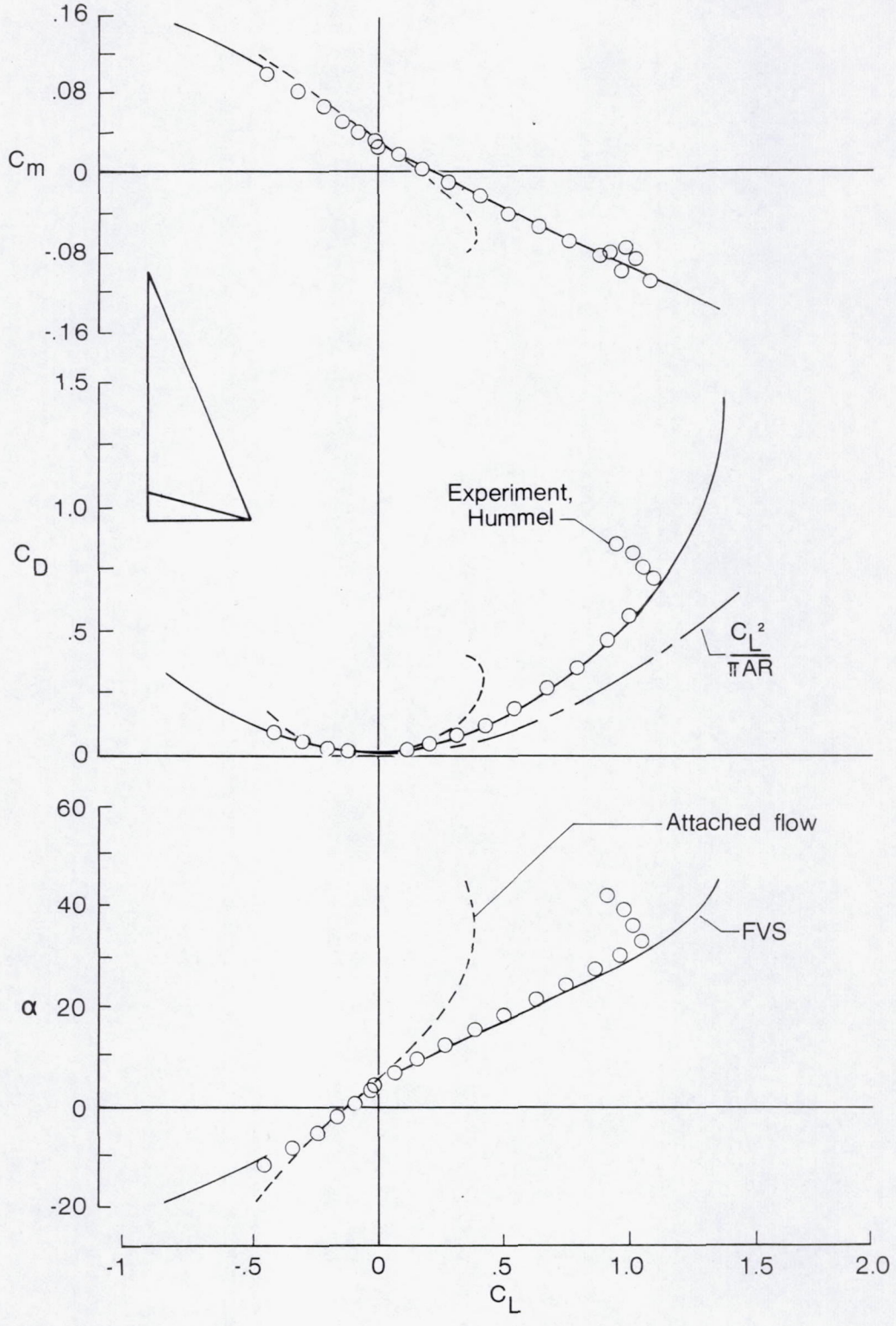

Figure 5.4- Calculation of force/moment properties.
AR = 1 delta wing.

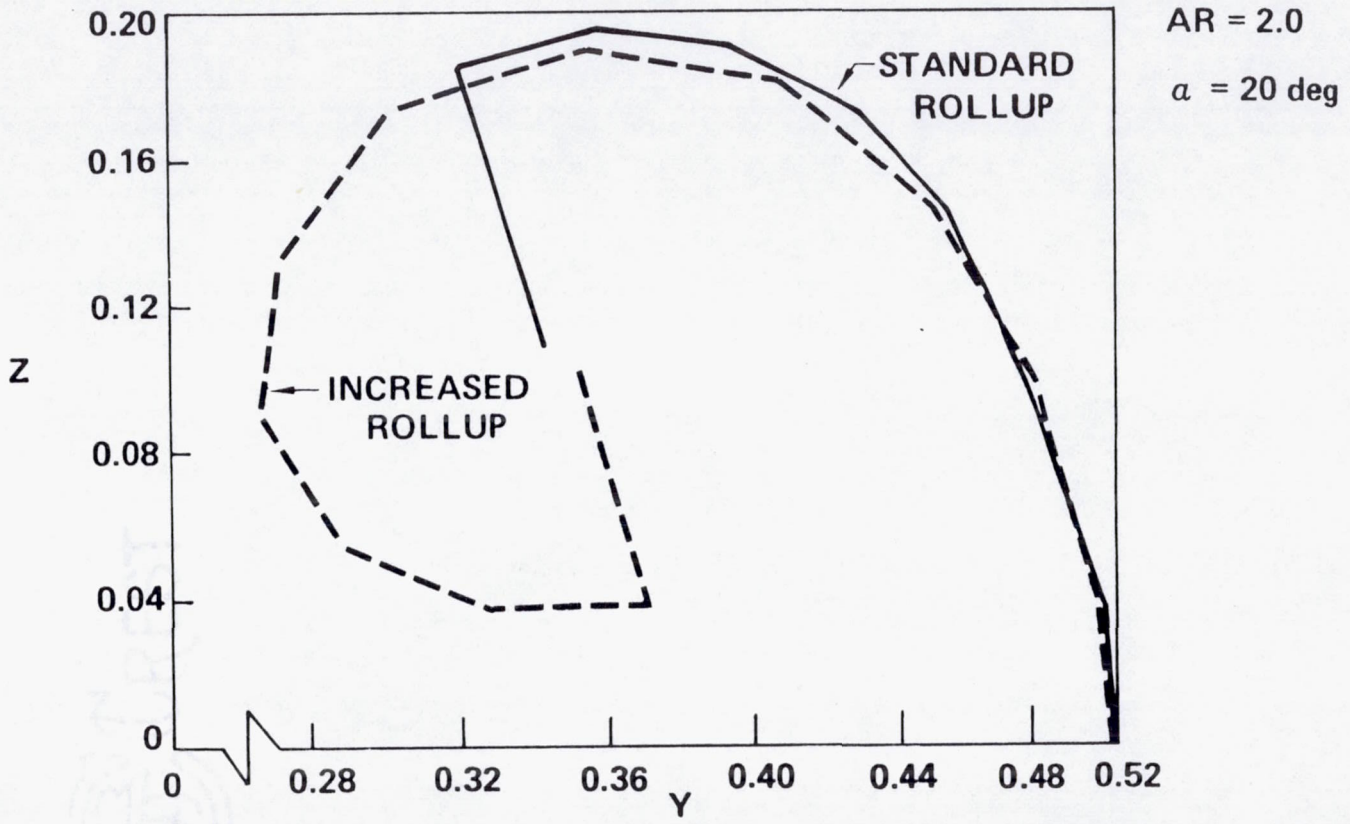

a) vortex geometry

Figure 6.1- Sheet rollup effects on global solution properties.
From Johnson, et al. (1980).

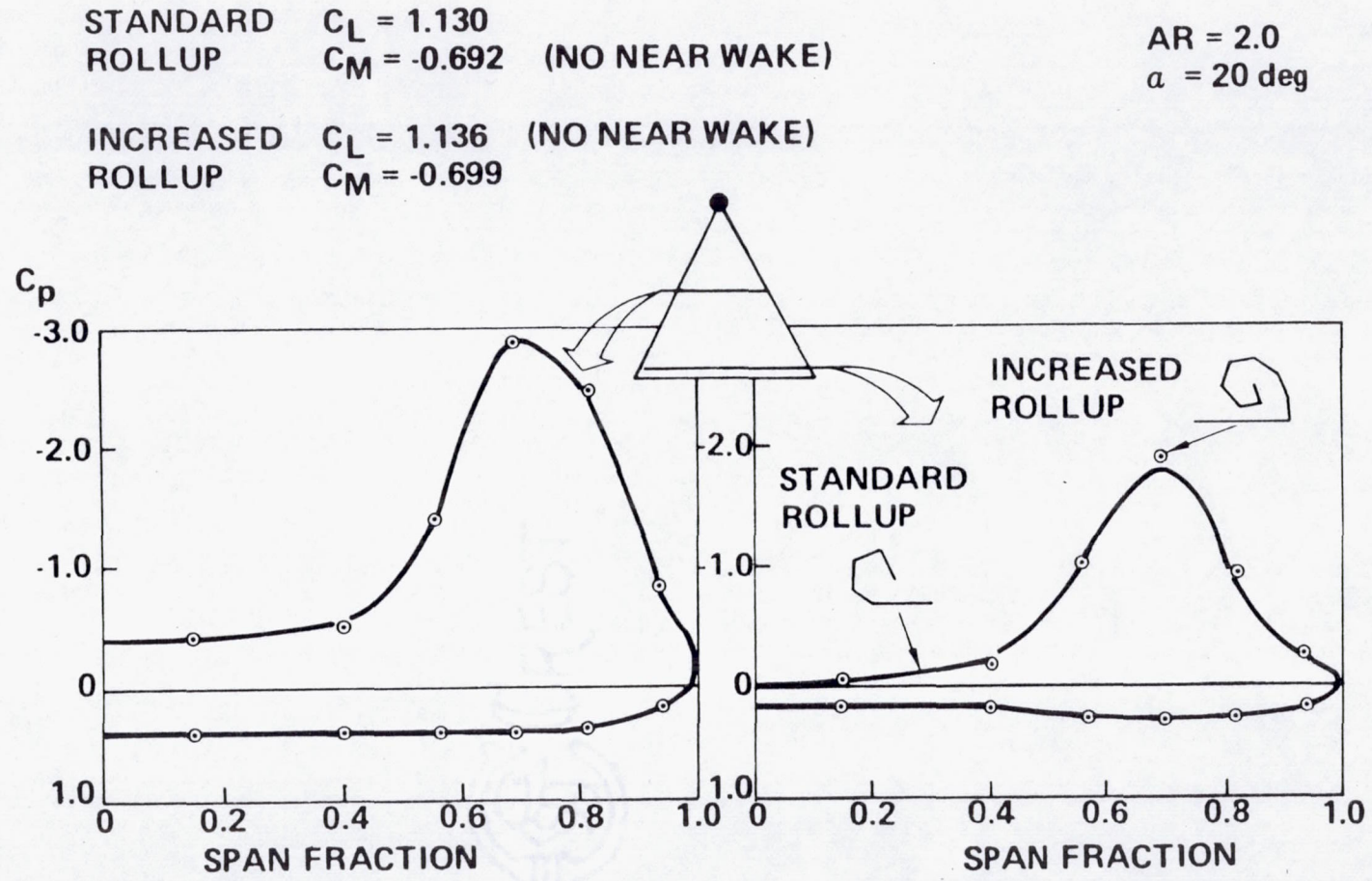

b) wing pressures

Figure 6.1- Concluded.

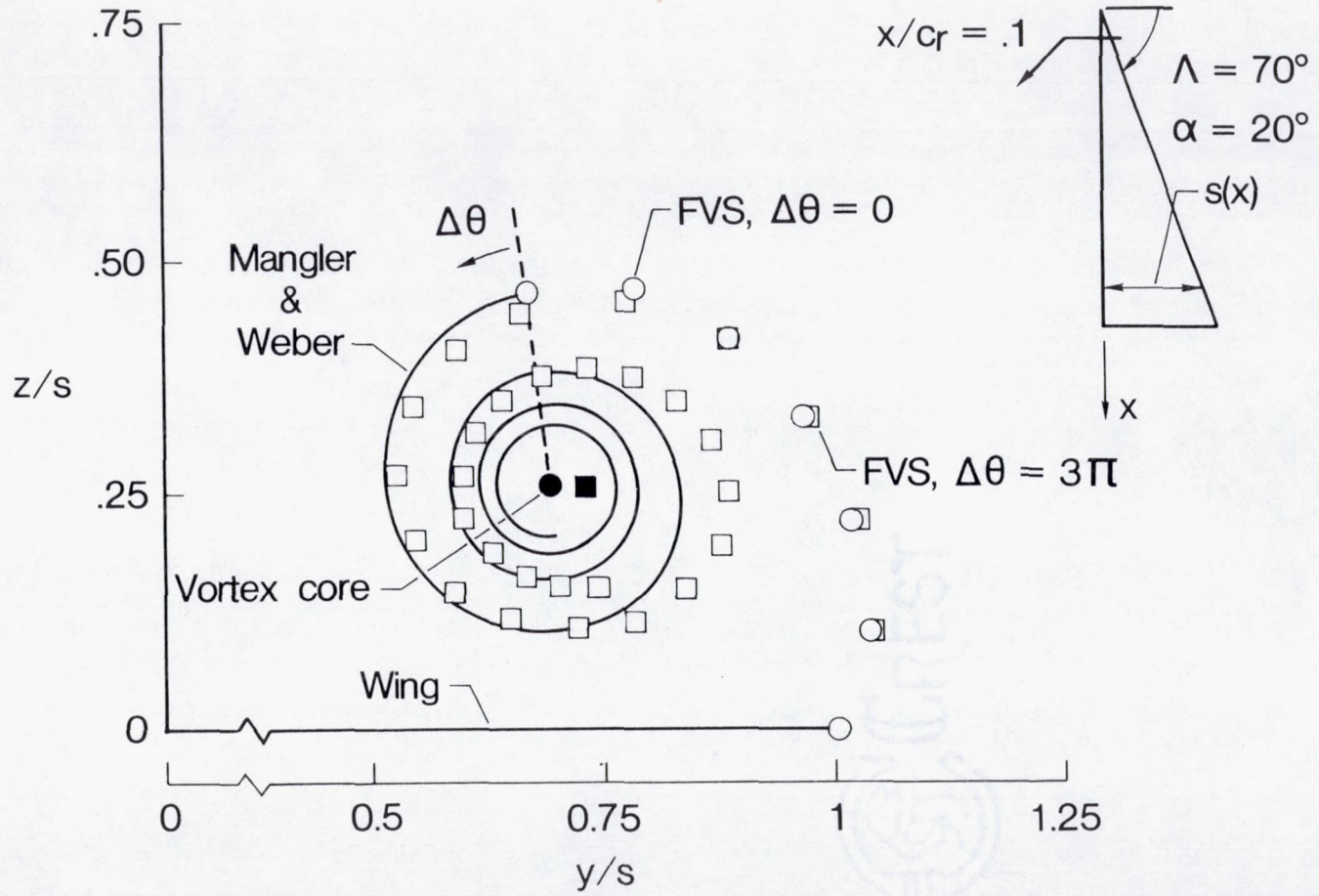

Figure 6.2- Comparison of vortex sheet trajectories.

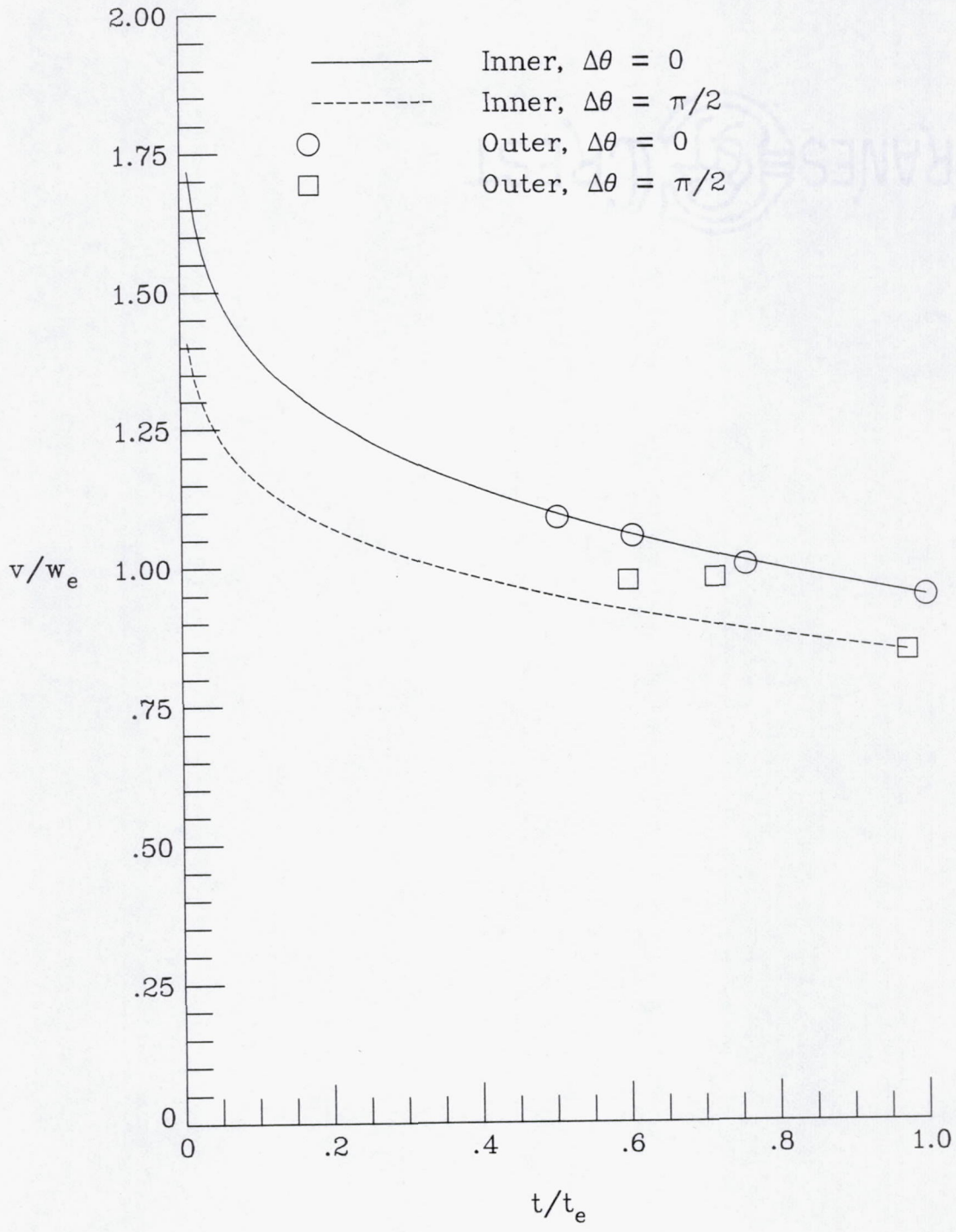

a) angular velocity

Figure 6.3- Inner- to outer-flow matching.

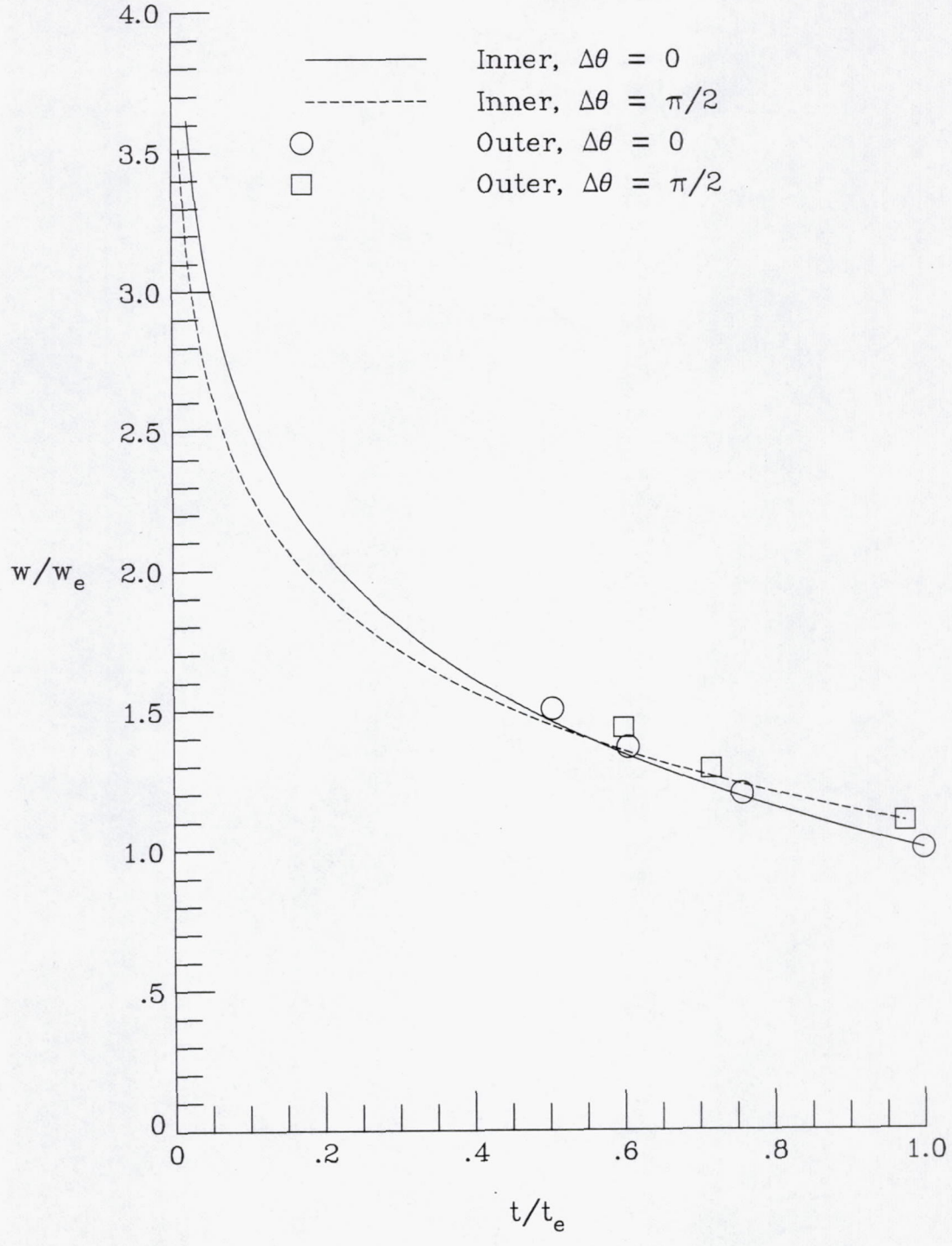

b) axial velocity

Figure 6.3- Continued

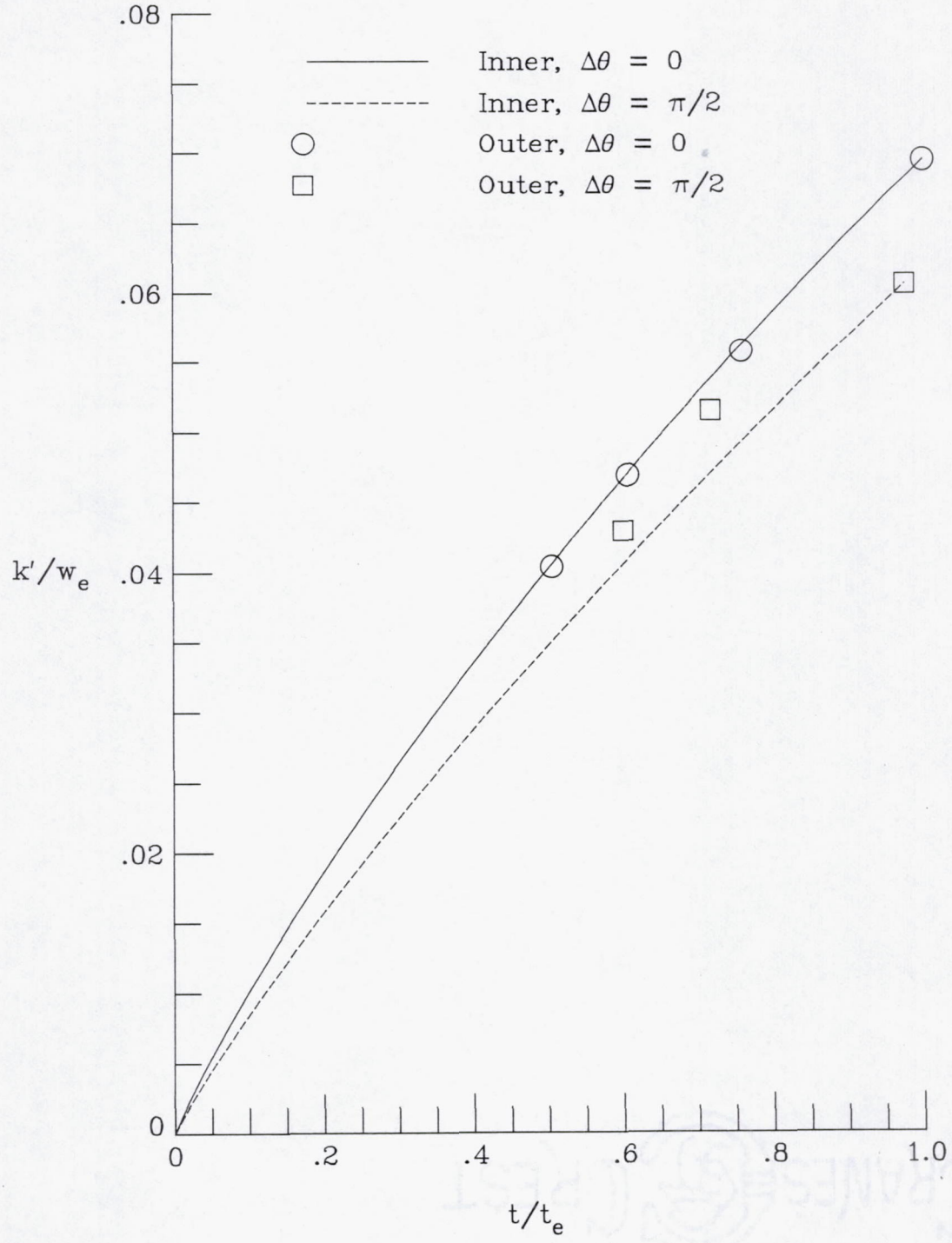

c) circulation gradient

Figure 6.3- Concluded.

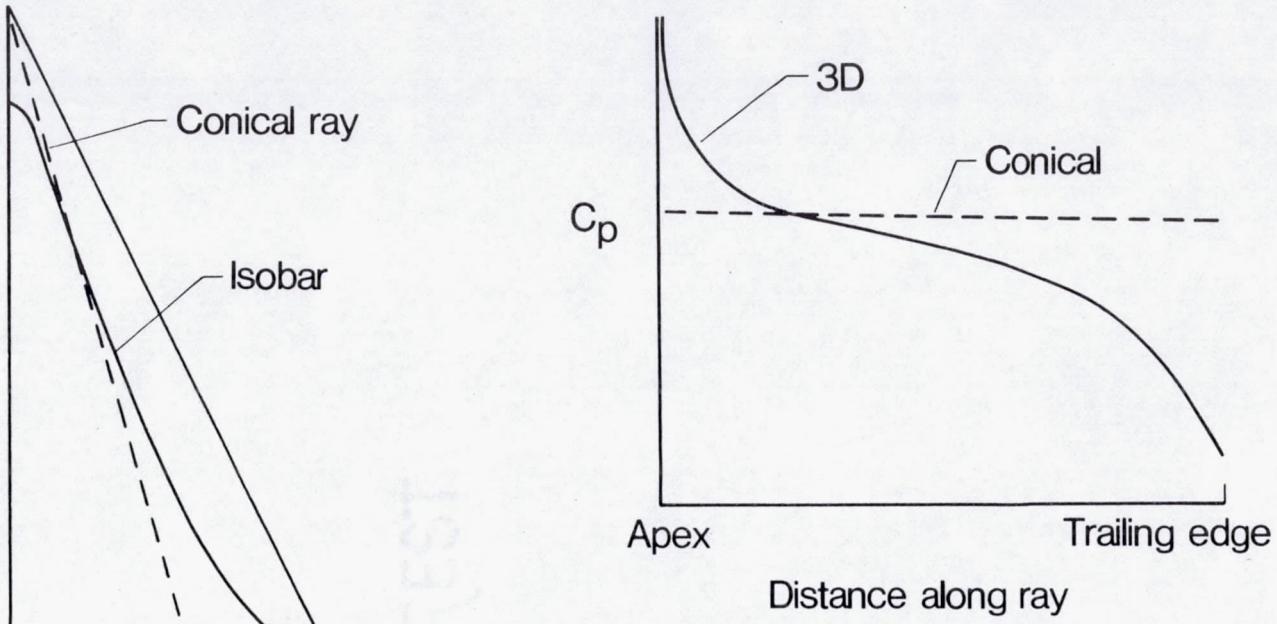

Figure 6.4- Nonconical effects. $M_\infty < 1$.

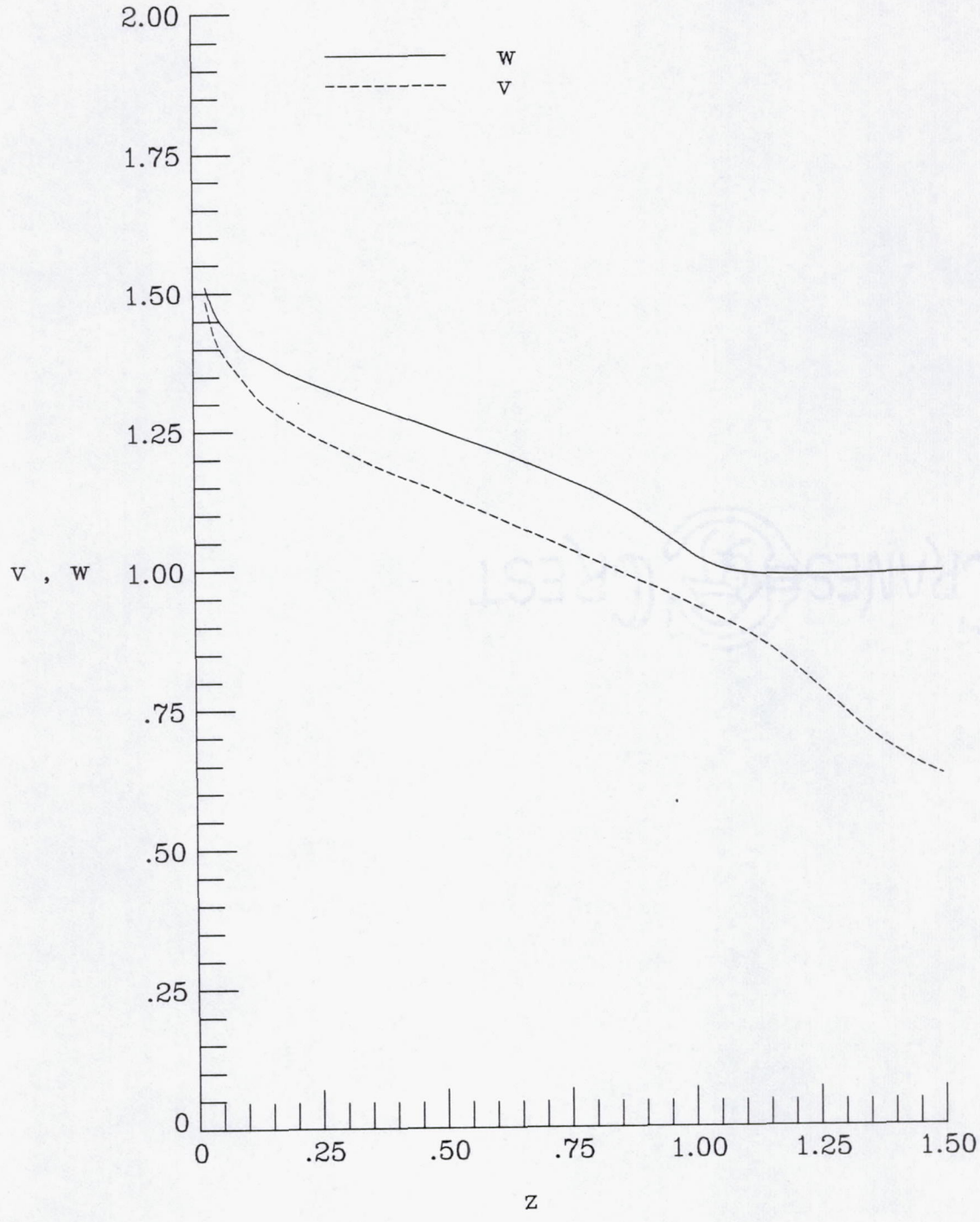

Figure 6.5- Representative boundary conditions. $\Lambda = 75°$, $\alpha = 15°$.

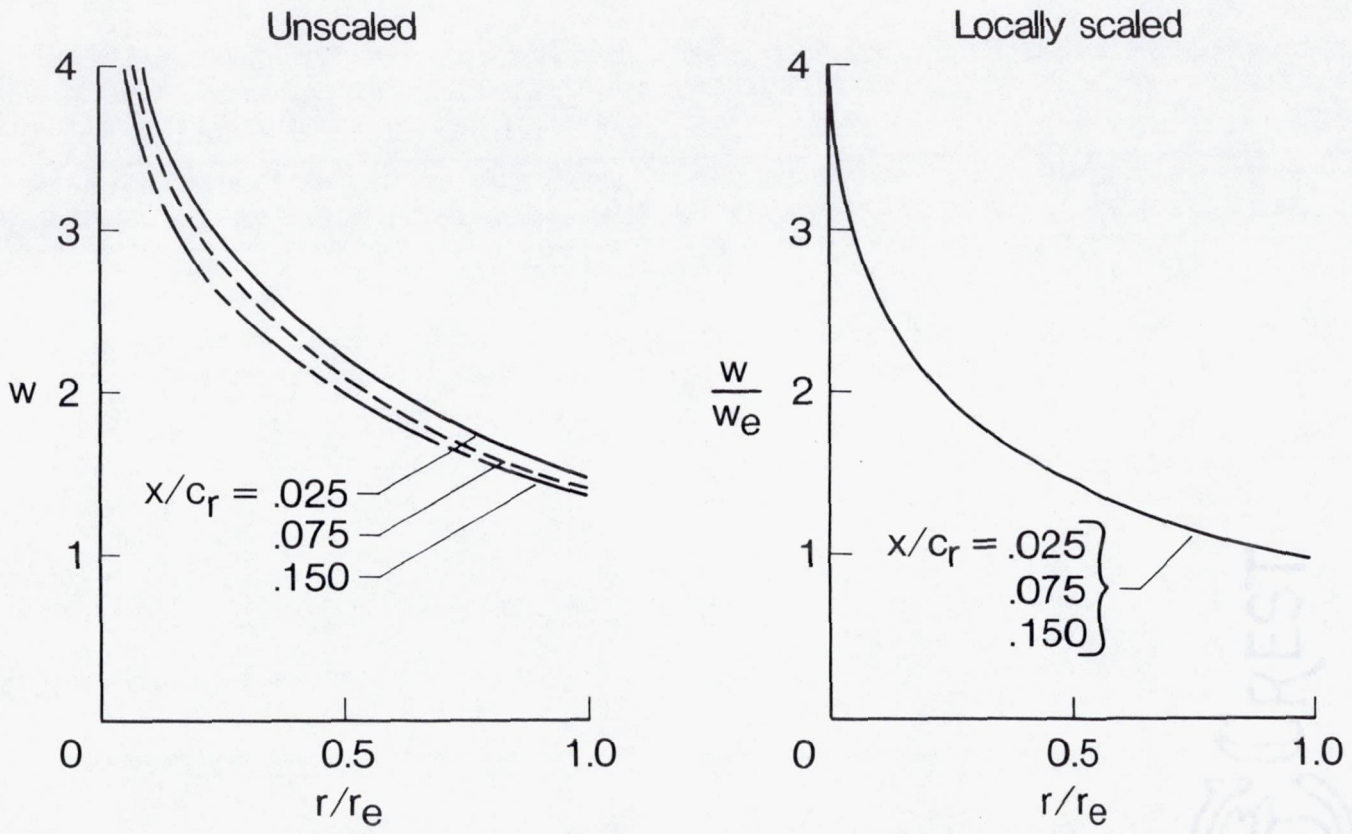

Figure 6.6- Longitudinal scaling effect.

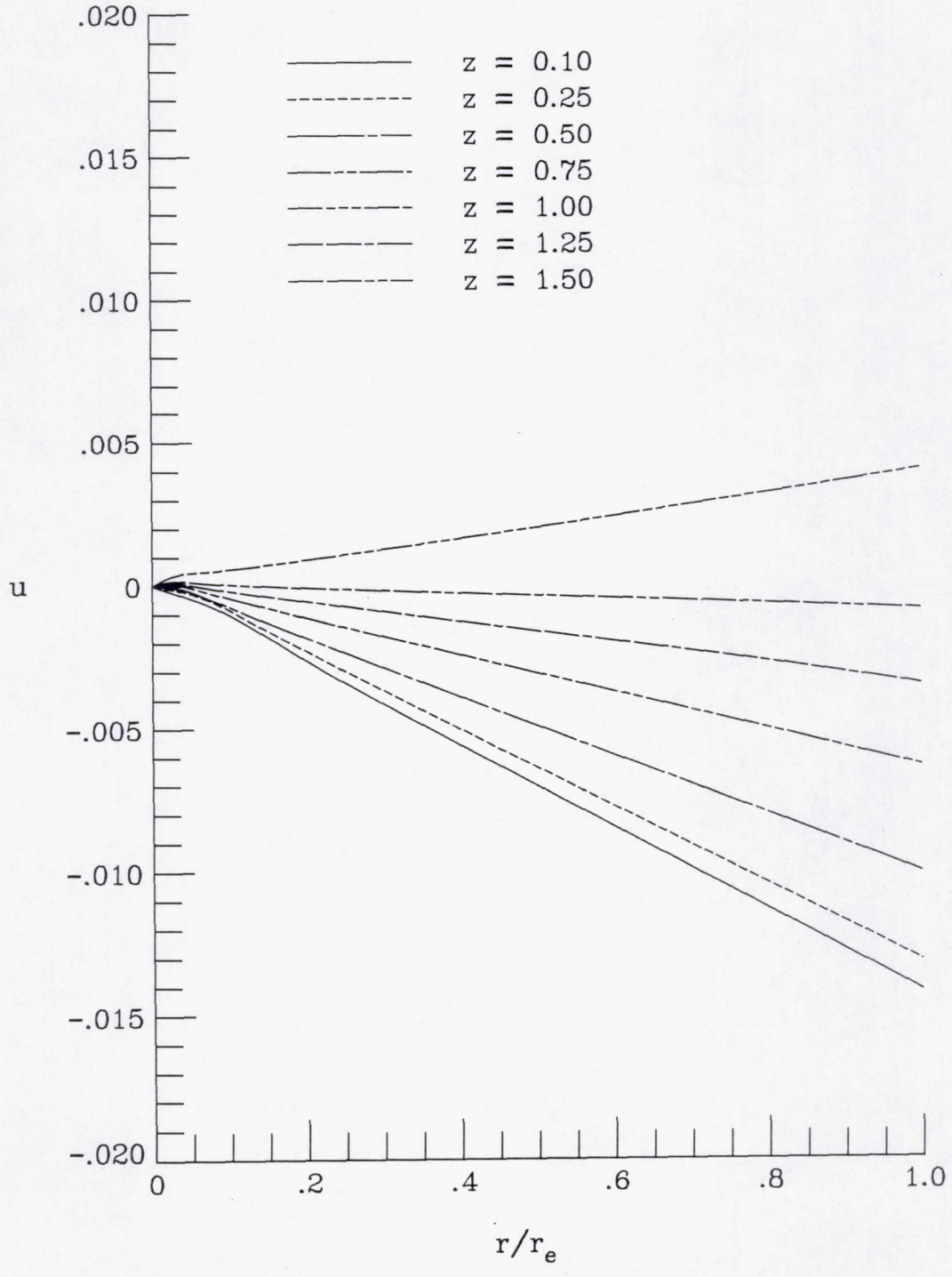

a) radial velocity

Figure 7.1- Representative delta wing solution - scaled radial distribution. $\Lambda = 75°$, $\alpha = 15°$.

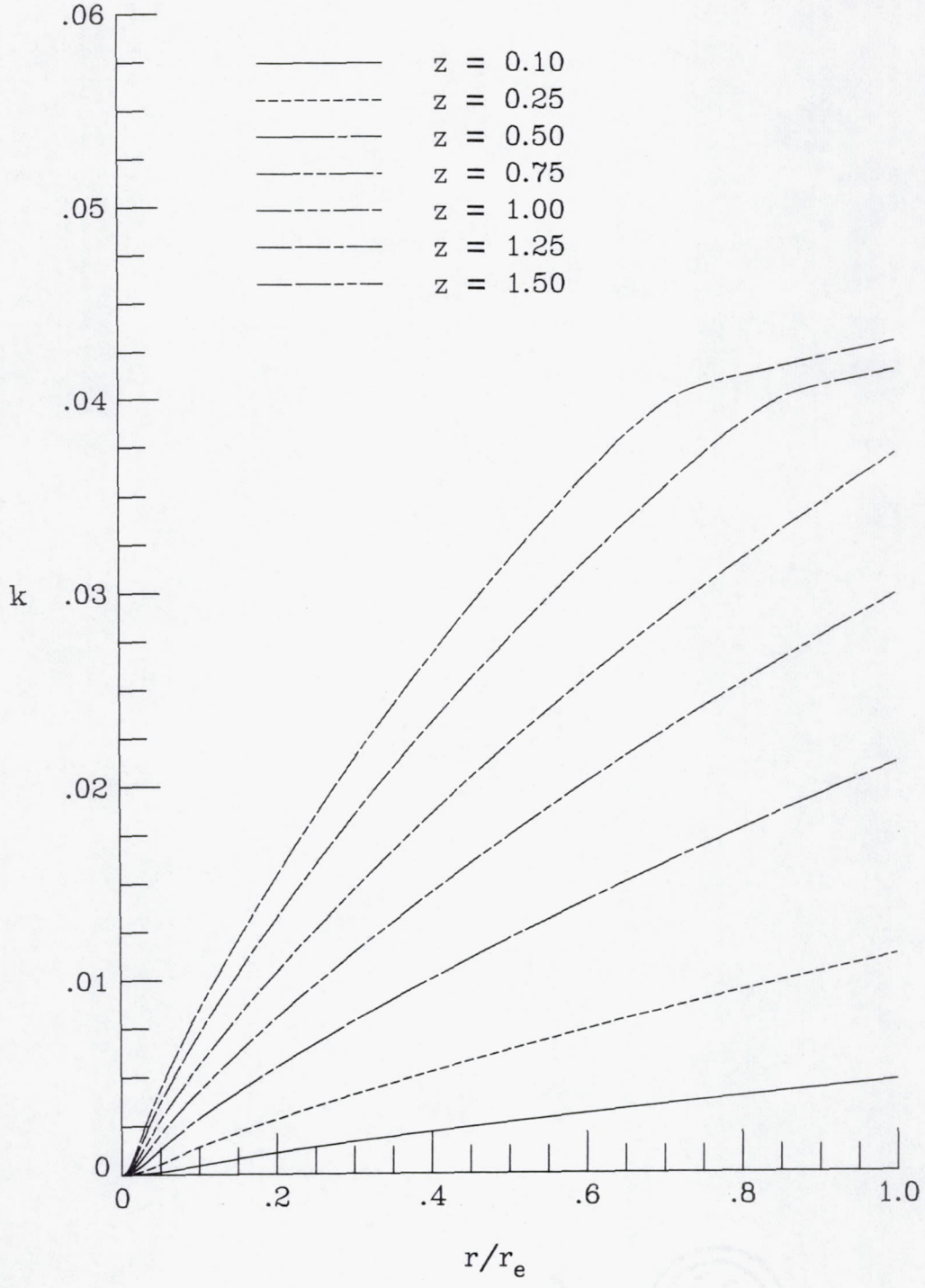

b) circulation parameter

Figure 7.1- Continued

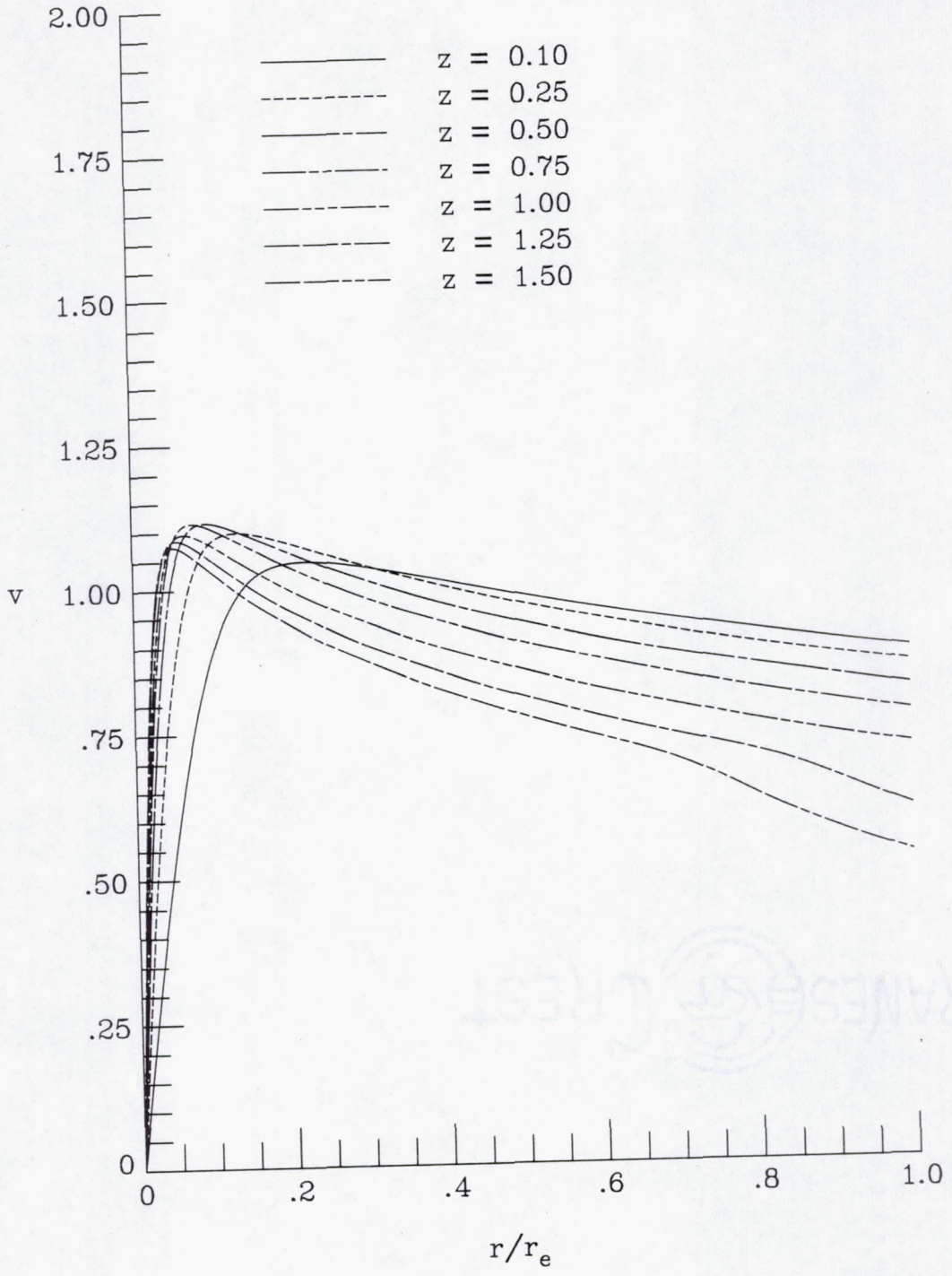

c) angular velocity

Figure 7.1- Continued

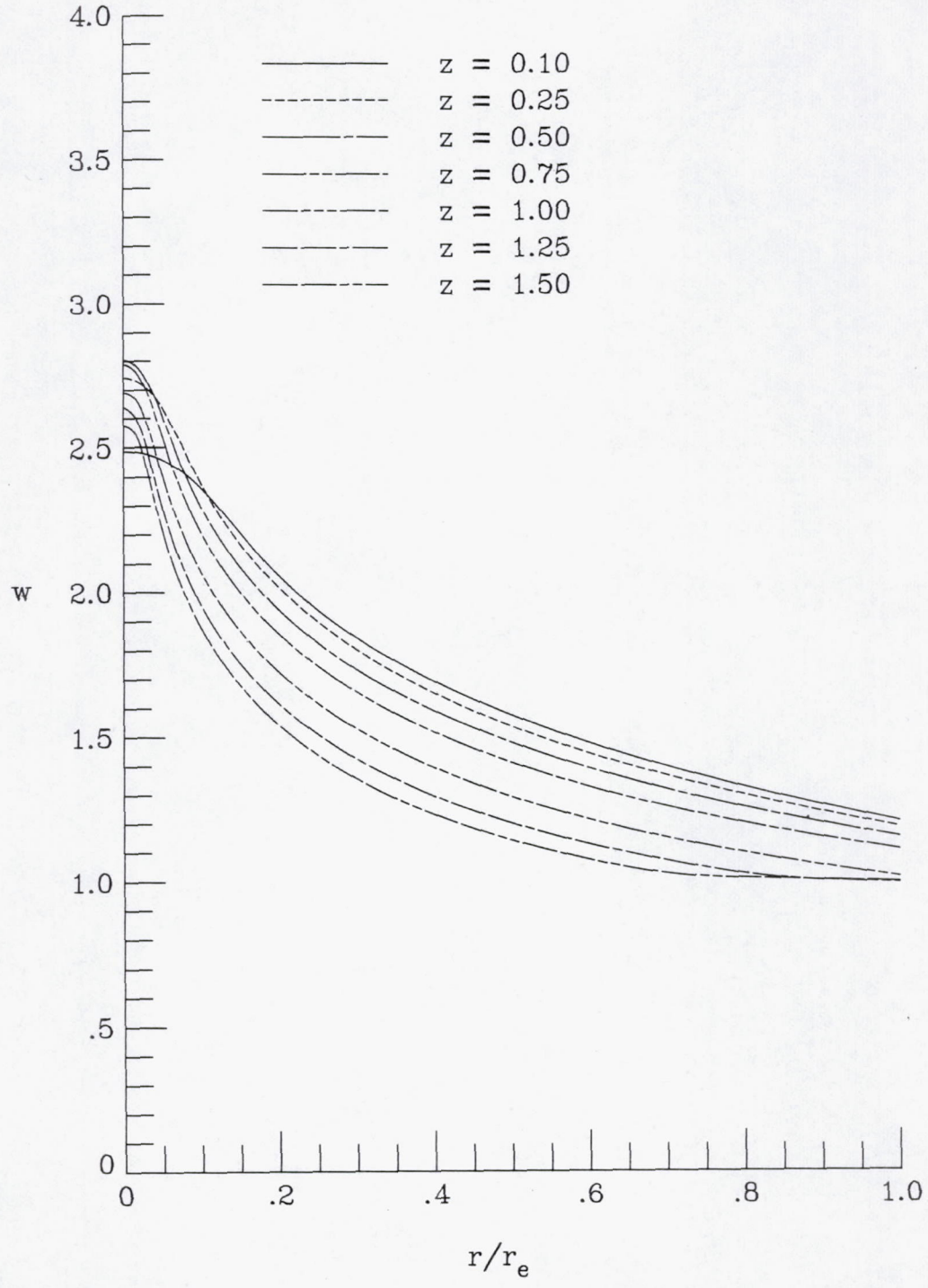

d) axial velocity

Figure 7.1- Continued

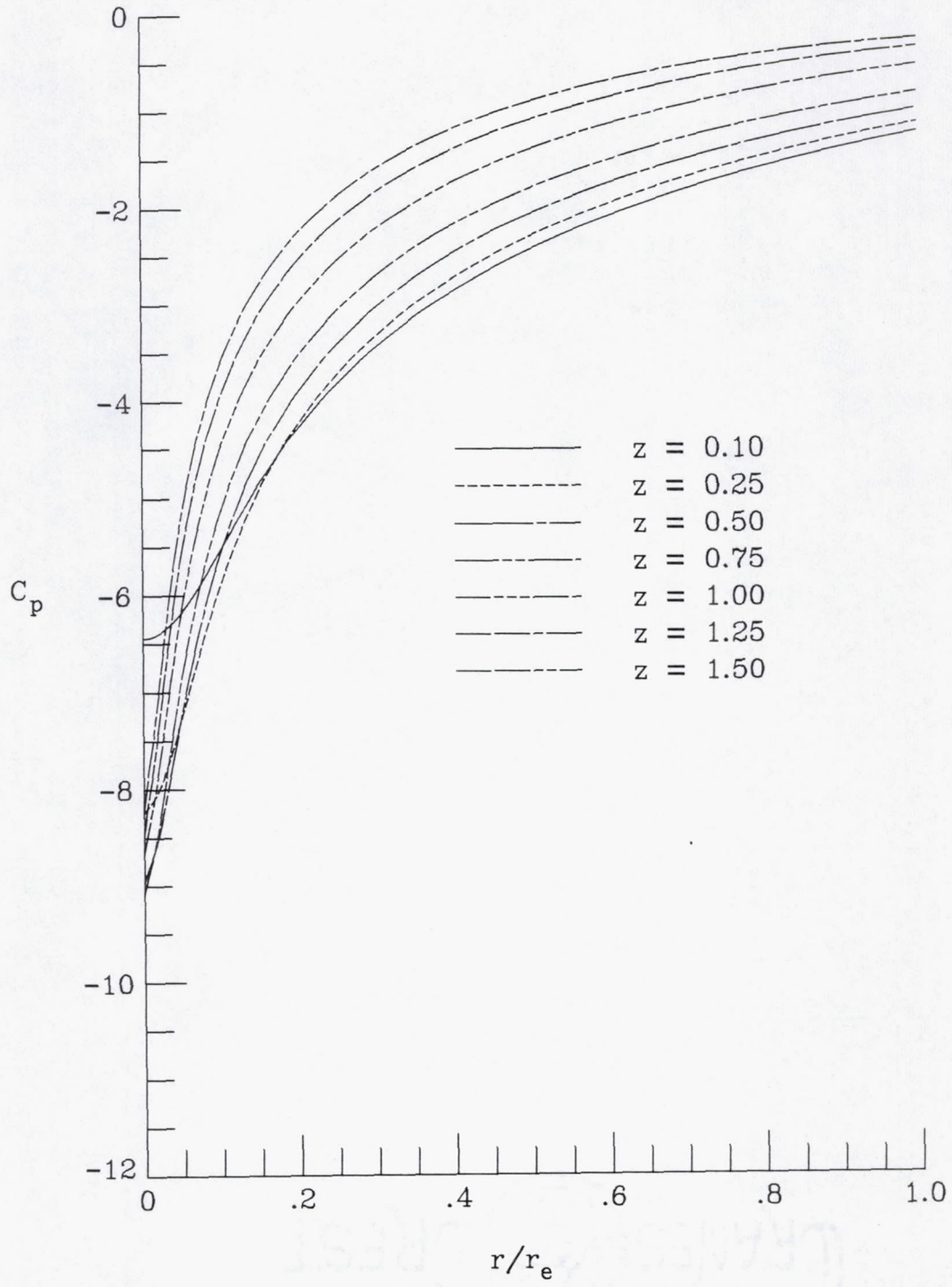

e) static pressure

Figure 7.1- Continued

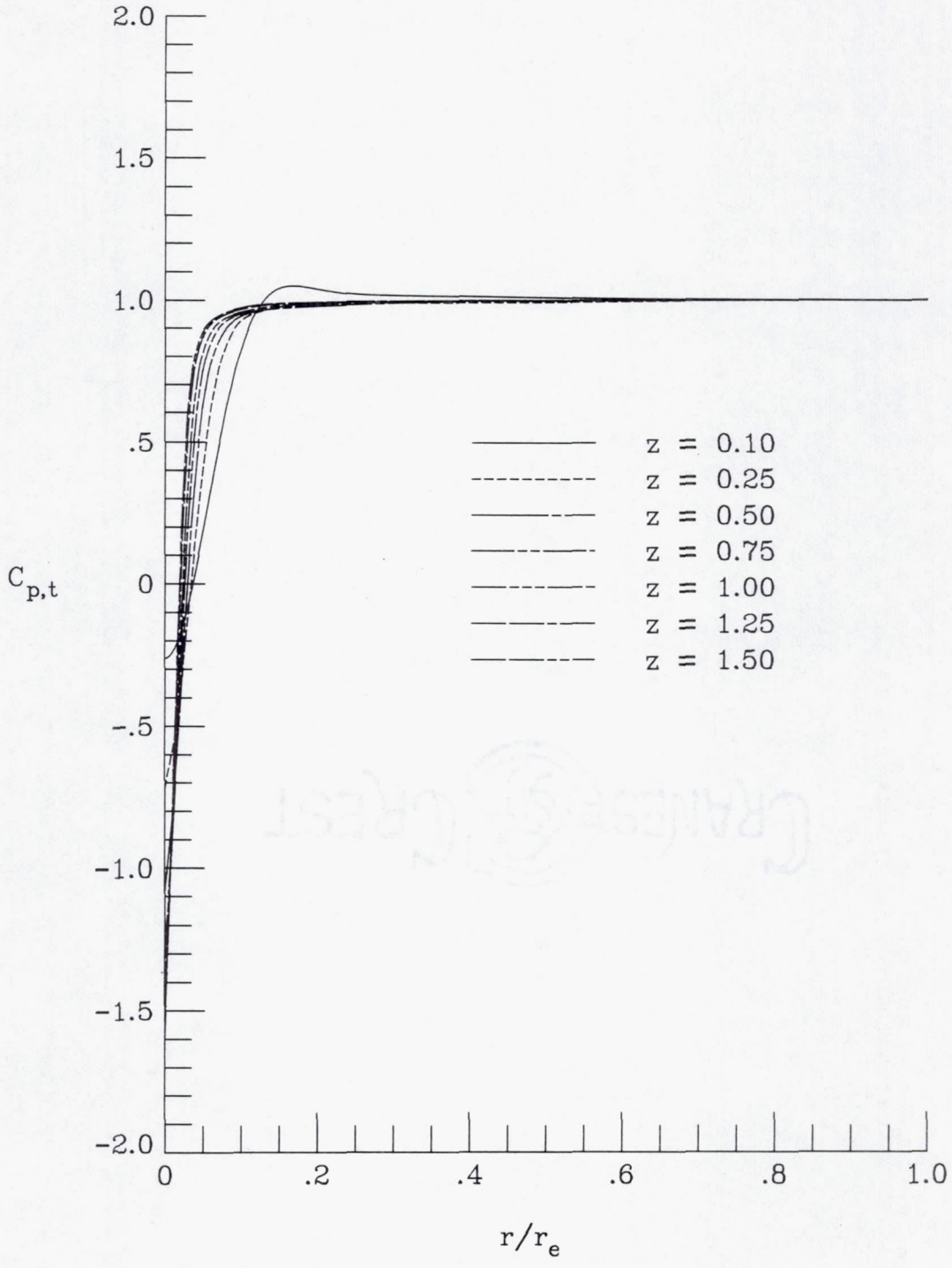

f) total pressure

Figure 7.1- Concluded.

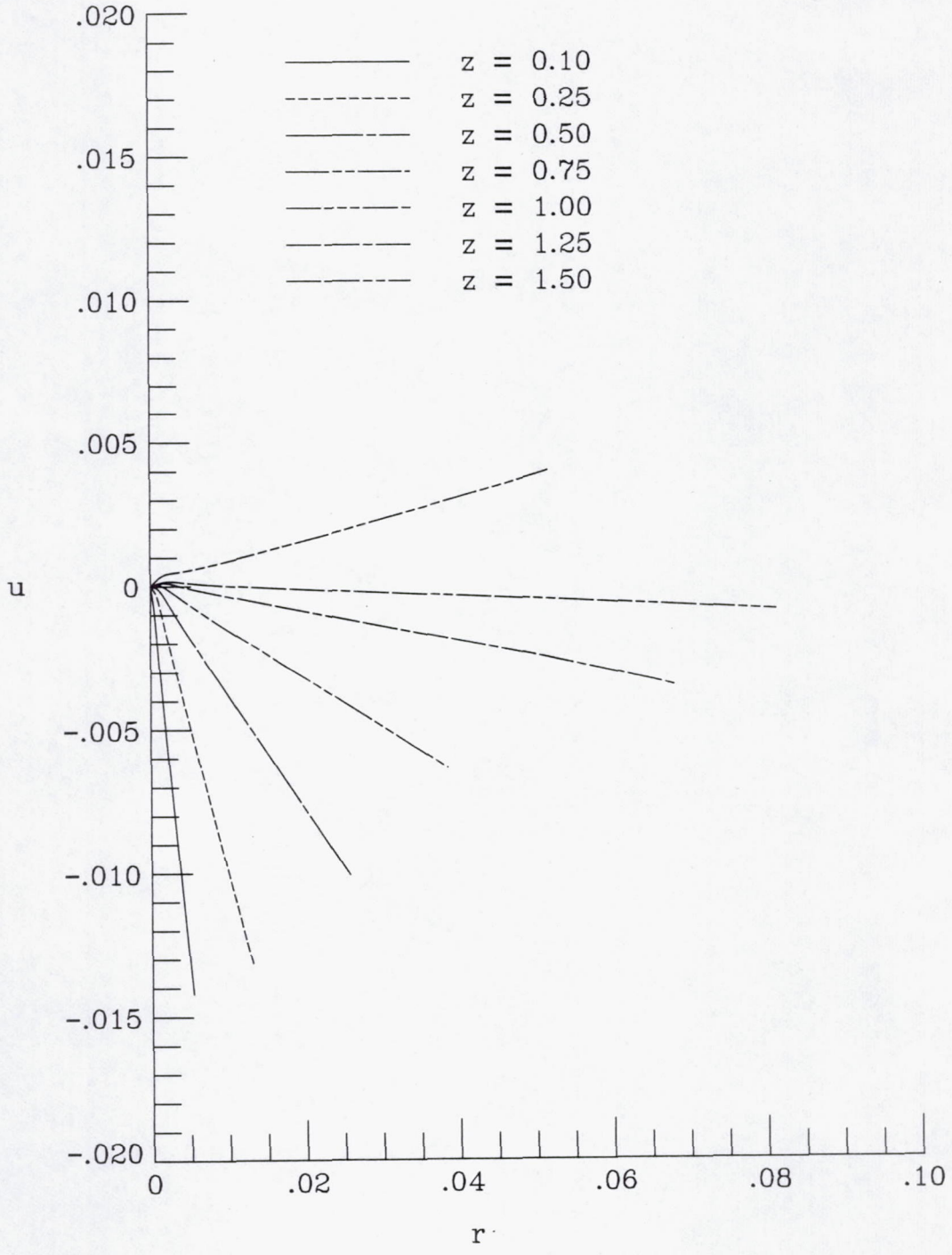

a) radial velocity

Figure 7.2- Representative delta wing solution - unscaled radial distribution. $\Lambda = 75^0$, $\alpha = 15^0$.

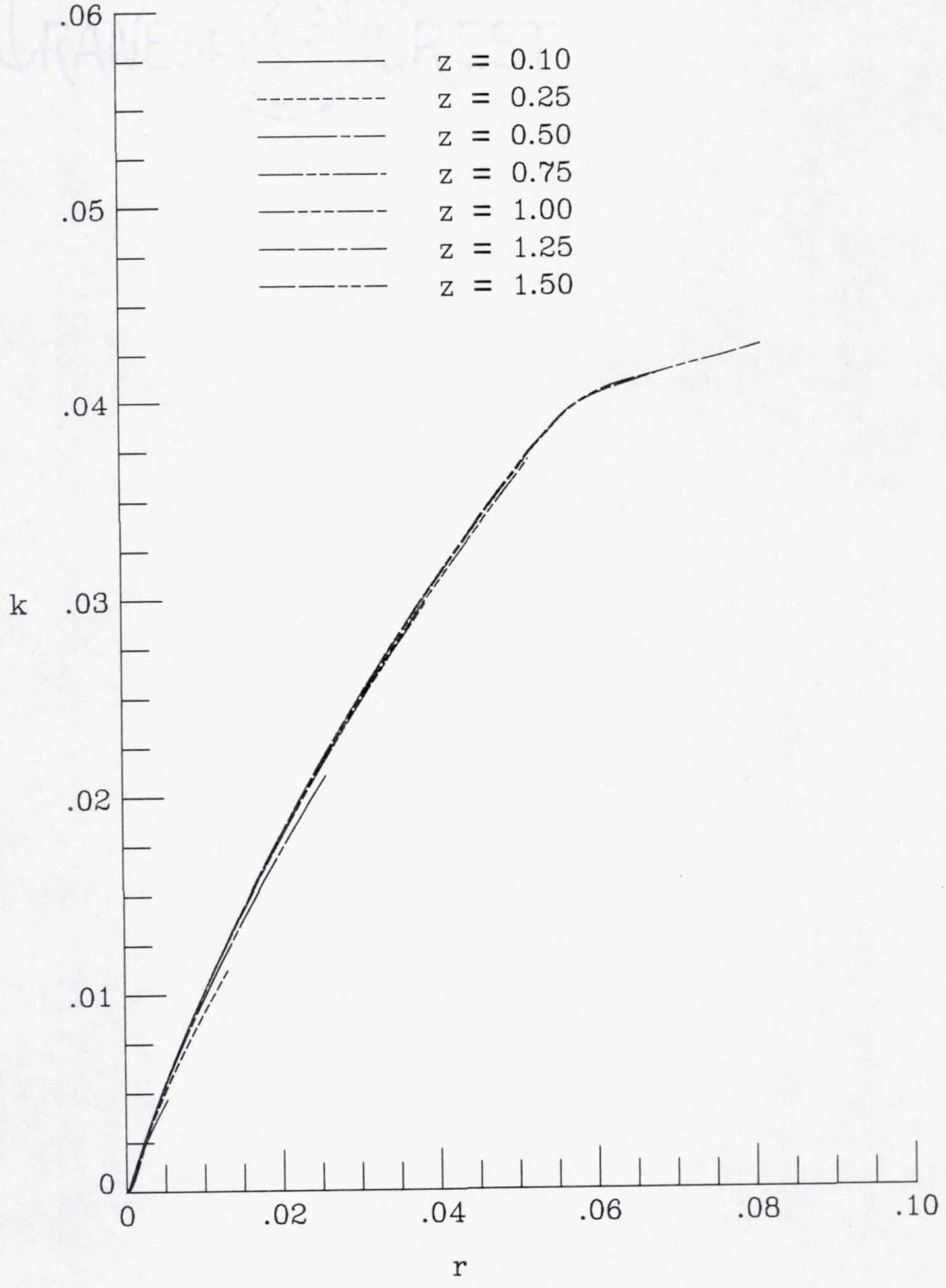

b) circulation parameter

Figure 7.2- Continued

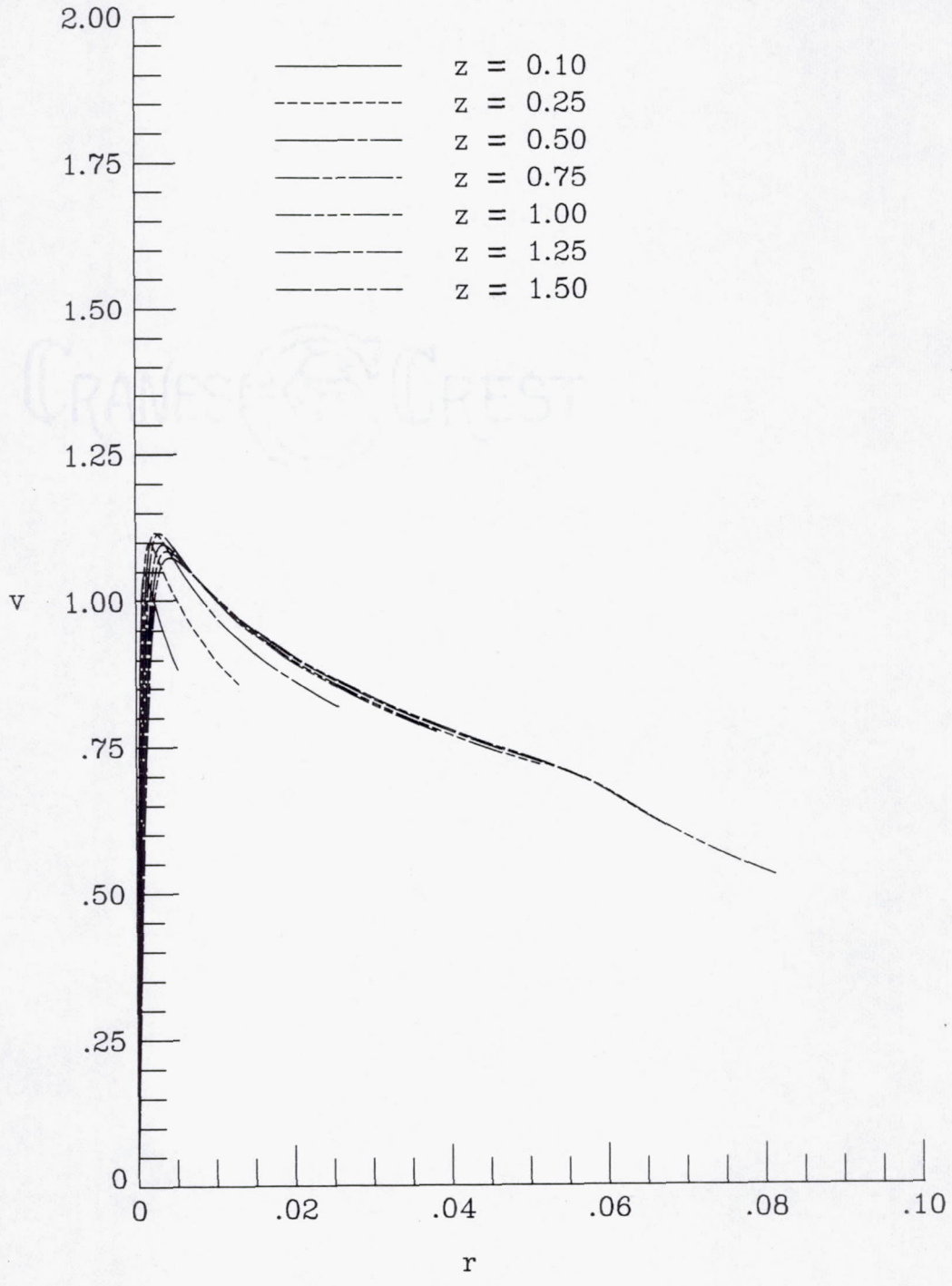

c) angular velocity

Figure 7.2- Continued

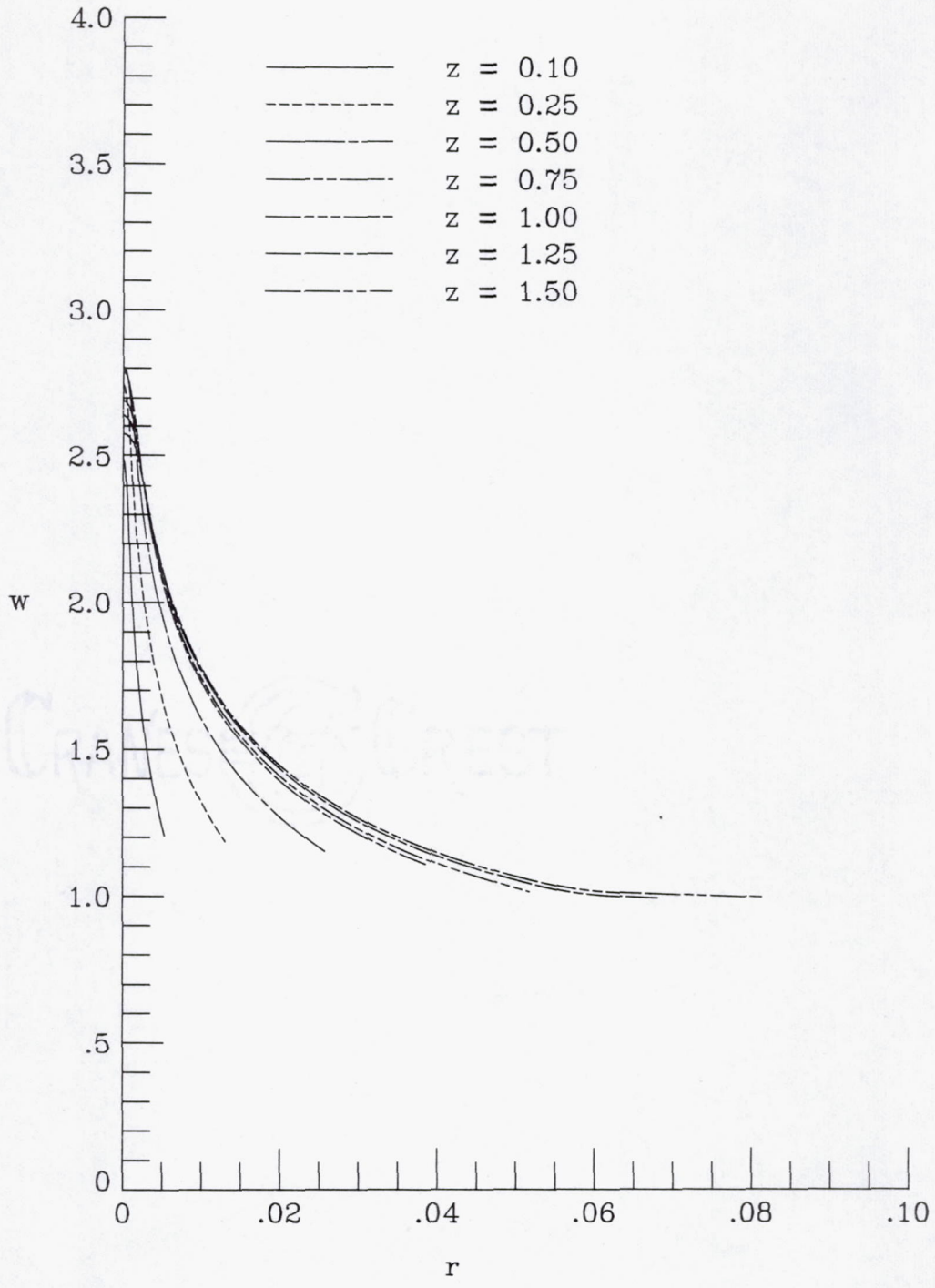

d) axial velocity

Figure 7.2- Continued

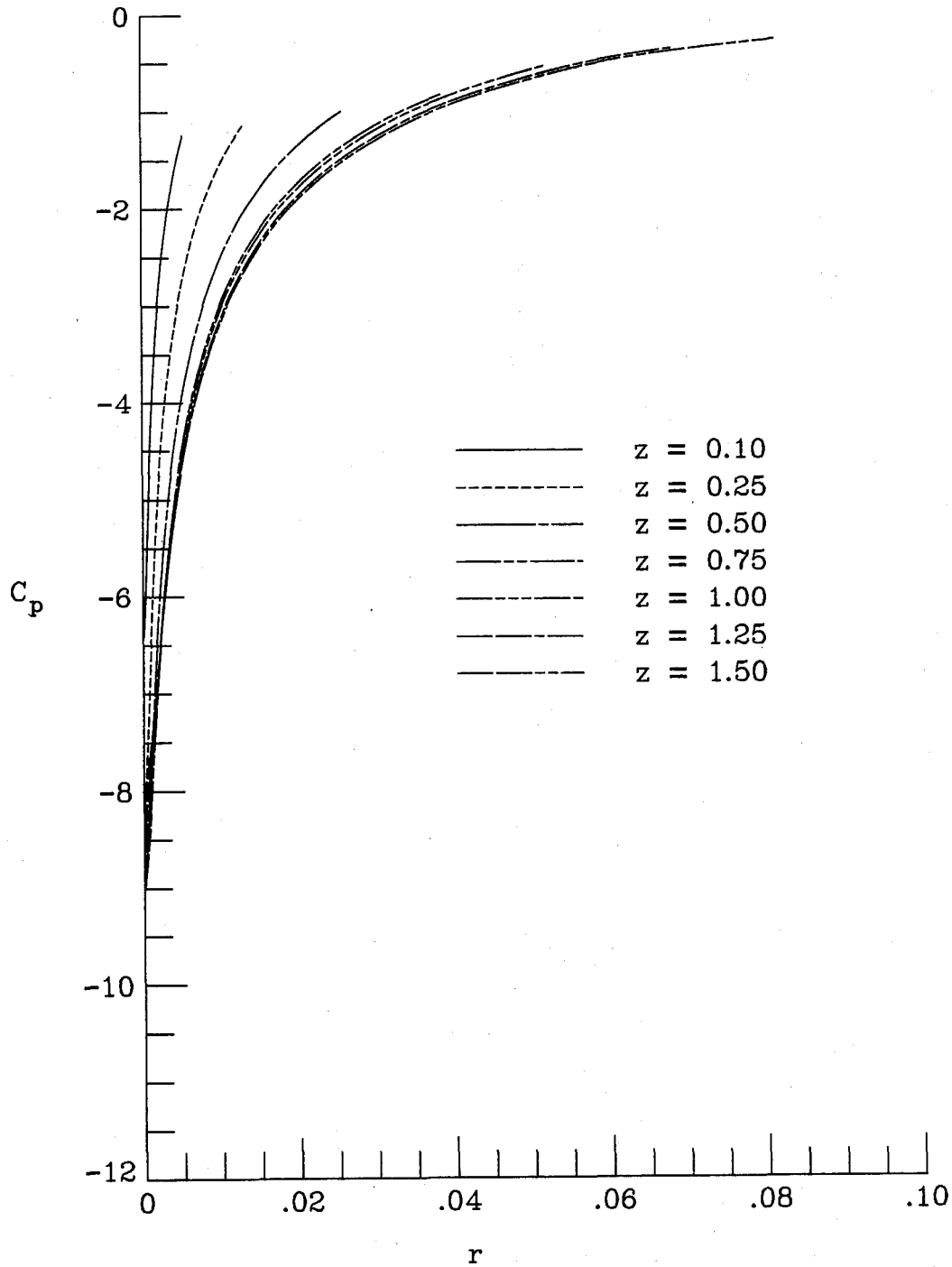

e) static pressure

Figure 7.2- Continued

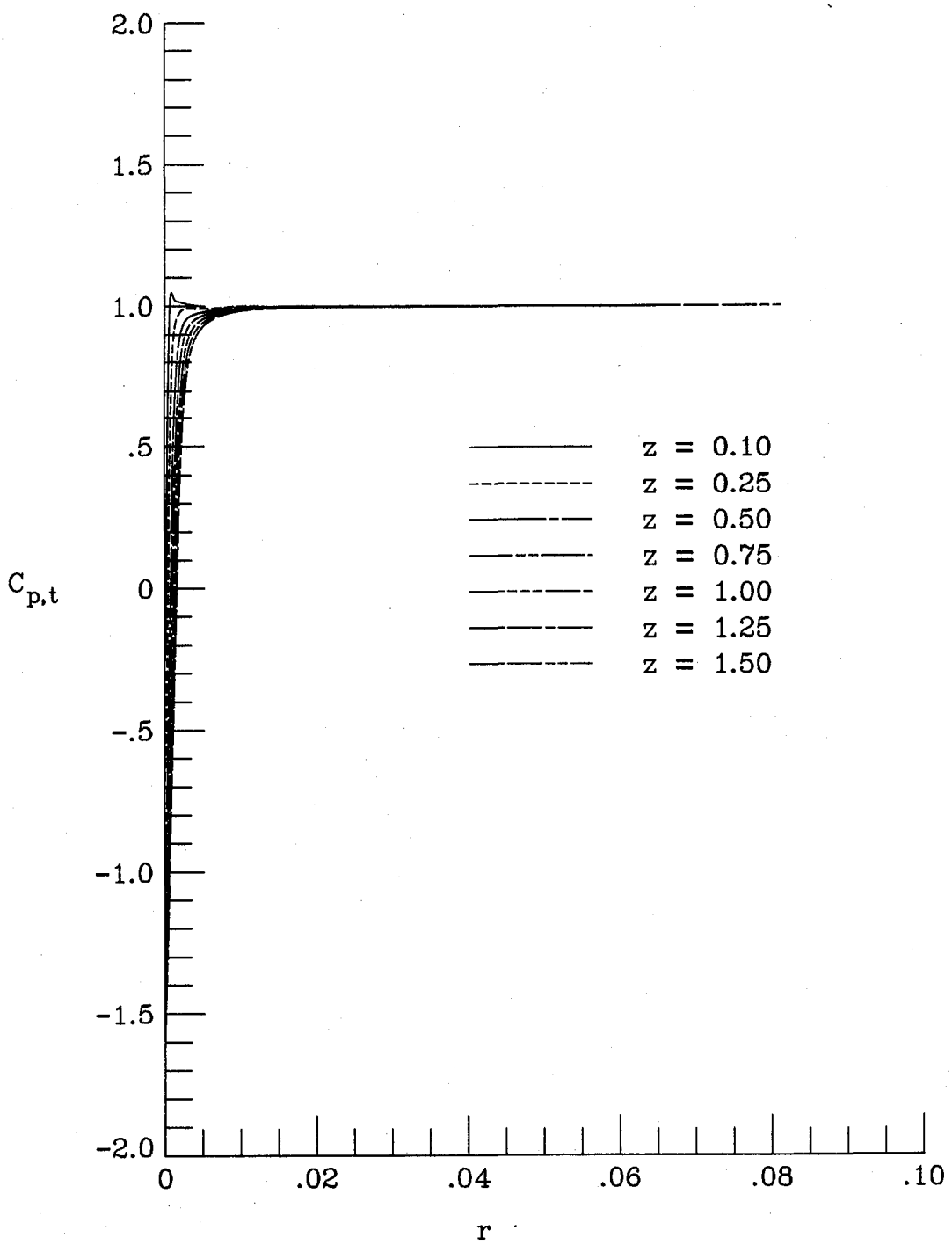

f) total pressure

Figure 7.2- Concluded.

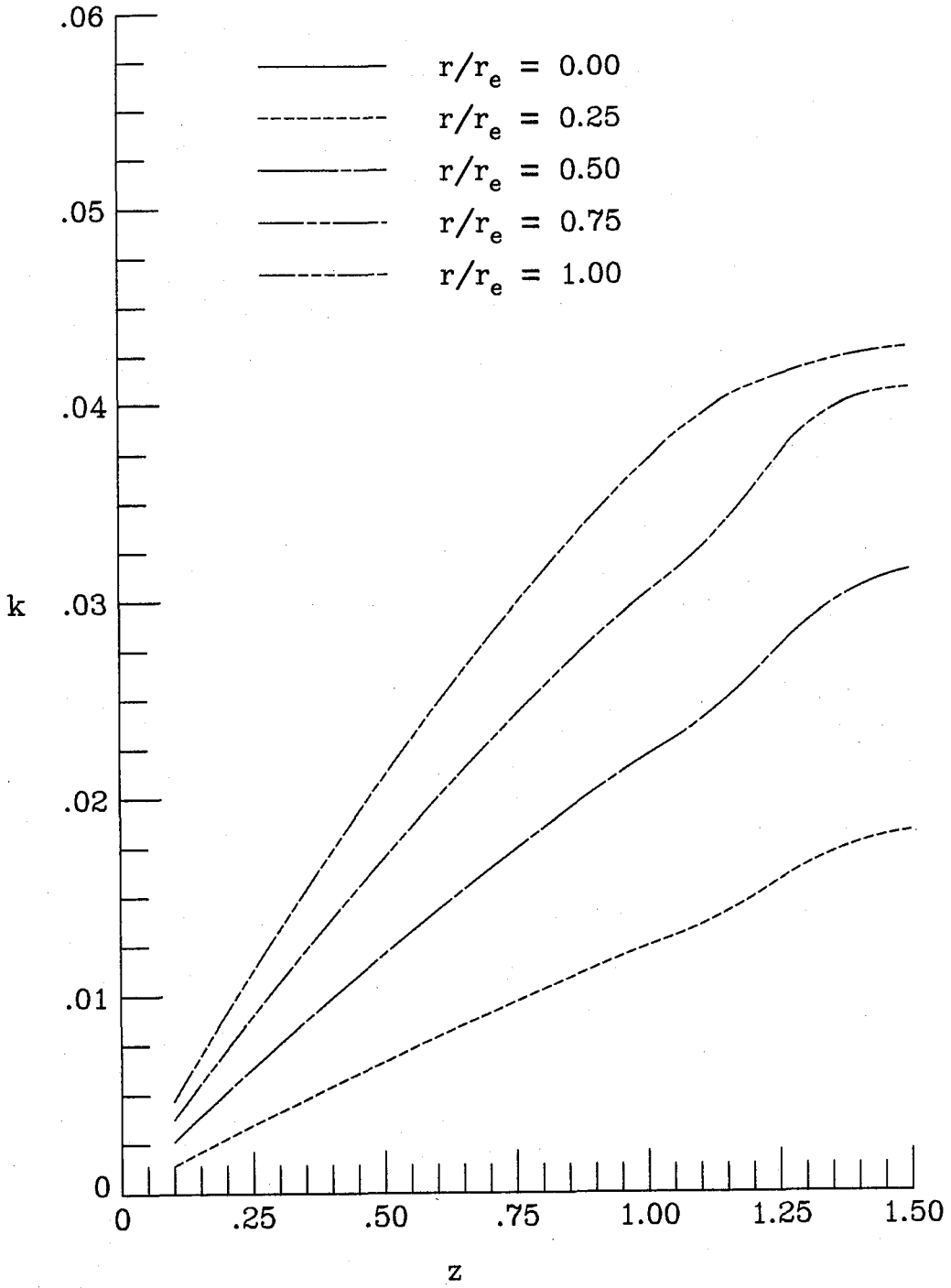

a) circulation parameter

Figure 7.3- Representative delta wing solution - longitudinal distribution. $\Lambda = 75^0$, $\alpha = 15^0$.

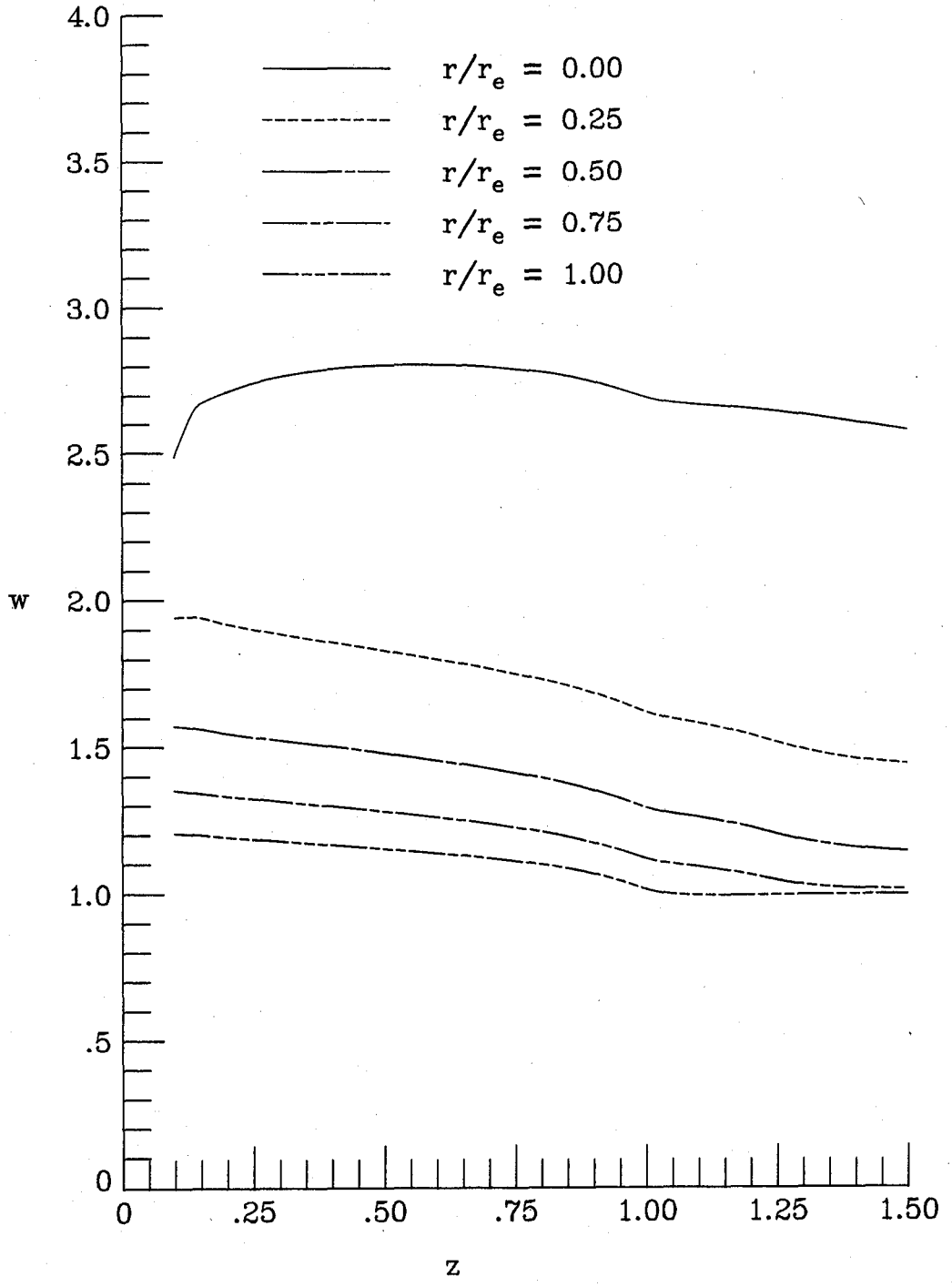

b) axial velocity

Figure 7.3- Continued

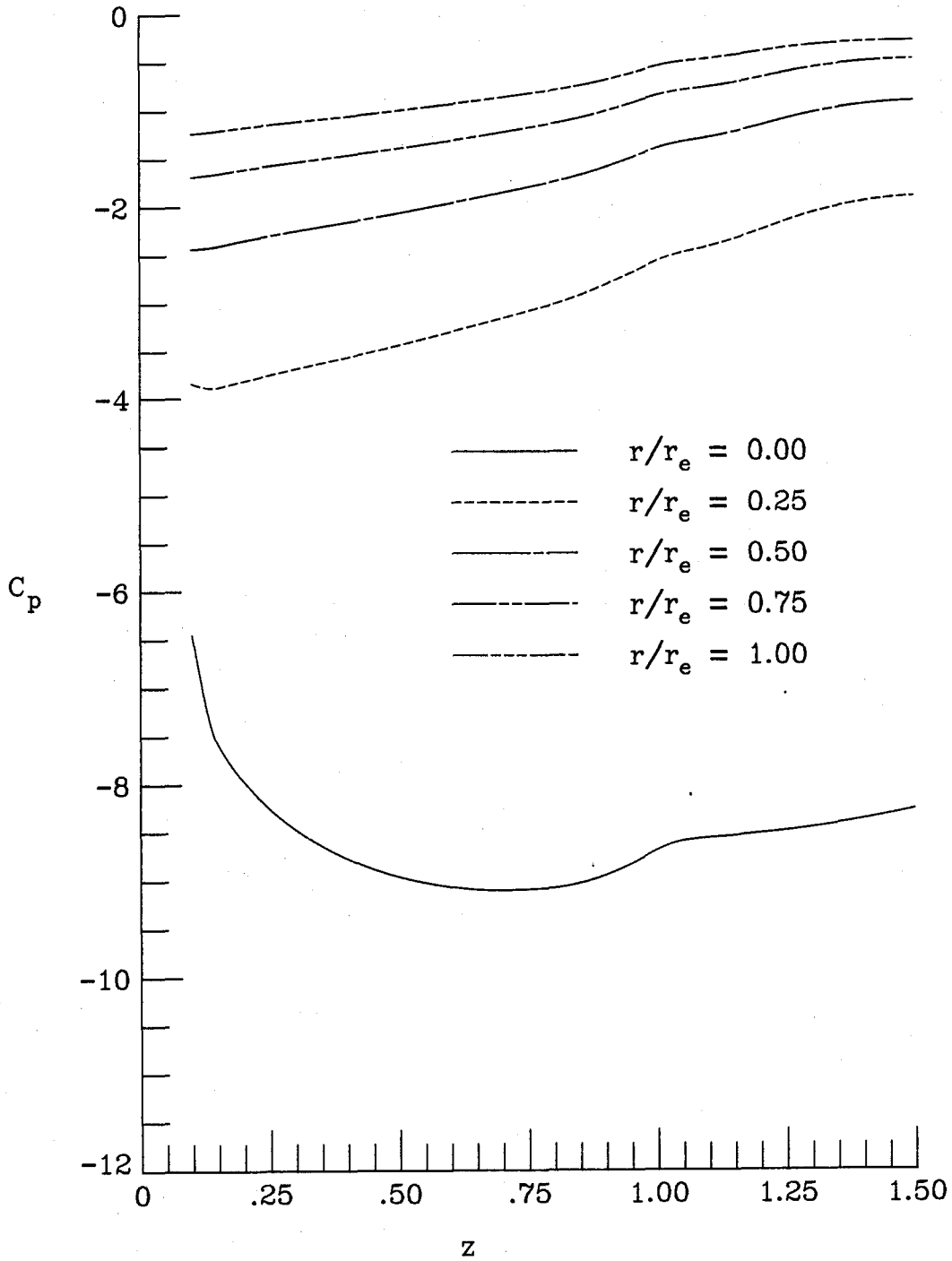

c) static pressure

Figure 7.3- Continued

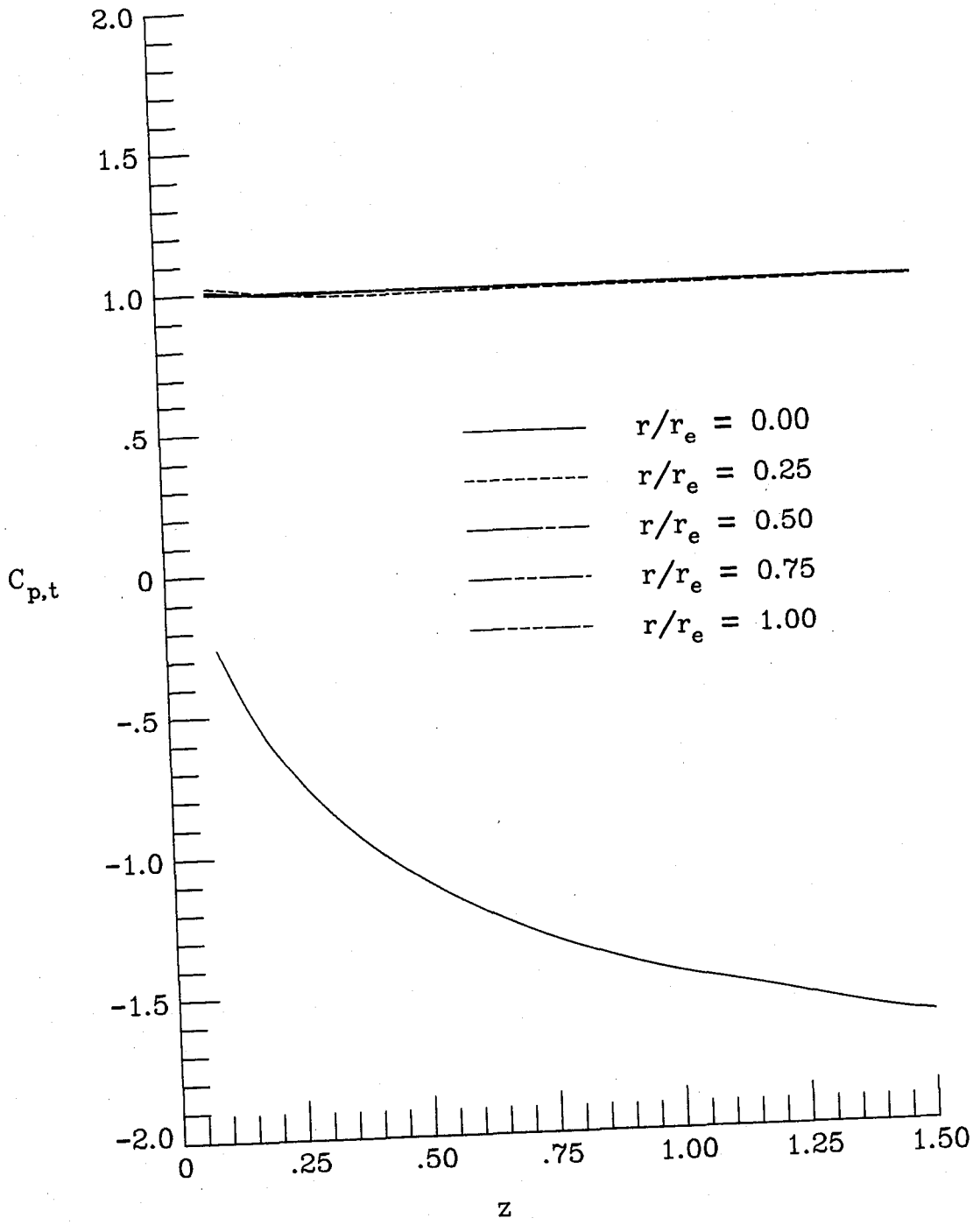

d) total pressure

Figure 7.3- Concluded.

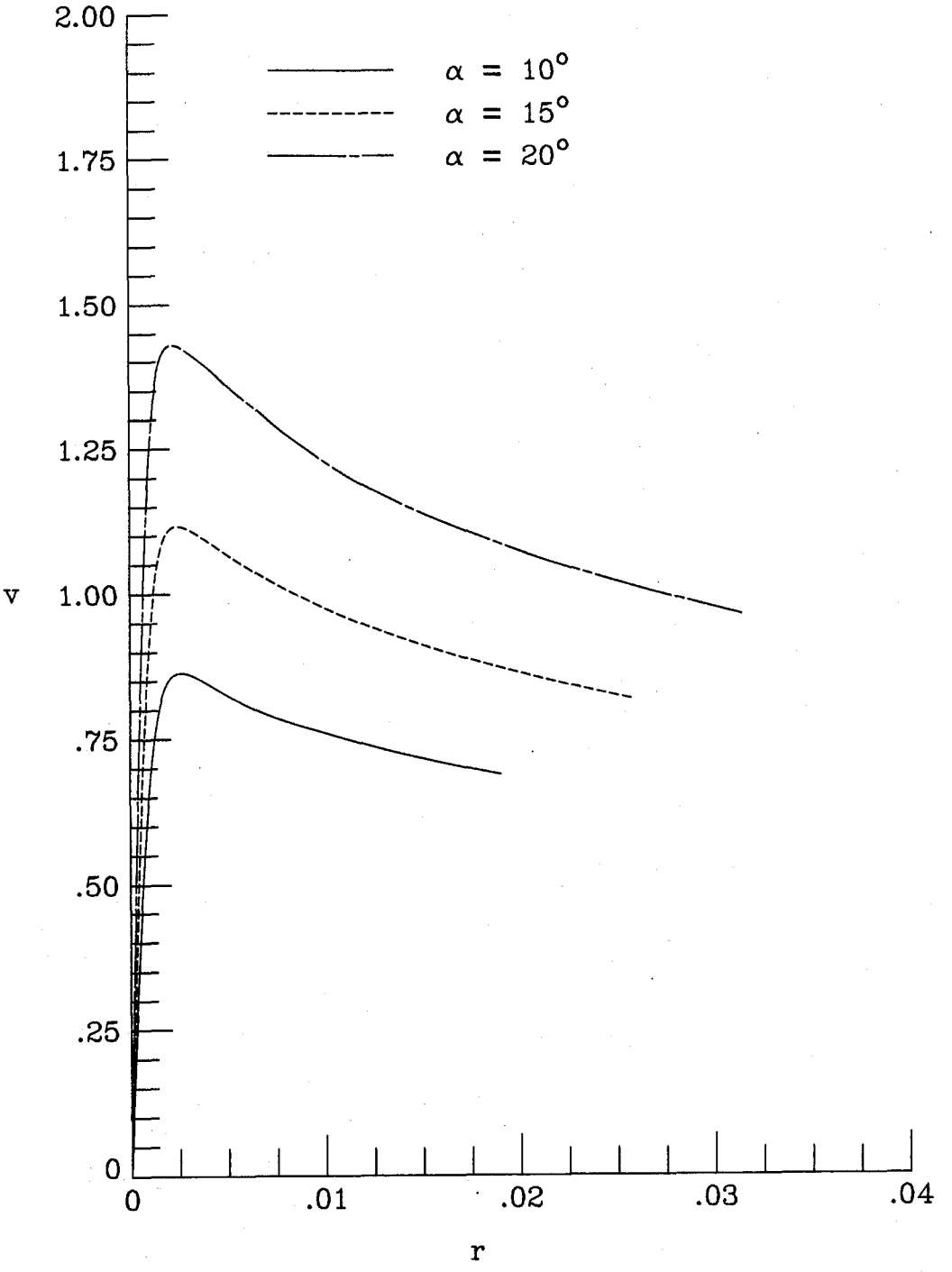

a) angular velocity

Figure 7.4- Angle-of-attack effect. $\Lambda = 75^0$.

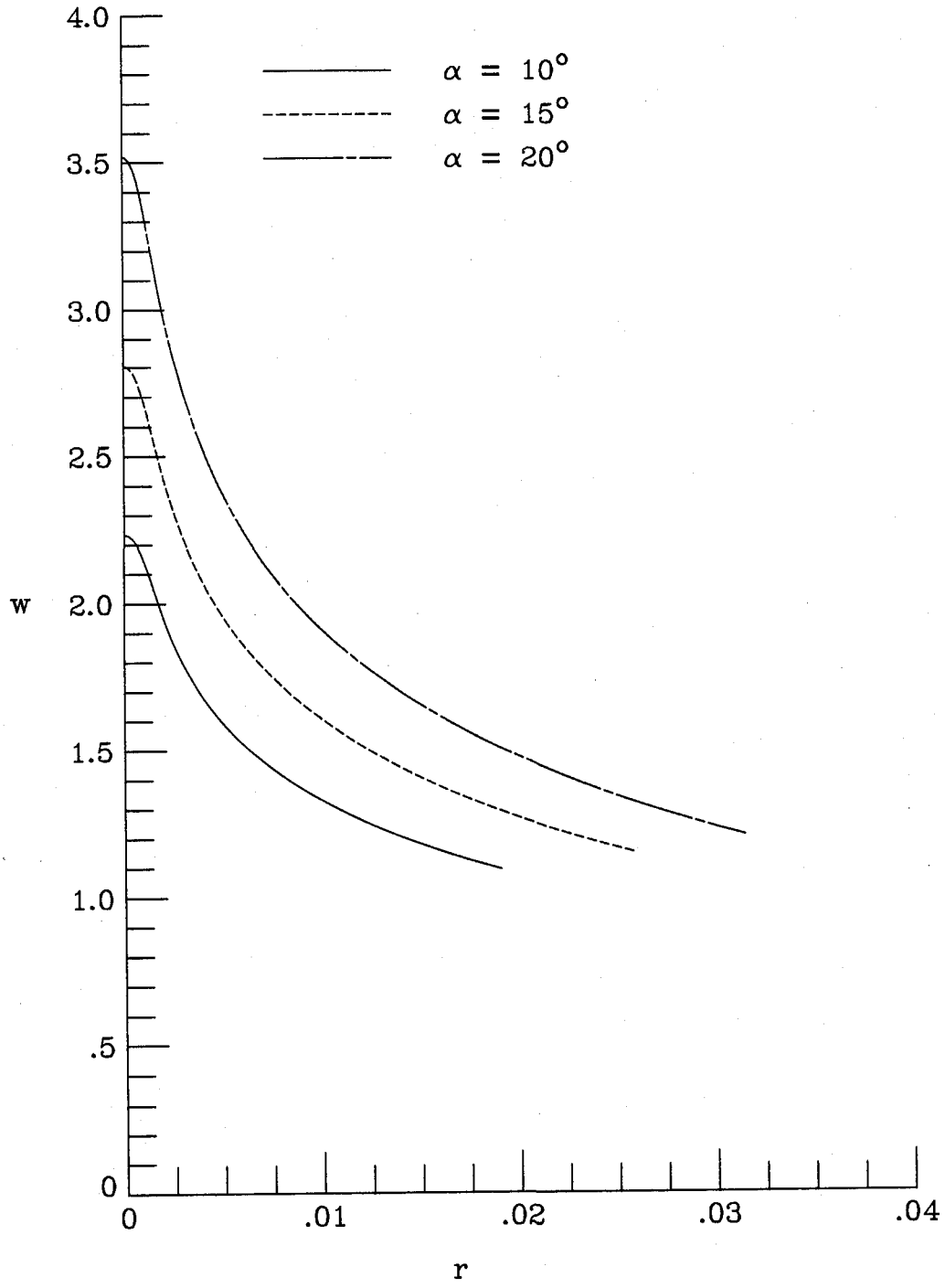

b) axial velocity

Figure 7.4- Continued

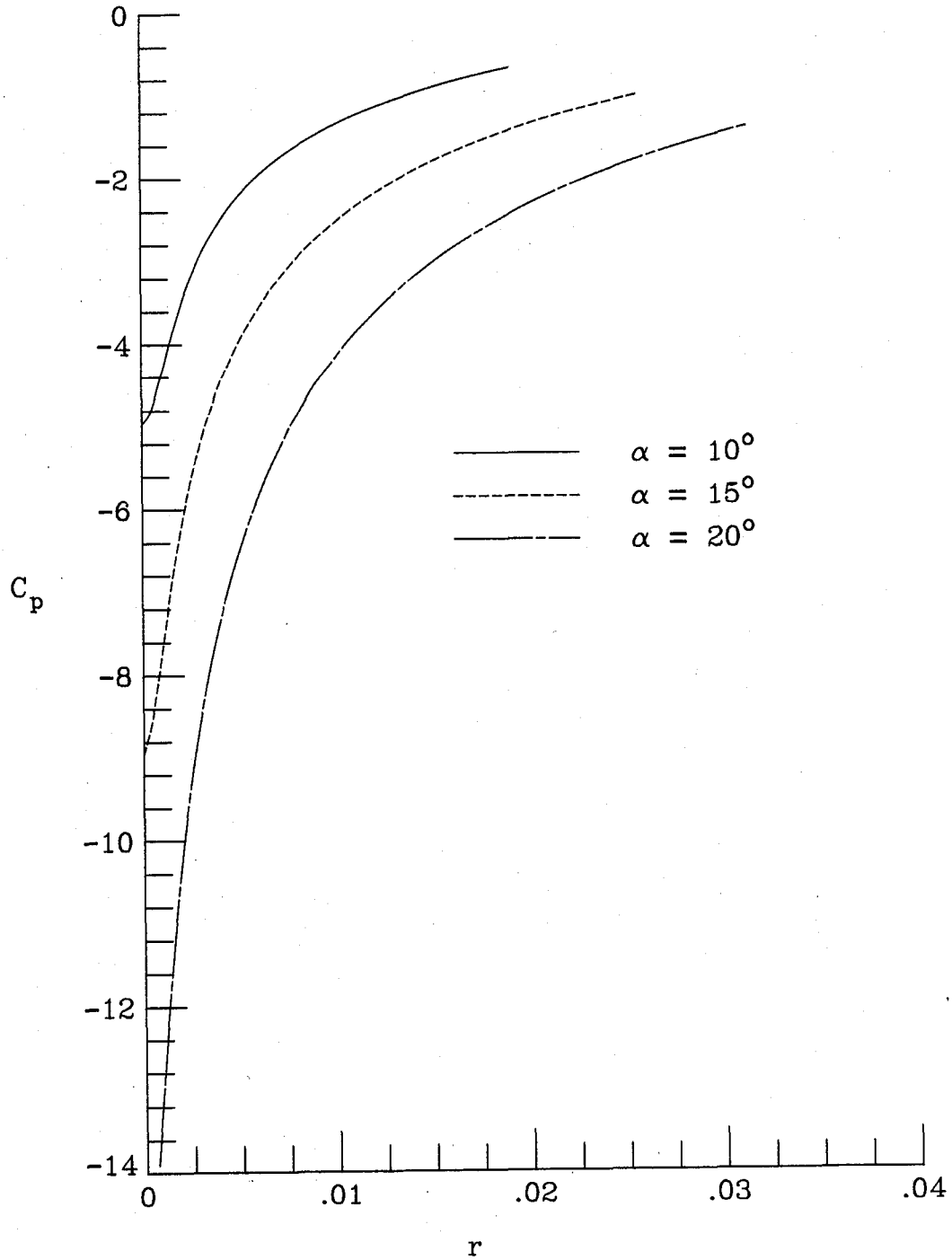

c) static pressure

Figure 7.4- Continued

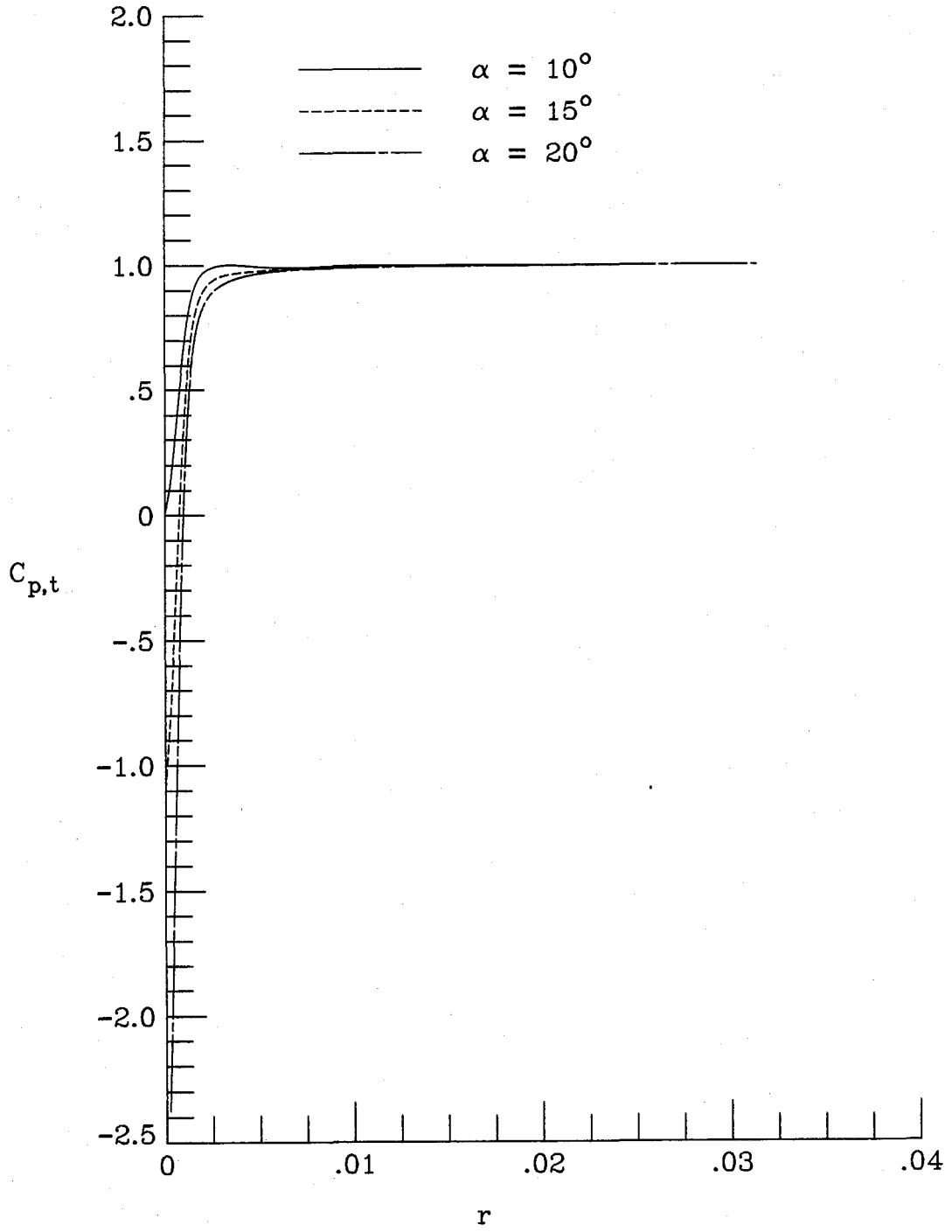

d) total pressure

Figure 7.4- Concluded.

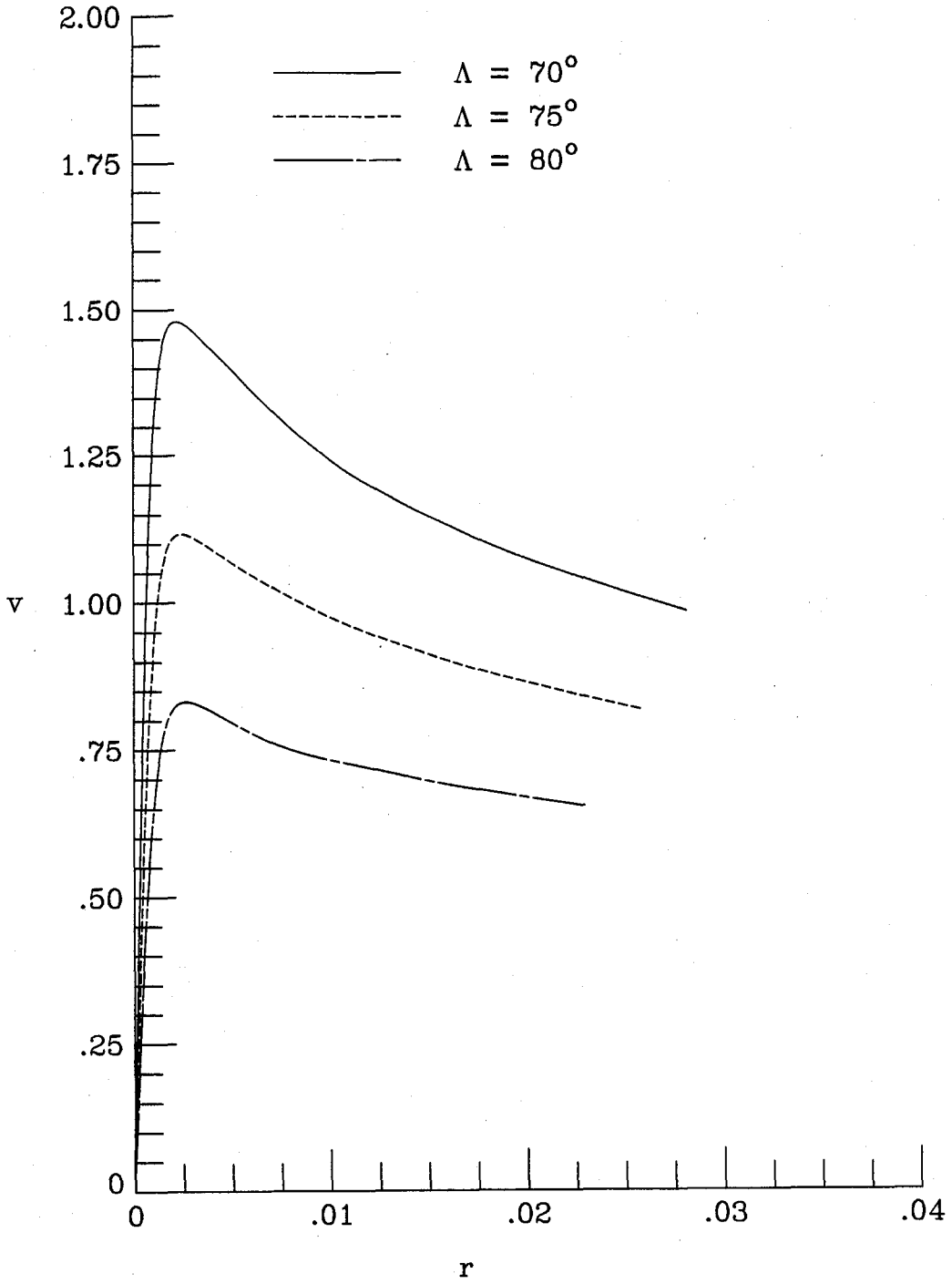

a) angular velocity

Figure 7.5- Leading-edge sweep effect - delta wings. $\alpha = 15^0$.

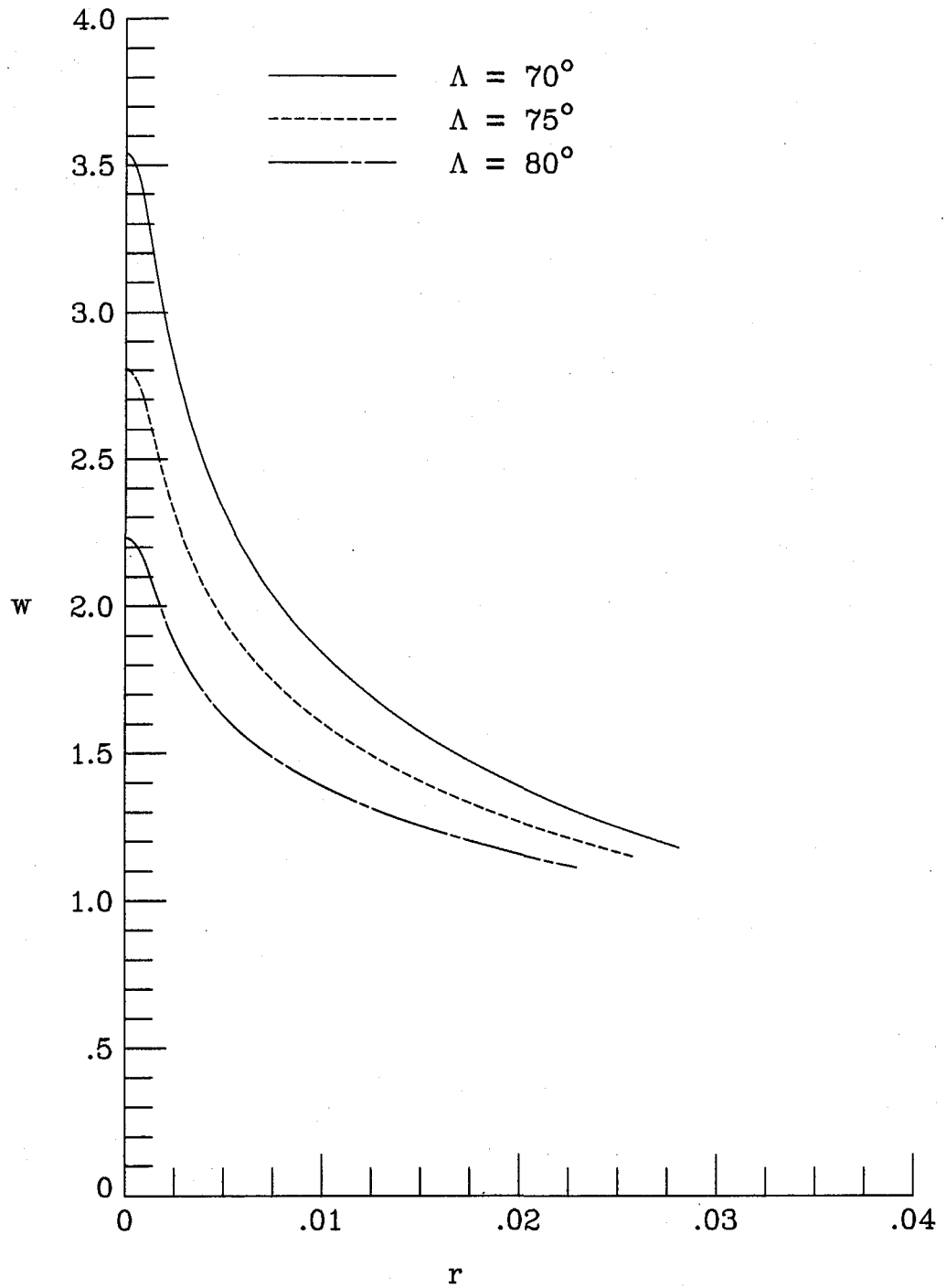

b) axial velocity

Figure 7.5- Continued

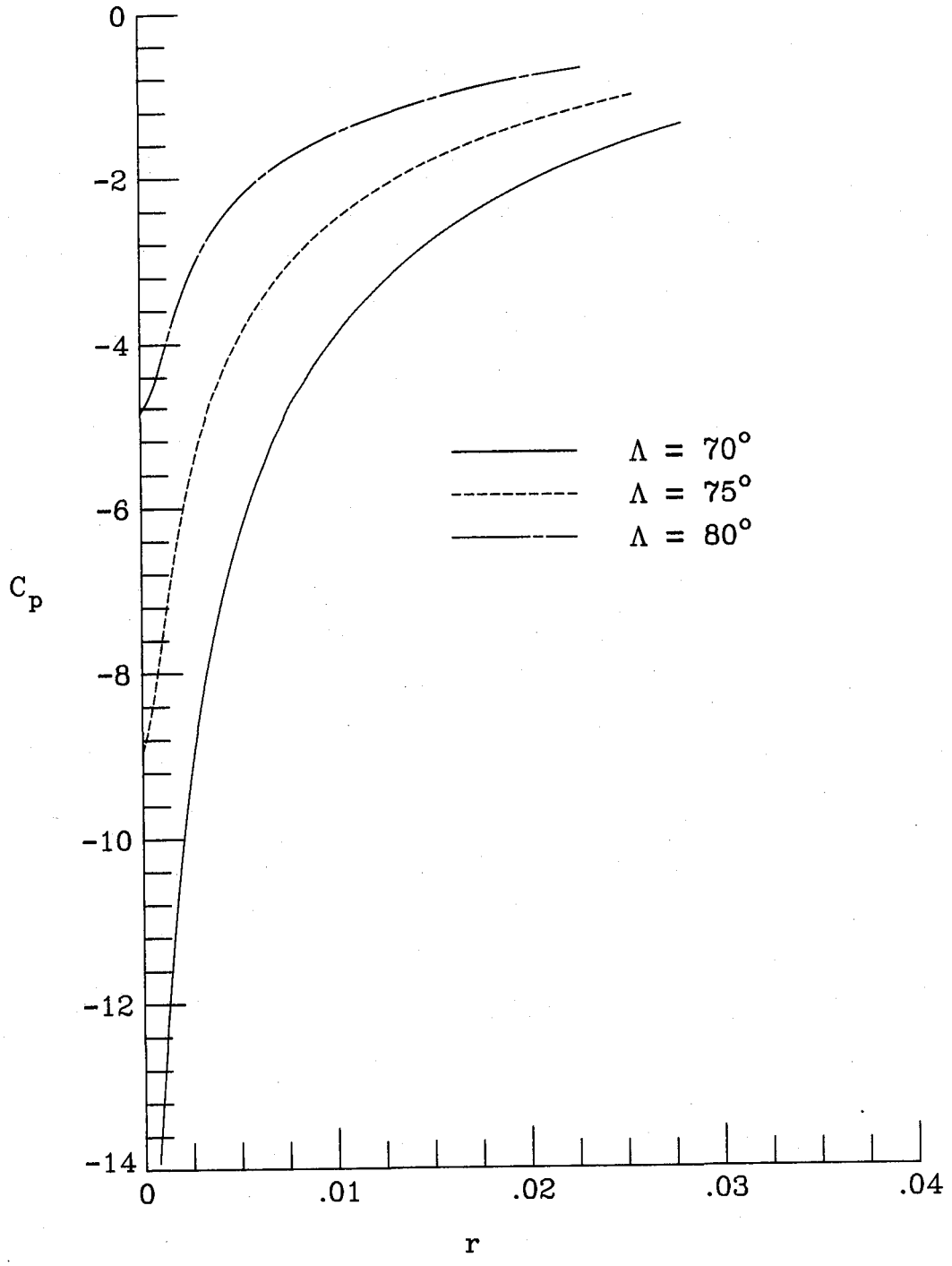

c) static pressure

Figure 7.5- Continued

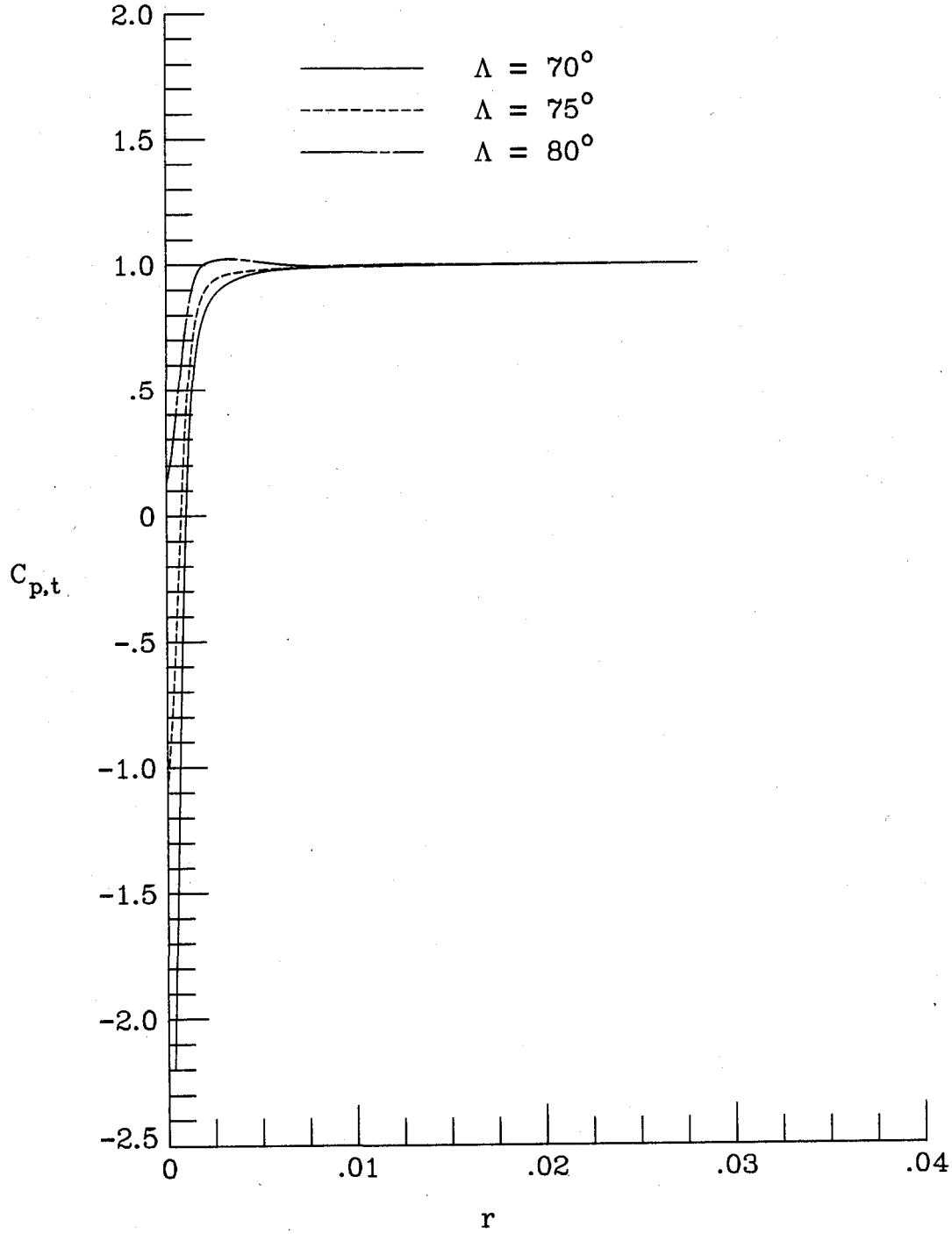

d) total pressure

Figure 7.5- Concluded.

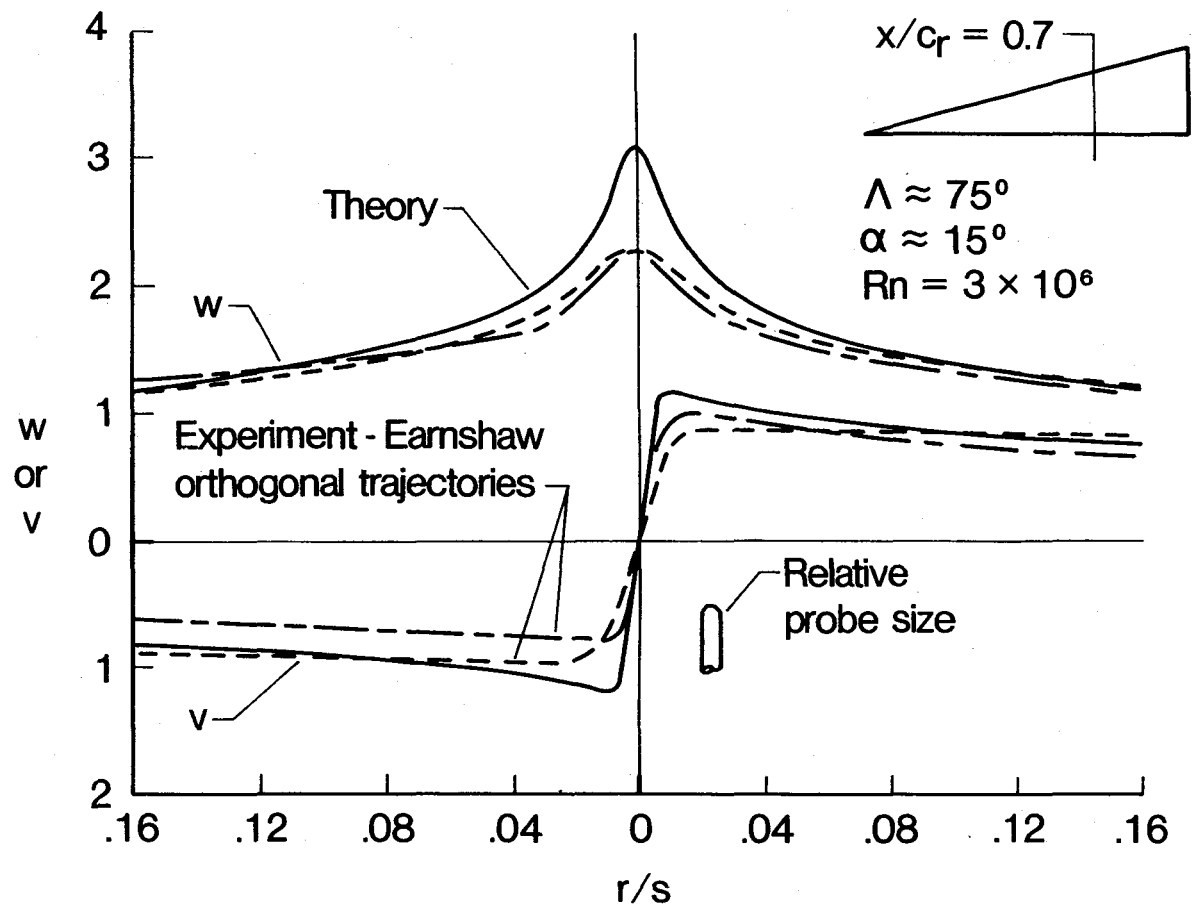

a) velocities

Figure 7.6- Experimental correlation.

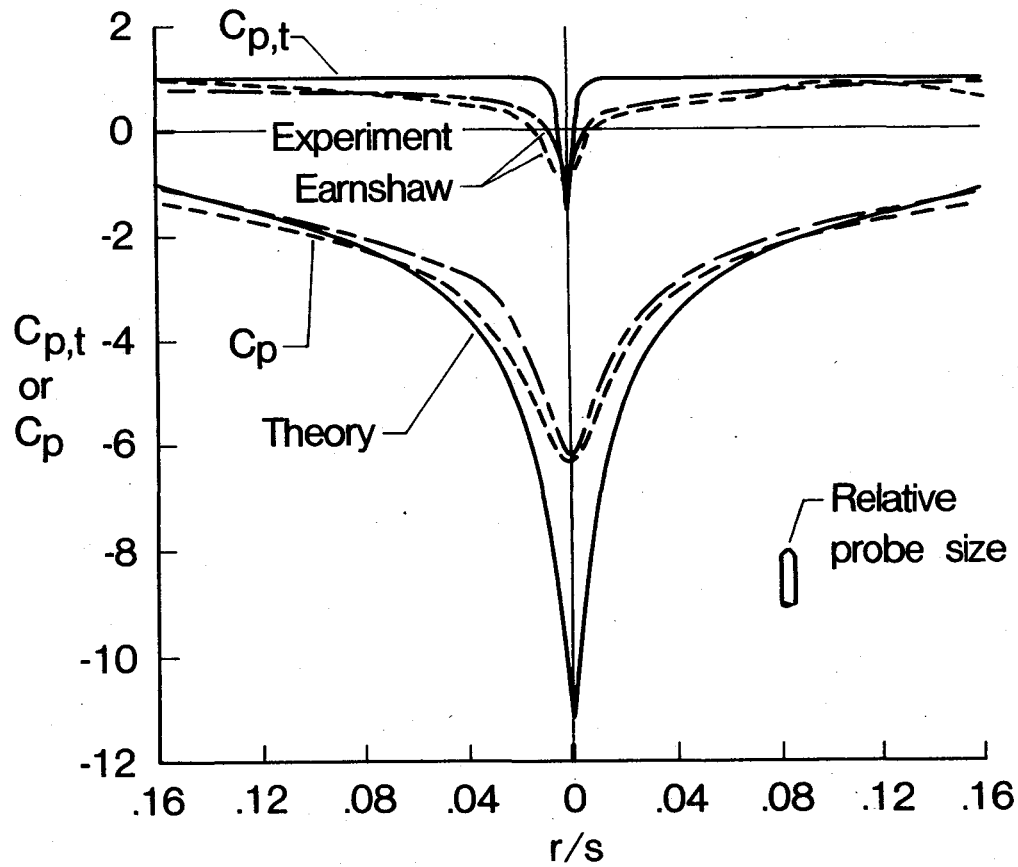

b) pressures

Figure 7.6- Concluded.

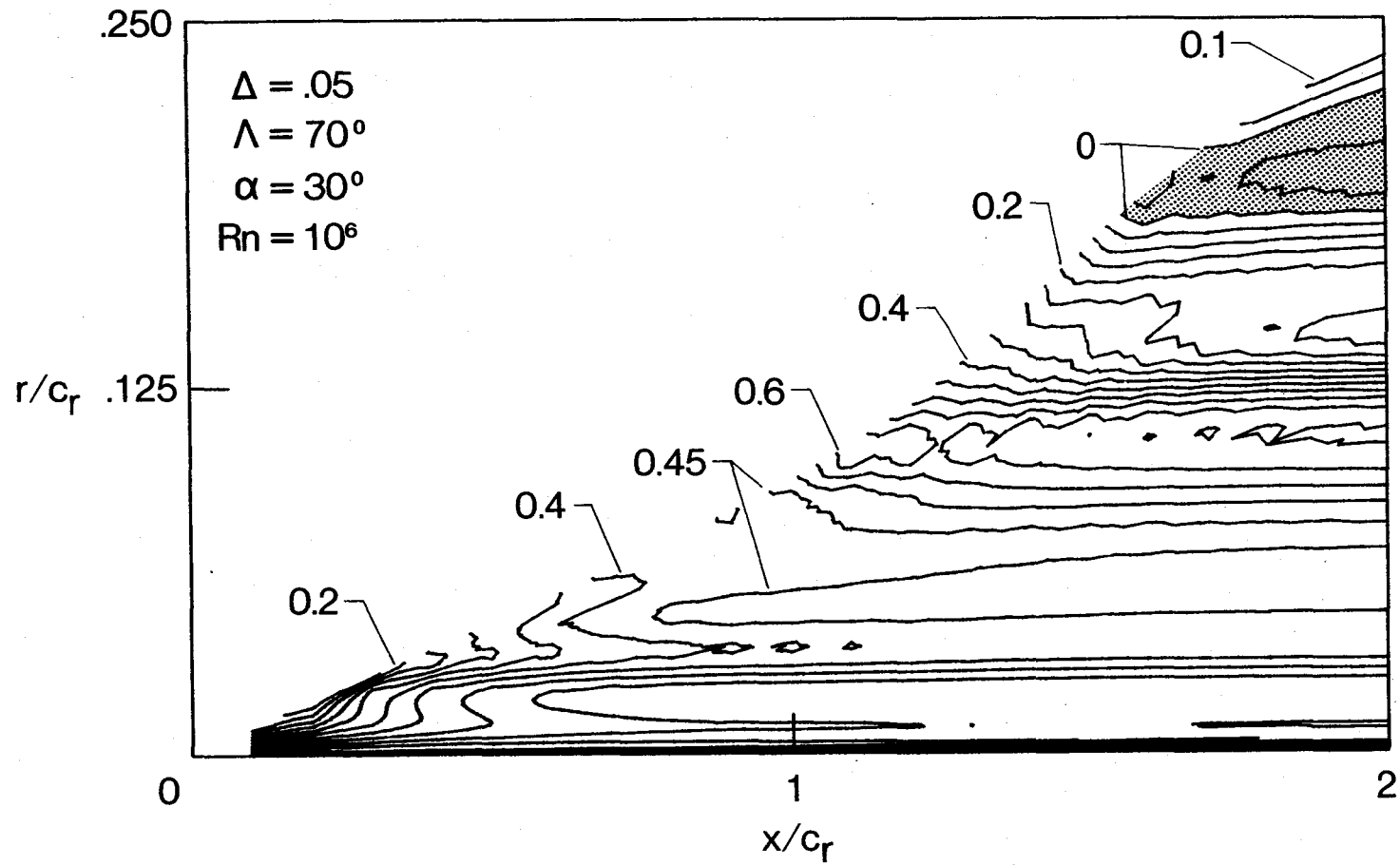

Figure 7.7- Stability contours. $\Lambda = 70^0$, $\alpha = 30^0$.

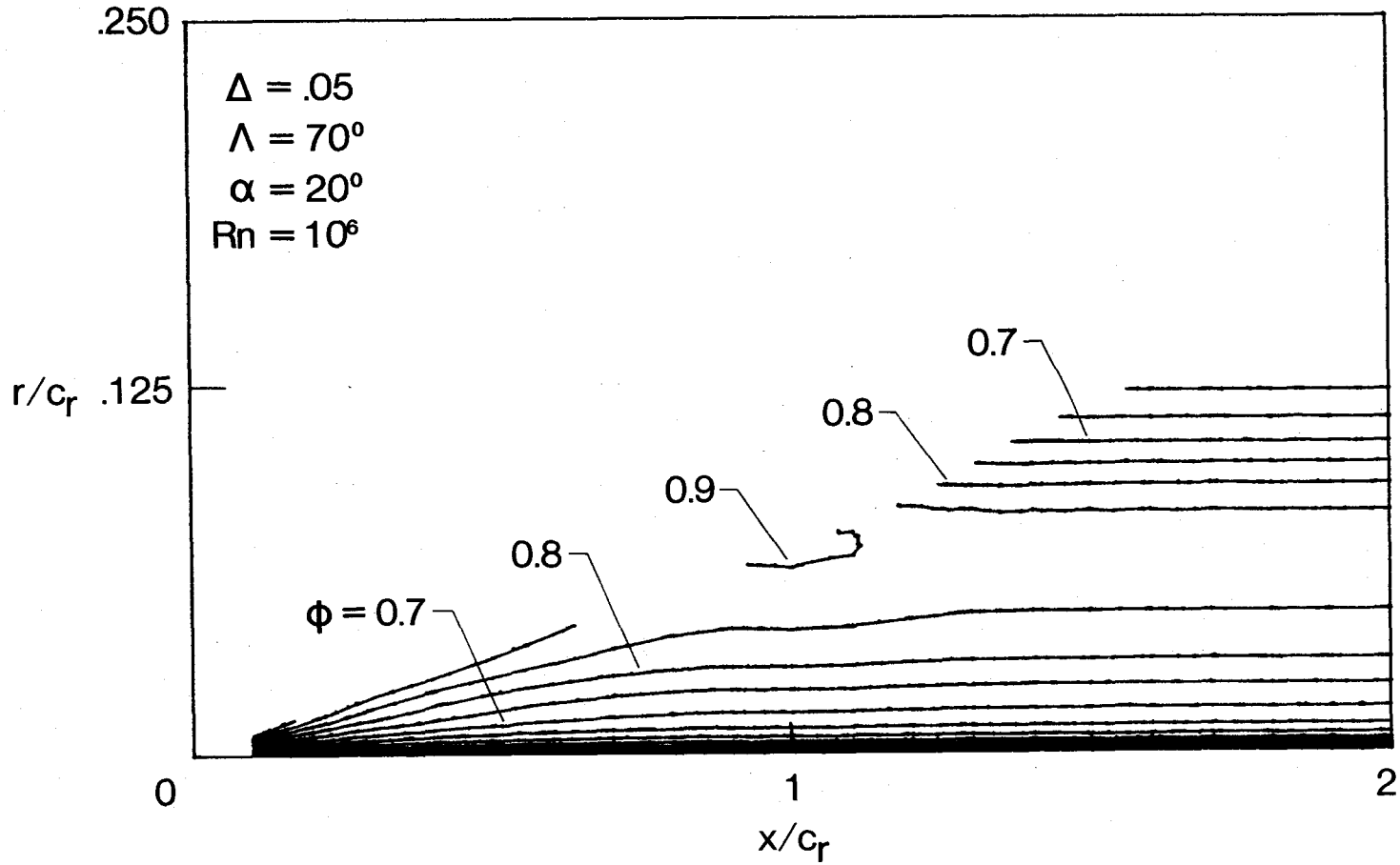

a) $\alpha = 20^0$

Figure 7.8- Helix angle contours. $\Lambda = 70^0$.

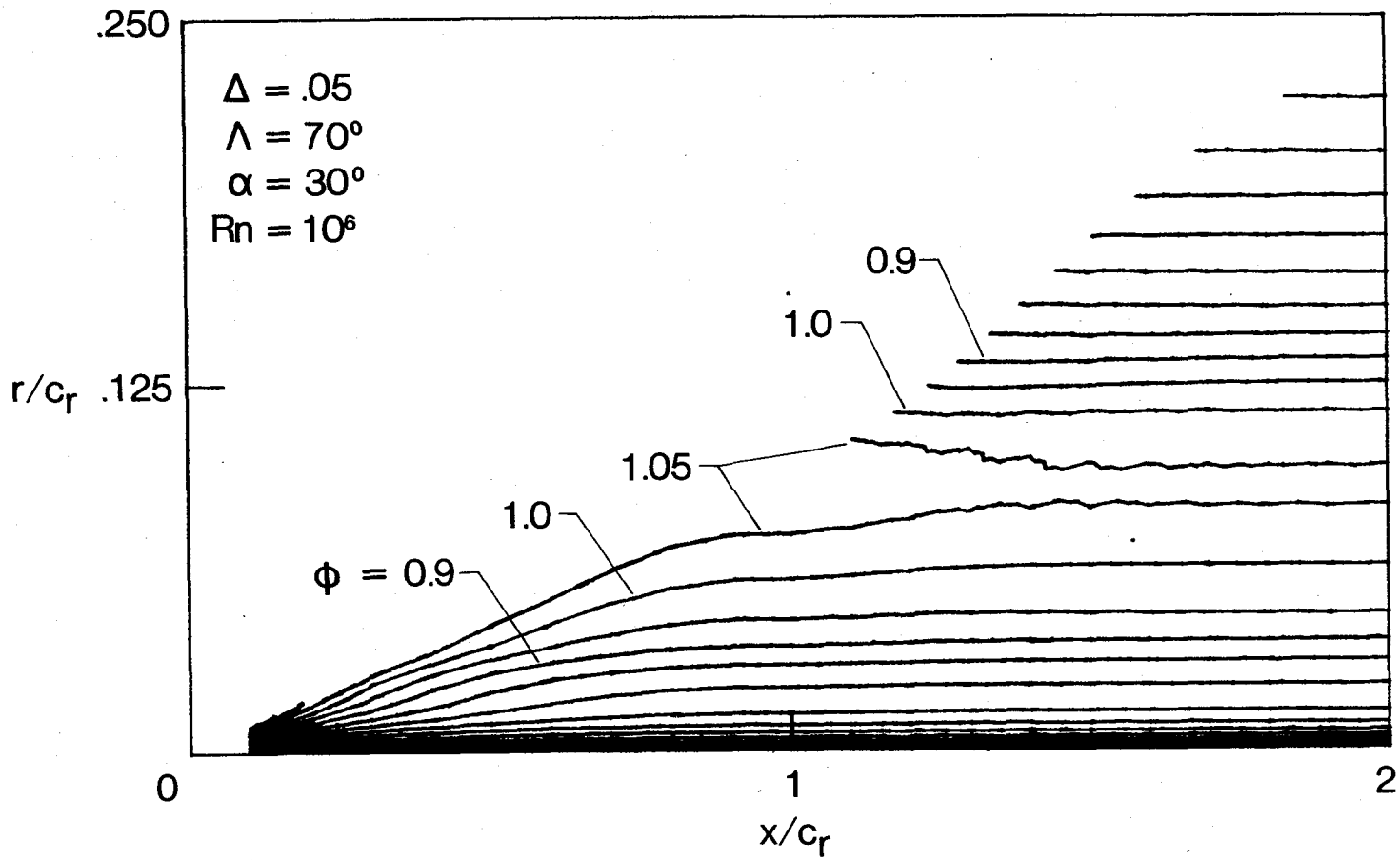

b) $\alpha = 30^0$

Figure 7.8- Continued

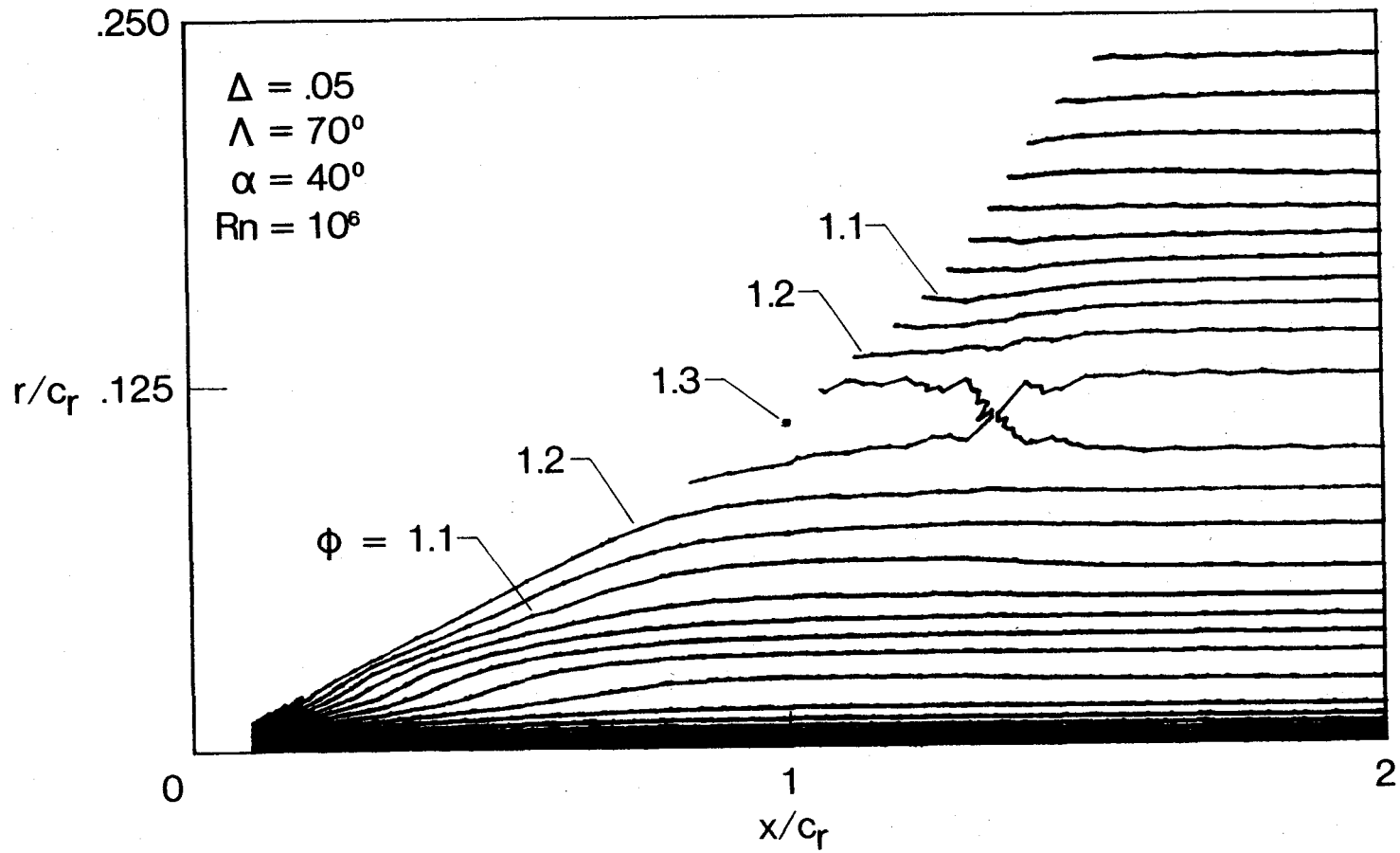

c) $\alpha = 40^0$

Figure 7.8- Concluded.

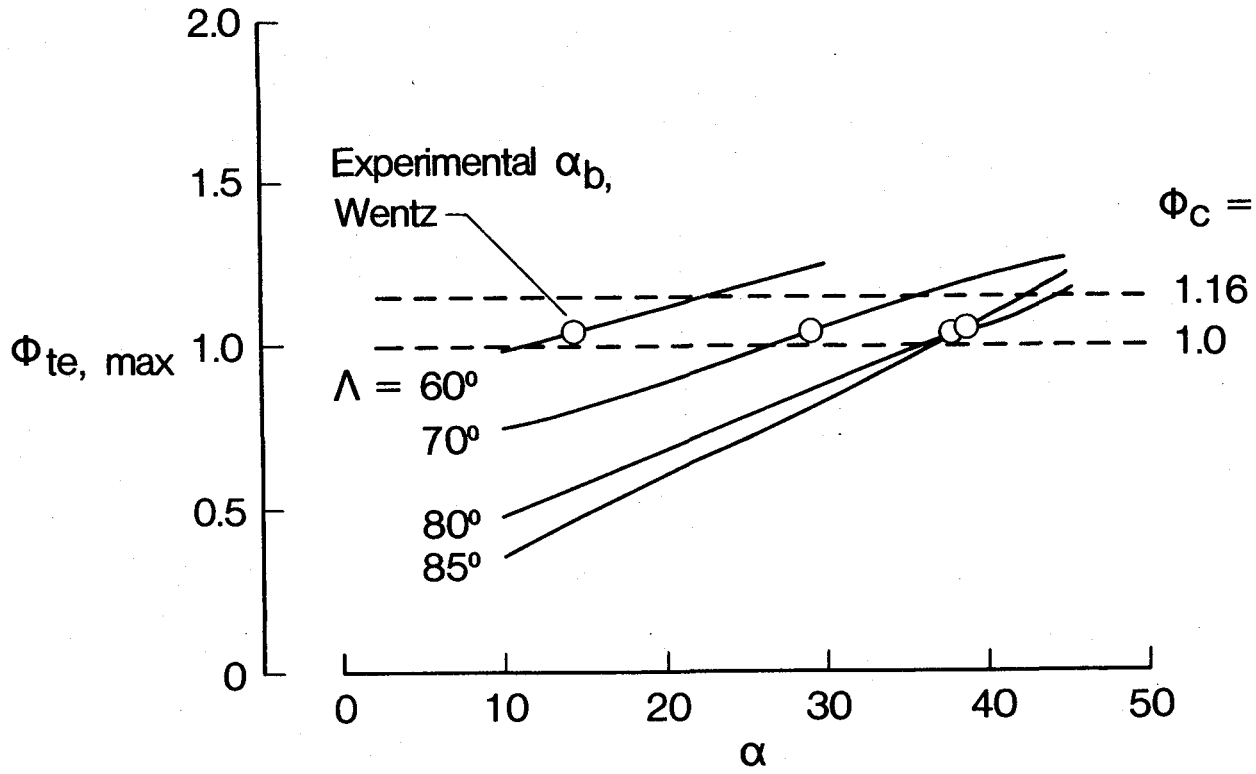

Figure 7.9- Trailing-edge maximum helix angle - delta wings.

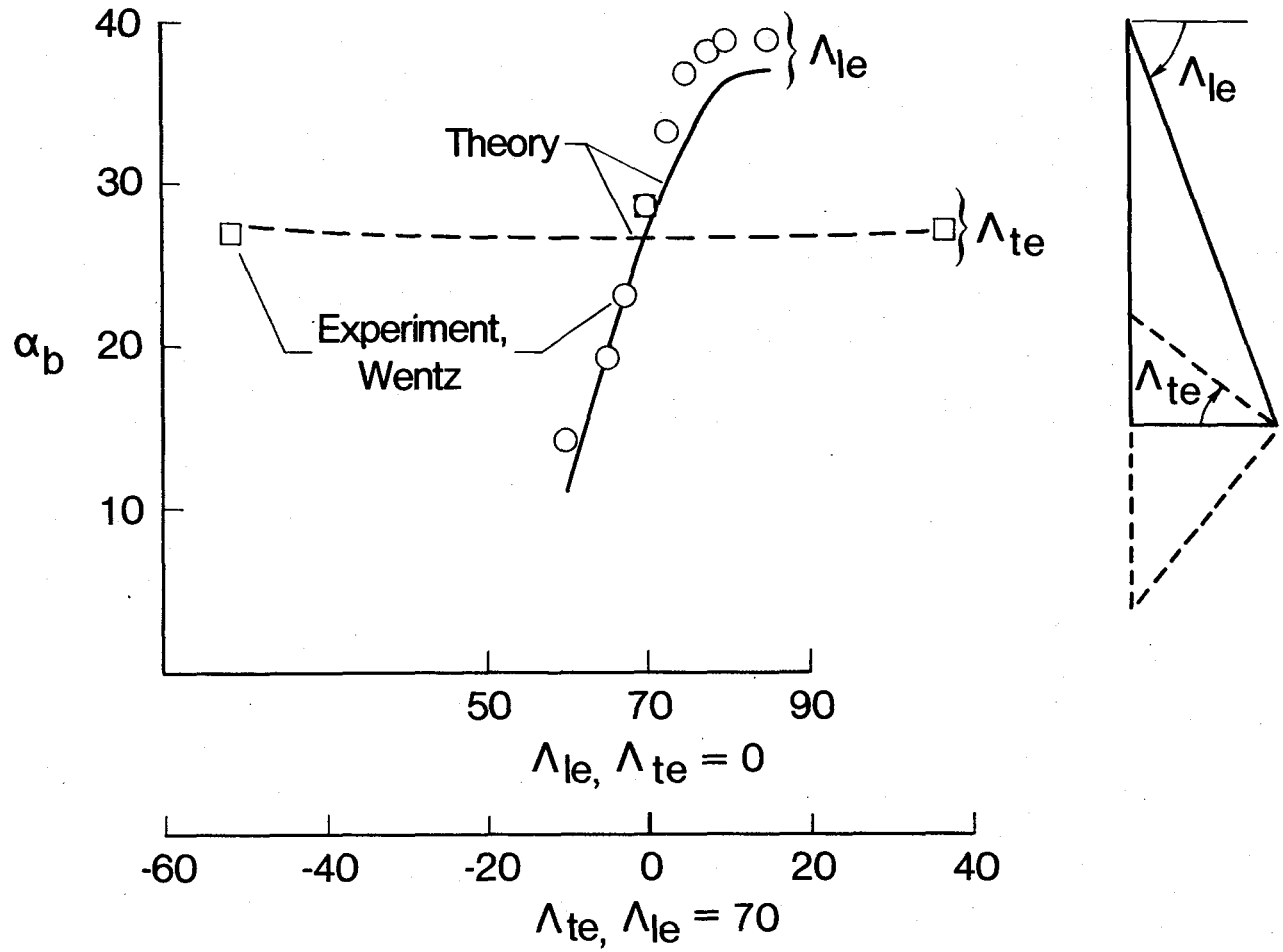

Figure 7.10- Vortex breakdown boundary.